MATHEMATICAL ANALYSIS AND NUMERICAL SIMULATION OF SOME NONLINEAR PROBLEMS IN SOLID MECHANICS

María Teresa Sánchez Rúa
Departamento de Matemática Aplicada
Universidade de Santiago de Compostela

PhD Dissertation

December 2009

Doña Peregrina Quintela Estévez, catedrática del Departamento de Matemática Aplicada de la Universidade de Santiago de Compostela, y Doña Patricia Barral Rodiño, profesora titular del Departamento de Matemática Aplicada de la Universidade de Santiago de Compostela, informan que la memoria titulada:

MATHEMATICAL ANALYSIS AND NUMERICAL SIMULATION OF SOME NONLINEAR PROBLEMS IN SOLID MECHANICS

fue realizada bajo su dirección por Doña María Teresa Sánchez Rúa, estimando que la interesada se encuentra en condiciones de optar al grado de Doctor en Ciencias Matemáticas, por lo que solicitan que sea admitida a trámite para su lectura y defensa pública.

En Santiago de Compostela, a 29 de julio de 2009.

Las directoras:

Prof. Dr. Peregrina Quintela Estévez

Prof. Dr. Patricia Barral Rodiño

La doctoranda: María Teresa Sánchez Rúa

Contents

Preface

Nowadays, a complete understanding of phenomena in solids mechanics is fundamental in order to develop new methods or techniques which allow saving huge amounts of money and time in applied fields like aluminium or ceramics industries. Historically, engineers have considered linear models in order to simulate these processes. However, real materials often exhibit a non-linear behavior and, at this moment, more and more new materials are emerging which push the linear models to their limits. Therefore, the use of nonlinear models has become more relevant in the numerical simulations of this type of industries.

In the present dissertation thesis, we distinguish three parts well defined and different but joined by a common topic: the mathematical study and numerical resolution of nonlinear problems in solid mechanics, arising from physical processes presented in the aluminium or ceramics industries. We consider real situations where different nonlinearities appear: behaviour laws of viscoplastic type, boundary conditions such as unilateral contact, etc. So, in the first part, we focus on the mathematical study of aluminium casting process, and we introduce some efficient algorithms to carry out its numerical simulation. In this problem, two nonlinearities appear: the nonlinear aluminium behaviour law and a contact condition with the block containing the metal. Then, the second part is devoted to the study of the well-known three-point bending experiment and the modulus of rupture of brittle materials. In this problem, again a contact condition introduces a nonlinearity in its formulation. Finally, the third part presents a mathematical analysis of an elasticity problem for catalyst supports.

In what follows, we describe every part and chapter in more detail.

Part 1. Aluminium casting processes: Efficient algorithms for their numerical simulation.

In this first part we propose two algorithms in order to solve numerically the deformation suffered for a slab in the aluminium casting process. We consider that the casting process is a quasi-static problem for a thermo-elasto-viscoplastic solid with a unilateral contact condition with the bottom block. In a first stage, to deal with the plastic and contact effects, the numerical solution was based on the well-known Bermúdez-Moreno algorithm and the numerical procedure was introduced in [5]. During the stationary stage, in which the contact condition does not have a significant influence, this algorithm worked well; however, during the start stage, when two nonlinearities worked together, the convergence was worse, increasing considerably the cpu-time. The objective of this first part is to design new strategies to obtain a computationally efficient algorithm, such as: generalized Newton methods, an adimensionalization of the constitutive law, a partial Cholesky

factorization or an automatic choice of algorithm parameters.

This first part is organized as follows:

- In Chapter 1, we give an introduction to the problem we want to solve and a description of the physical problem associated to the casting process.
- In Chapter 2, we introduce the mathematical model to simulate the butt curl deformation during the casting process, giving a description of the boundary conditions, equilibrium equations and the nonlinear behaviour law associated to aluminium casting.
- Chapter 3 summarizes the most important results for the mathematical analysis and the numerical solution of the butt curl deformation, introducing its weak formulation in terms of suitable functional spaces and some existence results. Finally, we recall a former numerical procedure, based in the Bermúdez-Moreno algorithm.
- Since this former algorithm did not give good convergence results in the butt curl deformation, Chapter 4 describes a new numerical procedure. To solve the nonlinear contact condition, we propose a generalized Newton method for nonsmooth equations and a penalization technique. To deal with the nonlinear behaviour law we propose two methods to improve the convergence: a Newton algorithm together with some numerical strategies designed to improve its efficiency and a Bermúdez-Moreno algorithm with variable parameters.
- In Chapter 5, we introduce some academic examples with known analytical solutions to validate the proposed algorithms and we present the numerical results for the simulation of the butt curl deformation, showing that the better results are obtained when considering the Newton algorithm for the contact, and the Bermúdez-Moreno one with variable parameters for the nonlinear behaviour law.
- Finally, in Chapter 6 we present the most important conclusions of Part I.

Part 2. Three-point bending tests: Mathematical study and numerical simulations.

This second part is devoted to the mathematical analysis of the three-point bending test and to the calculation of the modulus of rupture of brittle materials. In this type of tests, a sample of a brittle material is placed between three cylinders, without additional support, while the upper cylinder applies an increasing gradually force until the beam breaks. From this test, the modulus of rupture is obtained: the maximum surface stress of the bent beam at the instant of failure. In the engineering literature, this property is calculated by an explicit formula which involves the value of the load at failure, the distance between the two lower cylinders and the second moment of inertia of the transversal section of the beam. Firstly, in this part we carry out a complete mathematical analysis of the three-point bending test: we prove the existence of a unique solution to the elastic problem with frictionless unilateral contact that arises from this type of test and, in order to justify the classic formula for the modulus of rupture, we look for its limit model by using asymptotic analysis techniques. Secondly, we analyze analytically and numerically, from several perspectives, the modulus of rupture for brittle materials. In particular, we give four different approaches to the modulus of rupture: through the classical theory of beams; by means of the one

and three-dimensional numerical simulations; and by using an improved expression to the modulus of rupture obtained through its asymptotic analysis.

The second part is organized as follows:

- In Chapter 7, we give an introduction to the problem we want to solve and a description of the physical problem associated to the three-point bending tests.
- In Chapter 8, we introduce the mathematical model arising from the three-point bending test and we prove the existence of a unique solution under suitable conditions of compatibility on the data.
- Chapter 9 is devoted to the asymptotic analysis of this problem. We deduce the one-dimensional models associated to the displacement components, and we give the existence and uniqueness of solution for them. Moreover, we give an expression for the normal axial stress in the beam which is related to the MOR of brittle materials.
- In Chapter 10, we detail several examples for laboratory tests for cylindrical and rectangular beams made of porcelain and we deduce analytical solutions of the bending and axial displacements for them. Moreover, we introduce a new expression for the MOR, which takes into account not only the rupture load and the total length of the beam but also the distance between the two lower cylinders, the effect of the gravity and the distance between the ends of the beam and the lower cylinders.
- In Chapter 11 we present the numerical simulations of the real experiments introduced in the previous chapter and we compute the different approaches for the MOR described in this manuscript.
- Finally, in Chapter 12 we present the most important conclusions of Part II.

Part 3. An elasticity problem for catalyst supports: Unfolding method.

The study presented in this third part was carried out during a research stay in the Laboratoire Jacques-Louis Lion of the Univerist´é Pierre et Marie Curie. A catalytic converter in an automobile's exhaust system provides an environment for a chemical reaction where unburned hydrocarbons completely combust, in such a way that the pollution is reduced. In automotive industry, an enormous effort is being made with the purpose of developing appropriate supports and the catalyst itself. In some cases the correct support is what makes all the difference to the viability of a process. The goal of this third part is to study the asymptotic behaviour of catalyst supports in a linear elasticity problem when the catalyst support is a structure made of beams, placed periodically and with inner holes. To do that, we consider the unfolding method, which offers tools to study the asymptotic behavior and the homogenization of different structures formed by a large numbers of rods, plates or shells.

The third part is organized as follows:

- In Chapter 13, we give an introduction to the problem we want to solve and a description of the physical problem associated to the catalysis process.

- In Chapter 14 we introduce the three-dimensional elasticity problem for structures used as a catalyst support. These structures are made of a periodic family of elastic rods with a small thickness and inner holes.
- Chapter 15 is devoted to present some tools used when applying the unfolding method. Firstly, we introduce the unfolding operator related to the elasticity parameter and, secondly, we define the unfolding operator related to the periodicity parameter.
- In Chapter 16, under suitable hypotheses on the applied forces, we give the limit problem of the three-dimensional elastic problem when the elasticity and periodicity parameters go to zero, obtaining three uncoupled problems: The first problem defines the longitudinal displacement and the second one gives the transversal bending of the structure, while the third one defines the torsion angle.
- Finally, in Chapter 17, we present some conclusions of this third part.

Finally, the last part of the manuscript gathers the acknowledgments and a summary of this dissertation thesis in Spanish language.

Part I

Aluminium casting processes: Efficient algorithms for their numerical simulation

Table of Contents

Chapter 1

Introduction

The aim of Part I of this manuscript is to obtain efficient algorithms to solve nonlinearities arising from behaviour laws of viscoplastic type, or from boundary conditions such as unilateral contact. A real situation, where those two nonlinearities appear and which is the motivation of this research, is the casting process in aluminium production. During casting processes, the liquid aluminium is poured onto a water-cooled mold which is called bottom block; when the aluminium begins to solidify the bottom block starts to descend leaving room for more liquid metal (see Figure 1.1). A detailed description of the complete process can be found in [33, 41, 75].

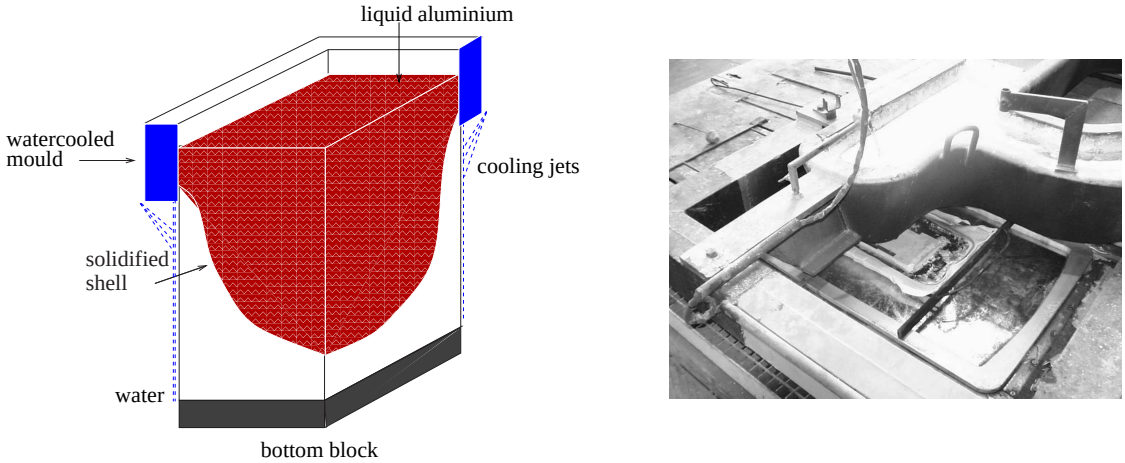

Figure 1.1: Scheme of a casting process and a photograph of the mold.

The casting process can be divided into two stages. During the start stage, the temperature field, the solidification front, and the slab shape change with time. The large thermal stresses due to the cooling jets cause the butt of the slab to bend and lose contact with the bottom block. This deformation is known as *butt curl* (see Figure 1.2). When the length of the slab is 1m, approximately, the temperature field has attained a steady state. In this stationary stage the solidified shell contracts inwards and the resulting cross-section has a "bone" shape.

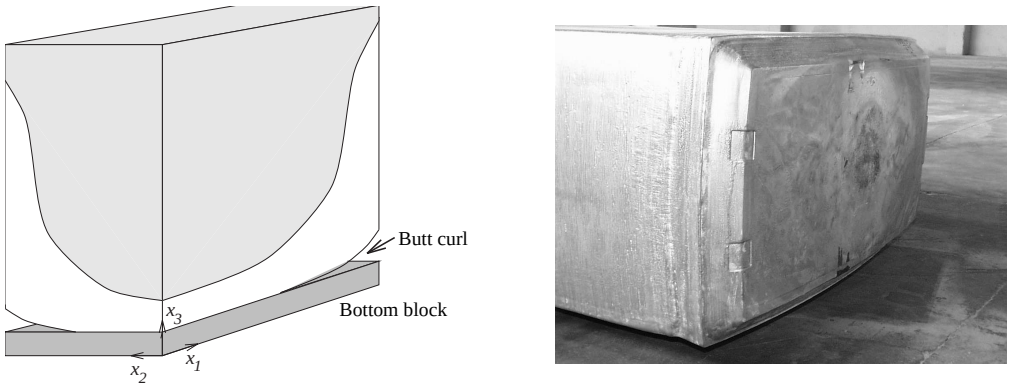

Figure 1.2: Butt curl deformation

The deformations of butt curl and of cross-sectional could be minimized by optimizing casting parameters but first it is necessary to be able to predict the deformations with fixed casting conditions. To predict casting behaviour, the main difficulties are due to coupling effects, to the presence of nonlinear terms, to the existence of free boundaries and to the computational domain which varies with time (see [6]). Specifically, in order to simulate the butt curl deformation we must solve a problem of frictionless unilateral contact between a thermo-elasto-viscoplastic body of Maxwell-Norton type and a rigid foundation.

This manuscript is the continuation of the research initiated in [5] and [9]-[13], where several mathematical aspects of this subject have been studied:

- The detailed formulation as a variational inequality.
- The establishment of sufficient conditions for the existence of a solution.
- The numerical implementation of the metallostatic pressure on the liquidus-solidus interphase.
- The numerical approximation of the variational inequality and the description of a numerical scheme to solve it.

In [5], an approximate solution of this problem was obtained by using an implicit Euler scheme in time and a finite element method in space. To deal with the nonlinearities, the numerical solution was based on the Bermúdez-Moreno algorithm with the participation of two multipliers: the viscoplastic multiplier (to take into account the nonlinearity from the behaviour law) and the contact multiplier (to avoid the nonlinearity due to the contact condition). These two multipliers were approximated by using fixed point algorithms (see [9, 10, 16]). During the stationary stage, in which the contact condition does not have a significant influence, this algorithm worked well; however, during the start stage, when two nonlinearities worked together, the convergence was worse, increasing considerably the cpu-time. Moreover, this algorithm presents a strong dependence on its parameters, which could not be determined *a priori*. These facts made difficult the massive usage of this algorithm to help in the understanding of the different effects in casting processes.

The fundamental objective of this research work is to develop efficient numerical methods that incorporate adaptive procedures to accelerate the treatment of the nonlinearities and hence, be able to simulate numerically the butt curl deformation in a reasonable cpu-time.

Several approaches are employed to achieve this objective:

- Contact condition. Approximating the contact multiplier using generalized Newton methods together with a penalization technique to conserve the matrix's symmetry (see [7, 14, 46, 54, 72]). The resultant algorithm for the treatment of the contact condition is fast, accurate and its convergence is independent of the algorithm parameters. Nevertheless, the stiffness matrix needs to be recalculated at each iteration. So, taking into account that usually the nonlinear boundary condition only involves a small part of the boundary, we propose to use a factorization of the stiffness matrix adapted to the problem's geometry.
- Viscoplastic law. Two options are considered:
  - Approximating the viscoplastic multiplier with standard Newton techniques without modification of the stiffness matrix at each iteration (see [7, 14]).
  - Approximating the viscoplastic multiplier with a generalization of the Bermúdez-Moreno algorithm with variable parameters automatically calculated (see [43]).

  When the nonlinearity coming from the viscoplastic law is solved by using Newton techniques, the strong thermal gradients of stresses force to employ some numerical techniques to obtain a good convergence: an adimensionalization technique, an Armijo rule and an optimization of the time step. We present academic problems in order to show the good behaviour of this methodology but, in the real casting process, the convergence is not always achieved. Due to this, we propose a second algorithm which is a generalization of the Bermúdez-Moreno algorithm with an automatic choice of its parameters.

The outline of this Part I is as follows:

In Chapter 2, we introduce the mathematical model to simulate the butt curl deformation during the casting process, giving a description of the boundary conditions, equilibrium equations and the nonlinear behaviour law associated to aluminium casting. The latter is a thermo-elasto-viscoplastic law, where the viscoplastic part is given by a nonlinear Maxwell-Norton law, and the thermal part is a generalization of Arrhenius law.

In Chapter 3, we make a review of the most important results for the mathematical analysis and the numerical solution of the butt curl deformation. We propose a weak formulation for the problem in terms of suitable functional spaces, following the works of Geymotat and Suquet (see [45]) and Barral and Quintela (see [13]). Moreover, some existence results proved by Barral and Quintela in [13] and Barral *et al* in [8] are presented. Finally, we recall the numerical procedure proposed in [5] to approximate the solution of the problem and to simulate the butt curl deformation. This procedure is based in the Bermúdez-Moreno algorithm.

With the aim of improving the poor convergence of the former algorithm in butt-curl simulation, Chapter 4 describes a new numerical procedure to approximate the solution of the problem. The contact condition is solved by means of the Bermúdez-Moreno algorithm (see [16]), in which the

contact multiplier is a fixed point of a nonlinear equation. To approximate this multiplier we propose a generalized Newton method for nonsmooth equations and a penalization technique. In order to deal with the nonlinear constitutive law we use again the Bermúdez-Moreno algorithm and we propose two methods to approximate the corresponding multiplier: a Newton algorithm together with some numerical strategies designed to improve its efficiency and a Bermúdez-Moreno algorithm with variable parameters.

In Chapter 5, we present some academic examples with known analytical solutions to validate the proposed algorithms. These examples have been designed to reproduce a behaviour analogous to semicontinuous casting behaviour: large gradients of stresses with respect to time and a gap between the computational domain and the rigid foundation which grows with time. Numerical results are given to compare the efficiency of these methodologies with the former Bermúdez-Moreno algorithm used in [9, 10]. Finally, we present the numerical results for the simulation of the butt curl deformation, showing that the better results are obtained when considering the Newton algorithm for the contact, and the Bermúdez-Moreno one with variable parameters for the viscoplasticity.

Chapter 2

Mathematical model

In this chapter we introduce a mathematical model to simulate the deformation suffered by an aluminium slab during the solidification process. For this purpose, we consider a quasi-static problem for a thermo-elasto-viscoplastic solid with a unilateral contact condition with the bottom block.

In this manuscript, coupling between thermal and mechanical models is not considered. The temperature field is computed *a priori* by using the code presented in [63] and used as a data in the mechanical simulation. A detailed description of the thermal model can be found in [6, 17, 63].

Several authors have studied the mechanical deformations in casting processes. In 1982, Kristiansson and Zetterlund (see [55]) studied the deformation in steel continuous casting by means of a two-dimensional viscoelastic model, formulated on a horizontal section. Later, in 1992, Mariaux *et al.* (see [59]) studied the butt curl simulation in aluminium casting and, in 1995, Drezet *et al.* (see [34]) simulated the cross-sectional deformation; both works considered a viscoelastic model. In 2005, Sengupta *et al.* (see [77]) presented a coupled thermal-stress model to simulate the start-up phase of the casting process. Nevertheless, all these works present numerical results, but they do not specify the used models or algorithms. Contrarily, in 2001 Barral (see [5]) presented a mathematical analysis and a numerical study of a quasistatic evolution problem to model the thermomechanical behaviour of an aluminium casting, identifying all the governing equations as well as the suitable functional spaces and numerical algorithms. In this manuscript we are going to use this mathematical model in order to simulate the butt-curl deformation arising from casting processes.

The outline of this chapter is as follows: In Section 1.1, we introduce some notations we will use hereafter in Part I, and the computational domain of the mechanical simulation. In Sections 1.2 and 1.3, we present the boundary conditions and equilibrium equations, respectively. Section 1.4 is devoted to introduce the nonlinear behaviour law; a thermo-elasto-viscoplastic law is considered, where the viscoplastic part is given by a nonlinear Maxwell-Norton law and the thermal part is a generalization of Arrhenius law. Finally, in Section 1.5, the initial conditions are given and in Section 1.6 we present the complete mathematical model.

2.1 Computational domain and notations

Let $Ox_1x_2x_3$ be a fixed system of rectangular Cartesian axes associated to the slab, whose origin coincides with the center of the slab base.

Hereafter in this manuscript, Latin subscripts are understood to range over the integers $\{1,2,3\}$, and Greek subscripts over the integers $\{1,2\}$. Einstein notation of summation over repeated subscripts is implied.

Given two vectors $\mathbf{u}, \mathbf{v} \in \mathbb{R}^3$, with components $(u_i)_{i=1,2,3}$, $(v_i)_{i=1,2,3}$, respectively, $\mathbf{u}\cdot\mathbf{v}$ denotes their scalar product. From now on, $\mathcal{S}_3$ denotes the space of symmetric second order tensors endowed with the usual scalar product

$$\boldsymbol{\tau} : \boldsymbol{\xi} = \tau_{ij}\xi_{ij},\ \boldsymbol{\tau}, \boldsymbol{\xi} \in \mathcal{S}_3.$$

Given $\boldsymbol{\tau}$ a tensor function in $\mathcal{S}_3$, we denote its divergence

$$\mathrm{div}(\boldsymbol{\tau})_i = \partial_j \tau_{ij},$$

and its trace

$$\mathrm{tr}(\boldsymbol{\tau}) = \sum_{k=1}^{3} \tau_{kk}.$$

Moreover, we introduce the following norm in $\mathcal{S}_3$:

$$|\boldsymbol{\tau}| = \sqrt{\mathrm{tr}(\boldsymbol{\tau} : \boldsymbol{\tau})}.$$

From here on, we will use a superposed dot to denote differentiation with respect to time.

Let $[0, t_f]$ be the time interval to carry out the mechanical simulation. Due to casting symmetry, $\Omega(t)$ represents a quarter of the slab at the instant $t \in [0, t_f]$. The temperature field $T(\mathbf{x}, t)$ at each point $\mathbf{x} \in \Omega(t)$ is previously computed by using the mathematical model developed in [63]. The mechanical domain at each time instant t corresponds to the solidified part of the slab, denoted by $\Omega_s(t)$, which is obtained from the solution of the thermal problem:

$$\Omega_s(t) = \{\mathbf{x} \in \Omega(t); T(\mathbf{x}, t) < T_l\},$$

where T_l is the liquidus temperature (see Figure 2.1). We assume that at the initial instant $t = 0$ there exists a solidified part of the slab, that is, $\Omega_s(0) \neq \emptyset$.

The mechanical problem consists of determining the displacement field $\mathbf{u}(\mathbf{x}, t)$ and the stress tensor field $\boldsymbol{\sigma}(\mathbf{x}, t)$ at each point $\mathbf{x} \in \Omega_s(t)$ and at each instant $t \in (0, t_f]$.

2.2 Boundary conditions

Let $\Gamma(t)$ be the boundary of $\Omega_s(t)$ and $\mathbf{n}$ the unit outward normal vector to $\Omega_s(t)$. Boundary $\Gamma(t)$ is split into five disjoint parts

$$\Gamma(t) = \bar{\Gamma}_{sl}(t) \cup \bar{\Gamma}_C \cup \bar{\Gamma}_{sym}(t) \cup \bar{\Gamma}_n^1(t) \cup \bar{\Gamma}_n^2(t),$$

where:

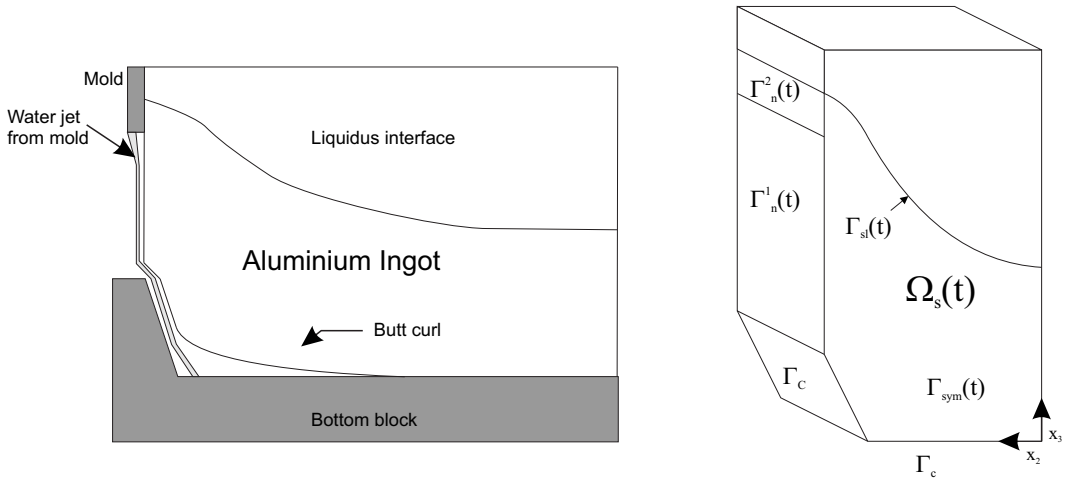

Figure 2.1: Computational domain $\Omega_s(t)$.

- The upper boundary $\Gamma_{sl}(t)$ is defined by the isotherm corresponding to the liquidus temperature T_l. This isotherm is the free boundary of the thermal problem and, therefore, it varies with time. $\Gamma_{sl}(t)$ is subjected to the metallostatic pressure exerted by the overlying liquid metal

$$\boldsymbol{\sigma}\mathbf{n} = p_r\mathbf{n},\ p_r(\mathbf{x},t) = \rho(T(\mathbf{x},t))g(x_3 - h(t)) \text{ on } \Gamma_{sl}(t),\ 0 < t \leq t_f,$$

  where ρ is the temperature-dependent mass density of the aluminium, g the gravitational acceleration and $h(t)$ the length of the slab at the instant t.

- Γ_C is the part of the slab susceptible to be in contact with the bottom block. This is assumed to be rigid, so aluminium cannot penetrate it, that is, the normal component of displacements, $u_n = \mathbf{u}\cdot\mathbf{n}$, cannot be positive:

$$u_n \leq 0 \text{ on } \Gamma_C \times (0, t_f].$$

  Moreover, due to the action-reaction principle, where an effective contact exists, $u_n = 0$, the bottom block exerts a pressure in the normal direction and upwards. So, the normal stress, $\sigma_n = \sigma_{ij}n_jn_i$, verifies $\sigma_n \leq 0$. Contrarily, where a contact does not exist, $u_n < 0$, the distance between the slab and the bottom block is not null and, consequently, the motion takes place freely, $\sigma_n = 0$. Therefore,

$$\sigma_n u_n = 0 \text{ on } \Gamma_C \times (0, t_f].$$

  Finally, taking into account that water is flowing down the slab sides, we assume that friction does not exist in the contact zone, that is, the tangential stress, $\boldsymbol{\sigma}_t = \boldsymbol{\sigma}\mathbf{n} - \sigma_n\mathbf{n}$, is null.

  Summing up, to reproduce the butt curl deformation, we consider a frictionless contact condition with the bottom block, known as Signorini unilateral frictionless contact condition

$$\boldsymbol{\sigma}_t = \mathbf{0},\ \sigma_n \leq 0,\ u_n \leq 0,\ \sigma_n u_n = 0 \text{ on } \Gamma_C \times (0, t_f].$$

  A detailed description of this contact condition can be found in [54].

- Boundary $\Gamma_n^1(t)$ denotes the part of the lateral outer faces which has already solidified; so, it is free of forces
$$\boldsymbol{\sigma}\mathbf{n} = \mathbf{0} \text{ on } \Gamma_n^1(t),\ 0 < t \leq t_f.$$

- The boundary $\Gamma_n^2(t)$ corresponds to the mushy region, which is confined by the mold; so,
$$\boldsymbol{\sigma}_t = \mathbf{0},\ u_n = 0 \text{ on } \Gamma_n^2(t),\ 0 < t \leq t_f.$$

- Finally, on $\Gamma_{sym}(t)$ we assume usual symmetry conditions:
$$\boldsymbol{\sigma}_t = \mathbf{0},\ u_n = 0 \text{ on } \Gamma_{sym}(t),\ 0 < t \leq t_f.$$

2.3 Equilibrium equations

Under the small strains assumption and in the quasistatic case, the slab behaviour is given by the equilibrium equations
$$-\mathrm{div}(\boldsymbol{\sigma}) = \mathbf{f} \text{ in } \Omega_s(t),$$
where $\mathbf{f}$ represents the volume forces due to the gravity, that is
$$\mathbf{f}(\mathbf{x}, t) = (0, 0, -\rho(T)g).$$

2.4 Behaviour law

Following the works of Drezet *et al.* [34], Mariaux *et al.* [59] and Barral *et al.* [9] where this type of deformations were studied, we assume that the aluminium is a nonlinear Maxwell-Norton thermo-elasto-viscoplastic solid; so, the strain rate tensor is the superposition of elastic, viscoplastic and thermal components:
$$\dot{\boldsymbol{\varepsilon}}(\mathbf{u}) = \dot{\boldsymbol{\varepsilon}}^e(\mathbf{u}) + \dot{\boldsymbol{\varepsilon}}^{vp}(\mathbf{u}) + \dot{\boldsymbol{\varepsilon}}^{th}(\mathbf{u}).$$
Here the strain tensor is related to the displacement field by the usual formula
$$\varepsilon_{ij}(\mathbf{u}) = \frac{1}{2}(\partial_j u_i + \partial_i u_j).$$
The elastic deformations $\boldsymbol{\varepsilon}^e$ are related to the stress tensor $\boldsymbol{\sigma}$ through Hooke's law with material parameters dependent on temperature
$$\boldsymbol{\varepsilon}^e(\mathbf{u}) = \Lambda_s(T)\boldsymbol{\sigma} = \frac{1+\nu(T)}{E(T)}\boldsymbol{\sigma} - \frac{\nu(T)}{E(T)}\mathrm{tr}(\boldsymbol{\sigma})\mathbf{I},$$
where E, ν denote the Young's modulus and Poisson's ratio, respectively, and $\mathbf{I}$ is the identity tensor. Reciprocally, the stress tensor $\boldsymbol{\sigma}$ can be written in terms of the strain tensor $\boldsymbol{\varepsilon}^e$,
$$\boldsymbol{\sigma} = (\Lambda_s(T))^{-1}\,\boldsymbol{\varepsilon}^e(\mathbf{u}) = \lambda(T)\mathrm{tr}(\boldsymbol{\varepsilon}^e(\mathbf{u}))\mathbf{I} + 2\mu(T)\boldsymbol{\varepsilon}^e(\mathbf{u}),$$

being λ and μ the Lamé coefficients related with E and ν with the usual expressions:

$$\lambda(T) = \frac{E(T)\nu(T)}{(1+\nu(T))(1-2\nu(T))},\ \mu(T) = \frac{E(T)}{2(1+\nu(T))}.$$

A detailed description of the elastic behaviour law can be found in [28, 52].

The thermal expansion is related to the temperature by a generalized Arrhenius law

$$\dot{\boldsymbol{\varepsilon}}^{th}(\mathbf{u}) = \alpha_s(T)\dot{T}\mathbf{I},$$

where α_s is the coefficient of thermal expansion, including volume changes due to possible phase transformations. A detailed description is found in [19, 59].

The viscoplastic part of the strain rate field, $\dot{\boldsymbol{\varepsilon}}^{vp}$, is governed by Norton-Hoff's law (see [42]). To describe this law, let us introduce the dissipation potential Φ_q defined on $\mathcal{S}_3$ by

$$\Phi_q(\boldsymbol{\tau}) = \frac{1}{q}\theta(T)|\boldsymbol{\tau}|^q,$$

$q \geq 2$ is a fixed real number and θ denotes a positive material parameter depending on temperature,

$$\theta(T) = \theta_0 \mathrm{e}^{\frac{-G}{R(T+273)}},$$

θ_0 being a material parameter, G the activation energy and R the universal gas constant.

Norton-Hoff's law may be written as (see [42])

$$\dot{\boldsymbol{\varepsilon}}^{vp}(\mathbf{u}) = \nabla\Phi_q(\boldsymbol{\sigma}^D) = \theta(T) \mid \boldsymbol{\sigma}^D \mid^{q-2} \boldsymbol{\sigma}^D,$$

where $\nabla\Phi_q$ denotes the gradient of Φ_q relative to the inner product on $\mathcal{S}_3$ and $\boldsymbol{\tau}^D$ denotes the deviatoric part of $\boldsymbol{\tau}$ given by

$$\boldsymbol{\tau}^D = \boldsymbol{\tau} - \frac{1}{3}\mathrm{tr}(\boldsymbol{\tau})\mathbf{I}.$$

Summing up, the constitutive law can be formulated as

$$\boldsymbol{\varepsilon}(\dot{\mathbf{u}})(t) = \dot{\widetilde{(\Lambda_s(T)\boldsymbol{\sigma})}}(t) + (\nabla\Phi_q(\boldsymbol{\sigma}^D))(t) + \left(\alpha_s(T)\dot{T}\right)(t)\mathbf{I} \text{ in } \Omega_s(t),\ 0 < t \leq t_f.$$

2.5 Initial conditions

In order to complete the mathematical model, we consider the following initial conditions:

$$\mathbf{u}(\mathbf{x},0) = \mathbf{u}_0(\mathbf{x}),\ \ \boldsymbol{\sigma}(\mathbf{x},0) = \boldsymbol{\sigma}_0(\mathbf{x}) \text{ in } \Omega_s(0),$$

where $\mathbf{u}_0$, $\boldsymbol{\sigma}_0$ verify suitable compatibility conditions detailed in Chapter 4.

2.6 Problem (P)

The problem we must solve is the following:

Problem (P):

Find the displacement field $\mathbf{u}(\mathbf{x},t)$ and the stress tensor field $\boldsymbol{\sigma}(\mathbf{x},t)$, at each point $\mathbf{x} \in \Omega_s(t)$ and at each instant $t \in (0, t_f]$ such that:

$$-\mathrm{div}(\boldsymbol{\sigma}) = \mathbf{f} \quad \text{in} \quad \Omega_s(t), \tag{2.1}$$

$$\boldsymbol{\sigma}\mathbf{n} = p_r\mathbf{n} \quad \text{on} \quad \Gamma_{sl}(t), \tag{2.2}$$

$$\boldsymbol{\sigma}\mathbf{n} = \mathbf{0} \quad \text{on} \quad \Gamma_n^1(t), \tag{2.3}$$

$$\boldsymbol{\sigma}_t = \mathbf{0},\ u_n = 0 \quad \text{on} \quad \Gamma_n^2(t) \cup \Gamma_{sym}(t), \tag{2.4}$$

$$\boldsymbol{\sigma}_t = \mathbf{0},\ \sigma_n \leq 0,\ u_n \leq 0,\ \sigma_n u_n = 0 \quad \text{on} \quad \Gamma_C, \tag{2.5}$$

$$\boldsymbol{\varepsilon}(\dot{\mathbf{u}}) = \dot{\widetilde{(\Lambda_s(T)\boldsymbol{\sigma})}} + \nabla\Phi_q(\boldsymbol{\sigma}^D) + \alpha_s(T)\dot{T}\mathbf{I} \quad \text{in} \quad \Omega_s(t), \tag{2.6}$$

$$\mathbf{u}(0) = \mathbf{u}_0,\ \ \boldsymbol{\sigma}(0) = \boldsymbol{\sigma}_0 \quad \text{in} \quad \Omega_s(0). \tag{2.7}$$

Chapter 3

State of the art

In this Chapter, we make a review of the most important results for the mathematical analysis and the numerical solution of Problem (P); many of these results can be found in the PhD Thesis [5].

In order to obtain a weak formulation of Problem (P), in Section 3.1, we introduce a suitable framework to treat the nonlinearities due to the behaviour law and the contact condition. Following the functional framework for Norton-Hoff's law studied by Geymotat and Suquet (see [45]), we present the functional subsets of admissible displacements and stresses.

In Section 3.2, we introduce the hypotheses on the temperature field, the applied forces and the initial conditions, needed to obtain a variational formulation of Problem (P).

In Section 3.3, we give a variational formulation of Problem (P) which involves an inequality due to the contact condition. A detailed description of variational formulations for different contact problems can be found in [54] for elastic materials, [27] for perfect plastic materials and [78] for some viscoplastic materials.

Section 3.4 is devoted to collect some results of existence of solution for Maxwell-Norton materials.

Finally, in Section 3.5, we recall the numerical algorithm proposed in the PhD Thesis [5]: First, we extend Problem (VP) to the entire slab using a fictitious domain method to implement the metallostatic pressure on the interphase. In order to solve numerically the variational formulation, we employ a finite element method to discretize the problem in space. In order to solve the nonlinearities due to the contact condition and the constitutive law, we use the Bermúdez-Moreno algorithm which involves two multipliers. In Section 3.6 we summarize the complete Bermúdez-Moreno algorithm to solve a casting problem, coupling the two nonlinearities due to the contact and the viscoplasticity.

3.1 Functional framework

From now on, we assume that at each instant $t \in (0, t_f]$, $\Omega_s(t)$ is an open, bounded, connected region in $\mathbb{R}^3$ with a Lipschitz boundary. Let us assume that the exponent of the viscoplastic law verifies $2 \leq q < +\infty$ and so its conjugate exponent p verifies $1 < p \leq 2$.

We consider the space of displacement fields as

$$\mathbf{V}^p(t) = \{\mathbf{v} \in [W^{1,p}(\Omega_s(t))]^3;\ \mathrm{div}(\mathbf{v}) \in L^2(\Omega_s(t))\},$$

which is a Banach space endowed with the norm

$$\|\mathbf{v}\|_{\mathbf{V}^p(t)} = \|\mathbf{v}\|_{[L^p(\Omega_s(t))]^3} + \|\boldsymbol{\varepsilon}^D(\mathbf{v})\|_{[L^p(\Omega_s(t))]^9} + \|\mathrm{div}(\mathbf{v})\|_{L^2(\Omega_s(t))}.$$

Let $\mathbf{U}^p(t)$ be the subspace of $\mathbf{V}^p(t)$ obtained when considering the confinement condition in the mushy region and the symmetry condition (see (2.4)):

$$\mathbf{U}^p(t) = \{\mathbf{v} \in \mathbf{V}^p(t); v_n = 0 \text{ on } \Gamma_n^2(t) \cup \Gamma_{sym}(t)\}.$$

The subset of kinematically admissible displacements at each instant t is

$$\mathbf{U}^p_{ad}(t) = \{\mathbf{v} \in \mathbf{U}^p(t);\ v_n \leq 0 \text{ on } \Gamma_C\}.$$

We define the space of stress fields

$$\mathbf{X}^q(t) = \{\boldsymbol{\tau} = (\tau_{ij});\ \tau_{ij} = \tau_{ji},\ \boldsymbol{\tau}^D \in [L^q(\Omega_s(t))]^9,\ \mathrm{tr}(\boldsymbol{\tau}) \in L^2(\Omega_s(t))\},$$

which is a Banach space endowed with the norm

$$\|\boldsymbol{\tau}\|_{\mathbf{X}^q(t)} = \|\boldsymbol{\tau}^D\|_{[L^q(\Omega_s(t))]^9} + \|\mathrm{tr}(\boldsymbol{\tau})\|_{L^2(\Omega_s(t))}.$$

We introduce the subspace of $\mathbf{X}^q(t)$

$$\mathbf{H}^q(t) = \{\boldsymbol{\tau} \in \mathbf{X}^q(t);\ \mathrm{div}(\boldsymbol{\tau}) \in [L^q(\Omega_s(t))]^3\},$$

which is also a Banach space endowed with the norm

$$\|\boldsymbol{\tau}\|_{\mathbf{H}^q(t)} = \|\boldsymbol{\tau}\|_{\mathbf{X}^q(t)} + \|\mathrm{div}(\boldsymbol{\tau})\|_{[L^q(\Omega_s(t))]^3}.$$

It can be proved that the space of distributions $[\mathcal{D}(\overline{\Omega}_s(t))]^9$ is dense in $\mathbf{H}^q(t)$ (see [45]). Moreover, the following properties are verified:

Lemma 3.1.1. *The application*

$$\boldsymbol{\tau} \in \mathbf{H}^q(t) \to \boldsymbol{\tau}\mathbf{n} \in [W^{-\frac{1}{q},q}(\Gamma(t))]^3,$$

is linear and continuous. Moreover, the following Green's formula is verified:

$$\int_{\Omega_s(t)} \boldsymbol{\tau} : \boldsymbol{\varepsilon}(\mathbf{v}) dx + \int_{\Omega_s(t)} \mathrm{div}(\boldsymbol{\tau}) \cdot \mathbf{v} dx = \langle \boldsymbol{\tau}\mathbf{n}, \mathbf{v} \rangle_{\Gamma(t)},\ \forall \boldsymbol{\tau} \in \mathbf{H}^q(t),\ \forall \mathbf{v} \in \mathbf{V}^p(t),$$

where $\langle \cdot, \cdot \rangle_{\Gamma(t)}$ denotes the duality product between $[W^{-\frac{1}{q},q}(\Gamma(t))]^3$ and $[W^{1-\frac{1}{p},p}(\Gamma(t))]^3$.

The subset of kinematically admissible stresses at each instant t is

$$\mathbf{H}^q_{ad}(t) = \big\{\boldsymbol{\tau} \in \mathbf{H}^q(t); -\mathrm{div}(\boldsymbol{\tau}) = \mathbf{f}(t) \text{ in } \Omega_s(t),\ \boldsymbol{\tau}\mathbf{n} = \mathbf{0} \text{ on } \Gamma_n^1(t),\ \boldsymbol{\tau}\mathbf{n} = p_r(t)\mathbf{n} \text{ on } \Gamma_{sl}(t),$$
$$\boldsymbol{\tau}_t = \mathbf{0} \text{ on } \Gamma_C \cup \Gamma_{sym}(t) \cup \Gamma_n^2(t),\ \tau_n \leq 0 \text{ on } \Gamma_C\big\}.$$

Boundary conditions

Given $t \in (0, t_f]$, consider $\hat{\Gamma}(t) \subset \Gamma(t)$, with $\hat{\Gamma}(t) \cap \Gamma_C = \emptyset$ and $\text{meas}(\hat{\Gamma}(t)) > 0$, and $\hat{\mathbf{h}} \in [L^q(\hat{\Gamma}(t))]^3$.

Definition 3.1.2. *Let $\boldsymbol{\tau} \in \mathbf{H}^q(t)$. Then $\boldsymbol{\tau}\mathbf{n} = \hat{\mathbf{h}}$ on $\hat{\Gamma}(t)$ if*

$$\langle \boldsymbol{\tau}\mathbf{n}, \mathbf{v} \rangle_{\Gamma(t)} = \int_{\hat{\Gamma}(t)} \hat{\mathbf{h}} \cdot \mathbf{v} d\Gamma,$$

for all $\mathbf{v} \in [W^{1-\frac{1}{p},p}(\Gamma(t))]^3$ such that $\mathbf{v} = \mathbf{0}$ on $\Gamma(t) \setminus \hat{\Gamma}(t)$.

Definition 3.1.3. *Let $\boldsymbol{\tau} \in \mathbf{H}^q(t)$ be such that $\boldsymbol{\tau}\mathbf{n} = \hat{\mathbf{h}}$ on $\hat{\Gamma}(t)$. Then $\boldsymbol{\tau}_t = \mathbf{0}$ on Γ_C if*

$$\langle \boldsymbol{\tau}\mathbf{n}, \mathbf{v} \rangle_{\Gamma(t)} = \int_{\hat{\Gamma}} \hat{\mathbf{h}} \cdot \mathbf{v} d\Gamma,$$

for all $\mathbf{v} \in [W^{1-\frac{1}{p},p}(\Gamma(t))]^3$ such that $\mathbf{v} = \mathbf{0}$ on $\Gamma(t) \setminus (\Gamma_C \cup \hat{\Gamma}(t))$ and $v_n = 0$ on Γ_C.

Definition 3.1.4. *Let $\boldsymbol{\tau} \in \mathbf{H}^q(t)$ be such that $\boldsymbol{\tau}\mathbf{n} = \hat{\mathbf{h}}$ on $\hat{\Gamma}(t)$ and $\boldsymbol{\tau}_t = \mathbf{0}$ on Γ_C. Then $\tau_n \leq 0$ on Γ_C if*

$$\langle \boldsymbol{\tau}\mathbf{n}, \mathbf{v} \rangle_{\Gamma(t)} \geq \int_{\hat{\Gamma}} \hat{\mathbf{h}} \cdot \mathbf{v} d\Gamma,$$

for all $\mathbf{v} \in [W^{1-\frac{1}{p},p}(\Gamma(t))]^3$ such that $\mathbf{v} = \mathbf{0}$ on $\Gamma(t) \setminus (\Gamma_C \cup \hat{\Gamma})$ and $v_n \leq 0$ on Γ_C.

3.2 Assumptions on the data of Problem (P)

From now on, we assume that the following hypotheses are satisfied:

(H1) The temperature field $T \in W^{1,\infty}(0, t_f; L^\infty(\Omega_s(t)))$.

(H2) The metallostatic pressure $p_r \in W^{1,\infty}(0, t_f; W^{-\frac{1}{q},q}(\Gamma(t)) \cap L^q(\Gamma_{sl}(t)))$, the volume forces $\mathbf{f} \in W^{1,\infty}(0, t_f; [L^q(\Omega_s(t))]^3)$ and the density is such that $\rho(s) \geq \rho_0 > 0$, $\forall s \in \mathbb{R}$.

(H3) The elasticity tensor $\Lambda_s \in [W^{1,\infty}(\mathbb{R})]^{81}$ is symmetric and:

$$\exists\, \beta > 0;\ \Lambda_s \boldsymbol{\tau} : \boldsymbol{\tau} \geq \beta |\boldsymbol{\tau}|^2,\ \forall \boldsymbol{\tau} \in \mathcal{S}_3,\ \text{a.e. in } \mathbb{R}.$$

(H4) The coefficient of thermal expansion $\alpha_s \in L^\infty(\mathbb{R})$ and the coefficient of the viscoplastic law $\theta \in L^\infty(\mathbb{R})$.

(H5) $\boldsymbol{\sigma}_0 \in \mathbf{H}^q_{ad}(0)$, $\mathbf{u}_0 \in \mathbf{U}^p_{ad}(0)$ and verify the natural compatibility conditions which are described in Chapter 4.

3.3 Variational inequality. Problem (VP)

Proposition 3.3.1. *Under assumptions* $(\mathbf{H1})-(\mathbf{H5})$*, if* $\boldsymbol{\tau}\in\mathbf{H}^q(t)$ *and* $\mathbf{u}(t)\in\mathbf{U}^p_{ad}(t)$ *verify*

$$\int_{\Omega_s(t)}\boldsymbol{\tau}:\boldsymbol{\varepsilon}(\mathbf{v}-\mathbf{u}(t))dx\geq\int_{\Omega_s(t)}\mathbf{f}\cdot(\mathbf{v}-\mathbf{u}(t))dx+\int_{\Gamma_{sl}(t)}p_r(t)\mathbf{n}\cdot(\mathbf{v}-\mathbf{u}(t))d\Gamma,\ \forall\mathbf{v}\in\mathbf{U}^p_{ad}(t),$$

then $\boldsymbol{\tau}\in\mathbf{H}^q_{ad}(t)$.

Proof. It is easy to prove from Green's formula in Lemma 3.1.1 and taking into account boundary conditions introduced in Definitions 3.1.2-3.1.4. □

Therefore, the variational formulation of Problem (P) we consider is:

Problem (VP):

Find $\mathbf{u}\in W^{1,\infty}(0,t_f;\mathbf{U}^p_{ad}(t))$ and $\boldsymbol{\sigma}\in W^{1,\infty}(0,t_f;\mathbf{H}^q(t))$ such that *a.e.* $t\in(0,t_f]$

$$\int_{\Omega_s(t)}\boldsymbol{\sigma}(t):\boldsymbol{\varepsilon}(\mathbf{v}-\mathbf{u}(t))\,dx\geq\int_{\Omega_s(t)}\mathbf{f}(t)\cdot(\mathbf{v}-\mathbf{u}(t))\,dx+\int_{\Gamma_{sl}(t)}p_r(t)\mathbf{n}\cdot(\mathbf{v}-\mathbf{u}(t))\,d\Gamma,\quad\forall\mathbf{v}\in\mathbf{U}^p_{ad}(t),\tag{3.1}$$

$$\boldsymbol{\varepsilon}(\dot{\mathbf{u}})(t)=\dot{\widetilde{(\Lambda_s(T)\boldsymbol{\sigma})}}(t)+(\nabla\Phi_q(\boldsymbol{\sigma}^D))(t)+\left(\alpha_s(T)\dot{T}\right)(t)\mathbf{I},\ \text{in }\Omega_s(t),\tag{3.2}$$

$$\mathbf{u}(0)=\mathbf{u}_0,\ \ \boldsymbol{\sigma}(0)=\boldsymbol{\sigma}_0,\ \text{in }\Omega_s(0).\tag{3.3}$$

Proposition 3.3.2. *If* $(\mathbf{u}(t),\boldsymbol{\sigma}(t))$ *is a smooth solution of Problem* (VP) *at the instant* t*, then* $(\mathbf{u}(t),\boldsymbol{\sigma}(t))$ *is a solution of Problem* (P)*. The reciprocal is also true.*

Proofs of Propositions 3.3.1 and 3.3.2 can be found in the PhD Thesis [5].

3.4 Existence of solution

In [56] the existence of solution for Maxwell-Norton problems with classic boundary conditions of type Dirichlet-Neumann is given. Later, in [24] the previous result is generalized for a Maxwell-Norton law depending on time. Nevertheless, these results are not applicable to Problem (P) since they use variational formulations in velocities, which are not valid to solve Signorini contact conditions.

In [13] it is proved a result of existence of solution for an analogous problem to that presented here, over a domain independent of time and without considering the thermal effects. In this result, the authoresses based their proof in that given in [32] for a Maxwell-Norton quasi-static problem with mixed boundary conditions.

3.4.1 Elasto-viscoplastic problem of Maxwell-Norton type with contact conditions

Let Ω be a bounded, open, connected region of $\mathbb{R}^3$ such that $\Omega \in \mathcal{C}^{1,1}$. Moreover, its boundary is partitioned into three non-empty, open and disjointed parts Γ_D, Γ_N and Γ_C satisfying

$$\Gamma = \partial\Omega = \bar{\Gamma}_D \cup \bar{\Gamma}_N \cup \bar{\Gamma}_C,$$

with $\text{meas}(\Gamma_D) > 0$.

Problem $(\tilde{P})$:

Find the displacement field $\mathbf{u}$ and the stress tensor $\boldsymbol{\sigma}$ verifying

$$\begin{aligned}
-\text{div}(\boldsymbol{\sigma}) &= \mathbf{f}, \text{ in } (0,t_f]\times\Omega,\\
\boldsymbol{\varepsilon}(\dot{\mathbf{u}}) &= \Lambda_s\dot{\boldsymbol{\sigma}} + \nabla\Phi_q(\boldsymbol{\sigma}^D), \text{ in } (0,t_f]\times\Omega,\\
\mathbf{u} &= \mathbf{0}, \text{ on } (0,t_f]\times\Gamma_D,\\
\boldsymbol{\sigma}\mathbf{n} &= \mathbf{h}, \text{ on } (0,t_f]\times\Gamma_N,\\
u_n \le 0, \sigma_n \le 0, \boldsymbol{\sigma}_t &= \mathbf{0}, \sigma_n u_n = 0, \text{ on } (0,t_f]\times\Gamma_C,\\
\mathbf{u}(0) = \mathbf{u}_0,\ \boldsymbol{\sigma}(0) &= \boldsymbol{\sigma}_0, \text{ in } \Omega.
\end{aligned}$$

Assumptions

($\widetilde{\mathbf{H1}}$) The elasticity tensor Λ_s is independent of time, symmetric and $\Lambda_s \in [L^\infty(\Omega)]^{81}$. Furthermore,

$$\exists\ \beta > 0;\ \Lambda_s\boldsymbol{\tau} : \boldsymbol{\tau} \ge \beta|\boldsymbol{\tau}|^2,\ \forall\boldsymbol{\tau} \in \mathcal{S}_3,\ \text{a.e. in } \mathbb{R}.$$

($\widetilde{\mathbf{H2}}$) The applied forces satisfy

$$\begin{aligned}
\mathbf{f} &\in W^{2,\infty}(0,t_f;[L^q(\Omega)]^3)\\
\mathbf{h} &\in W^{2,\infty}(0,t_f;[W^{-\frac{1}{q},q}(\Gamma)]^3 \cap [L^q(\Gamma_N)]^3).
\end{aligned}$$

($\widetilde{\mathbf{H3}}$) The initial stress field $\boldsymbol{\sigma}_0$ and the corresponding initial displacement verify

$$\begin{aligned}
-\text{div}(\boldsymbol{\sigma}_0) &= \mathbf{f}(0) \text{ in } \Omega,\\
\boldsymbol{\sigma}_0\mathbf{n} &= \mathbf{h}(0) \text{ on } \Gamma_N,\\
\mathbf{u}_0 &= \mathbf{0} \text{ on } \Gamma_D,\\
u_{0n} \le 0, \sigma_{0n} \le 0, \boldsymbol{\sigma}_{0t} &= \mathbf{0}, \sigma_{0n}u_{0n} = 0 \text{ on } \Gamma_C.
\end{aligned}$$

($\widetilde{\mathbf{H4}}$) The exponent q verifies $2 \le q < 6$, and therefore $6/5 < p \le 2$.

Theorem 3.4.1. *Under the above assumptions* ($\widetilde{\mathbf{H1}}$) – ($\widetilde{\mathbf{H4}}$), *there exists a solution* $(\mathbf{u},\boldsymbol{\sigma}) \in W^{1,2}(0,t_f;\tilde{\mathbf{U}}^p_{ad}) \times \left(W^{1,2}(0,t_f;\mathbf{X}^2) \cap L^\infty(0,t_f;\mathbf{X}^q)\right)$ *of Problem* $(\tilde{P})$, *where*

$$\tilde{\mathbf{U}}^p_{ad} = \{\mathbf{v} \in \mathbf{V}^p;\ \mathbf{v} = \mathbf{0} \text{ on } \Gamma_D,\ v_n \le 0 \text{ on } \Gamma_C\}.$$

3.4.2 Thermo-elasto-viscoplastic problem of Maxwell-Norton type

In [8] it was proved the existence and uniqueness of solution for a quasistatic thermo-elasto-viscoplastic problem of Maxwell-Norton type with coefficients depending on temperature when it is verified that $\dot{T} \geq 0$. In this case, contact conditions were not considered.

Let Ω be a bounded, open, connected region of $\mathbb{R}^3$ with a Lipschitz boundary. Moreover, its boundary is partitioned into two non-empty, open and disjointed parts Γ_D and Γ_N satisfying

$$\Gamma = \partial\Omega = \bar{\Gamma}_D \cup \bar{\Gamma}_N,$$

with $\text{meas}(\Gamma_D) > 0$.

Problem $(\hat{P})$:

Given the temperature field T, find the displacement field $\mathbf{u}$ and the stress tensor $\boldsymbol{\sigma}$ verifying

$$\begin{aligned}
-\text{div}(\boldsymbol{\sigma}) &= \mathbf{f}, \text{ in } (0,t_f] \times \Omega, \\
\boldsymbol{\varepsilon}(\dot{\mathbf{u}}) = \dot{\widetilde{(\Lambda_s(T)\boldsymbol{\sigma})}} + \nabla\Phi_q(\boldsymbol{\sigma}^D) + \alpha_s(T)\dot{T}\mathbf{I}&, \text{ in } (0,t_f] \times \Omega, \\
\mathbf{u} &= \mathbf{u}_d, \text{ on } (0,t_f] \times \Gamma_D, \\
\boldsymbol{\sigma}\mathbf{n} &= \mathbf{h}, \text{ on } (0,t_f] \times \Gamma_N, \\
\mathbf{u}(0) = \mathbf{u}_0,\ \boldsymbol{\sigma}(0) &= \boldsymbol{\sigma}_0, \text{ in } \Omega,
\end{aligned}$$

Assumptions

($\widehat{\mathbf{H1}}$) The temperature field $T \in W^{2,\infty}(0,t_f;L^\infty(\Omega))$. Moreover it is positive and $\dot{T} \geq 0$ *a.e.* in Ω, $\forall t \in [0,t_f]$.

($\widehat{\mathbf{H2}}$) The applied forces satisfy

$$\mathbf{f} \in W^{2,\infty}(0,t_f;[L^q(\Omega)]^3)$$

$$\mathbf{h} \in W^{2,\infty}(0,t_f;[W^{-\frac{1}{q},q}(\Gamma)]^3 \cap [L^q(\Gamma_N)]^3).$$

($\widehat{\mathbf{H3}}$) The elasticity tensor Λ_s is symmetric and the following hold true:

- $\Lambda_s \in [W^{2,\infty}(\mathbb{R})]^{81}$, therefore, there exists $\beta_1 > 0$ such that $|\Lambda_s(r)\boldsymbol{\tau}| \leq \beta_1|\boldsymbol{\tau}|$ and there exists $\beta_2 > 0$ such that $|\Lambda_s'(r)\boldsymbol{\tau}| \leq \beta_2|\boldsymbol{\tau}|$, $\forall\boldsymbol{\tau} \in \mathcal{S}_3$, $\forall r \in \mathbb{R}$.
- There exists $\beta > 0$ such that $\Lambda_s(r)\boldsymbol{\tau} : \boldsymbol{\tau} \geq \beta|\boldsymbol{\tau}|^2$, $\forall\boldsymbol{\tau} \in \mathcal{S}_3, \forall r \in \mathbb{R}$.
- $\Lambda_s'(r)\boldsymbol{\tau} : \boldsymbol{\tau} \geq 0$, $\forall\boldsymbol{\tau} \in \mathcal{S}_3, \forall r \in \mathbb{R}$.

($\widehat{\mathbf{H4}}$)The coefficient of thermal expansion $\alpha_s \in W^{1,\infty}(\mathbb{R})$.

($\widehat{\mathbf{H5}}$) The coefficient of the viscoplastic law $\theta \in L^\infty(\mathbb{R})$ and $\theta(r) \geq \theta_c > 0$, $\forall r \in \mathbb{R}$.

($\widehat{\mathbf{H6}}$) The initial stress field $\boldsymbol{\sigma}_0 \in \mathbf{H}^q$ and the initial displacement $\mathbf{u}_0 \in \mathbf{V}^p$ verify

$$\begin{aligned} -\mathrm{div}(\boldsymbol{\sigma}_0) &= \mathbf{f}(0) \text{ in } \Omega, \\ \boldsymbol{\sigma}_0\mathbf{n} &= \mathbf{h}(0) \text{ on } \Gamma_N, \\ \mathbf{u}_0 &= \mathbf{u}_d(0) \text{ on } \Gamma_D, \\ \varepsilon(\mathbf{u}_0) &= \Lambda_s(T_0)\boldsymbol{\sigma}_0 \text{ in } \Omega. \end{aligned}$$

($\widehat{\mathbf{H7}}$)The boundary Dirichlet condition satisfies $\mathbf{u}_d \in W^{2,\infty}(0, t_f; [W^{1-(1/p),p}(\Gamma)]^3)$.

($\widehat{\mathbf{H8}}$) The exponent q verifies $q \geq 2$, and its conjugate p is such that $1 < p \leq 2$.

Theorem 3.4.2. *Under the above assumptions* ($\widehat{\mathbf{H1}}$)$-$($\widehat{\mathbf{H8}}$) *there exists a unique solution* $(\mathbf{u}, \boldsymbol{\sigma}) \in W^{1,2}(0, t_f; \mathbf{V}^p) \times \left(W^{1,2}(0, t_f; \mathbf{X}^2) \cap L^\infty(0, t_f; \mathbf{X}^q)\right)$ *of Problem* $(\hat{P})$.

3.5 Former numerical solution

In this section we are going to review the numerical resolution of Problem (VP) defined by (3.1)-(3.3), given in [5]. The main difficulties to overcome in the numerical solution of this problem were the following:

- The solidified part of the slab, which is the computational domain of the mechanical simulation, changes with time. Furthermore, on the upper boundary, which is the isotherm of the liquidus temperature and, therefore, the free boundary of the thermal problem, we must impose the metallostatic pressure due to the liquid metal. To deal with this difficulty, a fictitious domain method is considered.
- To model the butt curl, we must solve a contact condition between the slab and the bottom block. To deal with this nonlinear condition, the Bermúdez-Moreno algorithm, based on maximal monotone operator techniques, was considered.
- The aluminium behaviour is nonlinear and depends strongly on the temperature field. In order to avoid the nonlinearity of the constitutive law, again the Bermúdez-Moreno method was used.
- The computational domain grows with time and the zone with steep gradients changes. To overcome this difficulty, the meshes were constructed in a way adapted to the problem's geometry.

3.5.1 Imposing the metallostatic pressure

In the mechanical simulation of an aluminium casting, the computational domain is the solidified part of the slab. So, its upper boundary coincides with the isotherm corresponding to the liquidus temperature, denoted by $\Gamma_{sl}(t)$, which is the free boundary of the thermal problem. On this boundary, it is necessary to impose the metallostatic pressure exerted by the weight of the liquid

metal. In order to implement numerically this condition, we are going to use the fictitious domain method introduced in [11]. It consists of solving the problem over the entire slab, assuming that the liquid metal is a very elastic material under the action of the gravity forces; so, the liquid metal does not offer resistance to solid deformations. This methodology has the advantage that remeshing is not needed at each time instant to adjust the free boundary, and so the numerical implementation is easier.

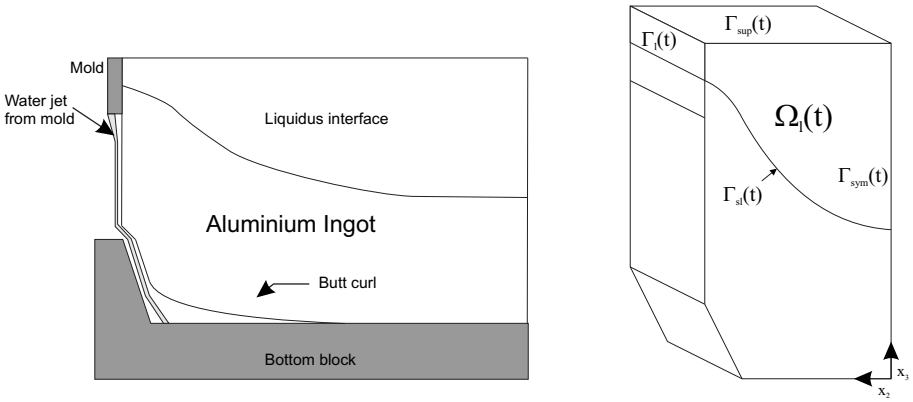

Figure 3.1: Fictitious domain $\Omega_l(t)$.

Let $\Omega_l(t)$ be the liquid zone of the slab at the instant t,

$$\Omega_l(t) = \{\mathbf{x} \in \Omega(t); T(\mathbf{x}, t) > T_l\}.$$

The boundary of $\Omega_l(t)$ is split into four disjoint parts:

$$\partial\Omega_l(t) = \bar{\Gamma}_{sup}(t) \cup \bar{\Gamma}_{sym}(t) \cup \bar{\Gamma}_l(t) \cup \bar{\Gamma}_{sl}(t),$$

where $\Gamma_{sup}(t)$ denotes the upper boundary, $\Gamma_{sym}(t)$ the symmetry boundary and $\Gamma_l(t)$ the outer lateral boundary (see Figure 3.1).

In the liquid domain, $\Omega_l(t)$, the applied forces are the following:

- To impose the weight of the liquid aluminium, we consider volume forces due to gravity, with constant density $\rho_l = \rho(T_l)$.
- Since the liquid must not offer resistance to solid deformations we consider that the surface forces on the upper boundary, $\Gamma_{sup}(t)$, are null.
- On the outer lateral boundary, $\Gamma_l(t)$, the aluminium is confined by the mold.

In order to impose that the liquid metal is a very elastic material, we consider that the behaviour law in the liquid domain is given by the Hooke's law depending on a small parameter ϵ,

$$\boldsymbol{\sigma}^\epsilon(\mathbf{u}^\epsilon) = \Lambda_l^{-1}\boldsymbol{\varepsilon}(\mathbf{u}^\epsilon) = \lambda_l^\epsilon \mathrm{div}(\mathbf{u}^\epsilon)\mathbf{I} + 2\mu_l^\epsilon \boldsymbol{\varepsilon}(\mathbf{u}^\epsilon),$$

where the Lamé coefficients of the liquid domain, $\lambda_l^\epsilon, \mu_l^\epsilon$, change with different length scale:

$$\lambda_l^\epsilon = \epsilon^\beta \overline{\lambda},\ \mu_l^\epsilon = \epsilon^\alpha \overline{\mu},$$

with $\overline{\lambda}$, $\overline{\mu}$, α and β real positive numbers independent of ϵ. Assuming that $\alpha > \beta$, this has the effect of applying the metallostatic pressure to the solidification front, as it was proved in [12] by using asymptotic expansion techniques. In order to simplify the notation, from now on, we omit the index ϵ in the behaviour law.

With this technique, the variational inequality (3.1) can be extended to the complete slab and the integral over the thermal free boundary $\Gamma_{sl}(t)$ disappears. Therefore, from now on, we will consider this new extended weak formulation over the entire slab $\Omega(t) = \text{int}(\Omega_s(t) \cup \Omega_l(t) \cup \Gamma_{sl}(t))$:

Problem (EVP)

Find $\mathbf{u} \in W^{1,\infty}(0, t_f; \mathbf{U}^p_{ad}(t))$ and $\boldsymbol{\sigma} \in W^{1,\infty}(0, t_f; \mathbf{H}^q(t))$ verifying *a.e.* in $(0, t_f]$:

$$\int_{\Omega(t)} \boldsymbol{\sigma}(t) : \boldsymbol{\varepsilon}(\mathbf{v} - \mathbf{u}(t))\, dx \geq \int_{\Omega(t)} \mathbf{f}(t) \cdot (\mathbf{v} - \mathbf{u}(t))\, dx, \forall \mathbf{v} \in \mathbf{U}^p_{ad}(t), \tag{3.4}$$

$$\boldsymbol{\varepsilon}(\dot{\mathbf{u}})(t) = \begin{cases} \dot{\widetilde{(\Lambda_s(T)\boldsymbol{\sigma})}}(t) + (\nabla \Phi_q(\boldsymbol{\sigma}^D))(t) + \left(\alpha_s(T)\dot{T}\right)(t)\mathbf{I} & \text{in } \Omega_s(t), \\ \dot{\widetilde{(\Lambda_l \boldsymbol{\sigma})}}(t) & \text{in } \Omega_l(t), \end{cases} \tag{3.5}$$

$$\mathbf{u}(0) = \mathbf{u}_0, \;\; \boldsymbol{\sigma}(0) = \boldsymbol{\sigma}_0, \text{ in } \Omega(0). \tag{3.6}$$

Remark 3.5.1. *Notice that the functional spaces are extended to the complete slab in the natural way.*

The initial data, $\mathbf{u}_0$ and $\boldsymbol{\sigma}_0$, should be extended to all $\Omega(0)$, ensuring that the following compatibility conditions are satisfied:

$$\begin{aligned} -\text{div}(\boldsymbol{\sigma}_0) = \mathbf{f}(0) \text{ in } \Omega(0), \\ \boldsymbol{\sigma}_0 \mathbf{n} = \mathbf{0} \text{ on } \Gamma_{sup}(0) \cup \Gamma^1_n(0), \\ \boldsymbol{\sigma}_{0t} = \mathbf{0}, \; u_{0n} = 0 \text{ on } \Gamma_{sym}(0) \cup \Gamma^2_n(0) \cup \Gamma_l(0), \\ \boldsymbol{\sigma}_{0t} = \mathbf{0}, \; \sigma_{0n} \leq 0, \; u_{0n} \leq 0, \; \sigma_{0n} u_{0n} = 0 \text{ on } \Gamma_C, \end{aligned}$$

$$\boldsymbol{\varepsilon}(\mathbf{u}_0) = \begin{cases} \Lambda_s(T_0)\boldsymbol{\sigma}_0 & \text{in } \Omega_s(0), \\ \Lambda_l \boldsymbol{\sigma}_0 & \text{in } \Omega_l(0). \end{cases}$$

Remark 3.5.2. *In casting processes the temperature at $t = 0$, T_0, corresponds with the liquidus temperature T_l.*

3.5.2 Discretization in space

Finite element approximation to simulate the model is considered in the usual way. Displacements are discretized in space using the Lagrange tetrahedral finite element method of degree one. Stresses are assumed constant within each element. Let $\mathcal{T}_h(t)$ be a tetrahedral mesh on the computational domain $\bar{\Omega}(t)$ compatible with the boundary partition. As usual, h denotes the maximum diameter of $\mathcal{T}_h(t)$ and

$$\Sigma_h(t) = \{b_i\}_{1 \leq i \leq N_h(t)},$$

the nodes set of the tetrahedral mesh. Moreover, $\mathcal{S}_h$ and $\mathcal{Z}_h(t)$ are the triangulations induced on the contact boundary Γ_C and the boundaries $\Gamma_n^2(t) \cup \Gamma_l(t)$, respectively.

We construct a family of finite dimensional subspaces $\mathbf{V}_h(t)$ of $\mathbf{V}^p(t)$ by approximating the test functions $\mathbf{v}$ by piecewise polynomials of degree one over the tetrahedral mesh $\mathcal{T}_h(t)$ on the computational domain $\bar{\Omega}(t)$:

$$\mathbf{V}_h(t) = \{\mathbf{v}_h \in [\mathcal{C}^0(\Omega(t))]^3; \mathbf{v}_h|_K \in [P_1(K)]^3, \forall K \in \mathcal{T}_h(t)\},$$
$$\mathbf{U}_h(t) = \{\mathbf{v}_h \in \mathbf{V}_h(t); (v_h)_\alpha = 0 \text{ on } [x_\alpha = 0],\ \mathbf{v}_{h|C} \cdot \mathbf{n}_{|C} = 0, \forall C \in \mathcal{Z}_h(t)\},$$

where $P_i(K)$ denotes the space of polynomials of degree i defined on K and $\mathbf{v}_{h|C}$ (resp. $\mathbf{n}_{|C}$) denotes the value of $\mathbf{v}_h$ (resp. $\mathbf{n}$) on the barycenter of C. Therefore, the discrete space of admissible displacements is

$$\mathbf{U}_{ad_h}(t) = \{\mathbf{v}_h \in \mathbf{U}_h(t); \mathbf{v}_{h|C} \cdot \mathbf{n}_{|C} \leq 0, \forall C \in \mathcal{S}_h\}.$$

Stresses are assumed constant within each element. We denote by $\mathbf{X}_h(t)$ the discretized space of stresses

$$\mathbf{X}_h(t) = \{\boldsymbol{\xi}_h; (\xi_h)_{ij} = (\xi_h)_{ji}, \boldsymbol{\xi}_h|_K \in [P_0(K)]^9, \forall K \in \mathcal{T}_h(t)\}.$$

In this space, we consider the norm induced by $\mathbf{L}^2$.

Functions $\mathbf{v}_h \in \mathbf{V}_h(t)$ are characterized for their values in the vertices of the elements,

$$\mathbf{v}_h(x) = \sum_{i=1}^{N_h(t)} \mathbf{v}_h(b_i)\phi_i(x),$$

where $\{\phi_i\}_{i=1,\ldots,N_h(t)}$ are the corresponding shape functions. Elements $\boldsymbol{\xi}_h \in \mathbf{X}_h(t)$ are characterized for their value in the barycenter of each element,

$$\boldsymbol{\xi}_h(x) = \sum_{K \in \mathcal{T}_h(t)} \boldsymbol{\xi}_h|_K \mathcal{X}_K(x),$$

where $\mathcal{X}_K$ denotes the characteristic function of the element K. Moreover, T_h denotes the discretized temperature field, which is considered constant by element.

Finally, at each time instant t we consider the operator

$$\begin{array}{rccl} \boldsymbol{\varepsilon}_h : & \mathbf{V}_h(t) & \longrightarrow & \mathbf{X}_h(t) \\ & \mathbf{v}_h & \longrightarrow & \boldsymbol{\varepsilon}_h(\mathbf{v}_h) = \displaystyle\sum_{K \in \mathcal{T}_h(t)} \boldsymbol{\varepsilon}(\mathbf{v}_h|_K)\mathcal{X}_K, \end{array}$$

and we denote by $\boldsymbol{\varepsilon}_h^*$ its adjoint operator.

With this notation, the discretized variational formulation corresponding to Problem (EVP) is the following:

Problem (DVP):

Find $\mathbf{u}_h \in W^{1,\infty}(0,t_f;\mathbf{U}_{ad_h}(t))$ and $\boldsymbol{\sigma} \in W^{1,\infty}(0,t_f;\mathbf{X}_h(t))$ verifying *a.e.* in $(0,t_f)$:

$$\int_{\Omega(t)} \boldsymbol{\sigma}_h(t) : \boldsymbol{\varepsilon}_h(\mathbf{v}_h - \mathbf{u}_h(t))\,dx \geq \int_{\Omega(t)} \mathbf{f}(t)\cdot(\mathbf{v}_h - \mathbf{u}_h(t))\,dx, \forall \mathbf{v}_h \in \mathbf{U}_{ad_h}(t), \tag{3.7}$$

$$\boldsymbol{\varepsilon}_h(\dot{\mathbf{u}}_h)(t) = \begin{cases} \dot{\overbrace{(\Lambda_s(T_h)\boldsymbol{\sigma}_h)}}(t) + (\nabla\Phi_q(\boldsymbol{\sigma}_h^D))(t) + \left(\alpha_s(T_h)\dot{T}_h\right)(t)\mathbf{I} & \text{in } \Omega_s(t), \\ \dot{\overbrace{(\Lambda_l\boldsymbol{\sigma}_h)}}(t) & \text{in } \Omega_l(t), \end{cases} \tag{3.8}$$

$$\mathbf{u}_h(0) = \mathbf{u}_0, \;\; \boldsymbol{\sigma}_h(0) = \boldsymbol{\sigma}_0, \text{ in } \Omega(0). \tag{3.9}$$

To simplify the notation, from now on we omit the index h to denote the elements of the discretized spaces.

3.5.3 Bermúdez-Moreno algorithm for the numerical solution of the contact problem

Both the contact condition and the viscoplastic behaviour, generate nonlinearities. A simple way to transform these nonlinearities is to use the well-known Bermúdez-Moreno lemma (see [16]). This lemma is the main idea of the algorithm developed in [9] and that we introduce in the following.

In order to introduce an algorithm to deal with the nonlinearity due to the contact condition, we focus on solving a simplified problem, corresponding to Problem (DVP) suppressing the viscoplastic part in the constitutive law. Therefore, the discretized variational problem remains:

$$\int_{\Omega(t)} \boldsymbol{\sigma}(t) : \boldsymbol{\varepsilon}(\mathbf{v} - \mathbf{u}(t))\,dx \geq \int_{\Omega(t)} \mathbf{f}(t)\cdot(\mathbf{v} - \mathbf{u}(t))\,dx, \forall \mathbf{v} \in \mathbf{U}_{ad_h}(t), \tag{3.10}$$

$$\boldsymbol{\varepsilon}(\mathbf{u})(t) = \begin{cases} (\Lambda_s(T)\boldsymbol{\sigma})(t) + \left(\displaystyle\int_{T_l}^{T} \alpha_s(r)dr\right)\mathbf{I} & \text{in } \Omega_s(t), \\ (\Lambda_l\boldsymbol{\sigma})(t) & \text{in } \Omega_l(t), \end{cases} \tag{3.11}$$

$$\mathbf{u}(0) = \mathbf{u}_0, \;\; \boldsymbol{\sigma}(0) = \boldsymbol{\sigma}_0, \text{ in } \Omega(0). \tag{3.12}$$

Remark 3.5.3. *If we remove the viscoplastic behaviour from the constitutive equation (3.8), we have*

$$\boldsymbol{\varepsilon}(\dot{\mathbf{u}}) = \begin{cases} \dot{\overbrace{(\Lambda_s(T)\boldsymbol{\sigma})}} + \left(\alpha_s(T)\dot{T}\right)\mathbf{I} & \textit{in } \Omega_s(t), \\ \dot{\overbrace{(\Lambda_l\boldsymbol{\sigma})}} & \textit{in } \Omega_l(t). \end{cases}$$

Therefore, if we integrate this equation in time, assuming that $\mathbf{u}_0$, $\boldsymbol{\sigma}_0$ *verify the elastic law at* $t = 0$, *we obtain the constitutive equations (3.11).*

In [85], it can be found an overview of different methods to solve contact problems. For numerical reasons, following [16, 27], to deal with the inequality in (3.10), we introduce a Lagrange

multiplier. For that purpose we consider the following notations:

$$E_h = \{p_h \in L^\infty(\Gamma_C);\ p_h|_C \in P_0(C),\ \forall C \in \mathcal{S}_h\},$$
$$Q_h = \{p_h \in E_h;\ p_h|_C \leq 0,\ \forall C \in \mathcal{S}_h\}.$$

In [9], it is proved that the discretized problem in space (3.10)-(3.12) can be formulated as a weak equality in the following manner:

Theorem 3.5.4. *Every solution of the discretized problem (3.10)-(3.12) is a solution of the problem:*

Find $\mathbf{u} \in W^{1,\infty}(0,t_f;\mathbf{U}_{ad_h}(t))$, $\boldsymbol{\sigma} \in W^{1,\infty}(0,t_f;\mathbf{X}_h(t))$ *and* $p \in W^{1,\infty}(0,t_f;E_h)$ *such that:*

$$\int_{\Omega(t)} \boldsymbol{\sigma}(t) : \boldsymbol{\varepsilon}(\mathbf{v})dx + \int_{\Gamma_C} \gamma_c u_n v_n d\Gamma = \int_{\Omega(t)} \mathbf{f}(t)\cdot\mathbf{v}dx - \int_{\Gamma_C} p(t)\ v_n d\Gamma,\ \forall \mathbf{v} \in \mathbf{U}_h(t), \tag{3.13}$$

$$\boldsymbol{\varepsilon}(\mathbf{u})(t) = \begin{cases} (\Lambda_s(T)\boldsymbol{\sigma})(t) + \left(\displaystyle\int_{T_l}^{T} \alpha_s(r)dr\right)\mathbf{I} & \text{in } \Omega_s(t), \\ (\Lambda_l\boldsymbol{\sigma})(t) & \text{in } \Omega_l(t), \end{cases} \tag{3.14}$$

$$p(t) = G_{\lambda_c}^{\gamma_c}(u_n(t) + \lambda_c\ p(t)) \text{ on } \Gamma_C, \tag{3.15}$$

for all $t \in (0,t_f]$, *and the initial conditions given in (3.12). Here* λ_c, γ_c *denote real numbers such that* $\lambda_c > 0$, $0 \leq \lambda_c\gamma_c < 1$ *and* $G_{\lambda_c}^{\gamma_c}$ *is the Yosida approximation of* $G^{\gamma_c} = G - \gamma_c\mathbf{I}$, $G = \partial I_{Q_h}$ *being the indicator function of the closed convex* Q_h.

Remark 3.5.5. *The Lagrange multiplier* $p(t)$ *takes into account the nonlinearity due to the contact condition and it will be called contact multiplier.*

In order to introduce an iterative algorithm to deal with the contact condition, we discretize the problem (3.13)-(3.15) in time using the following notation: The time interval of interest is divided into N steps

$$t^0 = 0,\ t^{j+1} = t^j + \Delta t,\ j = 0,...,N-1,\ \Delta t = \frac{t_f}{N}.$$

From now on we denote by g^j an approximation of a given function $g(t)$ at time t^j.

It is easy to prove that the Yosida approximation of G^{γ_c} is given by the expression (see [16])

$$G_{\lambda_c}^{\gamma_c}(\varphi) = \frac{1}{\lambda_c}\left(\varphi - \Pi_{Q_h}\left(\frac{1}{1-\lambda_c\gamma_c}\varphi\right)\right),\ \varphi \in E_h,$$

where Π_{Q_h} is the orthogonal projection over Q_h

$$\Pi_{Q_h}(p_h) = \begin{cases} p_h & \text{if } p_h \leq 0, \\ 0 & \text{if } p_h > 0. \end{cases}$$

Then, from Theorem 3.5.4, we obtain the following fixed point algorithm to solve Problem (3.10)-(3.12) introduced in [5]:

- Let $(\mathbf{u}_0, \boldsymbol{\sigma}_0, p^0)$ be given and γ_c, $\lambda_c > 0$ such that $\lambda_c \gamma_c < 1$.
- Then, for $j \geq 0$, $(\mathbf{u}^j,\ \boldsymbol{\sigma}^j,\ p^j)$ known at time t^j, we determine $(\mathbf{u}^{j+1}, \boldsymbol{\sigma}^{j+1},\ p^{j+1})$ at time t^{j+1}, an approximated weak solution of Problem (3.10)-(3.12). To do so, we propose the following iterative algorithm:

  i) Given $(\mathbf{u}_{k-1}^{j+1}, \boldsymbol{\sigma}_{k-1}^{j+1}, p_{k-1}^{j+1})$, we compute $(\mathbf{u}_k^{j+1}, \boldsymbol{\sigma}_k^{j+1}) \in \mathbf{U}_{ad_h}(t^{j+1}) \times \mathbf{X}_h(t^{j+1})$ by solving the variational equality

$$\int_{\Omega^{j+1}} \boldsymbol{\sigma}_k^{j+1} : \boldsymbol{\varepsilon}(\mathbf{v}) dx + \int_{\Gamma_C} \gamma_c \left(u_k^{j+1}\right)_n v_n d\Gamma =$$
$$\int_{\Omega^{j+1}} \mathbf{f}^{j+1} \cdot \mathbf{v} dx - \int_{\Gamma_C} p_{k-1}^{j+1}\ v_n d\Gamma,\ \forall \mathbf{v} \in \mathbf{U}_h(t^{j+1}),$$

  where

$$\boldsymbol{\sigma}_k^{j+1} = \begin{cases} \left(\Lambda_s(T^{j+1})\right)^{-1} \left(\boldsymbol{\varepsilon}(\mathbf{u}_k^{j+1}) - \alpha_s(T^{j+1})(T^{j+1} - T_l)\mathbf{I}\right) & \text{in } \Omega_s^{j+1}, \\ \Lambda_l^{-1} \boldsymbol{\varepsilon}(\mathbf{u}_k^{j+1}) & \text{in } \Omega_l^{j+1}. \end{cases}$$

  ii) The updated contact multiplier is given by relation

$$p_k^{j+1} = \frac{1}{\lambda_c} \left[\left(u_k^{j+1}\right)_n + \lambda_c p_{k-1}^{j+1} - \Pi_{Q_h} \left(\frac{\left(u_k^{j+1}\right)_n + \lambda_c p_{k-1}^{j+1}}{1 - \lambda_c \gamma_c} \right) \right].$$

Remark 3.5.6. *It can be proved that the weight of the entire slab is the total reaction force exerted by the bottom block over the slab. This property is used to initialize the contact multiplier (see [9]).*

3.5.4 Bermúdez-Moreno algorithm for the numerical solution of the nonlinear constitutive law

In order to avoid the nonlinearity due to the constitutive law (3.8), the numerical resolution is based on the Bermúdez-Moreno algorithm which involves a viscoplastic multiplier, which is a fixed point of a nonlinear equation. In a first stage, as in the contact case, the problem was solved in [10] by using fixed point techniques, which let to design an algorithm that we introduce in the following.

As we have done in previous subsection, we are going to consider a simplified problem, corresponding to Problem (DVP), replacing the contact boundary condition by a null Dirichlet condition. Therefore, the discretized variational problem remains:

$$\int_{\Omega(t)} \boldsymbol{\sigma}(t) : \boldsymbol{\varepsilon}(\mathbf{v}) dx = \int_{\Omega(t)} \mathbf{f}(t) \cdot \mathbf{v} dx, \forall \mathbf{v} \in \mathbf{U}_{ad_h}(t), \tag{3.16}$$

$$\boldsymbol{\varepsilon}(\dot{\mathbf{u}})(t) = \begin{cases} \dot{\overbrace{(\Lambda_s(T)\boldsymbol{\sigma})}}(t) + (\nabla \Phi_q(\boldsymbol{\sigma}^D))(t) + \left(\alpha_s(T)\dot{T}\right)(t)\mathbf{I} & \text{in } \Omega_s(t), \\ \dot{\overbrace{(\Lambda_l \boldsymbol{\sigma})}}(t) & \text{in } \Omega_l(t), \end{cases} \tag{3.17}$$

$$\mathbf{u}(0) = \mathbf{u}_0, \;\; \boldsymbol{\sigma}(0) = \boldsymbol{\sigma}_0, \text{ in } \Omega(0), \tag{3.18}$$

where

$$\mathbf{U}_{ad_h}(t) = \{\mathbf{v}_h \in \mathbf{U}_h(t); \mathbf{v}_h = \mathbf{0} \text{ on } \Gamma_C\}.$$

As in previous section, the thermo-elasto-viscoplastic law (3.17) is discretized in time by using an implicit Euler scheme:

$$\begin{aligned}\boldsymbol{\varepsilon}(\mathbf{u}^{j+1}) - \boldsymbol{\varepsilon}(\mathbf{u}^j) = &\left(\Lambda_s(T^{j+1})\boldsymbol{\sigma}^{j+1} - \Lambda_s(T^j)\boldsymbol{\sigma}^j\right) + \alpha_s(T^{j+1})(T^{j+1} - T^j)\mathbf{I} + \\ &\Delta t \; \nabla\Phi_q\left(\left(\boldsymbol{\sigma}^{j+1}\right)^D\right) \text{ in } \Omega_s^{j+1}, \\ \boldsymbol{\varepsilon}(\mathbf{u}^{j+1}) - \boldsymbol{\varepsilon}(\mathbf{u}^j) = &\Lambda_l\boldsymbol{\sigma}^{j+1} - \Lambda_l\boldsymbol{\sigma}^j \text{ in } \Omega_l^{j+1}.\end{aligned}$$

Once we have discretized the constitutive law, our objective is to obtain an explicit expression for $\boldsymbol{\sigma}^{j+1}$ and to substitute it in the mixed variational formulation (3.16). However, the nonlinearity of the viscoplastic function makes difficult to compute the stress tensor in $\Omega_s(t)$. In order to solve this difficulty, we are going to use again maximal monotone operator techniques.

The proofs of the following results can be found in [5].

Proposition 3.5.7. *At each time step t^{j+1}, $j = 0, \ldots, N-1$, the stress tensor in Ω_s^{j+1} is given by the relation*

$$\boldsymbol{\sigma}^{j+1} = \mathcal{V}(T^{j+1})\left(\boldsymbol{\varepsilon}(\mathbf{u}^{j+1}) - \Delta t\mathbf{q}^{j+1} + \frac{\Delta t\gamma_p s^{j+1}}{3}\mathrm{tr}(\boldsymbol{\varepsilon}(\mathbf{u}^{j+1}))\mathbf{I} + \mathbf{F}^j\right), \tag{3.19}$$

where $\mathbf{q}^{j+1}$ is the viscoplastic multiplier at the time step t^{j+1}

$$\mathbf{q}^{j+1} = (\nabla\Phi_q)^{\gamma_p}\left(\left(\boldsymbol{\sigma}^{j+1}\right)^D\right) = (\nabla\Phi_q - \gamma_p\mathbf{I})\left(\left(\boldsymbol{\sigma}^{j+1}\right)^D\right), \tag{3.20}$$

and $\mathbf{F}^j$ is the history of the solidified metal up to time t^j together with the expansional effects of the temperature changes at the time interval $[t^j, t^{j+1}]$

$$\begin{aligned}\mathbf{F}^j = -\boldsymbol{\varepsilon}(\mathbf{u}^j) + \Lambda_s(T^j)\boldsymbol{\sigma}^j - \alpha_s(T^{j+1})(T^{j+1} - T^j)\left(1 + \Delta t\gamma_p s^{j+1}\right)\mathbf{I} + \\ \frac{\Delta t\gamma_p s^{j+1}}{3}\left(\frac{1}{s^j}\mathrm{tr}(\boldsymbol{\sigma}^j) - \mathrm{tr}(\boldsymbol{\varepsilon}(\mathbf{u}^j))\right)\mathbf{I},\end{aligned} \tag{3.21}$$

where $\gamma_p \geq 0$ and

$$s^j = \frac{E(T^j)}{1 - 2\nu(T^j)}.$$

In (3.19), the automorphism $\mathcal{V}(T)$ is defined by

$$\mathcal{V}(T)\boldsymbol{\tau} = \widetilde{\lambda}(T)\mathrm{tr}(\boldsymbol{\tau})\mathbf{I} + 2\widetilde{\mu}(T)\boldsymbol{\tau},$$

being

$$\widetilde{\lambda}(T) = \frac{E(T)\nu(T)}{(L(T) - 2\nu(T))(L(T) + \nu(T))}, \;\; \widetilde{\mu}(T) = \frac{E(T)}{2(L(T) + \nu(T))},$$

and $L(T) = 1 + \gamma_p E(T)\Delta t$.

Lemma 3.5.8. *At each time step t^{j+1}, $j = 0, \ldots, N-1$, the viscoplastic multiplier $\mathbf{q}^{j+1}$ is a fixed point of the equation*

$$\mathbf{q}^{j+1} = (\nabla\Phi_q)_{\lambda_p}^{\gamma_p}\left(\left(\boldsymbol{\sigma}^{j+1}\right)^D + \lambda_p\mathbf{q}^{j+1}\right), \tag{3.22}$$

for λ_p a real positive number such that $\lambda_p\gamma_p < 1$. In this equation, $(\nabla\Phi_q)_{\lambda_p}^{\gamma_p}$ denotes the Moreau-Yosida approximation of $(\nabla\Phi_q)^{\gamma_p}$ given by the expression

$$(\nabla\Phi_q)_{\lambda_p}^{\gamma_p}(\boldsymbol{\zeta}) = \frac{\boldsymbol{\zeta}}{\lambda_p}\left(1 - \frac{1}{\eta^{j+1}(1-\lambda_p\gamma_p)}\right),\ \boldsymbol{\zeta} \in \mathcal{S}_3,$$

where $\eta^{j+1} = \eta(\boldsymbol{\zeta})$ is the unique root of the equation

$$\eta^{q-1} - \eta^{q-2} - \frac{\lambda_p\theta(T^{j+1})}{(1-\lambda_p\gamma_p)^{q-1}}|\boldsymbol{\zeta}|^{q-2} = 0, \tag{3.23}$$

in the interval $[1, +\infty)$.

Here we summarize the Bermúdez-Moreno algorithm to solve Problem (3.16)-(3.18) introduced in [5] and based on the results of Lemma 3.5.8:

- Let $(\mathbf{u}_0, \boldsymbol{\sigma}_0)$ be given and γ_p, $\lambda_p > 0$ such that $\lambda_p\gamma_p < 1$; we compute $\mathbf{q}^0 = (\nabla\Phi_q)^{\gamma_p}(\boldsymbol{\sigma}_0^D)$.
- Then, for $j \geq 0$, $(\mathbf{u}^j,\ \boldsymbol{\sigma}^j,\ \mathbf{q}^j)$ known at time t^j, we determine $(\mathbf{u}^{j+1}, \boldsymbol{\sigma}^{j+1},\ \mathbf{q}^{j+1})$ at time t^{j+1}, an approximated weak solution of Problem (3.16)-(3.18). To do so, we propose the following iterative algorithm:

  i) Given $(\mathbf{u}_{k-1}^{j+1}, \boldsymbol{\sigma}_{k-1}^{j+1}, \mathbf{q}_{k-1}^{j+1})$, we compute $(\mathbf{u}_k^{j+1}, \boldsymbol{\sigma}_k^{j+1}) \in \mathbf{U}_{ad_h}(t^{j+1}) \times \mathbf{X}_h(t^{j+1})$ by solving the variational equality, obtained by substituting expression (3.19) in equality (3.16),

$$\int_{\Omega_s^{j+1}} \mathcal{V}(T^{j+1})\left[\boldsymbol{\varepsilon}(\mathbf{u}_k^{j+1}) + \frac{\Delta t\gamma_p s^{j+1}}{3}\mathrm{tr}(\boldsymbol{\varepsilon}(\mathbf{u}_k^{j+1}))\mathbf{I}\right] : \boldsymbol{\varepsilon}(\mathbf{v})dx + \int_{\Omega_l^{j+1}} \Lambda_l^{-1}\boldsymbol{\varepsilon}(\mathbf{u}_k^{j+1}) : \boldsymbol{\varepsilon}(\mathbf{v})dx =$$
$$\int_{\Omega_s^{j+1}} \left[\mathcal{V}(T^{j+1})\Delta t\mathbf{q}_{k-1}^{j+1}\right] : \boldsymbol{\varepsilon}(\mathbf{v})dx - \int_{\Omega_s^{j+1}} \left[\mathcal{V}(T^{j+1})\mathbf{F}^j\right] : \boldsymbol{\varepsilon}(\mathbf{v})dx +$$
$$\int_{\Omega^{j+1}} \mathbf{f}^{j+1} \cdot \mathbf{v}dx\ \forall\mathbf{v} \in \mathbf{U}_{ad_h}(t^{j+1}),$$

  where $\mathbf{F}^j$ is given by expression (3.21), and

$$\boldsymbol{\sigma}_k^{j+1} = \begin{cases} \mathcal{V}(T^{j+1})\left(\boldsymbol{\varepsilon}(\mathbf{u}_k^{j+1}) - \Delta t\mathbf{q}_{k-1}^{j+1} + \dfrac{\Delta t\gamma_p s^{j+1}}{3}\mathrm{tr}(\boldsymbol{\varepsilon}(\mathbf{u}_k^{j+1}))\mathbf{I} + \mathbf{F}^j\right) & \text{in } \Omega_s^{j+1}, \\ \Lambda_l^{-1}\boldsymbol{\varepsilon}(\mathbf{u}_k^{j+1}) & \text{in } \Omega_l^{j+1}. \end{cases}$$

  ii) The updated viscoplastic multiplier is given by relation

$$\mathbf{q}_k^{j+1} = \frac{\left(\boldsymbol{\sigma}_k^{j+1}\right)^D + \lambda_p\mathbf{q}_{k-1}^{j+1}}{\lambda_p}\left(1 - \frac{1}{\eta_k^{j+1}(1-\lambda_p\gamma_p)}\right),$$

in Ω_s^{j+1}, where

$$\eta_k^{j+1} = \eta\left(\left(\boldsymbol{\sigma}_k^{j+1}\right)^D + \lambda_p \mathbf{q}_{k-1}^{j+1}\right),$$

is the solution of equation (3.23) in $[1, +\infty)$.

3.6 Bermúdez-Moreno algorithm to solve the casting problem: FPM algorithm

In this section we are going to summarize the Bermúdez-Moreno algorithm for the numerical resolution of the complete model (3.7)-(3.9). To do this, we must combine the algorithm introduced in Section 3.5.3 to solve the contact condition, with that introduced in Section 3.5.4 to deal with the constitutive law.

1. Let $(\mathbf{u}_0, \boldsymbol{\sigma}_0)$ be given and let consider p^0 as the weight of the liquid metal column for each point and $\mathbf{q}^0 = (\nabla\Phi_q)^{\gamma_p}(\boldsymbol{\sigma}_0^D)$.

2. Then, for $j \geq 0$, $(\mathbf{u}^j,\ \boldsymbol{\sigma}^j,\ \mathbf{q}^j,\ p^j)$ known at time t^j, we determine $(\mathbf{u}^{j+1}, \boldsymbol{\sigma}^{j+1},\ \mathbf{q}^{j+1},\ p^{j+1})$ at time t^{j+1}, an approximated weak solution of Problem (3.7)-(3.9). To do so, we propose the following iterative algorithm:

   2.1. Initialize $\mathbf{u}_0^{j+1} = \mathbf{u}^j$, $p_0^{j+1} = p^j$ and

$$\mathbf{q}_0^{j+1} = \begin{cases} \mathbf{q}^j & \text{in } \Omega_s^j, \\ \mathbf{0} & \text{in } \Omega_l^{j+1} \backslash \Omega_s^j. \end{cases}$$

   2.2. With $\mathbf{q}_{k-1}^{j+1}$, p_{k-1}^{j+1} known, calculate $\mathbf{u}_k^{j+1}$ by solving the variational equality

$$\begin{aligned} &\int_{\Omega_s^{j+1}} \mathcal{V}(T^{j+1}) \left[\boldsymbol{\varepsilon}(\mathbf{u}_k^{j+1}) + \frac{\Delta t \gamma_p s^{j+1}}{3} \mathrm{tr}(\boldsymbol{\varepsilon}(\mathbf{u}_k^{j+1}))\mathbf{I}\right] : \boldsymbol{\varepsilon}(\mathbf{v}) dx + \\ &\qquad \int_{\Omega_l^{j+1}} \Lambda_l^{-1} \boldsymbol{\varepsilon}(\mathbf{u}_k^{j+1}) : \boldsymbol{\varepsilon}(\mathbf{v}) dx + \int_{\Gamma_C} \gamma_c \left(u_k^{j+1}\right)_n v_n d\Gamma = \\ &\int_{\Omega_s^{j+1}} \left[\mathcal{V}(T^{j+1}) \Delta t \mathbf{q}_{k-1}^{j+1}\right] : \boldsymbol{\varepsilon}(\mathbf{v}) dx - \int_{\Omega_s^{j+1}} \left[\mathcal{V}(T^{j+1}) \mathbf{F}^j\right] : \boldsymbol{\varepsilon}(\mathbf{v}) dx - \\ &\qquad \int_{\Gamma_C} p_{k-1}^{j+1}\ v_n d\Gamma + \int_{\Omega^{j+1}} \mathbf{f}^{j+1} \cdot \mathbf{v} dx \ \ \forall \mathbf{v} \in \mathbf{U}_{ad_h}(t^{j+1}), \end{aligned} \tag{3.24}$$

   where $\mathbf{F}^j$ is given by expression (3.21).

   2.3. The updated stress tensor is defined by

$$\boldsymbol{\sigma}_k^{j+1} = \begin{cases} \mathcal{V}(T^{j+1}) \left(\boldsymbol{\varepsilon}(\mathbf{u}_k^{j+1}) - \Delta t \mathbf{q}_{k-1}^{j+1} + \dfrac{\Delta t \gamma_p s^{j+1}}{3} \mathrm{tr}(\boldsymbol{\varepsilon}(\mathbf{u}_k^{j+1}))\mathbf{I} + \mathbf{F}^j\right) & \text{in } \Omega_s^{j+1}, \\ \Lambda_l^{-1} \boldsymbol{\varepsilon}(\mathbf{u}_k^{j+1}) & \text{in } \Omega_l^{j+1}. \end{cases}$$

2.4. The updated contact multiplier is given by

$$p_k^{j+1} = \frac{1}{\lambda_c}\left[\left(u_k^{j+1}\right)_n + \lambda_c p_{k-1}^{j+1} - \Pi_{Q_h}\left(\frac{\left(u_k^{j+1}\right)_n + \lambda_c p_{k-1}^{j+1}}{1-\lambda_c\gamma_c}\right)\right].$$

2.5. The updated viscoplastic multiplier is given by

$$\mathbf{q}_k^{j+1} = \frac{\left(\boldsymbol{\sigma}_k^{j+1}\right)^D + \lambda_p \mathbf{q}_{k-1}^{j+1}}{\lambda_p}\left(1 - \frac{1}{\eta_k^{j+1}(1-\lambda_p\gamma_p)}\right),$$

in Ω_s^{j+1}, where

$$\eta_k^{j+1} = \eta\left(\left(\boldsymbol{\sigma}_k^{j+1}\right)^D + \lambda_p \mathbf{q}_{k-1}^{j+1}\right),$$

is the solution of equation

$$\eta^{q-1} - \eta^{q-2} - \frac{\lambda_p \theta(T^{j+1})}{(1-\lambda_p\gamma_p)^{q-1}}\left|\left(\boldsymbol{\sigma}_k^{j+1}\right)^D + \lambda_p \mathbf{q}_{k-1}^{j+1}\right|^{q-2} = 0,$$

in the interval $[1, +\infty)$.

Remark 3.6.1. *The only difficulty remaining in the variational formulation (3.24) is how to impose the confinement condition on the liquid and mushy zones:*

$$\mathbf{v}_{|C} \cdot \mathbf{n}_{|C} = 0,\ \forall C \in \mathcal{Z}_h(t),$$

included in the definition of the space of displacements fields $\mathbf{U}_h(t)$.

In three-dimensional simulations, since the transversal section of the slab is not rectangular, this difficulty is overcome by using a penalization technique in the liquid and mushy region. In two-dimensional simulations, this condition does not imply a coupling between the components of the displacement field.

Remark 3.6.2. *In practice, updating the contact and viscoplastic multipliers is performed with a relaxation parameter* ϑ. *For example, the updated viscoplastic multiplier is obtained by formula*

$$\mathbf{q}_k^{j+1} = \vartheta \mathbf{q}_k^{j+1} + (1-\vartheta)\mathbf{q}_{k-1}^{j+1}, \quad 0 < \vartheta \leq 1.$$

Chapter 4

Improved numerical solution

The Bermúdez-Moreno algorithm presented in Section 3.6 is robust and converges well in academic tests. Moreover, this algorithm is very efficient to solve the stationary stage in casting processes. Nevertheless, when it is applied to the simulation of the butt-curl deformation, its convergence gets worse due to its strong dependence on the parameters and the large gradients of the thermal stresses. Due to this, it is necessary to find efficient strategies in order to improve the convergence, which is the objective of this chapter.

The main difficulties we must overcome to improve the numerical solution of this problem are the following:

- To model the butt curl, we must solve a contact condition between the slab and the bottom block. To deal with this nonlinear condition, we use the Bermúdez-Moreno algorithm, based on maximal monotone operator techniques, together with a generalized Newton method.

- The aluminium behaviour is nonlinear and depends strongly on the temperature field. In order to avoid the nonlinearity of the constitutive law we use again the Bermúdez-Moreno method that is combined with two different techniques: an algorithm using Newton techniques and another one improving the Bermúdez-Moreno algorithm by considering that their parameters are variable.

The outline of this chapter is as follows: In Section 3.1, we take again the algorithm presented in Section 3.5.3 to treat the contact between the slab and the bottom block; to approximate the contact multiplier which is a fixed point of a nonlinear equation, we propose a generalized Newton method for nonsmooth equations combined with a penalization technique. In Section 3.2, to deal with the constitutive law we use again the Bermúdez-Moreno algorithm presented in 3.5.4 and we describe two methods to approximate the viscoplastic multiplier: the Newton algorithm and the Bermúdez-Moreno algorithm with variable parameters. Finally, in Section 3.3, we summarize the two algorithms to solve a casting problem, that put together the two nonlinearities due to the contact and the viscoplasticity.

4.1 Newton algorithm to approximate the contact multiplier

The fixed point algorithm introduced in Section 3.5.3 is robust and converges well for academic tests; nevertheless, the greater the problem's magnitude, the slower its convergence. In casting processes, in which we must join two nonlinearities -contact and viscoplasticity-, this difficulty becomes more apparent. In this section we will use a generalized Newton method based on the Lipschitzian properties of G_{λ_C} (see [39, 64, 72]) in order to improve the fixed point algorithm for the nonlinear equation (3.15). This new algorithm was published in [7].

In order to introduce a new algorithm to solve the contact condition, we consider $\gamma_c = 0$ and $\lambda_c > 0$ in Theorem 3.5.4 and, therefore, every solution of the discretized problem (3.10)-(3.12) is a solution of the problem:

$$\int_{\Omega(t)} \boldsymbol{\sigma}(t) : \boldsymbol{\varepsilon}(\mathbf{v}) dx + \int_{\Gamma_C} p(t)\ v_n d\gamma = \int_{\Omega(t)} \mathbf{f}(t) \cdot \mathbf{v} dx,\ \forall \mathbf{v} \in \mathbf{U}_h(t), \tag{4.1}$$

$$\boldsymbol{\varepsilon}(\mathbf{u})(t) = \begin{cases} (\Lambda_s(T)\boldsymbol{\sigma})(t) + \left(\displaystyle\int_{T_l}^{T} \alpha_s(r) dr\right) \mathbf{I} & \text{in } \Omega_s(t), \\ \\ (\Lambda_l \boldsymbol{\sigma})(t) & \text{in } \Omega_l(t), \end{cases} \tag{4.2}$$

$$p(t) = G_{\lambda_c}(u_n(t) + \lambda_c\ p(t)) \text{ on } \Gamma_C, \tag{4.3}$$

where

$$G_{\lambda_c}(\varphi) = \frac{1}{\lambda_c} \left(I - \Pi_{Q_h}\right)(\varphi),\ \varphi \in E_h, \tag{4.4}$$

Π_{Q_h} being the projection of E_h onto the closed convex Q_h.

Remark 4.1.1. *It is easy to prove that G_{λ_c} is contractive for $\lambda_c \geq 1$. So, given $u_n \in E_h$, p is the unique fixed point of (4.3) (see [16, 26, 86]).*

Notice that, from (4.4), at each $\varphi \in E_h$,

$$G_{\lambda_c}(\varphi)_{|C} = \hat{G}_{\lambda_c}(\varphi_{|C}),\ \forall C \in \mathcal{S}_h,$$

where

$$\hat{G}_{\lambda_c}(s) = \begin{cases} 0, & \text{if } s \leq 0, \\ s/\lambda_c, & \text{if } s > 0, \end{cases} \tag{4.5}$$

at each point $s \in \mathbb{R}$. Moreover, $\hat{G}_{\lambda_c}$ is differentiable at each point $s \neq 0$. In order to obtain an approximation of $\hat{G}_{\lambda_c}$ at $s = 0$, we need to introduce the following definitions which generalize the concepts of subdifferential and Jacobian (see [64]):

Definition 4.1.2. *Let $F : \mathbb{R}^n \to \mathbb{R}^m$ be a locally Lipschitz function. The B-subdifferential, $\partial_B F$, of F at $\mathbf{x} \in \mathbb{R}^n$ is defined by*

$$\partial_B F(\mathbf{x}) = \{V \in \mathbb{R}^{m \times n}; V = \lim_{\mathbf{x}_i \to \mathbf{x}} JF(\mathbf{x}_i),\ F \text{ is differentiable at } \mathbf{x}_i \text{ for all } i\},$$

where JF is the Jacobian matrix of F.

Definition 4.1.3. *Let $F : \mathbb{R}^n \to \mathbb{R}^m$ be a locally Lipschitz function. The Clarke generalized Jacobian of F at $\mathbf{x} \in \mathbb{R}^n$, denoted by $\partial F(\mathbf{x})$, is the convex hull of its B-subdifferential $\partial_B F(\mathbf{x})$.*

Remark 4.1.4. *Let $F : \mathbb{R}^n \to \mathbb{R}$ be a locally Lipschitz function. If F is convex, the Clarke generalized Jacobian $\partial F(\mathbf{x})$ is the subdifferential of F in $\mathbf{x}$ (see [60]).*

The Clarke generalized Jacobian is a powerful tool that allows to extend to non smooth functions many classical results for smooth functions. In particular, by using this tool, the classic Newton's method can be extended to semismooth functions (see [39, 65, 69, 79]). There are several equivalent ways to define this property but we use that definition found in [65]:

Definition 4.1.5. *A locally Lipschitz function $F : \mathbb{R}^n \to \mathbb{R}^m$ is semismooth at $\mathbf{x} \in \mathbb{R}^n$ if F is directionally differentiable near $\mathbf{x}$ and*

$$\lim_{\substack{\tilde{\mathbf{x}} \to \mathbf{x} \\ \tilde{\mathbf{x}} \neq \mathbf{x}}} \frac{\|F'(\tilde{\mathbf{x}}; \tilde{\mathbf{x}} - \mathbf{x}) - F'(\mathbf{x}; \tilde{\mathbf{x}} - \mathbf{x})\|}{\|\tilde{\mathbf{x}} - \mathbf{x}\|} = 0,$$

where $F'(\tilde{\mathbf{x}}; \tilde{\mathbf{x}} - \mathbf{x})$ denotes the directional derivative of F at $\tilde{\mathbf{x}}$ in the direction $\tilde{\mathbf{x}} - \mathbf{x}$.

Moreover, if F verifies that

$$\limsup_{\substack{\tilde{\mathbf{x}} \to \mathbf{x} \\ \tilde{\mathbf{x}} \neq \mathbf{x}}} \frac{\|F'(\tilde{\mathbf{x}}; \tilde{\mathbf{x}} - \mathbf{x}) - F'(\mathbf{x}; \tilde{\mathbf{x}} - \mathbf{x})\|}{\|\tilde{\mathbf{x}} - \mathbf{x}\|^2} < \infty,$$

then F is strongly semismooth at $\mathbf{x}$.

The proof of the following Lemma can be found in [68, 69]:

Lemma 4.1.6. *Let $F : \mathbb{R}^n \to \mathbb{R}^m$ be a locally Lipschitz function. If F is semismooth at $\mathbf{x} \in \mathbb{R}^n$, then for any $\mathbf{h} \to \mathbf{0}$ and $V \in \partial F(\mathbf{x} + \mathbf{h})$,*

$$F(\mathbf{x} + \mathbf{h}) - F(\mathbf{x}) - V\mathbf{h} = o\left(\|\mathbf{h}\|\right).$$

If F is strongly semismooth at $\mathbf{x}$, then

$$F(\mathbf{x} + \mathbf{h}) - F(\mathbf{x}) - V\mathbf{h} = O\left(\|\mathbf{h}\|^2\right).$$

Remark 4.1.7. *In [79] it is proved that convex and piecewise smooth functions are semismooth. Moreover, in [39] it is proved that piecewise affine functions are strongly semismooth.*

Application to the contact problem

It is easy to prove that the B-subdifferential of $\hat{G}_{\lambda_c}$ at $s = 0$ is

$$\partial_B \hat{G}_{\lambda_c}(0) = \left\{0, \frac{1}{\lambda_c}\right\},$$

and therefore, its Clarke generalized Jacobian is the interval

$$\partial \hat{G}_{\lambda_c}(0) = \left[0, \frac{1}{\lambda_c}\right],$$

which coincides with its subdifferential.

Lemma 4.1.8. *At each point $s_0 \in \mathbb{R}$, the following approximation for $\hat{G}_{\lambda_c}(s_0)$ holds true:*

$$\hat{G}_{\lambda_c}(s_0) \cong \hat{G}_{\lambda_c}(s_1) + \begin{cases} 0, & \text{if } s_0 < 0, \\ -V s_1, & \text{if } s_0 = 0, \\ (s_0 - s_1)/\lambda_c, & \text{if } s_0 > 0, \end{cases} \tag{4.6}$$

for $s_1 \in \mathbb{R}$ close enough to s_0, where V belongs to the subdifferential $\partial \hat{G}_{\lambda_c}(s_0)$. Furthermore, the error of this approximation is of order $O\left(|s_0 - s_1|^2\right)$.

Proof. Since $\hat{G}_{\lambda_c}$, defined in (4.5), is differentiable at every point $s \neq 0$ and strongly semismooth, we can write for all $s_0, s_1 \in \mathbb{R}$ thanks to Lemma 4.1.6

$$\hat{G}_{\lambda_c}(s_0) = \hat{G}_{\lambda_c}(s_1) + V\,(s_0 - s_1) + O\left(|s_0 - s_1|^2\right),$$

where $V \in \partial \hat{G}_{\lambda_c}(s_0)$. Taking into account the definition of $\hat{G}_{\lambda_c}$ (see 4.5), we obtain (4.6). □

Remark 4.1.9. *To solve numerically the contact problem we consider the election $V = 0$ in (4.6).*

In order to introduce an iterative algorithm to deal with the contact condition, we discretize the problem (4.1)-(4.3) in time in the same way that in Section 3.5.3.

Then, from Lemma 4.1.8, at each time step t^{j+1}, given the starting values $(\mathbf{u}_0^{j+1}, \boldsymbol{\sigma}_0^{j+1}, p_0^{j+1})$, successive approximations $(\mathbf{u}_k^{j+1}, \boldsymbol{\sigma}_k^{j+1}, p_k^{j+1})$, $k \geq 1$, of the solution $(\mathbf{u}^{j+1}, \boldsymbol{\sigma}^{j+1}, p^{j+1})$ can be computed by using the recurrence formulas:

$$\int_{\Omega^{j+1}} \boldsymbol{\sigma}_k^{j+1} : \boldsymbol{\varepsilon}(\mathbf{v}) dx + \int_{\Gamma_C} p_k^{j+1}\, v_n d\gamma = \int_{\Omega^{j+1}} \mathbf{f}^{j+1} \cdot \mathbf{v} dx,\ \forall \mathbf{v} \in \mathbf{U}_h(t^{j+1}), \tag{4.7}$$

$$\boldsymbol{\sigma}_k^{j+1} = \begin{cases} \left(\Lambda_s(T^{j+1})\right)^{-1} \left(\boldsymbol{\varepsilon}(\mathbf{u}_k^{j+1}) - \alpha_s(T^{j+1})(T^{j+1} - T_l)\mathbf{I}\right) & \text{in } \Omega_s^{j+1}, \\ \Lambda_l^{-1} \boldsymbol{\varepsilon}(\mathbf{u}_k^{j+1}) & \text{in } \Omega_l^{j+1}. \end{cases} \tag{4.8}$$

$$p_k^{j+1} = p_{k-\frac{1}{2}}^{j+1} + \begin{cases} 0, & \text{if } s_{k-1}^{j+1} \leq 0, \\ \left(s_k^{j+1} - s_{k-1}^{j+1}\right)/\lambda_c, & \text{if } s_{k-1}^{j+1} > 0, \end{cases} \tag{4.9}$$

where

$$s_k^{j+1} = \left(u_k^{j+1}\right)_n + \lambda_c\, p_k^{j+1}, \tag{4.10}$$

$$p_{k-\frac{1}{2}}^{j+1} = \hat{G}_{\lambda_c}(s_{k-1}^{j+1}). \tag{4.11}$$

Notice that approximation (4.9) corresponds to the choice $s_1 = s_{k-1}^{j+1}$, $s_0 = s_k^{j+1}$ and $V = 0$ for $s_0 = 0$ in (4.6).

Remark 4.1.10. *Note that at each iteration the variational equality corresponding to (4.7) is equivalent to the linear problem*

$$-\text{div}\left(\boldsymbol{\sigma}_k^{j+1}\right) = \mathbf{f}^{j+1} \text{ in } \Omega^{j+1}, \tag{4.12}$$

$$(u_k^{j+1})_n = 0,\ (\boldsymbol{\sigma}_k^{j+1})_t = \mathbf{0} \text{ on } \Gamma_n^2(t^{j+1}) \cup \Gamma_l(t^{j+1}) \cup \Gamma_{sym}(t^{j+1}), \tag{4.13}$$

$$\boldsymbol{\sigma}_k^{j+1}\mathbf{n} = \mathbf{0} \text{ on } \Gamma_n^1(t^{j+1}) \cup \Gamma_{sup}(t^{j+1}), \tag{4.14}$$

$$(\sigma_k^{j+1})_n = -p_k^{j+1},\ (\boldsymbol{\sigma}_k^{j+1})_t = \mathbf{0} \text{ on } \Gamma_C, \tag{4.15}$$

in the distributional sense; so the contact multiplier p_k^{j+1} represents the obstacle reaction on Γ_C.

When analyzing formulas (4.7)-(4.11), we notice that there exists a coupling between the displacements and the contact multiplier on the boundary Γ_C; furthermore, from (4.15), normal stresses only depend on the contact multiplier on this boundary. In what follows, our objective is to split Γ_C at each iteration into two parts: on the first part we will know the contact multiplier –and, in turn, the normal stresses–, on the second part the normal displacements will be null. This procedure will first allow us to compute displacements and stresses at each iteration, and then to compute the contact multiplier.

Lemma 4.1.11. *Let us consider the following sets:*

$$(\Gamma_{C,k}^-)^{j+1} = \{C \in S_h;\ s_k^{j+1} \leq 0\}, \tag{4.16}$$

$$(\Gamma_{C,k}^+)^{j+1} = \{C \in S_h;\ s_k^{j+1} > 0\}. \tag{4.17}$$

Then,

$$\begin{aligned} p_k^{j+1} &= 0 \text{ on } (\Gamma_{C,k-1}^-)^{j+1}, \\ \left(u_k^{j+1}\right)_n &= 0 \text{ on } (\Gamma_{C,k-1}^+)^{j+1}. \end{aligned} \tag{4.18}$$

Proof. With the notation introduced in (4.16) and (4.17), relation (4.9) can be rewritten as

$$p_k^{j+1} = \begin{cases} 0, & \text{on } (\Gamma_{C,k-1}^-)^{j+1}, \\ p_{k-\frac{1}{2}}^{j+1} + \left(s_k^{j+1} - s_{k-1}^{j+1}\right)/\lambda_c, & \text{on } (\Gamma_{C,k-1}^+)^{j+1}, \end{cases}$$

since $\hat{G}_{\lambda_C}$ is null on each $C \in (\Gamma_{C,k-1}^-)^{j+1}$. So, we can easily update the multiplier p_k^{j+1} by zero on $(\Gamma_{C,k-1}^-)^{j+1}$. Nevertheless, on each face of $(\Gamma_{C,k-1}^+)^{j+1}$, taking into account (4.10) and (4.11), we must compute p_k^{j+1} verifying

$$p_k^{j+1} = \frac{s_{k-1}^{j+1}}{\lambda_c} + \frac{\left(s_k^{j+1} - s_{k-1}^{j+1}\right)}{\lambda_c} = \frac{1}{\lambda_c}\left(u_k^{j+1}\right)_n + p_k^{j+1},$$

and this equality can only be verified if $\left(u_k^{j+1}\right)_n = 0$ on $(\Gamma_{C,k-1}^+)^{j+1}$. □

Thus, at each iteration the boundary Γ_C is split into two parts:

- $(\Gamma^+_{C,k-1})^{j+1}$, where the normal displacements and the tangential component of stresses are null,
- $(\Gamma^-_{C,k-1})^{j+1}$, where the normal and tangential stresses are null.

It is very important to note that this division of Γ_C is the only data which is modified at each iteration.

There are several ways to achieve the solution using formulas (4.7)-(4.11), but since our objective is to couple the contact effects with the viscoplastic ones, in the next subsection we propose an algorithm based on two steps. In the first one, we compute $(\mathbf{u}_k^{j+1}, \boldsymbol{\sigma}_k^{j+1})$ using Lemma 4.1.11 and Remark 4.1.10 to remove the contact multiplier in equation (4.7). Afterwards, we compute p_k^{j+1} and update $(\Gamma^+_{C,k})^{j+1}$.

Newton algorithm to solve the contact problem

The proposed algorithm to solve Problem (3.10)-(3.12) is the following:

- Given $\mathbf{u}_0$, $\boldsymbol{\sigma}_0$, we choose $p^0 = -(\sigma_0)_n$.
- Then, for $j \geq 0$, $(\mathbf{u}^j,\ \boldsymbol{\sigma}^j, p^j)$ known at time t^j, we determine $(\mathbf{u}^{j+1}, \boldsymbol{\sigma}^{j+1}, p^{j+1})$ at time t^{j+1}, an approximated weak solution of Problem (3.10)-(3.12). To do so, we propose the following iterative algorithm:

  Step 1: Given $(\mathbf{u}_{k-1}^{j+1}, \boldsymbol{\sigma}_{k-1}^{j+1}, p_{k-1}^{j+1})$, we compute $(\mathbf{u}_k^{j+1}, \boldsymbol{\sigma}_k^{j+1}) \in \mathbf{U}_h^*(t^{j+1}) \times \mathbf{X}_h(t^{j+1})$ by solving the variational equality

$$\int_{\Omega^{j+1}} \boldsymbol{\sigma}_k^{j+1} : \boldsymbol{\varepsilon}(\mathbf{v}) dx = \int_{\Omega^{j+1}} \mathbf{f}^{j+1} \cdot \mathbf{v} dx,\ \forall \mathbf{v} \in \mathbf{U}_h^*(t^{j+1}),$$

  together with the constitutive law (4.8), where

$$\mathbf{U}_h^*(t^{j+1}) = \{\mathbf{v} \in \mathbf{U}_h(t^{j+1});\ v_n = 0 \text{ on } (\Gamma^+_{C,k-1})^{j+1}\}.$$

  In this first step the tangential component of $\boldsymbol{\sigma}_k^{j+1}$ is assumed to be null on Γ_C, but normal stresses due to the contact are unknown on $(\Gamma^+_{C,k-1})^{j+1}$. For the practical computation we impose the Dirichlet condition (4.18) on $(\Gamma^+_{C,k-1})^{j+1}$ by using a penalty method in the variational equation

$$\int_{\Omega^{j+1}} \boldsymbol{\sigma}_k^{j+1} : \boldsymbol{\varepsilon}\ (\mathbf{v}) dx + \frac{1}{\epsilon_c} \int_{(\Gamma^+_{C,k-1})^{j+1}} \left(u_k^{j+1}\right)_n v_n d\gamma = \int_{\Omega^{j+1}} \mathbf{f}^{j+1} \cdot \mathbf{v} dx, \qquad (4.19)$$

  for all $\mathbf{v} \in \mathbf{U}_h(t^{j+1})$, where ϵ_c is a small parameter.

Step 2: Known $(\mathbf{u}_k^{j+1}, \boldsymbol{\sigma}_k^{j+1})$ and given that $p_k^{j+1} = 0$ on $(\Gamma_{C,k-1}^-)^{j+1}$, we update p_k^{j+1} on $(\Gamma_{C,k-1}^+)^{j+1}$ thanks to the variational equality (4.7):

$$\int_{(\Gamma_{C,k-1}^+)^{j+1}} p_k^{j+1} v_n d\gamma = -\int_{\Omega^{j+1}} \boldsymbol{\sigma}_k^{j+1} : \boldsymbol{\varepsilon}(\mathbf{v}) dx + \int_{\Omega^{j+1}} \mathbf{f}^{j+1} \cdot \mathbf{v} dx, , \tag{4.20}$$

for all $\mathbf{v} \in \mathbf{U}_h(t^{j+1})$ and we update $(\Gamma_{C,k}^+)^{j+1}$ using (4.17).

Then, taking into account expression (4.19) when updating p_k^{j+1} on $(\Gamma_{C,k-1}^+)^{j+1}$, we obtain that

$$\int_{(\Gamma_{C,k-1}^+)^{j+1}} p_k^{j+1} v_n d\gamma = \frac{1}{\epsilon_c} \int_{(\Gamma_{C,k-1}^+)^{j+1}} \left(u_k^{j+1}\right)_n v_n d\gamma, \, \forall \mathbf{v} \in \mathbf{U}_h(t^{j+1}),$$

that is,

$$p_k^{j+1} = \frac{1}{\epsilon_c} \left(u_k^{j+1}\right)_n \text{ on } (\Gamma_{C,k-1}^+)^{j+1}. \tag{4.21}$$

Matrix factorization

To solve the matrix of equations system resulting from applying the finite element method we use a direct method of resolution. Although it might seem reasonable to employ an iterative method, such as the conjugate gradient, several factors discourage us from its use: the large gradients of temperature and stresses, the penalty term of the contact condition and the multiscale nature of the fictitious domain technique to impose the metallostatic pressure. Due to this, we decided to use a classical resolution method using a Cholesky factorization.

The mean disadvantage of the Newton algorithm presented here is the need to factorize the stiffness matrix at each iteration, which implies an important increase in the computational cost with respect to the fixed point algorithm presented in Section 3.5.3. In order to avoid this difficulty, taking into account that the contact condition only involves a small part of the boundary, we propose to use a factorization of the stiffness matrix adapted to the problem's geometry.

For this purpose, we take into account that the computational domain grows with time far from the contact region. Then, there are two possibilities:

- To consider a lower factorization $\mathbf{K} = \mathbf{L}\mathbf{D}\mathbf{L}^T$ –where $\mathbf{D}$ is a diagonal matrix and $\mathbf{L}$ is a lower triangular matrix with unitary diagonal– and number the mesh in such a way that the last nodes correspond to the contact nodes. This method is not advisable in the casting case since the computational domain grows with time far from the contact region, and the mesh is constructed by layers to model the filling process.
- To consider an upper factorization $\mathbf{K} = \mathbf{U}\mathbf{D}\mathbf{U}^{\mathbf{T}}$ where $\mathbf{U}$ is an upper triangular matrix with unitary diagonal (see Figure 4.1) and number the mesh in such a way that the first nodes correspond to the contact nodes.

The factorization is carried out in the following way:

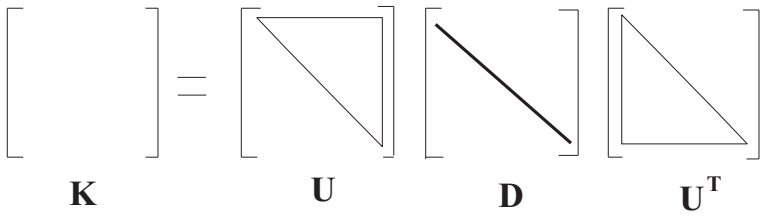

Figure 4.1: Scheme of the upper factorization

Adapted partial factorization. We consider the upper factorization $\mathbf{K} = \mathbf{U}\mathbf{D}\mathbf{U}^{\mathbf{T}}$ where $\mathbf{U}$ is an upper triangular matrix with unitary diagonal and it is easy to prove that $\mathbf{D}$ and $\mathbf{U}$ are characterized by the following formulae:

$$
\begin{aligned}
& d_{nn} = k_{nn}, \\
& i = n-1, n-2, \ldots, 1 \\
& \qquad u_{in} = \frac{k_{in}}{d_{nn}}, \\
& \qquad u_{ij} = \frac{k_{ij} - \displaystyle\sum_{l=j+1}^{n} u_{il} d_{ll} u_{jl}}{d_{jj}}, \quad j = n-1, n-2, \ldots, i+1, \\
& \qquad d_{ii} = k_{ii} - \sum_{l=i+1}^{n} u_{il}^2 d_{ll}.
\end{aligned}
$$

In the practice, the factorization is stored in the matrix $\mathbf{K}$ itself: $\mathbf{D}$ will be the diagonal of $\mathbf{K}$ and $\mathbf{U}$ its upper triangular submatrix. The pseudocode of the factorization is the following:

for $i = n-1$ to 1 **do**
  $k_{in} = k_{in}/k_{nn}$
  for $j = n-1$ to i **do**
    for $l = j+1$ to n **do**
      $k_{ij} = k_{ij} - k_{il} k_{ll} k_{jl}$
    end for
    if $i \neq j$ **then**
      $k_{ij} = k_{ij}/k_{jj}$
    end if
  end for
end for

Since with this methodology the contact rows are the first ones of the matrix, if we compute the factorization row by row from downwards to upwards and from the right to the left, during a time step we can conserve all the rows of the factorized matrix except those corresponding to the contact nodes (see Figure 4.3). So, at each iteration we must only compute and factorize the first rows of the matrix, corresponding to the contact nodes.

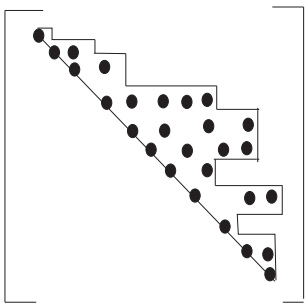

Figure 4.2: Upper skyline by rows

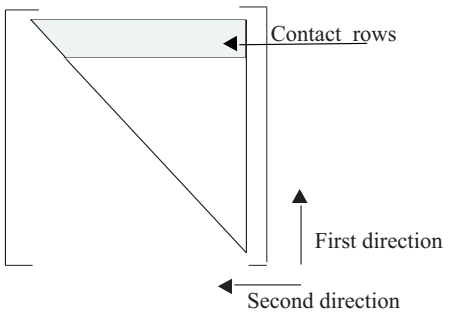

Figure 4.3: Direction of the upper factorization

Matrix storage. In order to storage the matrix $\mathbf{K}$, we employ a non standard storage by means of an upper skyline by rows. So, we store the upper matrix of $\mathbf{K}$ in vector form, row by row from upwards to downwards and from the left to the right. We denote by μ_K the array defined by

$$\begin{aligned}
&(\mu_K)_1 = 0,\\
&(\mu_K)_2 = 1,\\
&(\mu_K)_{i+1} = (\mu_K)_i + \mu_{i-1} - (i-1) + 1,
\end{aligned}$$

where $(\mu_K)_{i+1}$ gives the position of the diagonal term K_{ii}, μ_i being the column corresponding to the last non null element of the ith row of the matrix $\mathbf{K}$ (see Figure 4.2).

Figure 4.4 shows a flowchart of the Newton algorithm with the new matrix factorization. After initializing variables (Step 1 in Figure 4.4), a time step loop is carried out. In this loop, at the $j+1$ iteration, the displacement vector $\mathbf{u}^{j+1}$ is computed by constructing the fixed stiffness matrix (Step 2) and solving iteratively (Steps 5-8) equations (4.19) and (4.21), where the variable stiffness matrix is constructed at each iteration (Step 5).

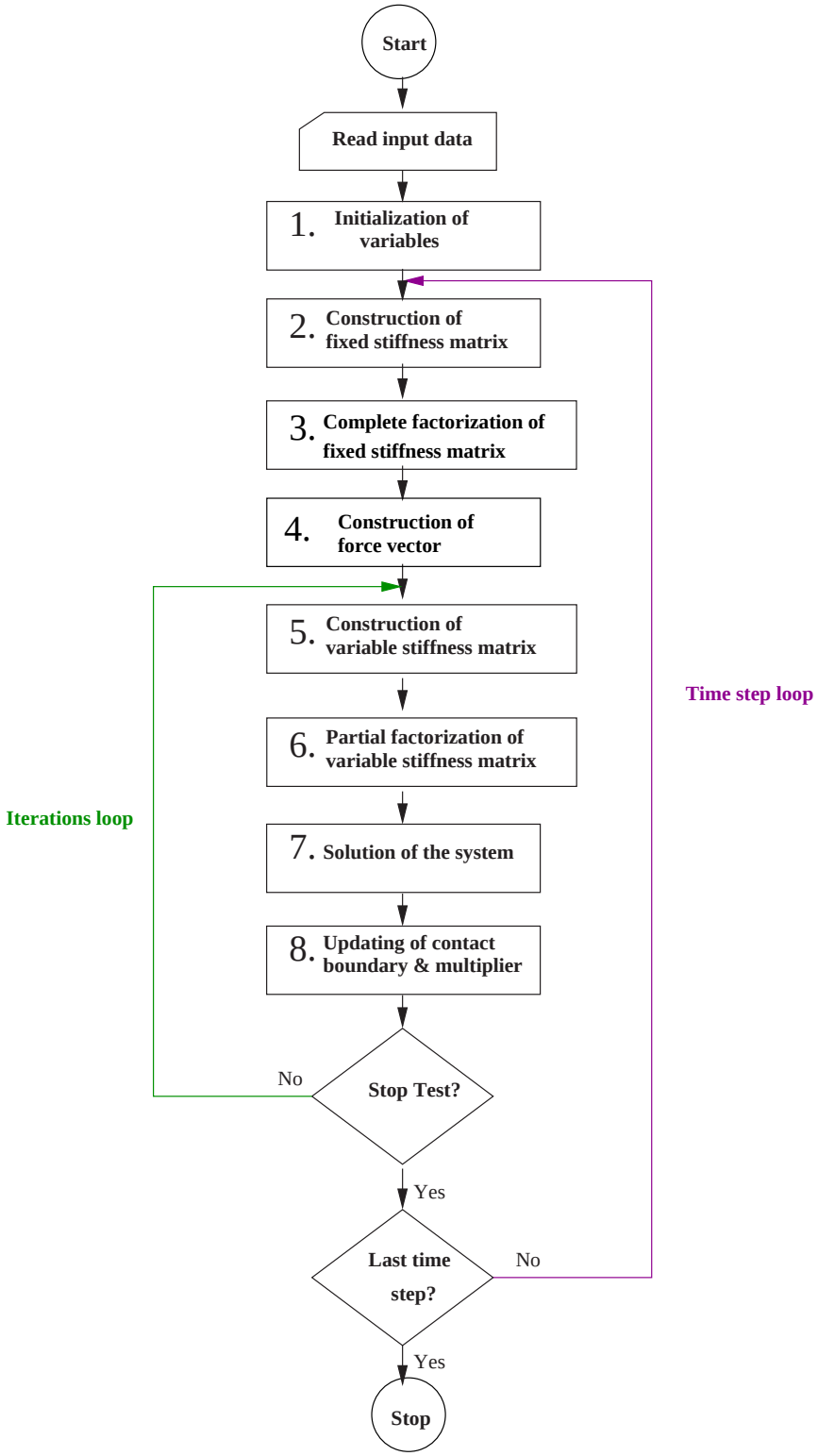

Figure 4.4: Flowchart of Newton algorithm with adapted factorization.

4.2 Algorithms for the numerical solution of the nonlinear constitutive law

In order to avoid the nonlinearity due to the constitutive law (3.5), the numerical solution is based on the Bermúdez-Moreno algorithm which involves a viscoplastic multiplier, which is a fixed point of a nonlinear equation. In a first stage, as in the contact case, the problem was solved in [10] by using the Bermúdez-Moreno algorithm described in Section 3.5.4. Although this algorithm was very robust, its convergence turned out to be slow in butt curl simulation. In order to improve its efficiency, we propose two new methodologies:

- To apply a Newton method to compute the multiplier.
- To consider the Bermúdez-Moreno algorithm with variable parameters introduced in [43].

As we have done in previous subsection, we are going to consider a simplified problem, corresponding to Problem (DVP), replacing the contact boundary condition by a null Dirichlet condition. Therefore, recall that the discretized variational (3.16)-(3.18) is:

$$\int_{\Omega(t)} \boldsymbol{\sigma}(t) : \boldsymbol{\varepsilon}(\mathbf{v}) dx = \int_{\Omega(t)} \mathbf{f}(t) \cdot \mathbf{v} dx, \forall \mathbf{v} \in \mathbf{U}_{ad_h}(t),$$

$$\boldsymbol{\varepsilon}(\dot{\mathbf{u}})(t) = \begin{cases} \dot{\widetilde{(\Lambda_s(T)\boldsymbol{\sigma})}}(t) + (\nabla \Phi_q(\boldsymbol{\sigma}^D))(t) + \left(\alpha_s(T)\dot{T}\right)(t)\mathbf{I} & \text{in } \Omega_s(t), \\ \dot{\widetilde{(\Lambda_l \boldsymbol{\sigma})}}(t) & \text{in } \Omega_l(t), \end{cases}$$

$$\mathbf{u}(0) = \mathbf{u}_0, \;\; \boldsymbol{\sigma}(0) = \boldsymbol{\sigma}_0, \text{ in } \Omega(0),$$

where

$$\mathbf{U}_{ad_h}(t) = \{\mathbf{v}_h \in \mathbf{U}_h(t); \mathbf{v}_h = \mathbf{0} \text{ on } \Gamma_C\}.$$

As in Section 3.5.4, the thermo-elasto-viscoplastic law is discretized in time by using an implicit Euler scheme:

$$\begin{aligned} \boldsymbol{\varepsilon}(\mathbf{u}^{j+1}) - \boldsymbol{\varepsilon}(\mathbf{u}^j) = &\left(\Lambda_s(T^{j+1})\boldsymbol{\sigma}^{j+1} - \Lambda_s(T^j)\boldsymbol{\sigma}^j\right) + \alpha_s(T^{j+1})(T^{j+1} - T^j)\mathbf{I} + \\ &\Delta t \; \nabla \Phi_q \left(\left(\boldsymbol{\sigma}^{j+1}\right)^D\right) \text{ in } \Omega_s^{j+1}, \\ \boldsymbol{\varepsilon}(\mathbf{u}^{j+1}) - \boldsymbol{\varepsilon}(\mathbf{u}^j) = &\Lambda_l \boldsymbol{\sigma}^{j+1} - \Lambda_l \boldsymbol{\sigma}^j \text{ in } \Omega_l^{j+1}. \end{aligned} \tag{4.22}$$

4.2.1 Newton algorithm to approximate the viscoplastic multiplier

In order to introduce a Newton algorithm to approximate the viscoplastic multiplier, in this section, we consider $\gamma_p = 0$ and $\lambda_p > 0$ a real positive number in Proposition 3.5.7 and Lemma 3.5.8. Therefore, we obtain the following expression for the stress tensor in $\Omega_s(t^{j+1})$:

$$\boldsymbol{\sigma}^{j+1} = (\Lambda_s(T^{j+1}))^{-1} \left(\boldsymbol{\varepsilon}(\mathbf{u}^{j+1}) - \Delta t \mathbf{q}^{j+1} + \mathbf{F}^j\right), \tag{4.23}$$

where

$$\mathbf{F}^j = -\boldsymbol{\varepsilon}(\mathbf{u}^j) + \Lambda_s(T^j)\boldsymbol{\sigma}^j - \alpha_s(T^{j+1})(T^{j+1} - T^j)\mathbf{I}, \tag{4.24}$$

is the history of the solidified metal up to time t^j and the viscoplastic multiplier $\mathbf{q}^{j+1}$ verifies

$$\mathbf{q}^{j+1} = (\nabla\Phi_q)_{\lambda_p}\left(\left(\boldsymbol{\sigma}^{j+1}\right)^D + \lambda_p\mathbf{q}^{j+1}\right), \tag{4.25}$$

being

$$(\nabla\Phi_q)_{\lambda_p}(\boldsymbol{\zeta}) = \frac{1}{\lambda_p}\left(1 - \frac{1}{\eta^{j+1}}\right)\boldsymbol{\zeta}, \tag{4.26}$$

where $\eta^{j+1} = \eta(\boldsymbol{\zeta})$ is the unique root of the equation

$$\eta^{q-1} - \eta^{q-2} - \lambda_p\theta(T^{j+1})|\boldsymbol{\zeta}|^{q-2} = 0, \tag{4.27}$$

in the interval $[1, +\infty)$.

Remark 4.2.1. *Since $\nabla\Phi_q$ is a maximal monotone operator, $(\nabla\Phi_q)_{\lambda_p}$ is contractive for $\lambda_p > 1$ (see [16, 26, 86]). Then, the fixed point of (4.25) is unique.*

In order to couple the two nonlinearities due to the contact condition and the constitutive law in casting processes, a key component of our procedure must be that the stiffness matrix is preserved and we do not need to recalculate it at each iteration. At the same time we wish to achieve the efficiency of Newton techniques. To this end, assuming that the stress tensor is known, we linearize the equation (4.25) to obtain an approximation of the viscoplastic multiplier.

Lemma 4.2.2. *Given any $\boldsymbol{\sigma} \in \mathcal{S}_3$ and $\lambda_p > 1$, the fixed point $\mathbf{q} \in \mathcal{S}_3$ of the equation*

$$\mathbf{q} = (\nabla\Phi_q)_{\lambda_p}\left(\boldsymbol{\sigma}^D + \lambda_p\mathbf{q}\right), \tag{4.28}$$

can be approximated by

$$\mathbf{q} \cong (\nabla\Phi_q)_{\lambda_p}(\boldsymbol{\sigma}^D + \lambda_p\hat{\mathbf{q}}) + \left(1 - \frac{1}{\eta}\right)(\mathbf{q} - \hat{\mathbf{q}}) + \bar{\eta}\left(\left(\boldsymbol{\sigma}^D + \lambda_p\hat{\mathbf{q}}\right) : (\mathbf{q} - \hat{\mathbf{q}})\right)\left(\boldsymbol{\sigma}^D + \lambda_p\hat{\mathbf{q}}\right), \tag{4.29}$$

for $\hat{\mathbf{q}} \in \mathcal{S}_3$ close enough to $\mathbf{q}$ and provided that $\boldsymbol{\sigma}^D + \lambda_p\hat{\mathbf{q}} \neq \mathbf{0}$. Here $\eta = \eta\left(\boldsymbol{\sigma}^D + \lambda_p\hat{\mathbf{q}}\right)$, and $\bar{\eta}$ is given by the expression

$$\bar{\eta} = \frac{(q-2)(\eta-1)}{\eta\left((q-1)\eta - (q-2)\right)|\boldsymbol{\sigma}^D + \lambda_p\hat{\mathbf{q}}|^2}. \tag{4.30}$$

The order of this approximation is $O\left(|\mathbf{q} - \hat{\mathbf{q}}|^2\right)$.

Proof. Since $(\nabla\Phi_q)_{\lambda_p}(\boldsymbol{\xi})$ is twice-differentiable for $\boldsymbol{\xi} \neq \mathbf{0}$, we can apply Taylor's formula to approximate $\mathbf{q}$. Then, for $\hat{\mathbf{q}} \in \mathcal{S}_3$ close enough, if $\boldsymbol{\sigma}^D + \lambda_p\hat{\mathbf{q}} \neq \mathbf{0}$, we obtain from (4.28)

$$\mathbf{q} = (\nabla\Phi_q)_{\lambda_p}(\boldsymbol{\sigma}^D + \lambda_p\hat{\mathbf{q}}) + D(\nabla\Phi_q)_{\lambda_p}(\boldsymbol{\sigma}^D + \lambda_p\hat{\mathbf{q}})(\lambda_p(\mathbf{q} - \hat{\mathbf{q}})) + O\left(|\mathbf{q} - \hat{\mathbf{q}}|^2\right). \tag{4.31}$$

From expression (4.26) we deduce that

$$D\left(\nabla\Phi_q\right)_{\lambda_p}(\boldsymbol{\tau})(\boldsymbol{\xi}) = \frac{\boldsymbol{\xi}}{\lambda_p}\left(1-\frac{1}{\eta(\boldsymbol{\tau})}\right) + \frac{\boldsymbol{\tau}}{\lambda_p}\frac{D\eta(\boldsymbol{\tau})(\boldsymbol{\xi})}{\eta(\boldsymbol{\tau})^2}, \quad \forall \boldsymbol{\tau},\boldsymbol{\xi}\in\mathcal{S}_3. \tag{4.32}$$

Deriving implicitly with respect to $\boldsymbol{\xi}$ in expression (4.27),

$$D\eta(\boldsymbol{\tau})(\boldsymbol{\xi}) = \frac{\lambda_p\theta(T)(q-2)|\boldsymbol{\tau}|^{q-4}}{(q-1)\eta(\boldsymbol{\tau})^{q-2}-(q-2)\eta(\boldsymbol{\tau})^{q-3}}(\boldsymbol{\tau}:\boldsymbol{\xi}),\ \forall\boldsymbol{\tau},\boldsymbol{\xi}\in\mathcal{S}_3. \tag{4.33}$$

From (4.32) and (4.33),

$$D\left(\nabla\Phi_q\right)_{\lambda_p}(\boldsymbol{\tau})(\boldsymbol{\xi}) = \frac{\boldsymbol{\xi}}{\lambda_p}\left(1-\frac{1}{\eta(\boldsymbol{\tau})}\right) + \frac{\theta(T)(q-2)|\boldsymbol{\tau}|^{q-4}(\boldsymbol{\tau}:\boldsymbol{\xi})}{(q-1)\eta(\boldsymbol{\tau})^{q}-(q-2)\eta(\boldsymbol{\tau})^{q-1}}\boldsymbol{\tau}.$$

Therefore, from (4.31),

$$\begin{aligned}\mathbf{q} = &\left(\nabla\Phi_q\right)_{\lambda_p}\left(\boldsymbol{\sigma}^D+\lambda_p\hat{\mathbf{q}}\right) + \left(1-\frac{1}{\eta}\right)\left(\mathbf{q}-\hat{\mathbf{q}}\right) + \\ &\bar{\eta}\left(\left(\boldsymbol{\sigma}^D+\lambda_p\hat{\mathbf{q}}\right):\left(\mathbf{q}-\hat{\mathbf{q}}\right)\right)\left(\boldsymbol{\sigma}^D+\lambda_p\hat{\mathbf{q}}\right) + O\left(|\mathbf{q}-\hat{\mathbf{q}}|^2\right),\end{aligned}$$

where $\eta = \eta\left(\boldsymbol{\sigma}^D+\lambda_p\hat{\mathbf{q}}\right)$ and

$$\bar{\eta} = \frac{\lambda_p\theta(T)\left(q-2\right)\left|\boldsymbol{\sigma}^D+\lambda_p\hat{\mathbf{q}}\right|^{q-4}}{\left(q-1\right)\eta^q-\left(q-2\right)\eta^{q-1}}.$$

Taking into account expression (4.27), we can simplify the expression for $\bar{\eta}$ in the following form:

$$\begin{aligned}\bar{\eta} &= \frac{\lambda_p\theta(T)\left(q-2\right)\left|\boldsymbol{\sigma}^D+\lambda_p\hat{\mathbf{q}}\right|^{q-4}}{\left(q-1\right)\eta^q-\left(q-2\right)\eta^{q-1}} = \frac{\left(q-2\right)\left|\boldsymbol{\sigma}^D+\lambda_p\hat{\mathbf{q}}\right|^{-2}(\eta^{q-1}-\eta^{q-2})}{\left(q-1\right)\eta^q-\left(q-2\right)\eta^{q-1}} = \\ &= \frac{\left(q-2\right)\left(\eta-1\right)}{\eta\left(\left(q-1\right)\eta-\left(q-2\right)\right)\left|\boldsymbol{\sigma}^D+\lambda_p\hat{\mathbf{q}}\right|^2},\end{aligned}$$

and therefore, expression (4.30) is obtained. A detailed explanation of this procedure can be found in [73]. □

Remark 4.2.3. *The case* $\boldsymbol{\sigma}^D+\lambda_p\hat{\mathbf{q}}=\mathbf{0}$ *was excluded from Lemma 4.2.2 since from equation (4.25), if* $\boldsymbol{\sigma}^D+\lambda_p\mathbf{q}=\mathbf{0}$*, then* $\mathbf{q}=\mathbf{0}$ *is the fixed point.*

Summing up, if we replace expression (4.23) in equality (3.16) at time step t^{j+1}, we obtain a variational formulation in displacements of our problem. So, we propose the following iterative algorithm:

At each time step t^{j+1}, given the starting values $(\mathbf{u}_0^{j+1},\boldsymbol{\sigma}_0^{j+1},\mathbf{q}_0^{j+1})$, successive approximations $(\mathbf{u}_k^{j+1},\boldsymbol{\sigma}_k^{j+1},\mathbf{q}_k^{j+1})$, $k\geq 1$, of the solution $(\mathbf{u}^{j+1},\boldsymbol{\sigma}^{j+1},\mathbf{q}^{j+1})$ can be computed by using the recurrence formulas:

$$\begin{aligned}&\int_{\Omega_s^{j+1}}\left(\Lambda_s(T^{j+1})\right)^{-1}\boldsymbol{\varepsilon}(\mathbf{u}_k^{j+1}):\boldsymbol{\varepsilon}(\mathbf{v})dx + \int_{\Omega_l^{j+1}}\Lambda_l^{-1}\boldsymbol{\varepsilon}(\mathbf{u}_k^{j+1}):\boldsymbol{\varepsilon}(\mathbf{v})dx = \\ &\int_{\Omega_s^{j+1}}\left(\Lambda_s(T^{j+1})\right)^{-1}\left(\Delta t\mathbf{q}_{k-1}^{j+1}\right):\boldsymbol{\varepsilon}(\mathbf{v})dx - \int_{\Omega_s^{j+1}}\left(\Lambda_s(T^{j+1})\right)^{-1}\mathbf{F}^j:\boldsymbol{\varepsilon}(\mathbf{v})dx + \\ &\int_{\Omega^{j+1}}\mathbf{f}^{j+1}\cdot\mathbf{v}dx\ \forall\mathbf{v}\in\mathbf{U}_{ad_h}(t^{j+1}),\end{aligned} \tag{4.34}$$

where $\mathbf{F}^j$ is given by expression (4.24).

The stress tensor and the viscoplastic multiplier are updated by the following expressions:

$$\boldsymbol{\sigma}_k^{j+1} = \begin{cases} \left(\Lambda_s(T^{j+1})\right)^{-1}\left(\boldsymbol{\varepsilon}(\mathbf{u}_k^{j+1}) - \Delta t\mathbf{q}_{k-1}^{j+1} + \mathbf{F}^j\right) & \text{in } \Omega_s^{j+1}, \\ \\ \Lambda_l^{-1}\boldsymbol{\varepsilon}(\mathbf{u}_k^{j+1}) & \text{in } \Omega_l^{j+1}, \end{cases} \tag{4.35}$$

$$\mathbf{q}_k^{j+1} = \begin{cases} \mathbf{0}, & \text{if } \boldsymbol{\kappa}_k^{j+1} = \mathbf{0}, \\ \\ (\nabla\Phi_q)_{\lambda_p}(\boldsymbol{\kappa}_k^{j+1}) + \left(1 - \frac{1}{\eta_k^{j+1}}\right)\left(\mathbf{q}_k^{j+1} - \mathbf{q}_{k-1}^{j+1}\right) & \\ \quad + \bar{\eta}_k^{j+1}\left(\boldsymbol{\kappa}_k^{j+1} : (\mathbf{q}_k^{j+1} - \mathbf{q}_{k-1}^{j+1})\right)\boldsymbol{\kappa}_k^{j+1}, & \text{if } \boldsymbol{\kappa}_k^{j+1} \neq \mathbf{0}, \end{cases} \tag{4.36}$$

in Ω_s^{j+1}, where

$$\boldsymbol{\kappa}_k^{j+1} = \left(\boldsymbol{\sigma}_k^{j+1}\right)^D + \lambda_p\,\mathbf{q}_{k-1}^{j+1}, \tag{4.37}$$

and $\bar{\eta}_k^{j+1}$ is given by

$$\bar{\eta}_k^{j+1} = \frac{(q-2)\left(\eta_k^{j+1} - 1\right)}{\eta_k^{j+1}\left((q-1)\,\eta_k^{j+1} - (q-2)\right)|\boldsymbol{\kappa}_k^{j+1}|^2}, \tag{4.38}$$

for $\eta_k^{j+1} = \eta(\boldsymbol{\kappa}_k^{j+1})$.

The fixed point of (4.36) can be explicitly computed thanks to the following lemma.

Lemma 4.2.4. *At each time step t^{j+1}, $j = 0, \ldots, N-1$, and at each iteration $k > 0$, the fixed point $\mathbf{q}_k^{j+1}$ of equation (4.36) can be computed using the recurrence formula*

$$\mathbf{q}_k^{j+1} = \begin{cases} \mathbf{0}, & \textit{if } \boldsymbol{\kappa}_k^{j+1} = \mathbf{0}, \\ \\ \dfrac{\left(\eta_k^{j+1} - 1\right)}{\lambda_p}\left(\left(\boldsymbol{\sigma}_k^{j+1}\right)^D + \left(\eta_k^{j+1} - 1\right)\dfrac{q-2}{\eta_k^{j+1}}\boldsymbol{\kappa}_k^{j+1}\right) & \\ \quad - \left(\eta_k^{j+1} - 1\right)\dfrac{q-2}{|\boldsymbol{\kappa}_k^{j+1}|^2}\left(\mathbf{q}_{k-1}^{j+1} : \boldsymbol{\kappa}_k^{j+1}\right)\boldsymbol{\kappa}_k^{j+1}, & \textit{if } \boldsymbol{\kappa}_k^{j+1} \neq \mathbf{0}, \end{cases} \tag{4.39}$$

in $\Omega_s(t^{j+1})$, where $\boldsymbol{\kappa}_k^{j+1}$ is given by (4.37) and $\eta_k^{j+1} = \eta\left(\boldsymbol{\kappa}_k^{j+1}\right)$.

Proof. Let us consider $\boldsymbol{\kappa}_k^{j+1} \neq \mathbf{0}$. Taking into account the expression of $(\nabla\Phi_q)_{\lambda_p}$ given by (4.26), we obtain from (4.36) the equality

$$\mathbf{q}_k^{j+1} = \left(1 - \frac{1}{\eta_k^{j+1}}\right)\left(\frac{1}{\lambda_p}\boldsymbol{\kappa}_k^{j+1} + \left(\mathbf{q}_k^{j+1} - \mathbf{q}_{k-1}^{j+1}\right)\right) + \bar{\eta}_k^{j+1}\left(\boldsymbol{\kappa}_k^{j+1} : \left(\mathbf{q}_k^{j+1} - \mathbf{q}_{k-1}^{j+1}\right)\right)\boldsymbol{\kappa}_k^{j+1}, \tag{4.40}$$

where $\bar{\eta}_k^{j+1}$ is given by (4.38). In order to obtain an explicit expression for $\mathbf{q}_k^{j+1}$, we multiply equation (4.40) by $\boldsymbol{\kappa}_k^{j+1}$:

$$\begin{aligned}\left(\mathbf{q}_k^{j+1} : \boldsymbol{\kappa}_k^{j+1}\right) &= \left(1-\frac{1}{\eta_k^{j+1}}\right)\left(\frac{1}{\lambda_p}|\boldsymbol{\kappa}_k^{j+1}|^2 + (\mathbf{q}_k^{j+1}-\mathbf{q}_{k-1}^{j+1} : \boldsymbol{\kappa}_k^{j+1})\right)\\ &\quad +\bar{\eta}_k^{j+1}\left(\boldsymbol{\kappa}_k^{j+1}:\mathbf{q}_k^{j+1}-\mathbf{q}_{k-1}^{j+1}\right)|\boldsymbol{\kappa}_k^{j+1}|^2\\ &= \left(1-\frac{1}{\eta_k^{j+1}}\right)\frac{1}{\lambda_p}|\boldsymbol{\kappa}_k^{j+1}|^2 - \left(1-\frac{1}{\eta_k^{j+1}}+\bar{\eta}_k^{j+1}|\boldsymbol{\kappa}_k^{j+1}|^2\right)(\mathbf{q}_{k-1}^{j+1} : \boldsymbol{\kappa}_k^{j+1})\\ &\quad +\left(1-\frac{1}{\eta_k^{j+1}}+\bar{\eta}_k^{j+1}|\boldsymbol{\kappa}_k^{j+1}|^2\right)(\mathbf{q}_k^{j+1} : \boldsymbol{\kappa}_k^{j+1}).\end{aligned}$$

This allows us to rewrite $\left(\mathbf{q}_k^{j+1} : \boldsymbol{\kappa}_k^{j+1}\right)$ as

$$\left(\mathbf{q}_k^{j+1} : \boldsymbol{\kappa}_k^{j+1}\right) = \chi_k^{j+1}\left(1-\frac{1}{\eta_k^{j+1}}\right)\frac{|\boldsymbol{\kappa}_k^{j+1}|^2}{\lambda_p} - \chi_k^{j+1}\left(1-\frac{1}{\eta_k^{j+1}}+\bar{\eta}_k^{j+1}|\boldsymbol{\kappa}_k^{j+1}|^2\right)\left(\mathbf{q}_{k-1}^{j+1} : \boldsymbol{\kappa}_k^{j+1}\right), \tag{4.41}$$

where

$$\chi_k^{j+1} = \frac{\eta_k^{j+1}}{1-\eta_k^{j+1}\bar{\eta}_k^{j+1}|\boldsymbol{\kappa}_k^{j+1}|^2}.$$

Taking into account the definition of $\bar{\eta}_k^{j+1}$,

$$\chi_k^{j+1} = \frac{\eta_k^{j+1}}{1-\frac{(q-2)(\eta_k^{j+1}-1)}{(q-1)\eta_k^{j+1}-(q-2)}} = (q-1)\eta_k^{j+1}-(q-2),$$

and we deduce that

$$\chi_k^{j+1} = (q-1)\eta_k^{j+1}-(q-2). \tag{4.42}$$

Besides, by doing simple calculations, we have that

$$\begin{aligned}\chi_k^{j+1}\left(1-\frac{1}{\eta_k^{j+1}}+\bar{\eta}_k^{j+1}|\boldsymbol{\kappa}_k^{j+1}|^2\right) &= \frac{\eta_k^{j+1}}{1-\eta_k^{j+1}\bar{\eta}_k^{j+1}|\boldsymbol{\kappa}_k^{j+1}|^2}\left(1-\frac{1}{\eta_k^{j+1}}+\bar{\eta}_k^{j+1}|\boldsymbol{\kappa}_k^{j+1}|^2\right) =\\ = \frac{\eta_k^{j+1}-1+\eta_k^{j+1}\bar{\eta}_k^{j+1}|\boldsymbol{\kappa}_k^{j+1}|^2}{1-\eta_k^{j+1}\bar{\eta}_k^{j+1}|\boldsymbol{\kappa}_k^{j+1}|^2} &= -\frac{1-\eta_k^{j+1}-\eta_k^{j+1}\bar{\eta}_k^{j+1}|\boldsymbol{\kappa}_k^{j+1}|^2}{1-\eta_k^{j+1}\bar{\eta}_k^{j+1}|\boldsymbol{\kappa}_k^{j+1}|^2} = -(1-\chi_k^{j+1}).\end{aligned}$$

Thus, expression (4.41) remains

$$\left(\mathbf{q}_k^{j+1} : \boldsymbol{\kappa}_k^{j+1}\right) = \chi_k^{j+1}\left(1-\frac{1}{\eta_k^{j+1}}\right)\frac{|\boldsymbol{\kappa}_k^{j+1}|^2}{\lambda_p} + \left(\mathbf{q}_{k-1}^{j+1} : \boldsymbol{\kappa}_k^{j+1}\right)\left(1-\chi_k^{j+1}\right).$$

Replacing this expression in equation (4.40) we deduce that

$$\mathbf{q}_k^{j+1} = \left(1-\frac{1}{\eta_k^{j+1}}\right)\left(\frac{1}{\lambda_p}\boldsymbol{\kappa}_k^{j+1} + \left(\mathbf{q}_k^{j+1}-\mathbf{q}_{k-1}^{j+1}\right)\right) - \bar{\eta}_k^{j+1}\left(\boldsymbol{\kappa}_k^{j+1}\colon \mathbf{q}_{k-1}^{j+1}\right)\boldsymbol{\kappa}_k^{j+1} + \bar{\eta}_k^{j+1}\left\{\chi_k^{j+1}\left(1-\frac{1}{\eta_k^{j+1}}\right)\frac{|\boldsymbol{\kappa}_k^{j+1}|^2}{\lambda_p} + \left(\mathbf{q}_{k-1}^{j+1} : \boldsymbol{\kappa}_k^{j+1}\right)\left(1-\chi_k^{j+1}\right)\right\}\boldsymbol{\kappa}_k^{j+1}.$$

So, the updated viscoplastic multiplier is characterized by the explicit expression

$$\begin{aligned}\mathbf{q}_k^{j+1} &= \frac{\left(\eta_k^{j+1}-1\right)}{\lambda_p}\left(\boldsymbol{\sigma}_k^{j+1}\right)^D - \eta_k^{j+1}\bar{\eta}_k^{j+1}\left(\boldsymbol{\kappa}_k^{j+1}\colon \mathbf{q}_{k-1}^{j+1}\right)\boldsymbol{\kappa}_k^{j+1} \\ &\quad + \bar{\eta}_k^{j+1}\left\{\chi_k^{j+1}\left(\eta_k^{j+1}-1\right)\frac{|\boldsymbol{\kappa}_k^{j+1}|^2}{\lambda_p} + \left(\mathbf{q}_{k-1}^{j+1} : \boldsymbol{\kappa}_k^{j+1}\right)\eta_k^{j+1}\left(1-\chi_k^{j+1}\right)\right\}\boldsymbol{\kappa}_k^{j+1} \\ &= \frac{\left(\eta_k^{j+1}-1\right)}{\lambda_p}\left(\left(\boldsymbol{\sigma}_k^{j+1}\right)^D + \bar{\eta}_k^{j+1}\chi_k^{j+1}|\boldsymbol{\kappa}_k^{j+1}|^2\boldsymbol{\kappa}_k^{j+1}\right) - \eta_k^{j+1}\bar{\eta}_k^{j+1}\chi_k^{j+1}\left(\mathbf{q}_{k-1}^{j+1} : \boldsymbol{\kappa}_k^{j+1}\right)\boldsymbol{\kappa}_k^{j+1}.\end{aligned}$$

Finally, taking into account expressions (4.38) and (4.42) we obtain formula (4.39) to update the viscoplastic multiplier. □

Newton algorithm to solve the viscoplastic problem

Summing up, the proposed algorithm to solve Problem (3.16)-(3.18) is:

- Let $(\mathbf{u}_0, \boldsymbol{\sigma}_0)$ be given; we compute $\mathbf{q}^0 = \nabla\Phi_q(\boldsymbol{\sigma}_0^D)$.
- Then, for $j \geq 0$, $(\mathbf{u}^j,\ \boldsymbol{\sigma}^j,\ \mathbf{q}^j)$ known at time t^j, we determine $(\mathbf{u}^{j+1}, \boldsymbol{\sigma}^{j+1},\ \mathbf{q}^{j+1})$ at time t^{j+1}, an approximated weak solution of Problem (3.16)-(3.18). To do so, we propose the following iterative algorithm:

  i) Given $(\mathbf{u}_{k-1}^{j+1}, \boldsymbol{\sigma}_{k-1}^{j+1}, \mathbf{q}_{k-1}^{j+1})$, we compute $(\mathbf{u}_k^{j+1}, \boldsymbol{\sigma}_k^{j+1}) \in \mathbf{U}_{ad_h}(t^{j+1}) \times \mathbf{H}_h(t^{j+1})$ by solving the variational equality

$$\int_{\Omega_s^{j+1}} \left(\Lambda_s(T^{j+1})\right)^{-1}\boldsymbol{\varepsilon}(\mathbf{u}_k^{j+1}) : \boldsymbol{\varepsilon}(\mathbf{v})dx + \int_{\Omega_l^{j+1}} \Lambda_l^{-1}\boldsymbol{\varepsilon}(\mathbf{u}_k^{j+1}) : \boldsymbol{\varepsilon}(\mathbf{v})dx = \int_{\Omega_s^{j+1}} \left(\Lambda_s(T^{j+1})\right)^{-1}\left(\Delta t\mathbf{q}_{k-1}^{j+1}\right) : \boldsymbol{\varepsilon}(\mathbf{v})dx - \int_{\Omega_s^{j+1}} \left(\Lambda_s(T^{j+1})\right)^{-1}\mathbf{F}^j : \boldsymbol{\varepsilon}(\mathbf{v})dx + \int_{\Omega^{j+1}} \mathbf{f}^{j+1}\cdot\mathbf{v}dx,\ \forall\mathbf{v} \in \mathbf{U}_{ad_h}(t^{j+1}),$$

  where

$$\mathbf{F}^j = \Lambda_s(T^j)\boldsymbol{\sigma}^j - \boldsymbol{\varepsilon}(\mathbf{u}^j) - \alpha_s(T^{j+1})(T^{j+1}-T^j)\mathbf{I} \text{ in } \Omega_s^{j+1},$$

and

$$\boldsymbol{\sigma}_k^{j+1} = \begin{cases} \left(\Lambda_s(T^{j+1})\right)^{-1}\left(\boldsymbol{\varepsilon}(\mathbf{u}_k^{j+1}) - \Delta t \mathbf{q}_{k-1}^{j+1} + \mathbf{F}^j\right) & \text{in } \Omega_s^{j+1}, \\ \Lambda_l^{-1}\boldsymbol{\varepsilon}(\mathbf{u}_k^{j+1}) & \text{in } \Omega_l^{j+1}. \end{cases}$$

ii) The updated viscoplastic multiplier is given by relation (4.39).

Adimensionalization technique

Due to the large thermal gradients that appear in the ingot during casting, sometimes convergence is not achieved when using the Newton algorithm described above to simulate Problem (3.16)-(3.18), as we will show in Section 5.2. To solve this unexpected difficulty, we propose to employ an adimensionalization technique on the stresses. This technique consists of choosing a reference stress and introducing new nondimensional unknowns in order to transfer the magnitude of the stresses to the coefficients of the behaviour law (3.17) to solve a similar problem for these new unknowns.

Let η and $\delta > 0$, such that $\eta^{-\delta}$ is the size of reference stress; let introduce the new nondimensional unknown

$$\boldsymbol{\sigma}_\delta(\mathbf{x}, t) = \eta^\delta \boldsymbol{\sigma}(\mathbf{x}, t).$$

For the displacement and the temperature fields we consider:

$$\mathbf{u}_\delta(\mathbf{x}, t) = \mathbf{u}(\mathbf{x}, t),\ T_\delta(\mathbf{x}, t) = T(\mathbf{x}, t).$$

The new mechanical coefficients considered in $\Omega_s(t)$ are

$$\Lambda_s^\xi(T_\delta) = \eta^\xi \Lambda_s(T_\delta),\ \theta^\beta(T_\delta) = \eta^\beta \theta(T_\delta),$$

where ξ and β must be calculated in order to obtain the same solution when the problem is formulated in terms of these new unknowns and coefficients. In particular:

- Behaviour law: $\mathbf{u}_\delta$, $\boldsymbol{\sigma}_\delta$ and T_δ must verify

$$\boldsymbol{\varepsilon}(\dot{\mathbf{u}}_\delta) = \overset{\cdot}{\overbrace{(\Lambda_s^\xi(T_\delta)\boldsymbol{\sigma}_\delta)}} + \theta^\beta(T_\delta)|\boldsymbol{\sigma}_\delta^D|^{q-2}\boldsymbol{\sigma}_\delta^D + (\alpha_s(T_\delta)\dot{T}_\delta)\mathbf{I},\ \text{in } \Omega_s(t).$$

For this reason, the following expression must be satisfied:

$$\overset{\cdot}{\overbrace{(\Lambda_s(T)\boldsymbol{\sigma})}} + \theta(T)|\boldsymbol{\sigma}^D|^{q-2}\boldsymbol{\sigma}^D + (\alpha_s(T)\dot{T})\mathbf{I} =$$
$$\eta^{-(\xi+\delta)}\overset{\cdot}{\overbrace{(\Lambda_s^\xi(T_\delta)\boldsymbol{\sigma}_\delta)}} + \eta^{-\beta-\delta(q-1)}\theta^\beta(T_\delta)|\boldsymbol{\sigma}_\xi^D|^{q-2}\boldsymbol{\sigma}_\xi^D + (\alpha_s(T_\delta)\dot{T}_\delta)\mathbf{I},$$

in $\Omega_s(t)$, which implies that we must take $\xi = -\delta$ and $\beta = -\delta(q-1)$.

The same procedure is also applied to the behaviour law in the liquid domain $\Omega_l(t)$:

$$\boldsymbol{\varepsilon}(\dot{\mathbf{u}}_\delta) = \Lambda_l^{-\delta}\dot{\boldsymbol{\sigma}}_\delta,\ \Lambda_l^{-\delta} = \eta^{-\delta}\Lambda_l.$$

- Equilibrium equation: $\boldsymbol{\sigma}_\delta$ verifies

$$-\mathrm{div}(\boldsymbol{\sigma}_\delta) = \mathbf{f}_\delta \text{ in } \Omega(t),$$

  if we consider the scaling down on the volume force $\mathbf{f}_\delta = \eta^\delta \mathbf{f}$.

- Boundary conditions: It is clear that $\mathbf{u}_\delta$ and $\boldsymbol{\sigma}_\delta$ verify the corresponding boundary conditions.

- Initial conditions: $\mathbf{u}_\delta$ and $\boldsymbol{\sigma}_\delta$ verify

$$\mathbf{u}_\delta(x,0) = \mathbf{u}_{0_\delta}(x), \;\; \boldsymbol{\sigma}_\delta(x,0) = \boldsymbol{\sigma}_{0_\delta}(x) \text{ in } \Omega(0),$$

  if we consider the scaling down on the initial data $\mathbf{u}_{0_\delta} = \mathbf{u}_0$, $\boldsymbol{\sigma}_{0_\delta} = \eta^\delta \boldsymbol{\sigma}_0$.

Summing up, the adimensionalized model, corresponding to Problem (3.16)-(3.18), to solve is

$$\left.\begin{array}{rcl}
-\mathrm{div}(\boldsymbol{\sigma}_\delta) = \mathbf{f}_\delta & \text{in} & \Omega(t), \\
\boldsymbol{\sigma}_\delta \mathbf{n} = \mathbf{0} & \text{on} & \Gamma_n^1(t), \\
(\boldsymbol{\sigma}_\delta)_t = \mathbf{0}, \; (u_\delta)_n = 0 & \text{on} & \Gamma_n^2(t) \cup \Gamma_{sym}(t) \cup \Gamma_l(t), \\
\mathbf{u}_\delta = \mathbf{0} & \text{on} & \Gamma_C, \\
\boldsymbol{\varepsilon}(\dot{\mathbf{u}}_\delta) = \dot{\overbrace{(\Lambda_s^{-\delta}(T_\delta)\boldsymbol{\sigma}_\delta)}} + \theta^{-\delta(q-1)}(T_\delta)|\boldsymbol{\sigma}_\delta^D|^{q-2}\boldsymbol{\sigma}_\delta^D + (\alpha_s(T_\delta)\dot{T}_\delta)\mathbf{I} & \text{in} & \Omega_s(t), \\
\boldsymbol{\varepsilon}(\dot{\mathbf{u}}_\delta) = \Lambda_l^{-\delta}\dot{\boldsymbol{\sigma}}_\delta & \text{in} & \Omega_l(t), \\
\mathbf{u}_\delta(x,0) = \mathbf{u}_{0_\delta}(x), \;\; \boldsymbol{\sigma}_\delta(x,0) = \boldsymbol{\sigma}_{0_\delta}(x) & \text{in} & \Omega(0).
\end{array}\right\}$$

Optimization of the time step and Armijo rule

Newton method is known to be an efficient method, but, unfortunately, in time-dependent problems, it is necessary to use a very small time step discretization. Since the time interval of interest in casting processes is about 150s to reproduce the butt curl deformation, if we want to apply Newton algorithm we should be able to increase the used time step. To solve this problem, we propose to use an optimization technique on the time step in such a way that, given Δt fixed, if convergence is not achieved, the time step is automatically reduced until the algorithm converges. When the convergence is stabilized, the time step is again automatically increased.

Furthermore, to stabilize the Newton method we employ an Armijo rule on the computation of the viscoplastic multiplier (see [20]) which consists of the following: Since the viscoplastic multiplier $\mathbf{q}^{j+1}$ is the fixed point of the equation (4.28) we define the error function

$$E(\mathbf{q}^{j+1}) = \left| \mathbf{q}^{j+1} - (\nabla \Phi_q)_{\lambda_p} \left(\left(\boldsymbol{\sigma}^{j+1}\right)^D + \lambda_p \mathbf{q}^{j+1} \right) \right|^2.$$

So, for the time step t^{j+1}, given two successive iterants $\mathbf{q}_k^{j+1}, \mathbf{q}_{k+1}^{j+1}$, we distinguish the two following possibilities:

- If $E(\mathbf{q}_{k+1}^{j+1}) \leq E(\mathbf{q}_k^{j+1})$, the algorithm works well.

- If $E(\mathbf{q}_{k+1}^{j+1}) > E(\mathbf{q}_k^{j+1})$, $\mathbf{q}_{k+1}^{j+1}$ moves far away from the fixed point. Then, by using an Armijo rule, we look for a constant ς such that

$$E(\mathbf{q}_k^{j+1} + \varsigma(\mathbf{q}_{k+1}^{j+1} - \mathbf{q}_k^{j+1})) \leq E(\mathbf{q}_k^{j+1}). \tag{4.43}$$

For that purpose, let us define

$$\phi(\varsigma) = E(\mathbf{q}_k^{j+1} + \varsigma(\mathbf{q}_{k+1}^{j+1} - \mathbf{q}_k^{j+1})), \quad \varsigma \in [0,1].$$

Then, from (4.43), ς must verify

$$\phi(\varsigma) < \phi(0).$$

Given $s > 0$, $\beta \in (0,1)$ and $m \in (0,1)$, the Armijo rule consists of choosing

$$\varsigma_n = \beta^{r_n} s,$$

where r_n is the first nonnegative integer such that

$$\phi(\varsigma_n) < \phi(0) + m\,\varsigma_n\,\phi'(0).$$

4.2.2 Bermúdez-Moreno algorithm with variable parameters to approximate the viscoplastic multiplier

As we will see in Chapter 5, numerical results in academic tests show that the previous combination of the Newton algorithm with the adimensionalization technique and the optimization of the time step works well in academic examples. Nevertheless, we find difficulties to achieve convergence in the real casting simulation. In these simulations, large thermal gradients appear, producing great variations in the viscoplastic multiplier. In this Section we propose to take advantage of the robustness of the method introduced in Section 3.5.4 and to improve it with the methodology proposed in [43, 67]. For this purpose, since the performance of the first algorithm strongly depends on the choice of the two constant parameters λ_p, γ_p, and the viscoplastic behaviour varies strongly depending if an element is recently solidified or not, we propose to replace the constant parameters by scalar functions depending on time and space.

Therefore, in this section, we consider that γ_p, λ_p are functions from $\Omega \times (0, t_f)$ to $\mathbb{R}$ and we propose the following algorithm, obtained when considering these modifications in that presented in Section 3.5.4:

At each time step t^{j+1}, given γ_p^j, λ_p^j and the starting values $(\mathbf{u}_0^{j+1}, \boldsymbol{\sigma}_0^{j+1}, \mathbf{q}_0^{j+1})$, successive approximations $(\mathbf{u}_k^{j+1}, \boldsymbol{\sigma}_k^{j+1}, \mathbf{q}_k^{j+1})$, $k \geq 1$, of the solution $(\mathbf{u}^{j+1}, \boldsymbol{\sigma}^{j+1}, \mathbf{q}^{j+1})$ can be computed by using the recurrence formulas:

$$\int_{\Omega_s^{j+1}} \mathcal{V}(T^{j+1}) \left[\boldsymbol{\varepsilon}(\mathbf{u}_k^{j+1}) + \frac{\Delta t \gamma_p^j s^{j+1}}{3} \mathrm{tr}(\boldsymbol{\varepsilon}(\mathbf{u}_k^{j+1}))\mathbf{I} \right] : \boldsymbol{\varepsilon}(\mathbf{v}) dx + \int_{\Omega_l^{j+1}} \Lambda_l^{-1} \boldsymbol{\varepsilon}(\mathbf{u}_k^{j+1}) : \boldsymbol{\varepsilon}(\mathbf{v}) dx =$$
$$\int_{\Omega_s^{j+1}} \left[\mathcal{V}(T^{j+1}) \Delta t \mathbf{q}_{k-1}^{j+1} \right] : \boldsymbol{\varepsilon}(\mathbf{v}) dx - \int_{\Omega_s^{j+1}} \left[\mathcal{V}(T^{j+1}) \mathbf{F}^j \right] : \boldsymbol{\varepsilon}(\mathbf{v}) dx +$$
$$\int_{\Omega^{j+1}} \mathbf{f}^{j+1} \cdot \mathbf{v} dx \ \forall \mathbf{v} \in \mathbf{U}_{ad_h}(t^{j+1}), \tag{4.44}$$

where

$$\mathbf{F}^j = -\boldsymbol{\varepsilon}(\mathbf{u}^j) + \Lambda_s(T^j)\boldsymbol{\sigma}^j - \alpha_s(T^{j+1})(T^{j+1}-T^j)\left(1+\Delta t\gamma_p^j s^{j+1}\right)\mathbf{I} + \frac{\Delta t\gamma_p^j s^{j+1}}{3}\left(\frac{1}{s^j}\mathrm{tr}(\boldsymbol{\sigma}^j) - \mathrm{tr}(\boldsymbol{\varepsilon}(\mathbf{u}^j))\right)\mathbf{I} \text{ in } \Omega_s^{j+1}, \tag{4.45}$$

and

$$\boldsymbol{\sigma}_k^{j+1} = \begin{cases} \mathcal{V}(T^{j+1})\left(\boldsymbol{\varepsilon}(\mathbf{u}_k^{j+1}) - \Delta t\mathbf{q}_{k-1}^{j+1} + \dfrac{\Delta t\gamma_p^j s^{j+1}}{3}\mathrm{tr}(\boldsymbol{\varepsilon}(\mathbf{u}_k^{j+1}))\mathbf{I} + \mathbf{F}^j\right) & \text{in } \Omega_s^{j+1}, \\ \Lambda_l^{-1}\boldsymbol{\varepsilon}(\mathbf{u}_k^{j+1}) & \text{in } \Omega_l^{j+1}, \end{cases} \tag{4.46}$$

The updated viscoplastic multiplier is given by

$$\mathbf{q}_k^{j+1} = \frac{\left(\boldsymbol{\sigma}_k^{j+1}\right)^D + \lambda_p^j\mathbf{q}_{k-1}^{j+1}}{\lambda_p^j}\left(1 - \frac{1}{\eta_k^{j+1}(1-\lambda_p^j\gamma_p^j)}\right) \text{ in } \Omega_s^{j+1}, \tag{4.47}$$

and $\eta_k^{j+1} = \eta\left(\left(\boldsymbol{\sigma}_k^{j+1}\right)^D + \lambda_p^j\,\mathbf{q}_{k-1}^{j+1}\right)$ is the unique root of the equation

$$\eta^{q-1} - \eta^{q-2} - \frac{\lambda_p^j\theta(T^{j+1})}{(1-\lambda_p^j\gamma_p^j)^{q-1}}\left|\left(\boldsymbol{\sigma}_k^{j+1}\right)^D + \lambda_p^j\,\mathbf{q}_{k-1}^{j+1}\right|^{q-2} = 0,$$

in the interval $[1, +\infty)$.

The main question is to determine the suitable technique to update the value of parameters γ_p^j, λ_p^j from the solution obtained at the time step t^j. Taking into account that the optimal parameters to convergence verify $\lambda_p^j\gamma_p^j = 1/2$ (see [16, 66]), the problem is reduced to calculate, for example, γ_p^j.

Application to plane strain case

Due to the great computational demands of the three-dimensional simulation in casting processes, in the numerical simulations presented in this manuscript we consider the two-dimensional associated problem under the plane strain assumption on the symmetry plane $[x_1 = 0]$. Due to this, in this section we present the algorithm to approximate the viscoplastic multiplier under this assumption. So, at each element $K \in \mathcal{T}_h(t^j)$, any $\boldsymbol{\tau} \in \mathbf{X}_h(t^j)$ can be written in the matrix form

$$\boldsymbol{\tau}_{|K} = \begin{pmatrix} \tau_{11} & 0 & 0 \\ 0 & \tau_{22} & \tau_{23} \\ 0 & \tau_{23} & \tau_{33} \end{pmatrix} \in \mathcal{M}_{3\times 3}(\mathbb{R}).$$

Taking into account that the Norton-Hoff's law (2.6) only involves the deviatoric part of the stress tensor, in this study we consider for each element $K \in \mathcal{T}_h(t^j)$:

$$\mathbf{V}^D = \{\boldsymbol{\tau} = (\tau_{ij}) \in \mathcal{M}_{3\times 3}(\mathbb{R}); \tau_{ij} = \tau_{ji}, \tau_{12} = \tau_{13} = 0, \tau_{11} = -(\tau_{22}+\tau_{33})\},$$

the space of matrices with null trace under the plane strain assumption. It is easy to prove that a basis of the space $\mathbf{V}^D$ is $B_{\mathbf{V}^D} = \left\{\boldsymbol{\tau}^1, \boldsymbol{\tau}^2, \boldsymbol{\tau}^3\right\}$ with

$$\boldsymbol{\tau}^1 = \begin{pmatrix} -1 & 0 & 0 \\ 0 & 1 & 0 \\ 0 & 0 & 0 \end{pmatrix}, \boldsymbol{\tau}^2 = \begin{pmatrix} -1 & 0 & 0 \\ 0 & 0 & 0 \\ 0 & 0 & 1 \end{pmatrix}, \boldsymbol{\tau}^3 = \begin{pmatrix} 0 & 0 & 0 \\ 0 & 0 & 1 \\ 0 & 1 & 0 \end{pmatrix}.$$

We recall that in Section 3.5.4 the following expression for the viscoplastic multiplier $\mathbf{q}^j$ was obtained from the Bermúdez-Moreno Lemma:

$$\mathbf{q}^j = (\nabla\Phi_q)^{\gamma_p}_{1/(2\gamma_p)} \left(\left(\boldsymbol{\sigma}^j\right)^D + \frac{1}{2\gamma_p}\mathbf{q}^j \right), \tag{4.48}$$

for $\gamma_p > 0$ and where $\boldsymbol{\sigma}^j$ is given by equation (4.46) at the time step t^j.

In order to simplify the notation, we denote by H the application of the dissipation potential

$$\begin{aligned} H : \mathbf{V}^D &\longrightarrow \mathbf{V}^D \\ \boldsymbol{\tau} &\longrightarrow H(\boldsymbol{\tau}) = (\nabla\Phi_q)(\boldsymbol{\tau}); \end{aligned}$$

the regularized Yosida of the perturbed operator $H - \gamma_p\mathbf{I}$,

$$\begin{aligned} H^{\gamma_p}_{1/(2\gamma_p)} : \mathbf{V}^D &\longrightarrow \mathbf{V}^D \\ \boldsymbol{\tau} &\longrightarrow H^{\gamma_p}_{1/(2\gamma_p)}(\boldsymbol{\tau}) = \left((\nabla\Phi_q)^{\gamma_p}_{1/(2\gamma_p)} \right)(\boldsymbol{\tau}); \end{aligned}$$

and, at the time step t^j,

$$\begin{aligned} \tilde{H}^{\gamma_p}_{1/(2\gamma_p)} : \mathbf{V}^D &\longrightarrow \mathbf{V}^D \\ \boldsymbol{\tau} &\longrightarrow \tilde{H}^{\gamma_p}_{1/(2\gamma_p)}(\boldsymbol{\tau}) = \left((\nabla\Phi_q)^{\gamma_p}_{1/(2\gamma_p)} \right) \left(\left(\boldsymbol{\sigma}^j\right)^D + \frac{1}{2\gamma_p}\boldsymbol{\tau} \right). \end{aligned}$$

So, with this notation, the viscoplastic multiplier $\mathbf{q}^j$ can be rewritten as:

$$\mathbf{q}^j|_K = H^{\gamma_p}_{1/(2\gamma_p)} \left(\left(\boldsymbol{\sigma}^j\right)^D|_K + \frac{1}{2\gamma_p}\mathbf{q}^j|_K \right) = \tilde{H}^{\gamma_p}_{1/(2\gamma_p)} \left(\mathbf{q}^j|_K\right), \forall K \in \mathcal{T}_h(t^j), \tag{4.49}$$

that is, $\mathbf{q}^j|_K$ is obtained as the fixed point of $\tilde{H}^{\gamma_p}_{1/(2\gamma_p)}$.

In [43], Gallardo *et al.* introduced a generalized Yosida regularization and they presented a generalization of the Bermúdez-Moreno algorithm that allows the use of very general operators as parameters. Moreover, as a particular case, they analyzed the use of scalar and matrix-valued parameters, proving that the optimal choice of the parameter γ_p^j would be a matrix-valued function. Furthermore, in [4], Arregui *et al.* presented an application of this generalized algorithm with scalar parameters in one-dimensional problems.

Taking into account the complexity of the real problem, in this study we propose to consider that the parameter γ_p is a scalar function. We will see in Chapter 5 that, although in [43] this choice did not give good results in academic cases, in the casting process the convergence improvement

is considerable. This fact is due to that the viscoplastic behaviour varies greatly from one element to another and from one time step to another, which explains the poor convergence results when considering γ_p constant.

Then, the strategy proposed in [43] consists of finding a parameter γ_p^j such that

$$D\tilde{H}^{\gamma_p^j}_{1/(2\gamma_p^j)}(\mathbf{q}^j|_K) = \mathbf{0}. \tag{4.50}$$

To simplify the notation, from now on in this section we will omit the restriction to an element $K \in \mathcal{T}_h(t^j)$.

Therefore, in order to give a scalar expression for γ_p, we try to minimize $\rho^j_{\gamma_p}$, the spectral radius of $D\tilde{H}^{\gamma_p^j}_{1/(2\gamma_p^j)}(\mathbf{q}^j)$. To do that, we give the following Lemma:

Lemma 4.2.5. *The differential $D\tilde{H}^{\gamma_p}_{1/(2\gamma_p)}(\mathbf{q}^j)$ is given by the expression*

$$D\tilde{H}^{\gamma_p}_{1/(2\gamma_p)}(\mathbf{q}^j) = \left[\mathbf{I} - \left(\frac{1}{2}\mathbf{I} + \frac{1}{2\gamma_p} DH\left(\left(\boldsymbol{\sigma}^j\right)^D\right)\right)^{-1}\right],$$

with $\mathbf{q}^j = (\nabla\Phi_q)^{\gamma_p}\left(\left(\boldsymbol{\sigma}^j\right)^D\right)$.

Proof. In [16] it is proved the following result:

$$H^{\gamma_p}_{\lambda_p}(\boldsymbol{\tau}) = \frac{1}{1-\lambda_p\gamma_p} H_{\frac{\lambda_p}{1-\lambda_p\gamma_p}}\left(\frac{1}{1-\lambda_p\gamma_p}\boldsymbol{\tau}\right) - \frac{\gamma_p}{1-\lambda_p\gamma_p}\boldsymbol{\tau}, \quad \boldsymbol{\tau} \in \mathbf{V}^D,$$

for all $\lambda_p, \gamma_p > 0$, $\lambda_p\gamma_p < 1$. So, for $\gamma_p\lambda_p = 1/2$ we have that

$$H^{\gamma_p}_{1/(2\gamma_p)}(\boldsymbol{\tau}) = 2H_{\frac{1}{\gamma_p}}(2\boldsymbol{\tau}) - 2\gamma_p\boldsymbol{\tau}.$$

By using the definition of the Yosida regularization, we obtain that

$$\begin{aligned} H^{\gamma_p}_{1/(2\gamma_p)}(\boldsymbol{\tau}) =& 2\gamma_p\left[\mathbf{I} - \left(\mathbf{I} + \frac{1}{\gamma_p}H\right)^{-1}\right](2\boldsymbol{\tau}) - 2\gamma_p\boldsymbol{\tau} = 2\gamma_p\left[\boldsymbol{\tau} - \left(\mathbf{I} + \frac{1}{\gamma_p}H\right)^{-1}(2\boldsymbol{\tau})\right] = \\ & 2\gamma_p\left[\boldsymbol{\tau} - \left(\frac{1}{2}\mathbf{I} + \frac{1}{2\gamma_p}H\right)^{-1}(\boldsymbol{\tau})\right] = 2\gamma_p\left[\mathbf{I} - \left(\frac{1}{2}\mathbf{I} + \frac{1}{2\gamma_p}H\right)^{-1}\right](\boldsymbol{\tau}). \end{aligned}$$

Then, applying the chain rule it results

$$\begin{aligned} DH^{\gamma_p}_{1/(2\gamma_p)}(\boldsymbol{\tau}) =& 2\gamma_p\left[\mathbf{I} - D\left(\left(\frac{1}{2}\mathbf{I} + \frac{1}{2\gamma_p}H\right)^{-1}\right)(\boldsymbol{\tau})\right] = \\ & 2\gamma_p\left[\mathbf{I} - \left(\frac{1}{2}\mathbf{I} + \frac{1}{2\gamma_p}DH(\boldsymbol{\eta})\right)^{-1}\right], \end{aligned} \tag{4.51}$$

for

$$\boldsymbol{\eta} = \left(\frac{1}{2}\mathbf{I} + \frac{1}{2\gamma_p}H\right)^{-1}(\boldsymbol{\tau}), \tag{4.52}$$

or equivalently,

$$\boldsymbol{\tau} = \left(\frac{1}{2}\mathbf{I} + \frac{1}{2\gamma_p}H\right)(\boldsymbol{\eta}) = \frac{1}{2}\boldsymbol{\eta} + \frac{1}{2\gamma_p}H(\boldsymbol{\eta}). \tag{4.53}$$

In particular, if we consider in (4.52)

$$\boldsymbol{\tau} = \left(\boldsymbol{\sigma}^j\right)^D + \frac{1}{2\gamma_p}\mathbf{q}^j, \tag{4.54}$$

and taking into account that $\mathbf{q}^j$ is defined as the perturbed operator of H with parameter γ_p (see (3.20)), we have that

$$\begin{aligned}\boldsymbol{\tau} = \left(\boldsymbol{\sigma}^j\right)^D + \frac{1}{2\gamma_p}\mathbf{q}^j = \left(\boldsymbol{\sigma}^j\right)^D + \frac{1}{2\gamma_p}\left[H\left(\left(\boldsymbol{\sigma}^j\right)^D\right) - \gamma_p\left(\boldsymbol{\sigma}^j\right)^D\right] = \\ \frac{1}{2}\left(\boldsymbol{\sigma}^j\right)^D + \frac{1}{2\gamma_p}H\left(\left(\boldsymbol{\sigma}^j\right)^D\right).\end{aligned} \tag{4.55}$$

From (4.53) and (4.55), we deduce that for $\boldsymbol{\tau}$ defined by (4.54) the corresponding $\boldsymbol{\eta}$ is $\boldsymbol{\eta} = \left(\boldsymbol{\sigma}^j\right)^D$. Then, from (4.49) and (4.51), we infer that

$$D\tilde{H}^{\gamma_p}_{1/(2\gamma_p)}(\mathbf{q}^j) = \frac{1}{2\gamma_p}DH^{\gamma_p}_{1/(2\gamma_p)}\left(\left(\boldsymbol{\sigma}^j\right)^D + \frac{1}{2\gamma_p}\mathbf{q}^j\right) = \left[\mathbf{I} - \left(\frac{1}{2}\mathbf{I} + \frac{1}{2\gamma_p}DH\left(\left(\boldsymbol{\sigma}^j\right)^D\right)\right)^{-1}\right],$$

and the Lemma is proved. □

Lemma 4.2.6. *Let assume that* $DH\left(\left(\boldsymbol{\sigma}^j\right)^D\right)$ *is positive definite and consider that* $0 < \omega_1^j \leq \omega_2^j \leq \omega_3^j$ *are its eigenvalues. Then,*

$$\frac{\omega_i^j - \gamma_p}{\omega_i^j + \gamma_p}$$

are the eigenvalues of $D\tilde{H}^{\gamma_p}_{1/(2\gamma_p)}(\mathbf{q}^j)$ *for* $\mathbf{q}^j = (\nabla\Phi_q)^{\gamma_p}\left(\left(\boldsymbol{\sigma}^j\right)^D\right)$ *and its spectral radius is*

$$\rho^j_{\gamma_p} = \max_{i=1,2,3}\left|\frac{\omega_i^j - \gamma_p}{\omega_i^j + \gamma_p}\right|. \tag{4.56}$$

Proof. Let μ_i^j be an eigenvalue of $D\tilde{H}^{\gamma_p}_{1/(2\gamma_p)}(\mathbf{q}^j)$; then, by using Lemma 4.2.5, there exists $\boldsymbol{\tau} \in \mathbf{V}^D$ such that

$$\left[\mathbf{I} - \left(\frac{1}{2}\mathbf{I} + \frac{1}{2\gamma_p}DH\left(\left(\boldsymbol{\sigma}^j\right)^D\right)\right)^{-1}\right](\boldsymbol{\tau}) = \mu_i^j\boldsymbol{\tau}.$$

By doing some simple calculations, we obtain

$$(1-\mu_i^j)\left(\frac{1}{2}\mathbf{I}+\frac{1}{2\gamma_p}DH\left(\left(\boldsymbol{\sigma}^j\right)^D\right)\right)(\boldsymbol{\tau})=\boldsymbol{\tau}$$

from where we deduce that

$$DH\left(\left(\boldsymbol{\sigma}^j\right)^D\right)(\boldsymbol{\tau})=\gamma_p\frac{1+\mu_i^j}{1-\mu_i^j}\boldsymbol{\tau}.$$

Let us denote

$$\omega_i^j=\gamma_p\frac{1+\mu_i^j}{1-\mu_i^j}, \tag{4.57}$$

then ω_i^j is an eigenvalue of $DH\left(\left(\boldsymbol{\sigma}^j\right)^D\right)$ and we can write the eigenvalue μ_i^j in terms of ω_i^j in the following manner:

$$\mu_i^j=\frac{\omega_i^j-\gamma_p}{\omega_i^j+\gamma_p}.$$

□

The optimal γ_p^j will be that minimizing (4.56). In the following result we give an expression for γ_p^j:

Proposition 4.2.7. *Under the assumptions of Lemma 4.2.6, the parameter γ_p^j minimizing ρ_{γ_p} is given by:*

$$\gamma_p^j=\sqrt{\omega_1^j\omega_3^j}. \tag{4.58}$$

Proof. The proof is similar to that given in [43] and it is based in the following property:

$$\forall\gamma_p>0,\quad \frac{\omega_1^j-\gamma_p}{\omega_1^j+\gamma_p}\leq\frac{\omega_2^j-\gamma_p}{\omega_2^j+\gamma_p}\leq\frac{\omega_3^j-\gamma_p}{\omega_3^j+\gamma_p}.$$

We have to analyze several cases depending on the position of γ_p with respect to eigenvalues ω_i^j:

- If $0<\gamma_p\leq\omega_1^j$, it is easy to prove that

$$\min_{0<\gamma_p\leq\omega_1^j}\rho_{\gamma_p}=\frac{\omega_3^j-\omega_1^j}{\omega_3^j+\omega_1^j}.$$

- Analogously,

$$\min_{\omega_3^j\leq\gamma_p}\rho_{\gamma_p}=\frac{\omega_3^j-\omega_1^j}{\omega_3^j+\omega_1^j}.$$

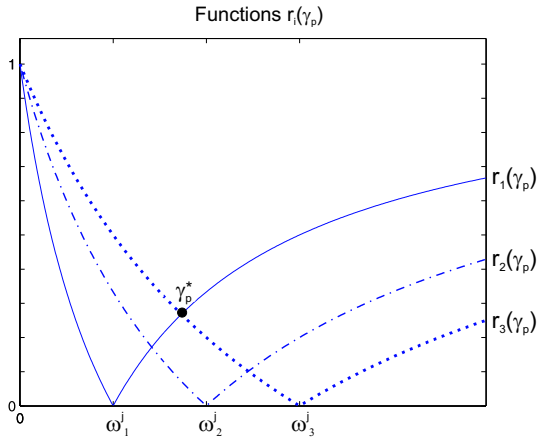

Figure 4.5: Functions $r_i(\gamma_p)$

- Finally, let suppose that $\gamma_p \in (\omega_1^j, \omega_3^j)$ and define

$$r_i(\gamma_p) = \left| \frac{\omega_i^j - \gamma_p}{\omega_i^j + \gamma_p} \right|.$$

Then, we have that (see Figure 4.5)

$$\rho_{\gamma_p} = \begin{cases} r_3(\gamma_p) & \text{if } \omega_1^j < \gamma_p \leq \gamma_p^*, \\ r_1(\gamma_p) & \text{if } \gamma_p^* < \gamma_p \leq \omega_3^j, \end{cases}$$

where γ_p^* is the unique element in the interval (ω_1^j, ω_3^j) such that $r_1(\gamma_p^*) = r_3(\gamma_p^*)$. A simple calculation gives $\gamma_p^* = \sqrt{\omega_1^j \omega_3^j}$.

Notice that

$$\min_{\omega_1^j < \gamma_p < \omega_3^j} \rho_{\gamma_p} = r_1(\gamma_p^*) = r_3(\gamma_p^*) \leq \frac{\omega_3^j - \omega_1^j}{\omega_3^j + \omega_1^j},$$

so the best choice for γ_p is precisely γ_p^*. □

Proposition 4.2.8. *The associated matrix of* $DH\left(\left(\boldsymbol{\sigma}^j\right)^D\right)$ *in terms of the basis* $B_{\mathbf{V}^D}$ *is:*

$$DH\left(\left(\boldsymbol{\sigma}^j\right)^D\right) = \begin{pmatrix} A^j C_{21}^j (\sigma^j)_{22}^D + B^j & A^j C_{31}^j (\sigma^j)_{22}^D & 2A^j (\sigma^j)_{23}^D (\sigma^j)_{22}^D \\ A^j C_{21}^j (\sigma^j)_{33}^D & A^j C_{31}^j (\sigma^j)_{33}^D + B^j & 2A^j (\sigma^j)_{23}^D (\sigma^j)_{33}^D \\ A^j C_{21}^j (\sigma^j)_{23}^D & A^j C_{31}^j (\sigma^j)_{23}^D & 2A^j (\sigma^j)_{23}^D (\sigma^j)_{23}^D + B^j \end{pmatrix},$$

where

$$A^j = \theta(T^j)(q-2)\left|\left(\boldsymbol{\sigma}^j\right)^D\right|^{q-4}, \tag{4.59}$$

$$B^j = \theta(T^j)\left|\left(\boldsymbol{\sigma}^j\right)^D\right|^{q-2}, \tag{4.60}$$

$$C_{21}^j = (\sigma^j)_{22}^D - (\sigma^j)_{11}^D,\ C_{31}^j = (\sigma^j)_{33}^D - (\sigma^j)_{11}^D.$$

The eigenvalues of $DH\left(\left(\boldsymbol{\sigma}^j\right)^D\right)$ *are given by the expressions:*

$$\omega_1^j = \omega_2^j = B^j, \quad \omega_3^j = B^j + \frac{2}{3}A^j\sigma_{eq}^2, \tag{4.61}$$

where σ_{eq}^2 *is the Von Mises equivalent stress defined by*

$$\sigma_{eq}^2 = \frac{3}{2}\left(\boldsymbol{\sigma}^j\right)^D : \left(\boldsymbol{\sigma}^j\right)^D.$$

Moreover, the eigenvalues verify that $\omega_i^j \geq 0$, $i = 1, 2, 3$.

Proof. It is easy to prove that $DH\left(\left(\boldsymbol{\sigma}^j\right)^D\right)$ is given by the expression

$$\begin{aligned} DH\left(\left(\boldsymbol{\sigma}^j\right)^D\right)\boldsymbol{\tau} =& \theta(T^j)(q-2)\left|\left(\boldsymbol{\sigma}^j\right)^D\right|^{q-4}\left(\left(\boldsymbol{\sigma}^j\right)^D : \boldsymbol{\tau}\right)\left(\boldsymbol{\sigma}^j\right)^D + \theta(T^j)\left|\left(\boldsymbol{\sigma}^j\right)^D\right|^{q-2}\boldsymbol{\tau} = \\ & A^j\left(\left(\boldsymbol{\sigma}^j\right)^D : \boldsymbol{\tau}\right)\left(\boldsymbol{\sigma}^j\right)^D + B^j\boldsymbol{\tau}, \end{aligned}$$

for all $\boldsymbol{\tau} \in \mathbf{V}^D$. Then, in order to obtain its associated matrix in terms of the basis $B_{\mathbf{V}^D}$, we calculate the image of each element $\boldsymbol{\tau}^i \in B_{\mathbf{V}^D}$, i=1,2,3, and we write them in terms of the basis $B_{\mathbf{V}^D}$:

$$\begin{aligned} DH\left(\left(\boldsymbol{\sigma}^j\right)^D\right)(\boldsymbol{\tau}^1) =& A^j\left((\sigma^j)_{22}^D - (\sigma^j)_{11}^D\right)\left(\boldsymbol{\sigma}^j\right)^D + B^j\boldsymbol{\tau}^1 = A^jC_{21}^j\left(\boldsymbol{\sigma}^j\right)^D + B^j\boldsymbol{\tau}^1 = \\ & \begin{pmatrix} A^jC_{21}^j(\sigma^j)_{11}^D - B^j & 0 & 0 \\ 0 & A^jC_{21}^j(\sigma^j)_{22}^D + B^j & A^jC_{21}^j(\sigma^j)_{23}^D \\ 0 & A^jC_{21}^j(\sigma^j)_{23}^D & A^jC_{21}^j(\sigma^j)_{33}^D \end{pmatrix} = \\ & \left(A^jC_{21}^j(\sigma^j)_{22}^D + B^j\right)\boldsymbol{\tau}^1 + A^jC_{21}^j(\sigma^j)_{33}^D\boldsymbol{\tau}^2 + A^jC_{21}^j(\sigma^j)_{23}^D\boldsymbol{\tau}^3, \\ DH\left(\left(\boldsymbol{\sigma}^j\right)^D\right)(\boldsymbol{\tau}^2) =& A^j\left((\sigma^j)_{33}^D - (\sigma^j)_{11}^D\right)\left(\boldsymbol{\sigma}^j\right)^D + B^j\boldsymbol{\tau}^2 = A^jC_{31}^j\left(\boldsymbol{\sigma}^j\right)^D + B^j\boldsymbol{\tau}^2 = \\ & \begin{pmatrix} A^jC_{31}^j(\sigma^j)_{11}^D - B^j & 0 & 0 \\ 0 & A^jC_{31}^j(\sigma^j)_{22}^D & A^jC_{31}^j(\sigma^j)_{23}^D \\ 0 & A^jC_{31}^j(\sigma^j)_{23}^D & A^jC_{31}^j(\sigma^j)_{33}^D + B^j \end{pmatrix} = \\ & A^jC_{31}^j(\sigma^j)_{22}^D\boldsymbol{\tau}^1 + \left(A^jC_{31}^j(\sigma^j)_{33}^D + B^j\right)\boldsymbol{\tau}^2 + A^jC_{31}^j(\sigma^j)_{23}^D\boldsymbol{\tau}^3, \\ DH\left(\left(\boldsymbol{\sigma}^j\right)^D\right)(\boldsymbol{\tau}^3) =& 2A^j(\sigma^j)_{23}^D\left(\boldsymbol{\sigma}^j\right)^D + B^j\boldsymbol{\tau}^3 = \\ & \begin{pmatrix} 2A^j(\sigma^j)_{23}^D(\sigma^j)_{11}^D & 0 & 0 \\ 0 & 2A^j(\sigma^j)_{23}^D(\sigma^j)_{22}^D & 2A^j(\sigma^j)_{23}^D(\sigma^j)_{23}^D + B^j \\ 0 & 2A^j(\sigma^j)_{23}^D(\sigma^j)_{23}^D + B^j & 2A^j(\sigma^j)_{23}^D(\sigma^j)_{33}^D \end{pmatrix} = \\ & 2A^j(\sigma^j)_{23}^D(\sigma^j)_{22}^D\boldsymbol{\tau}^1 + 2A^j(\sigma^j)_{23}^D(\sigma^j)_{33}^D\boldsymbol{\tau}^2 + \left(2A^j(\sigma^j)_{23}^D(\sigma^j)_{23}^D + B^j\right)\boldsymbol{\tau}^3. \end{aligned}$$

By using symbolic calculus, we obtain the eigenvalues of the associated matrix, that are given by expressions (4.61). □

Then, from Propositions 4.2.7 and 4.2.8, we can conclude the following result:

Corollary 4.2.9. *The optimal choice of parameters for the viscoplastic multiplier* $\mathbf{q}^j$ *is*

$$\gamma_p^j = \sqrt{\omega_1^j \omega_3^j}, \quad \lambda_p^j = \frac{1}{2\gamma_p^j},$$

where ω_1^j *and* ω_3^j *are given by expression (4.61).*

Bermúdez-Moreno algorithm with variable parameters to solve the viscoplastic problem under plane strain assumption

Summing up, the proposed algorithm to solve Problem (3.16)-(3.18) is:

- Let $(\mathbf{u}_0, \boldsymbol{\sigma}_0)$ and γ_p^0 be given; we compute $\mathbf{q}^0 = \nabla \Phi_q^{\gamma_p^0}(\boldsymbol{\sigma}_0^D)$.
- Then, for $j \geq 0$, $(\mathbf{u}^j,\ \boldsymbol{\sigma}^j, \mathbf{q}^j, \gamma_p^j)$ known at time t^j, we determine $(\mathbf{u}^{j+1}, \boldsymbol{\sigma}^{j+1},\ \mathbf{q}^{j+1}, \gamma_p^{j+1})$ at time t^{j+1}, an approximated weak solution of Problem (3.16)-(3.18). To do so, we propose the following iterative algorithm:

  i) Given $(\mathbf{u}_{k-1}^{j+1}, \boldsymbol{\sigma}_{k-1}^{j+1}, \mathbf{q}_{k-1}^{j+1})$, we compute $(\mathbf{u}_k^{j+1}, \boldsymbol{\sigma}_k^{j+1}) \in \mathbf{U}_{ad_h}(t^{j+1}) \times \mathbf{X}_h(t^{j+1})$ by solving the variational equality

$$\int_{\Omega_s^{j+1}} \mathcal{V}(T^{j+1}) \left[\boldsymbol{\varepsilon}(\mathbf{u}_k^{j+1}) + \frac{\Delta t \gamma_p^j s^{j+1}}{3} \mathrm{tr}(\boldsymbol{\varepsilon}(\mathbf{u}_k^{j+1}))\mathbf{I} \right] : \boldsymbol{\varepsilon}(\mathbf{v}) dx +$$
$$\int_{\Omega_l^{j+1}} \Lambda_l^{-1} \boldsymbol{\varepsilon}(\mathbf{u}_k^{j+1}) : \boldsymbol{\varepsilon}(\mathbf{v}) dx = \int_{\Omega_s^{j+1}} \left[\mathcal{V}(T^{j+1}) \Delta t \mathbf{q}_{k-1}^{j+1} \right] : \boldsymbol{\varepsilon}(\mathbf{v}) dx -$$
$$\int_{\Omega_s^{j+1}} \left[\mathcal{V}(T^{j+1}) \mathbf{F}^j \right] : \boldsymbol{\varepsilon}(\mathbf{v}) dx + \int_{\Omega^{j+1}} \mathbf{f}^{j+1} \cdot \mathbf{v} dx \ \forall \mathbf{v} \in \mathbf{U}_{ad_h}(t^{j+1}),$$

  where

$$\mathbf{F}^j = -\boldsymbol{\varepsilon}(\mathbf{u}^j) + \Lambda_s(T^j)\boldsymbol{\sigma}^j - \alpha_s(T^{j+1})(T^{j+1} - T^j)\left(1 + \Delta t \gamma_p^j s^{j+1}\right)\mathbf{I} +$$
$$\frac{\Delta t \gamma_p^j s^{j+1}}{3} \left(\frac{1}{s^j} \mathrm{tr}(\boldsymbol{\sigma}^j) - \mathrm{tr}(\boldsymbol{\varepsilon}(\mathbf{u}^j)) \right) \mathbf{I} \text{ in } \Omega_s^{j+1},$$

  and the updated stress tensor is given by

$$\boldsymbol{\sigma}_k^{j+1} = \begin{cases} \mathcal{V}(T^{j+1}) \left(\boldsymbol{\varepsilon}(\mathbf{u}_k^{j+1}) - \Delta t \mathbf{q}_{k-1}^{j+1} + \dfrac{\Delta t \gamma_p^j s^{j+1}}{3} \mathrm{tr}(\boldsymbol{\varepsilon}(\mathbf{u}_k^{j+1}))\mathbf{I} + \mathbf{F}^j \right) & \text{in } \Omega_s^{j+1}, \\ \Lambda_l^{-1} \boldsymbol{\varepsilon}(\mathbf{u}_k^{j+1}) & \text{in } \Omega_l^{j+1}, \end{cases}$$

  and the discretized space $\mathbf{U}_{ad_h}(t^{j+1})$ is restricted to the plane strain case in the usual way.

ii) The updated viscoplastic multiplier is given by

$$\mathbf{q}_k^{j+1} = 2\gamma_p^j \left[\left(\boldsymbol{\sigma}_k^{j+1} \right)^D + \frac{1}{2\gamma_p^j} \mathbf{q}_{k-1}^{j+1} \right] \left(1 - \frac{2}{\eta_k^{j+1}} \right).$$

- Once the convergence of the viscoplastic multiplier is achieved, the updated parameter γ_p^{j+1} is given by

$$\gamma_p^{j+1} = \sqrt{\omega_1^{j+1} \omega_3^{j+1}},$$

where $\omega_1^{j+1}, \omega_3^{j+1}$ are given by (4.61).

4.3 Two new algorithms to solve the casting problem

In this section, we are going to summarize two algorithms for the numerical resolution of the complete model (3.7)-(3.9). To do this, we combine the algorithm introduced in Section 4.1 to solve the contact condition with those introduced in Section 4.2 to deal with the constitutive law.

As we will see in the next chapter, in the numerical simulations presented in this manuscript, we consider the two-dimensional problem under the assumption of plane strain on the symmetry plane $[x_1 = 0]$. Due to this, we are going to introduce the algorithms in the particular case of plane strain. The two algorithms are the following:

- NM algorithm: In this case, we use the Bermúdez-Moreno algorithm together with Newton's techniques, introduced in Sections 4.1 and 4.2.1.
- NVPM algorithm: In order to overcome the poor convergence of the NM algorithm in the simulation of casting processes, we consider the following methodology: the Newton algorithm for the contact nonlinearity introduced in Section 4.1, together with the Bermúdez-Moreno algorithm with variable parameters for the viscoplastic nonlinearity presented in Section 4.2.2.

Let us summarize these algorithms in the following sections. Notice that the discretized spaces are restricted to the plane strain case in the usual way.

4.3.1 NM algorithm

1. Let $(\mathbf{u}_0, \boldsymbol{\sigma}_0)$ be given and let consider $p^0 = -(\sigma_0)_n$ and $\mathbf{q}^0 = \nabla \Phi_q \left(\boldsymbol{\sigma}_0^D \right)$.
2. Then, for $j \geq 0$, $(\mathbf{u}^j,\ \boldsymbol{\sigma}^j,\ \mathbf{q}^j,\ p^j)$ known at time t^j, we determine $(\mathbf{u}^{j+1}, \boldsymbol{\sigma}^{j+1},\ \mathbf{q}^{j+1},\ p^{j+1})$ at time t^{j+1}, an approximated weak solution of Problem (3.7)-(3.9). To do so, we propose the following iterative algorithm:

   2.1. Initialize $\mathbf{u}_0^{j+1} = \mathbf{u}^j$, $\mathbf{q}_0^{j+1} = \mathbf{q}^j$, $p_0^{j+1} = p^j$.

2.2. With $\mathbf{q}_{k-1}^{j+1}$, p_{k-1}^{j+1} known, calculate $(\mathbf{u}_k^{j+1}, p_k^{j+1})$ in two steps:

2.2.1. Solving the variational equality

$$\int_{\Omega_s^{j+1}} \left(\Lambda_s(T^{j+1})\right)^{-1} \boldsymbol{\varepsilon}(\mathbf{u}_k^{j+1}) : \boldsymbol{\varepsilon}(\mathbf{v}) dx + \int_{\Omega_l^{j+1}} \Lambda_l^{-1} \boldsymbol{\varepsilon}(\mathbf{u}_k^{j+1}) : \boldsymbol{\varepsilon}(\mathbf{v}) dx + \frac{1}{\epsilon_c} \int_{(\Gamma^+_{C,k-1})^{j+1}} \left(u_k^{j+1}\right)_n v_n d\gamma = \int_{\Omega^{j+1}} \mathbf{f}^{j+1} \cdot \mathbf{v} dx + \int_{\Omega_s^{j+1}} \left(\Lambda_s(T^{j+1})\right)^{-1} \left(\Delta t \mathbf{q}_{k-1}^{j+1} - \mathbf{F}^j\right) : \boldsymbol{\varepsilon}(\mathbf{v}) dx, \ \forall \mathbf{v} \in \mathbf{U}_h(t^{j+1}), \tag{4.62}$$

where

$$\mathbf{F}^j = \Lambda_s(T^j)\boldsymbol{\sigma}^j - \boldsymbol{\varepsilon}(\mathbf{u}^j) - \alpha_s(T^{j+1})(T^{j+1} - T^j)\mathbf{I} \text{ in } \Omega_s^{j+1}.$$

2.2.2. Updating the contact multiplier

$$p_k^{j+1} = \frac{1}{\epsilon_c} \left(u_k^{j+1}\right)_n \text{ on } (\Gamma^+_{C,k-1})^{j+1}, \tag{4.63}$$

and the effective contact boundary

$$(\Gamma^+_{C,k})^{j+1} = \{C \in S_h;\ s_k^{j+1} > 0\},\ s_k^{j+1} = \left(u_k^{j+1}\right)_n + \lambda_c\, p_k^{j+1}. \tag{4.64}$$

2.3. The updated stress tensor is defined by

$$\boldsymbol{\sigma}_k^{j+1} = \begin{cases} \left(\Lambda_s(T^{j+1})\right)^{-1} \left(\boldsymbol{\varepsilon}(\mathbf{u}_k^{j+1}) - \Delta t \mathbf{q}_{k-1}^{j+1} + \mathbf{F}^j\right) & \text{in } \Omega_s^{j+1}, \\ \Lambda_l^{-1} \boldsymbol{\varepsilon}(\mathbf{u}_k^{j+1}) & \text{in } \Omega_l^{j+1}. \end{cases} \tag{4.65}$$

2.4. The updated viscoplastic multiplier is given by

$$\mathbf{q}_k^{j+1} = \begin{cases} \mathbf{0}, & \text{if } \boldsymbol{\kappa}_k^{j+1} = \mathbf{0}, \\ \dfrac{\left(\eta_k^{j+1} - 1\right)}{\lambda_p} \left(\left(\boldsymbol{\sigma}_k^{j+1}\right)^D + \left(\eta_k^{j+1} - 1\right) \dfrac{q-2}{\eta_k^{j+1}} \boldsymbol{\kappa}_k^{j+1} \right) & \\ \quad - \left(\eta_k^{j+1} - 1\right) \dfrac{q-2}{|\boldsymbol{\kappa}_k^{j+1}|^2} \left(\mathbf{q}_{k-1}^{j+1} : \boldsymbol{\kappa}_k^{j+1}\right) \boldsymbol{\kappa}_k^{j+1}, & \text{if } \boldsymbol{\kappa}_k^{j+1} \neq \mathbf{0}, \end{cases} \tag{4.66}$$

in Ω_s^{j+1}, where $\boldsymbol{\kappa}_k^{j+1} = \left(\boldsymbol{\sigma}_k^{j+1}\right)^D + \lambda_p \mathbf{q}_{k-1}^{j+1}$, $\lambda_p > 1$ and η_k^{j+1} is the unique root of the equation

$$\eta^{q-1} - \eta^{q-2} - \lambda_p \theta_0 |\boldsymbol{\kappa}_k^{j+1}|^{q-2} = 0,$$

in the interval $[1, +\infty)$.

Figure 4.6 shows a flowchart of NM algorithm to solve aluminium casting problems. After initializing variables (Step 1 in Figure 4.6), a time step loop is carried out. In this loop, at the $j+1$ iteration, the displacement vector $\mathbf{u}^{j+1}$ is computed by constructing the fixed stiffness matrix (Step 2) and solving iteratively (Steps 5-7) equations (4.62)-(4.66), where the variable stiffness matrix is constructed at each iteration (Step 6).

4.3.2 NVPM algorithm

1. Let $(\mathbf{u}_0, \boldsymbol{\sigma}_0)$ and γ_p^0 be given and let consider $p^0 = -(\sigma_0)_n$ and $\mathbf{q}^0 = \nabla\Phi_q^{\gamma_p^0}(\boldsymbol{\sigma}_0^D)$.

2. Then, for $j \geq 0$, $(\mathbf{u}^j,\ \boldsymbol{\sigma}^j, \mathbf{q}^j, \gamma_p^j, p^j)$ known at time t^j, we determine $(\mathbf{u}^{j+1}, \boldsymbol{\sigma}^{j+1},\ \mathbf{q}^{j+1},\ \gamma_p^{j+1},\ p^{j+1})$ at time t^{j+1}, an approximated weak solution of Problem (3.7)-(3.9). To do so, we propose the following iterative algorithm:

   2.1. Initialize $\mathbf{u}_0^{j+1} = \mathbf{u}^j$, $\mathbf{q}_0^{j+1} = \mathbf{q}^j$, $p_0^{j+1} = p^j$.

   2.2. With $\mathbf{q}_{k-1}^{j+1}$, p_{k-1}^{j+1} known, calculate $(\mathbf{u}_k^{j+1}, p_k^{j+1})$ in two steps:

      2.2.1. Solving the variational equality

$$\int_{\Omega_s^{j+1}} \mathcal{V}(T^{j+1}) \left[\boldsymbol{\varepsilon}(\mathbf{u}_k^{j+1}) + \frac{\Delta t \gamma_p^j s^{j+1}}{3}\mathrm{tr}(\boldsymbol{\varepsilon}(\mathbf{u}_k^{j+1}))\mathbf{I}\right] : \boldsymbol{\varepsilon}(\mathbf{v})dx +$$
$$\int_{\Omega_l^{j+1}} \Lambda_l^{-1}\boldsymbol{\varepsilon}(\mathbf{u}_k^{j+1}) : \boldsymbol{\varepsilon}(\mathbf{v})dx + \frac{1}{\epsilon_c}\int_{(\Gamma_{C,k-1}^+)^{j+1}} \left(u_k^{j+1}\right)_n v_n d\gamma =$$
$$\int_{\Omega_s^{j+1}} \left[\mathcal{V}(T^{j+1})\Delta t \mathbf{q}_{k-1}^{j+1}\right] : \boldsymbol{\varepsilon}(\mathbf{v})dx - \int_{\Omega_s^{j+1}} \left[\mathcal{V}(T^{j+1})\mathbf{F}^j\right] : \boldsymbol{\varepsilon}(\mathbf{v})dx +$$
$$\int_{\Omega^{j+1}} \mathbf{f}^{j+1}\cdot\mathbf{v}dx\ \forall \mathbf{v} \in \mathbf{U}_h(t^{j+1}),$$

      where

$$\mathbf{F}^j = -\boldsymbol{\varepsilon}(\mathbf{u}^j) + \Lambda_s(T^j)\boldsymbol{\sigma}^j - \alpha_s(T^{j+1})(T^{j+1} - T^j)\left(1 + \Delta t\gamma_p^j s^{j+1}\right)\mathbf{I} +$$
$$\frac{\Delta t\gamma_p^j s^{j+1}}{3}\left(\frac{1}{s^j}\mathrm{tr}(\boldsymbol{\sigma}^j) - \mathrm{tr}(\boldsymbol{\varepsilon}(\mathbf{u}^j))\right)\mathbf{I} \text{ in } \Omega_s^{j+1}.$$

      2.2.2. Updating the contact multiplier

$$p_k^{j+1} = \frac{1}{\epsilon_c}\left(u_k^{j+1}\right)_n \text{ on } (\Gamma_{C,k-1}^+)^{j+1},$$

      and the effective contact boundary

$$(\Gamma_{C,k}^+)^{j+1} = \{C \in S_h;\ s_k^{j+1} > 0\},\ s_k^{j+1} = \left(u_k^{j+1}\right)_n + \lambda_c p_k^{j+1}.$$

   2.3. The updated stress tensor is defined by

$$\boldsymbol{\sigma}_k^{j+1} = \begin{cases} \mathcal{V}(T^{j+1})\left(\boldsymbol{\varepsilon}(\mathbf{u}_k^{j+1}) - \Delta t\mathbf{q}_{k-1}^{j+1} + \dfrac{\Delta t\gamma_p^j s^{j+1}}{3}\mathrm{tr}(\boldsymbol{\varepsilon}(\mathbf{u}_k^{j+1}))\mathbf{I} + \mathbf{F}^j\right) & \text{in } \Omega_s^{j+1}, \\ \Lambda_l^{-1}\boldsymbol{\varepsilon}(\mathbf{u}_k^{j+1}) & \text{in } \Omega_l^{j+1}. \end{cases}$$

   2.4. The updated viscoplastic multiplier is given by

$$\mathbf{q}_k^{j+1} = 2\gamma_p^j\left[\left(\boldsymbol{\sigma}_k^{j+1}\right)^D + \frac{1}{2\gamma_p^j}\mathbf{q}_{k-1}^{j+1}\right]\left(1 - \frac{2}{\eta_k^{j+1}}\right).$$

2.5. Once the convergence is achieved, the updated parameter γ_p^{j+1} is given by

$$\gamma_p^{j+1} = \sqrt{\omega_1^{j+1}\omega_3^{j+1}}, \quad \lambda_p^{j+1} = \frac{1}{2\gamma_p^{j+1}}$$

where

$$\omega_1^{j+1} = B^{j+1},$$
$$\omega_3^{j+1} = B^j + \frac{2}{3}A^j\sigma_{eq}^2,$$

being

$$A^{j+1} = \theta(T^{j+1})(q-2)\left|\left(\boldsymbol{\sigma}^{j+1}\right)^D\right|^{q-4},$$
$$B^{j+1} = \theta(T^{j+1})\left|\left(\boldsymbol{\sigma}^{j+1}\right)^D\right|^{q-2}.$$

The flowchart of NVPM algorithm is analogous to that in Figure 4.6, taking into account that, once the convergence is achieved in a time step, it is necessary to compute the value of parameter γ_p for the next time step.

Remark 4.3.1. *In practice, as in the case of the FPM algorithm, updating the contact and viscoplastic multipliers is performed with a relaxation parameter ϑ. For example, the updated viscoplastic multiplier is obtained by formula*

$$\mathbf{q}_k^{j+1} = \vartheta\mathbf{q}_k^{j+1} + (1-\vartheta)\mathbf{q}_{k-1}^{j+1}, \quad 0 < \vartheta \leq 1.$$

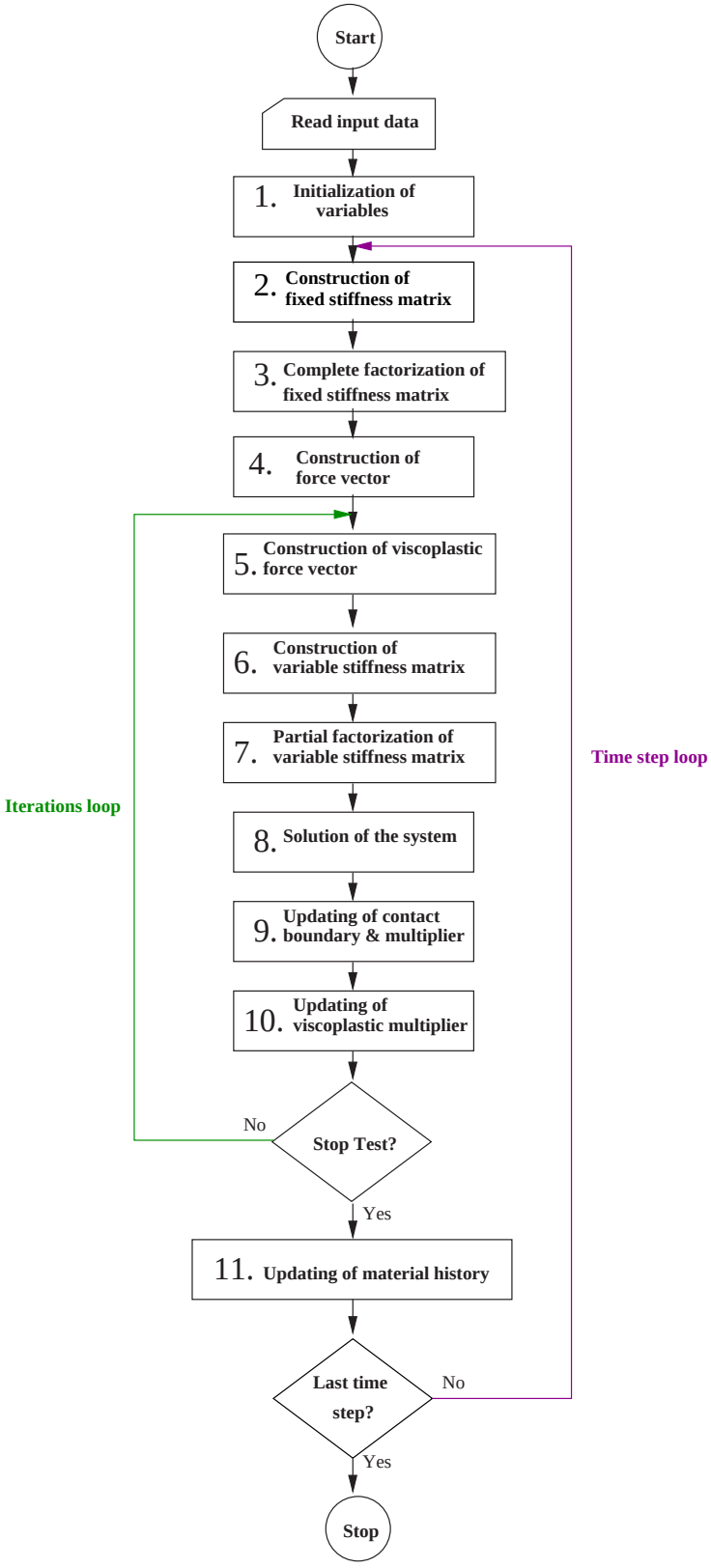

Figure 4.6: Flowchart for the NM algorithm.

Chapter 5

Numerical results

In this chapter, we compare and validate the algorithms proposed in Chapter 4 by applying a numerical code on several academic examples in plane strains. These tests have been designed to try to reproduce a behaviour analogous to semicontinuous real casting behaviour. To show the efficiency of the new algorithms, we compare the cpu-time[1], the number of iterations, and the displacement and stress errors between the new NM and NVPM algorithms and the former FPM algorithm. Finally, we present the results obtained in the simulation of a casting process.

5.1 Test 1: A growing butt curl

The aim of this test is to solve a contact problem when there is a gap which grows with time between the slab and the rigid foundation. This gap is similar to the butt curl deformation in a real aluminium casting process. For this purpose, we use the Newton algorithm introduced in Section 4.1, which involves an adapted matrix factorization. We compare the efficiency of this algorithm with the fixed point one described in Section 3.5.3.

Let $(0, 200\text{s}]$ be the time interval of interest and Ω be the cylindrical body whose axis is parallel to x_1-direction and its section the square of dimensions $0.5\text{m}\times 0.5\text{m}$ in the plane x_2x_3. For the sake of simplicity, we consider Ω independent of time. On $\partial\Omega$ we distinguish four parts:

$$\partial\Omega = \bar{\Gamma}_D \cup \bar{\Gamma}_N \cup \bar{\Gamma}_C \cup \bar{\Gamma}_{\pm},$$

where

$$\bar{\Gamma}_D = \partial\Omega \cap ([x_2 = 0] \cup [x_3 = 0.5]), \bar{\Gamma}_N = \partial\Omega \cap [x_2 = 0.5],$$
$$\bar{\Gamma}_C = \partial\Omega \cap [x_3 = 0],\ \bar{\Gamma}_{\pm} = \partial\Omega \cap [x_1 = \pm 1].$$

Let

$$T(t) = T_l + (100 - T_l)\frac{t}{200},\ t \in [0, 200] \tag{5.1}$$

[1]The numerical solution was computed on a PC with Intel Pentium IV 3.00GHz processor running on LINUX.

be the temperature function and $T_l = 649°\text{C}$. Notice that the slab temperature is constant at each time instant and lower than T_l at $t > 0$.

In this test we assume that the material is thermo-elastic and, then, the constitutive law corresponds to expression (3.11). We consider the elastic parameters $E = 10^9 \text{N/m}^2$, $\nu = 0.35$, independent of time and temperature, and we denote by λ, μ the corresponding Lamé coefficients. The coefficient of thermal expansion is given by

$$\alpha_s(T) = \begin{cases} -\dfrac{1}{3}\dfrac{\rho_l^{1/3}}{\rho(T)^{4/3}}\dfrac{d\rho(T)}{dT} & \text{if } T \le T_s, \\ \\ 0 & \text{if } T > T_s, \end{cases} \tag{5.2}$$

where the mass density function is (see [38])

$$\rho(T) = \begin{cases} 2700 - 0.23T & \text{if } T \le T_s, \\ 2360 & \text{if } T = T_l, \end{cases}$$

$T_s = 607°C$ being the solidus temperature. The values of $\rho(T)$ for $T \in (T_s, T_l)$ are approximated by linear interpolation. These data correspond to an aluminium alloy.

The problem to solve is

$$\left.\begin{aligned} -\text{div}(\boldsymbol{\sigma}) = \mathbf{f} \quad &\text{in} \quad \Omega, \\ \mathbf{u} = \widehat{\mathbf{u}} \quad &\text{on} \quad \Gamma_D, \\ \boldsymbol{\sigma}\mathbf{n} = (0, 0, 3\mu h^2) \quad &\text{on} \quad \Gamma_N, \\ \boldsymbol{\sigma}_\tau = \mathbf{0},\ u_n = 0 \quad &\text{on} \quad \Gamma_\pm, \\ \boldsymbol{\sigma}_\tau = \mathbf{m},\ \sigma_n \le 0,\ u_n \le 0,\ \sigma_n u_n = 0 \quad &\text{on} \quad \Gamma_C, \\ \boldsymbol{\varepsilon}(\mathbf{u}) = \Lambda\boldsymbol{\sigma} + \displaystyle\int_{T_l}^{T} \alpha_s(r)\, dr\, \mathbf{I} \quad &\text{in} \quad \Omega, \\ \mathbf{u}(0) = \widehat{\mathbf{u}}(0),\ \ \boldsymbol{\sigma}(0) = \widehat{\boldsymbol{\sigma}}(0) \quad &\text{in} \quad \Omega, \end{aligned}\right\}$$

with

$$h(x_2, t) = x_2 - 0.4 + 10^{-3}t,$$

$$\mathbf{f}(x,t) = \begin{cases} -3(\lambda+\mu)h^2\mathbf{e}_2 - 6\mu h x_3 \mathbf{e}_3, & \text{if } x_2 \le 0.4 - 10^{-3}t, \\ -6\mu h \mathbf{e}_3, & \text{if } x_2 > 0.4 - 10^{-3}t, \end{cases}$$

$$\mathbf{m}(x,t) = \begin{cases} -3h^2\mu x_3 \mathbf{e}_2, & \text{if } x_2 \le 0.4 - 10^{-3}t, \\ -3h^2\mu \mathbf{e}_2, & \text{if } x_2 > 0.4 - 10^{-3}t, \end{cases}$$

$$\widehat{\mathbf{u}}\,(x,t) = \frac{E}{2\mu}\left(\int_{T_l}^{T} \alpha(r)\, dr\right)(x_2\mathbf{e}_2 + x_3\mathbf{e}_3) + \begin{cases} h^3 x_3 \mathbf{e}_3, & \text{if } x_2 \le 0.4 - 10^{-3}t, \\ h^3 \mathbf{e}_3, & \text{if } x_2 > 0.4 - 10^{-3}t, \end{cases}$$

$$\widehat{\boldsymbol{\sigma}}(x,t) = -E\left(\int_{T_l}^{T} \alpha(r)\, dr\right)\mathbf{E}_1 + \begin{cases} \lambda h^3 \mathbf{I} + 2\mu h^3 \mathbf{E}_2 + 3\mu h^2 x_3 \mathbf{E}_3, & \text{if } x_2 \le 0.4 - 10^{-3}t, \\ \\ 3\mu h^2 \mathbf{E}_3, & \text{if } x_2 > 0.4 - 10^{-3}t, \end{cases}$$

where

$$\mathbf{E}_1 = \begin{pmatrix} 1 & 0 & 0 \\ 0 & 0 & 0 \\ 0 & 0 & 0 \end{pmatrix}, \mathbf{E}_2 = \begin{pmatrix} 0 & 0 & 0 \\ 0 & 0 & 0 \\ 0 & 0 & 1 \end{pmatrix}, \mathbf{E}_3 = \begin{pmatrix} 0 & 0 & 0 \\ 0 & 0 & 1 \\ 0 & 1 & 0 \end{pmatrix}.$$

We notice that in this test the frictionless condition on Γ_C has been replaced by a nonhomogeneous condition for the tangential stress when there is a gap. Although this condition has not physical meaning it is necessary in order to obtain the analytical solution for this test problem with an effective and nontrivial contact. The solution of this problem is

$$\mathbf{u} = \widehat{\mathbf{u}}, \boldsymbol{\sigma} = \widehat{\boldsymbol{\sigma}}.$$

As we have mentioned, to reduce the size of the problem and due to symmetry conditions we consider the corresponding plane strain problem over the plane x_2x_3 and we present the numerical simulation on the two-dimensional domain (see Figure 5.1). To solve this problem we use a uniform spatial mesh with 12800 triangles and 6561 vertices and for time discretization $\Delta t = 0.1$s. We initialize the contact multiplier by

$$p^0 = \begin{cases} 1, & \text{on } (\Gamma_C^+)^0, \\ 0, & \text{on } (\Gamma_C^-)^0. \end{cases}$$

Finally, we consider the following parameters:

- for the FPM algorithm:
$$\gamma_c = 0.5 \times 10^9,\ \lambda_c = 10^{-9},\ \vartheta = 0.9;$$
- for the NM algorithm:
$$\lambda_c = \frac{1}{\Delta t},\ \epsilon_c = 10^{-15},\ \vartheta = 0.9.$$

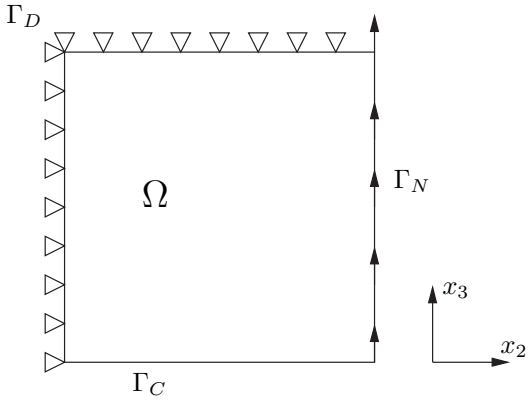

Figure 5.1: Computational domain.

The stopping test on the contact multiplier p is

$$\begin{aligned} |p_k - p_{k-1}| &< \tilde{\delta} \max\{\tilde{\delta}, |\, p_k|\},\ \forall C \in \mathcal{S}_h, \text{ and} \\ |p_k - G_{\lambda_c}(s_k)| &< \tilde{\delta} \max\{\tilde{\delta}, |\, G_{\lambda_c}(s_k)|\},\ \forall C \in \mathcal{S}_h, \end{aligned} \tag{5.3}$$

where $\tilde{\delta}$ is a small parameter and $s_k = (u_k)_n + \lambda_c p_k$. In this sample, $\tilde{\delta} = 10^{-3}$.

Remark 5.1.1. *Notice that, with stopping test (5.3), if the multiplier is close to zero we perform an absolute test with $\tilde{\delta}^2$ and, in the other case, a relative test with $\tilde{\delta}$.*

Figure 5.2 shows the displacements on the deformed configuration at two different time steps and the Von Mises norm of stresses at the last time step is represented in Figure 5.3.

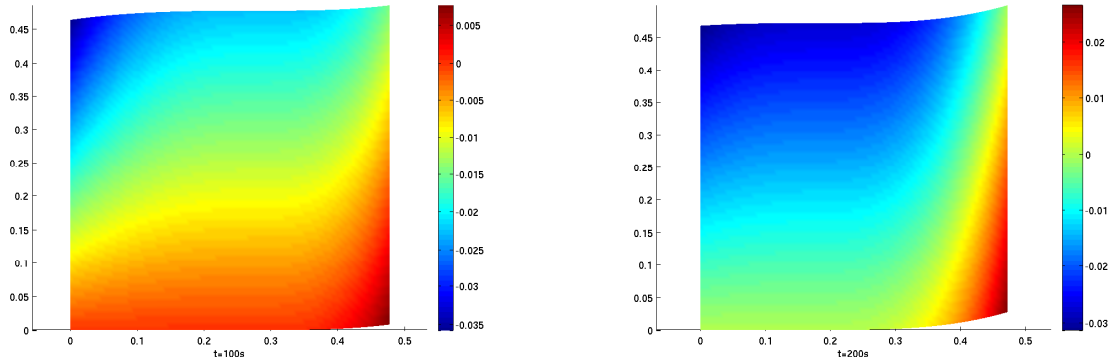

Figure 5.2: Displacements on the deformed configuration at two time steps.

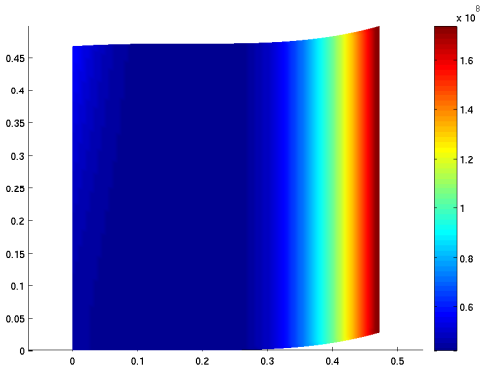

Figure 5.3: Von Mises norm of stresses at the last time step.

In this test we compare the results obtained with the NM algorithm with those obtained with the FPM one. The L^2 relative error at the last time step obtained with both algorithms is 3.957×10^{-4}m in displacements and 7.452×10^{-3}N/m^2 in stresses. Table 5.1 gathers the obtained results, showing that with NM algorithm the cpu-time decreases approximately 74% with respect to the FPM method and the number of iterations decreases 99%. In order to check the improvement of carrying out a matrix factorization adapted to the contact problem, the third column gathers the results for the NM algorithm without that factorization, denoted by NM*.

Method	FPM	NM	NM*
cpu-time (s)	17480.61	4615.30	7315.46
iterations	258	3	3

Table 5.1: Cpu-time and number of iterations for $\Delta t = 0.1$s.

5.2 Test 2: A problem with large gradients

In this second test we want to solve an elasto-viscoplastic problem with displacements and stresses whose gradients have a magnitude similar to that of real aluminium casting. Nevertheless, it does not reproduce the diverse behaviours which appear in the real process. For this purpose, we use the NM algorithm introduced in Section 4.3.1, which involves an adimensionalization technique and a time step optimization, and the NVPM algorithm described in Section 4.3.2. As in the previous test, we compare the obtained results with those of FPM algorithm.

Let $(0, 0.5\text{s}]$ be the time interval and Ω be the cylindrical body of Test 1 (its axis is parallel to x_1-direction and its section the square of dimensions $0.5\text{m}\times 0.5\text{m}$ in the plane x_2x_3). For the sake of simplicity, we consider Ω independent of time. On $\partial\Omega$ we distinguish four parts:

$$\partial\Omega = \bar{\Gamma}_D \cup \bar{\Gamma}_N \cup \bar{\Gamma}_C \cup \bar{\Gamma}_{\pm},$$

where

$$\bar{\Gamma}_D = \partial\Omega \cap [x_2 = 0],\ \bar{\Gamma}_N = \partial\Omega \cap ([x_2 = 0.5] \cup [x_3 = 0.5]),$$
$$\bar{\Gamma}_C = \partial\Omega \cap [x_3 = 0],\ \bar{\Gamma}_{\pm} = \partial\Omega \cap [x_1 = \pm 1].$$

In this test, we consider that Ω is already a solidified block with constant temperature. Then, there are not thermal stresses and the material parameters corresponding to the constitutive law, independent of the temperature T, are

$$E = 10^9\text{N/m}^2,\ \nu = 0.35,\ \theta_0 = 1.953125 \times 10^{-39}\text{m}^2/(\text{sN}),\ q = 6.$$

These data are similar to those of an aluminium alloy.

The problem to solve is

$$\left.\begin{array}{rcl} \operatorname{div}(\boldsymbol{\sigma}) = \mathbf{0} & \text{in} & \Omega, \\ \mathbf{u} = h\,(t)\,(0, x_2, -x_3) & \text{on} & \Gamma_D, \\ \boldsymbol{\sigma}\mathbf{n} = 10^8\mathbf{g} & \text{on} & \Gamma_N, \\ \boldsymbol{\sigma}_\tau = \mathbf{0},\ u_n = 0 & \text{on} & \Gamma_{\pm}, \\ \boldsymbol{\sigma}_\tau = \mathbf{0},\ \sigma_n \le 0,\ u_n \le 0,\ \sigma_n u_n = 0 & \text{on} & \Gamma_C, \\ \dot{\boldsymbol{\varepsilon}}(\mathbf{u}) = \Lambda\dot{\boldsymbol{\sigma}} + \theta_0 \mid \boldsymbol{\sigma}^D \mid^{q-2} \boldsymbol{\sigma}^D & \text{in} & \Omega, \\ \mathbf{u}(x,0) = \mathbf{0},\ \ \boldsymbol{\sigma}(x,0) = \mathbf{0} & \text{in} & \Omega, \end{array}\right\} \tag{5.4}$$

with $h\,(t) = 10^8\dfrac{1+\nu}{E}t + \dfrac{2}{3}10^{40}\theta_0 t^6$ and

$$\mathbf{g}(x,t) = \begin{cases} t\mathbf{n}, & \text{on } \Gamma_N \cap [x_2 = 0.5], \\ -t\mathbf{n}, & \text{on } \Gamma_N \cap [x_3 = 0.5]. \end{cases}$$

Its solution is readily verifiable

$$\mathbf{u}(x,t) = h\,(t)\,(0, x_2, -x_3)\,,\ \boldsymbol{\sigma}(x,t) = 10^8 \begin{pmatrix} 0 & 0 & 0 \\ 0 & t & 0 \\ 0 & 0 & -t \end{pmatrix}.$$

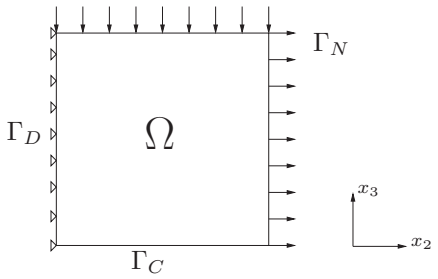

Figure 5.4: Computational domain.

As we have mentioned, to reduce the size of the problem we consider the corresponding plane strain problem over the symmetry plane $[x_1 = 0]$ (see Figure 5.4). To solve this problem we use a uniform spatial mesh with 800 elements and 441 nodes, corresponding to a discretization parameter $\Delta x = 0.025$ m. For time discretization we use a small time step ($\Delta t = 10^{-5}$) since the solution is nonlinear in time.

We initialize the multipliers in this way

$$\mathbf{q}^0 = \mathbf{0},\ p^0 = 10^{-5},$$

and we consider the following parameters:

- for the FPM algorithm:

$$\begin{aligned} &\gamma_c = 0.5 \times 10^{12},\ \lambda_c = 10^{-12}, \\ &\gamma_p = 10^{-6},\ \lambda_p = 0.5 \times 10^{6}, \\ &\vartheta = 0.9; \end{aligned}$$

- for the NM algorithm:

$$\lambda_c = \lambda_p = 1,\ \epsilon_c = 10^{-50},\ \vartheta = 0.9.$$

The test for convergence is performed on both multipliers. The stopping test on the contact multiplier p is detailed in (5.3).The stopping test on each component of the viscoplastic multiplier $\mathbf{q}$ is

$$\begin{aligned} |(q_k)_{il} - (q_{k-1})_{il}| < \tilde{\delta}\max\{\tilde{\delta}, |\,(q_k)_{il}|\},\ \forall K \in \mathcal{T}_h, \text{ and} \\ |(q_k)_{il} - \left(\nabla\Phi_q(\boldsymbol{\sigma}_k^D)\right)_{il}| < \tilde{\delta}\max\{\tilde{\delta}, |\,\left(\nabla\Phi_q(\boldsymbol{\sigma}_k^D)\right)_{il}|\},\ \forall K \in \mathcal{T}_h, \end{aligned} \tag{5.5}$$

where $\tilde{\delta}$ is a small parameter.

Firstly, we have tested the Newton algorithm for the elasto-viscoplastic law considering a Dirichlet condition on Γ_C. Nevertheless, convergence is not always achieved due to large gradient stresses. To overcome this difficulty, we use the adimensionalization technique introduced in Section 4.2.1 to reach the convergence of this algorithm.

Testing adimensionalization technique

We consider that the adimensionalization parameter is $\eta^{\delta} = 10^{-8}$. From now on, we will denote by NM$^{\bigstar}$ the Newton method together with this technique. Figure 5.5 shows the successive iterants calculated with and without adimensionalization. The cpu-time, the L^2 relative error at the last time step and the mean of the number of iterations are summarized in Table 5.2. Notice that with the NM$^{\bigstar}$ algorithm the number of iterations decreases approximately 95% and the cpu-time 85% with respect to the FPM algorithm.

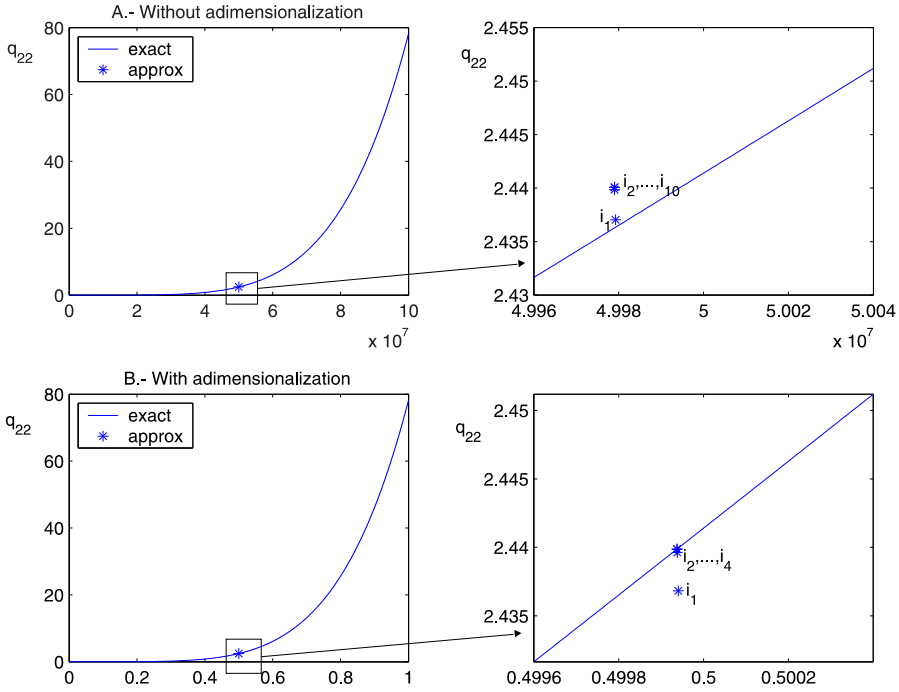

Figure 5.5: Numerical approximation of viscoplastic multiplier. The top row of figures without adimensionalization and the second one with the proposed adimensionalization technique. The $*$ shows the successive iterants with the NM$^{\bigstar}$ algorithm.

Table 5.2: Problem (5.4) without contact with $\Delta t = \tilde{\delta} = 10^{-5}$.

Method	FPM	NM$^{\bigstar}$
cpu-time (s)	18790.2	2744.0
iterations	57	3
$\mathbf{u}$ (m)-error	2.622×10^{-5}	2.621×10^{-5}
$\boldsymbol{\sigma}$ (N/m^2)-error	1.245×10^{-5}	1.244×10^{-5}

Finally, adding the contact condition on Γ_C to Problem (5.4), the reduction in cpu-time and in the number of iterations is analogous to that obtained previously (see Table 5.3).

Table 5.3: Problem (5.4) with $\Delta t = \tilde{\delta} = 10^{-5}$.

Method	FPM	NM$^\bigstar$
cpu-time (s)	25256.8	5365.2
iterations	69	3
$\mathbf{u}$ (m)-error	2.918×10^{-5}	2.917×10^{-5}
$\boldsymbol{\sigma}$ (N/m^2)-error	1.345×10^{-5}	1.345×10^{-5}

We notice that the NM$^\bigstar$ algorithm needs less iterations for convergence, and also less cpu-time, than the FPM algorithm. Nevertheless, the FPM algorithm is more robust and it does not need the adimensionalization technique.

Increasing the time step

Since the time interval of interest in the aluminium casting is about 150s, if we want to employ the NM$^\bigstar$ algorithm in casting simulation we must be able to increase the time step used in the previous simulations. If we do so, the FPM algorithm works well, but the NM$^\bigstar$ algorithm does not always converge due to the large gradients. To solve this problem, we use the optimization technique on the time step, introduced in Section 4.2.1: given Δt, if convergence is not achieved, we reduce the time step until the algorithm converges. Furthermore, to stabilize the Newton algorithm we employ an Armijo rule on the viscoplastic algorithm (see [20]). Summing up, we use the complete NM algorithm introduced in Section 4.3.1 to solve Problem 5.4.

Table 5.4 shows the obtained results; the NM algorithm obtains smaller displacement and stress errors than the FPM algorithm; in this case, the time step is reduced from 0.0625 to 1.5625×10^{-2}. Furthermore, the number of iterations with these techniques decreases 93% and the cpu-time 48%.

Table 5.4: Problem (5.4) with $\Delta t = 0.0625$ and $\tilde{\delta} = 10^{-3}$.

Method	FPM	NM
cpu-time (s)	6.58	3.39
iterations	254	18
$\mathbf{u}$ (m)-error	2.66×10^{-1}	7.30×10^{-2}
$\boldsymbol{\sigma}$ (N/m^2)-error	1.63×10^{-1}	2.70×10^{-2}

Testing the NVPM algorithm

From the above results we can state that NM method introduced in Section 4.3.1 is a good method to solve mechanical problems with elasto-viscoplastic laws of Maxwell-Norton type and a Signorini contact condition. Nevertheless, when using this method to solve the real casting

problem, convergence of NM method slows down dramatically. Due to this, we propose to use the NVPM algorithm where the Newton algorithm in viscoplasticity is replaced by the Bermúdez-Moreno algorithm with variable parameters. The considered parameters for this algorithm are:

$$\lambda_c = 1,\ \epsilon_c = 10^{-50},\ \gamma_p^0 = 0.1,\ \vartheta = 0.9.$$

Table 5.5 shows a comparison between the three mentioned algorithms. Although as expected the NM algorithm continues to obtain better results, the reduction in cpu-time (40%) and iterations (83%) of the NVPM algorithm with respect to the FPM one is considerable.

Table 5.5: Problem (5.4) with $\Delta t = 0.0625$ and $\tilde{\delta} = 10^{-3}$.

Method	FPM	NM	NVPM
cpu-time (s)	6.58	3.39	3.92
iterations	254	18	43
$\mathbf{u}$ (m)-error	2.66×10^{-1}	7.30×10^{-2}	2.03×10^{-1}
$\boldsymbol{\sigma}$ (N/m^2)-error	1.63×10^{-1}	2.70×10^{-2}	8.40×10^{-2}

5.3 Numerical simulation of casting processes

In this section we are going to present the results obtained in the numerical simulation of a real casting process. Real data have been provided by ALCOA-INESPAL S.A. (A Coruña, Spain). We compare the efficiency between the FPM, NM and NVPM algorithms.

The considered computational domain is shown in Figure 5.6.

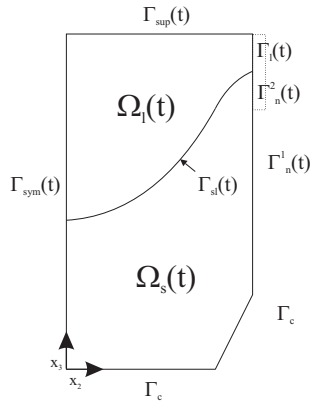

Figure 5.6: Computational domain.

Mesh construction

The mesh used for the simulation is built in a natural way. Firstly we make the mesh of the aluminium contained inside the bottom block before it begins to go down. After the start of the casting, at each time step we add the mesh of the liquid aluminium poured in that time interval.

The mesh construction takes into account the peculiarities of casting processes:

- The contact zone corresponds with the part of the slab rested on the mold. So, the mesh is constructed in such a way that the first nodes correspond to the contact nodes.
- The slab deformation depends strongly on the thermal gradients, which are larger in the recently solidified zone, that varies with the time. So, the mesh is finest-grained where the thermal gradients are larger.
- The computational domain grows with time. Then, the mesh is structured in layers to model the filling process and it is reconstructed at each time step adding the amount corresponding to the metal poured during that step.

Figure 5.7 shows the mesh of the computational domain at the start and the end of the casting process. The initial mesh has 1320 elements and 732 nodes while the final mesh has 2520 elements and 1342 nodes.

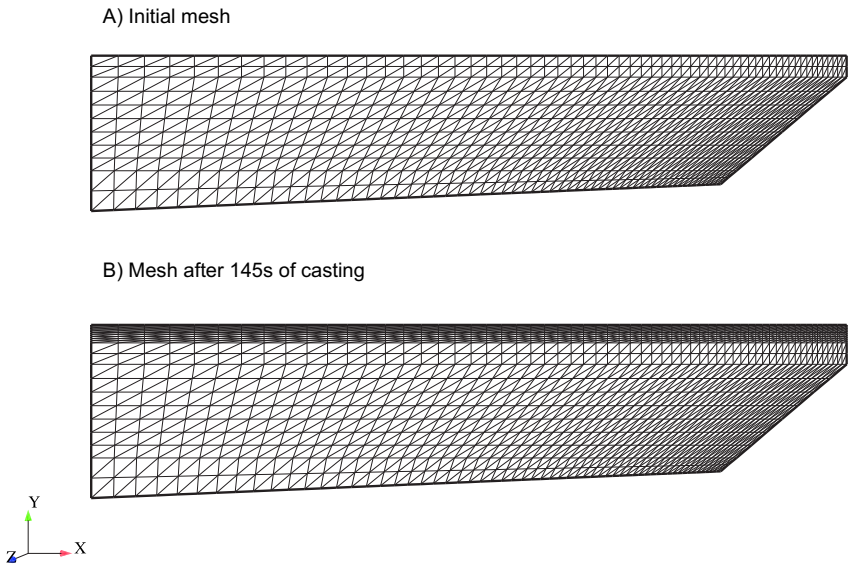

Figure 5.7: Initial mesh and mesh after 145 s of casting

The considered time interval is $(0, 145\text{s}]$ and in the numerical solution a time step $\Delta t = 1\text{s}$ is used. We must take into account that the NM algorithm has incorporated a time step optimization.

Behaviour law data

The parameters to characterize the thermo-elasto-viscoplastic law of aluminium (see (2.6)) have been introduced in the previous works [9, 10, 11] after carrying out a complete bibliographic search in the engineering literature (see [38, 57, 84]):

- Elastic law: Values for Young's modulus E and Poisson's coefficient ν depending on temperature are obtained from Table 5.6 by linear interpolation:

Table 5.6: Elastic law parameters.

$T(^\circ\mathrm{C})$	$E(10^9\mathrm{N/m^2})$	ν
126.9	67	0.3134
326.9	58	0.3448
526.9	40	0.45

- Viscoplastic law: The viscoplastic parameter θ_0 is computed from the data of Table 5.7 as

$$\theta_0 = \frac{\phi}{(\sqrt{2}k)^q}.$$

Table 5.7: Viscoplastic law parameters.

$\phi(\mathrm{s}^{-1})$	$k(10^9\mathrm{N/m^2})$	$G(\mathrm{Kcal/mol})$	q
4.0×10^{12}	15.72	37.3	6

- Thermal law: We consider the density function introduced in [38], given in $\mathrm{Kg/m^3}$:

$$\rho(T) = \begin{cases} 2700 - 0.23T & \text{if } T \leq T_s, \\ 2360 & \text{if } T = T_l, \end{cases}$$

where $T_s = 607^\circ\mathrm{C}$ and $T_l = 649^\circ\mathrm{C}$. The density values in (T_s, T_l) are computed by linear interpolation.

Algorithm parameters

In the following, we detail the parameters associated to the algorithms used in this simulation:

- for the FPM algorithm:

$$\gamma_c = 0.5 \times 10^6,\ \lambda_c = 10^{-6},$$
$$\gamma_p = 1.25 \times 10^{-12},\ \lambda_p = 0.4 \times 10^{12},$$
$$\vartheta = 0.9;$$

- for the NM algorithm:

$$\lambda_c = 1,\ \epsilon_c = 0.001,\ \lambda_p = 1,$$
$$\vartheta = 0.9,\ \eta^{\delta} = 10^{-9};$$

- for the NVPM algorithm:

$$\lambda_c = 1,\ \epsilon_c = 0.001,\ \gamma_p^0 = 1.25 \times 10^{-13},$$
$$\vartheta = 0.9,\ \eta^{\delta} = 10^{9};$$

- for the stopping test in both multipliers, $\tilde{\delta} = 10^{-4}$.

Finally, to impose the metallostatic pressure by using the fictitious domain method introduced in Section 3.5.1, we consider the following parameters in the liquid:

$$\bar{\lambda} = 1.2414 \times 10^{11},\ \bar{\mu} = 1.3793 \times 10^{10},\ \alpha = 2,\ \beta = 1,\ \epsilon = 10^{-3}.$$

Numerical results

Figure 5.8 shows the isotherms obtained with the code developed in [63] after carry out a parameter adjustment, and the butt curl obtained at the last time step.

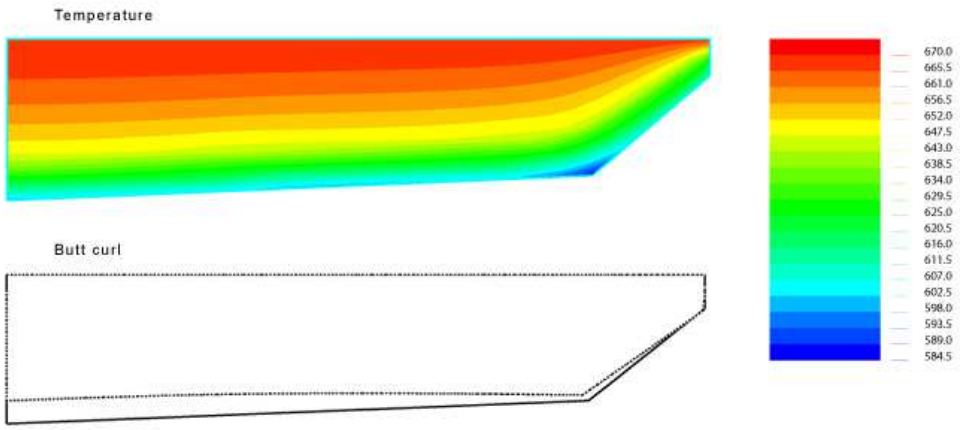

Figure 5.8: Isotherms and butt curl deformation after 150s.

The numerical simulation of the problem has been carried out by using the three algorithms. Although the NM algorithm has a very good convergence in the academic problems as we have seen in Sections 5.1 and 5.2, in real casting simulations, when a zone of the slab is recently solidified, sometimes the convergence is not achieved. Besides, the FPM algorithm has a good but slow convergence which depends strongly on the chosen parameters. Due to this, the NVPM algorithm incorporates the good convergence properties of the Newton algorithm in contact and

improves the convergence of the fixed point algorithm in viscoplasticity, computing automatically the parameters.

The cpu-time and the mean of the number of iterations obtained with the FPM and NVPM algorithms are summarized in Table 5.8. Data for the NM algorithm are not shown since, as we have said, convergence is not always achieved.

Method	FPM	NVPM
cpu-time (s)	2660.49	465.562
iterations	6593	89

Table 5.8: Cpu-time and number of iterations after $145s$ of casting.

Notice that with the NVPM algorithm the cpu-time decreases approximately 83% with respect to the FPM algorithm and the number of iterations decreases 99%.

Chapter 6

Conclusions

In Part I of this manuscript we have introduced two new algorithms to solve numerically a Signorini contact problem in Maxwell-Norton materials arising from an aluminium casting simulation. In [5], Barral presented a numerical method based on the Bermúdez-Moreno algorithm involving two multipliers which can be obtained as fixed points of two nonlinear equations. Due to the slow convergence of this algorithm and its strong dependence on the parameters, we propose two new techniques to improve its efficiency: firstly, taking advantage of the good convergence properties of Newton methods and secondly, by means of considering the parameters of the Bermuúdez-Moreno algorithm as variable scalar functions. The efficiency of these algorithms are compared with the fixed point algorithm introduced in [9, 10]. The three studied algorithms are:

- FPM algorithm: the Bermúdez-Moreno algorithm combined with fixed point techniques summarized in Sections 3.5.3 and 3.5.4 to deal with the two nonlinearities which was introduced in [5].
- NM algorithm: the Bermúdez-Moreno algorithm together with Newton techniques, introduced in Sections 4.1 and 4.2.1.
- NVPM algorithm: the Newton algorithm for the contact nonlinearity introduced in Section 4.1 together with the Bermúdez-Moreno algorithm with variable parameters for the viscoplastic nonlinearity presented in Section 4.2.2.

Numerical results show that:

- The FPM algorithm is slow and strongly dependent on its parameters, but in turn very robust.
- The NM algorithm combined with some numerical strategies is fast and accurate. It needs fewer iterations and less cpu-time that the FPM one. The numerical strategies presented here –the adapted matrix factorization to the problem geometry, an adimensionalization technique and a time step optimization– work well in academic examples but, when they are applied to the casting simulation, convergence is not always achieved. Our guess is that

this unexpected difficulty is due to the very different behaviours found in casting processes (between recently solidified zones and others already cold).

- The main disadvantage of the FPM algorithm is its strong dependence on the parameters (see [9]). The NVPM algorithm overcomes this difficulty since the parameters are considered variable scalar functions, depending on time and space and they are automatically calculated. Moreover, it takes advantage of the good convergence properties of Newton method when solving the nonlinear contact condition. Numerical results in casting simulation show that the NVPM algorithm is adequate to solve the butt curl deformation.

Part II

Three-point bending tests: Mathematical study and numerical simulations

Table of Contents

Chapter 7

Introduction

An increasing number of new challenges are constantly arising for engineers, comprising new applications, new materials or possibly both. Very often, the behaviour of a certain material under new conditions cannot be correctly predicted, and many trial tests are needed in order to determine whether it can be used or not. Therefore, an enormous effort is actually being made with the purpose of developing new prediction techniques that allow saving huge amounts of money and time in testing the materials. Strangely enough, there are very few studies about how to predict the behaviour of the different materials under simple conditions. Several factors, such as slight differences in the composition or in the microstructure, can dramatically affect the result of the considered tests, making useless previous tests to use on similar materials. This is particularly critical for the ceramic materials.

In the common applications, materials are subjected to different forces, with complicated components of bending, torsion, compression and usually combinations of all of them. To predict the behaviour of a certain material, without performing expensive destructive tests, it is necessary to understand the mechanisms that affect its resistance to select the suitable failure criteria. The properties of the material are carefully measured in laboratory tests on a sample of material; these tests determine the value of their mechanical properties by measuring the applied forces and the corresponding relative changes of length. There exist many tests to determine material properties, classified into several groups attending to the applied forces, the sample conditions at the experiment instant, the environment conditions, etc. The most important experiments are:

- Tensile or compression test: An axial load is applied to a sample in order to obtain a uniform stress distribution on the cross-section.
- Torsion test: This test determine the behaviour of samples subjected to a pair of loads.
- Bending or flexure test: This test determine the behaviour of materials subjected to simple loads, for example, concentrated or uniformly distributed loads.
- Fatigue test: Used to study the behaviour of materials subjected to variable loads.
- Impact test: This test is a particular case of previous tests; the load is applied suddenly.

Figure 7.1: Three-point bending experiment.

In Part II of this manuscript we will focus our study on bending tests. The relative simplicity of these tests has permitted its popularization for measuring the mechanical properties of brittle materials. One of the most common tests is the *three-point bending test*: a sample of a brittle material is placed between three cylinders, without additional support, while the upper cylinder applies an increasing gradually force until the beam breaks (see Figure 7.1). From this test a property known as *modulus of rupture* (MOR) is obtained, which represents the maximum surface stress of the bent beam at the instant of failure. In the engineering literature, the MOR is calculated by an explicit formula which involves the value of the load at failure, H, the distance, $2l$, between the two lower cylinders or supports, and the second moment of inertia, I_1, of the transversal section of the beam (see [25]).

Nevertheless, discrepancies by no means negligible for MOR values have been noticed in experimental measurements depending on the specimen size, the ratio between the area of its section and the overall length or the relation between the distance of the two lower cylinders and the overall length of the beam. The fact that samples of same material can lead to different values for the MOR is something quite common but so far there are not many studies about this behaviour.

The aim of Part II is to study the mathematical problem associated to three-point bending tests in order to increase the knowledge about the MOR for brittle materials. Specifically, we prove the existence of a unique solution to the elastic problem with frictionless unilateral contact that arises from the mechanical model of the three-point bending test. Furthermore, in order to justify the classic formula for the MOR, we are interested in finding its limit model by using asymptotic analysis techniques when the thickness of the sample beam goes to zero (see [2, 18, 36, 80, 81]). By using this method, classical theories like Bernouilli-Navier, Saint Venant, Timoshenko and Vlassov theories were studied and justified (see [18, 80]). Also beams with a unilateral contact with a rigid foundation have already been studied in [82, 83] but only when the beam is clamped at the ends. Despite the absence of Dirichlet conditions for the three-dimensional mechanical problem associated with the three-point bending test, the asymptotic method allow us to obtain the limit one-dimensional problems for bending and for traction and to identify the relationship between the failure load and the corresponding axial normal tension. All theoretical results are collected in [70].

Besides, we are interested in finding an effective method to compute the MOR from brittle materials. To do this, we use all the theoretical background presented here to compute various approximations of the MOR. The procedure is the following: Once we have carried out several laboratory tests with ceramic beams, we determine the maximum force that beams can support until breaking –the rupture load. By using the classic formula for the MOR, we calculate the first value for it –the theoretical MOR. Then, after making numerical simulations of the one and three-dimensional models, considering the rupture load, we compute two new approximations for the MOR –the 1d and 3d numerical MOR. Finally, we obtain a fourth approach for the MOR by using a new expression obtained from the asymptotic analysis of our problem. All these methodologies are applied for cylindrical and rectangular beams made of porcelain, which is a brittle material used very frequently in engineering.

The new theoretical formula obtained in this manuscript leads us to a better approximation of the MOR for brittle materials. This expression takes into account not only the rupture load and the total length of the beam but also the distance between the two lower cylinders, the effect of the gravity and the distance between the ends of the beam and the lower cylinders (see [51]).

The outline of Part II is as follows:

In Chapter 8, we study the static behaviour of a three-dimensional elastic beam when is subjected to a three-point bending test. Under suitable compatibility conditions on the applied forces and on the geometry of the beam, we prove the existence of a unique solution for the associated contact elastic problem. These conditions of compatibility on the data come from the absence of a Dirichlet condition on the beam boundary.

In Chapter 9, we study the asymptotic behaviour of this problem; in particular, we deduce the one-dimensional models associated to the displacement components, and we give the existence and uniqueness of solution for them. Moreover, we give an expression for the normal axial stress in the beam which is related to the MOR of brittle materials. In the final part of the chapter, we deal with the regularity of the solution for the bending problem and we prove some properties of the coincidence set.

In Chapter 10, several examples for laboratory tests for cylindrical and rectangular beams made of porcelain are detailed. We show that the previous assumptions of compatibility are satisfied for these real experiments. Moreover, we present analytical solutions of the bending and axial displacements for these real experiments. Their solutions are obtained from their differential formulations given by means of the asymptotic analysis. Moreover, we introduce a new expression for the MOR.

Finally, in Chapter 11 we gather all the approaches for the MOR of the porcelain by using the methodology described above. We apply this procedure for both cylindrical and rectangular beams. In Appendix A we offer a brief description of the classic expression for the MOR used in mechanics of materials given that this information is not usually included in the mathematical bibliography.

Chapter 8

Mathematical study of three-point bending tests

In this chapter we introduce a mathematical model to simulate the deformation suffered by a beam subjected to the three-point bending test as well as its associated variational formulation. Moreover, we obtain a result of existence and uniqueness of solution under suitable compatibility conditions.

In Section 8.1, we show the mathematical model associated with the three-point bending test: an elastic problem with a unilateral contact condition, without friction, formulated in displacements. In Section 8.2, we propose a weak formulation of the problem in the appropriate functional spaces. Despite not impose Dirichlet conditions, assuming a suitable condition of compatibility on the applied forces, we prove the existence of a solution in Section 8.3. Assuming additional conditions of symmetry in the geometry of the beam and in the applied forces, in Section 8.4 we demonstrate the uniqueness of the solution.

8.1 Mathematical model

As usual in solid mechanics, Latin subscripts are understood to range over the integers $\{1, 2, 3\}$ and Greek subscripts (other than ϵ) over the integers $\{1, 2\}$. Moreover, Einstein summation over repeated subscripts is implied.

Given two vectors $\mathbf{u}, \mathbf{v} \in \mathbb{R}^3$, with components (u_i), (v_i), respectively, $\mathbf{u} \cdot \mathbf{v} = u_i v_i$ represents their scalar product. We denote by $\mathbb{R}^9_s$ the space of second order symmetric tensors over $\mathbb{R}^3$, endowed with the usual scalar product

$$\boldsymbol{\sigma} : \boldsymbol{\tau} = \sigma_{ij}\tau_{ij}, \quad \boldsymbol{\sigma}, \boldsymbol{\tau} \in \mathbb{R}^9_s.$$

Let ω be a bounded, open, connected Lipschitz subset of $\mathbb{R}^2$ with area A. Given $0 < \epsilon \leq 1$, we define $\omega^\epsilon = \epsilon\,\omega$ and we consider the domain $\Omega^\epsilon = \omega^\epsilon \times (-L, L)$, $L > 0$, which corresponds to the reference configuration of the beam. Consequently, the beam length is $2L$ and the area of the

cross section is $A^\epsilon = \epsilon^2 A$. We refer the motion of the beam to a fixed Cartesian system $0x_1^\epsilon x_2^\epsilon x_3^\epsilon$ whose origin is situated at the center of gravity of the beam (see Figure 8.1).

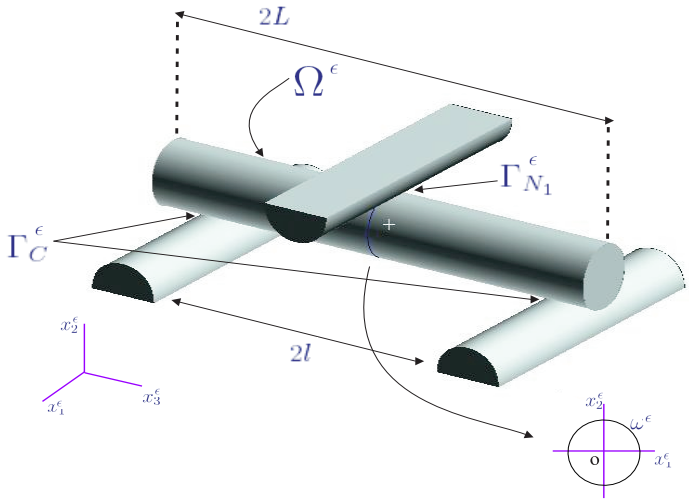

Figure 8.1: Sketch of the three-point bending test.

The physical problem consists of determining the displacement vector field, $\mathbf{u}^\epsilon$, and the stress tensor field, $\boldsymbol{\sigma}^\epsilon$, that the beam $\bar{\Omega}^\epsilon$ suffers when it is subjected to a three-point bending test.

8.1.1 Boundary conditions

Let Γ^ϵ be the boundary of the beam which is the union of the lateral boundary $\Gamma_l^\epsilon = \gamma^\epsilon \times [-L, L]$, where $\gamma^\epsilon = \partial\omega^\epsilon$, and the ends of the beam $\Gamma_\pm^\epsilon = \omega^\epsilon \times \{\pm L\}$; Γ^ϵ is assumed to be Lipschitz-continuous.

An arbitrary point of $\bar{\Omega}^\epsilon$ is denoted by $\mathbf{x}^\epsilon = (x_1^\epsilon, x_2^\epsilon, x_3^\epsilon)$ and $\mathbf{n}^\epsilon$ denotes the outward unit normal vector to Γ^ϵ. Notice that $\mathbf{n}^\epsilon(\mathbf{x}^\epsilon) = (n_1^\epsilon, n_2^\epsilon, 0)$ on the lateral boundary Γ_l^ϵ, where $(n_1^\epsilon(x_1^\epsilon, x_2^\epsilon), n_2^\epsilon(x_1^\epsilon, x_2^\epsilon))$ is the outward unit normal vector to ω^ϵ in $(x_1^\epsilon, x_2^\epsilon) \in \gamma^\epsilon$. Moreover, $\mathbf{n}^\epsilon = (0, 0, \pm 1)$ on $\Gamma_\pm^\epsilon$.

Lateral boundary Γ_l^ϵ is partitioned into three non-empty, open and disjointed parts Γ_C^ϵ, $\Gamma_{N_1}^\epsilon$ and $\Gamma_{N_2}^\epsilon$ satisfying $\bar{\Gamma}_l{}^\epsilon = \bar{\Gamma}_C^\epsilon \cup \bar{\Gamma}_{N_1}^\epsilon \cup \bar{\Gamma}_{N_2}^\epsilon$, where:

- $\bar{\Gamma}_C^\epsilon$ is the region of the beam where, due to the presence of the two lower cylinders, the normal component of the displacement cannot be positive. To impose this constraint and take into account the reaction force exerted by the two lower cylinders when the contact is effective, we consider a Signorini condition (see [54]):

$$\boldsymbol{\sigma}_\tau^\epsilon = \mathbf{0},\ \sigma_n^\epsilon \le 0,\ u_n^\epsilon \le 0,\ u_n^\epsilon \sigma_n^\epsilon = 0,\ \text{on } \Gamma_C^\epsilon \tag{8.1}$$

  where u_n^ϵ and σ_n^ϵ are the normal displacement and the normal stress at each point of the boundary, respectively, and $\mathbf{u}_\tau^\epsilon$ and $\boldsymbol{\sigma}_\tau^\epsilon$ are the tangential displacement and the tangential

component of $\boldsymbol{\sigma}^\epsilon \mathbf{n}^\epsilon$, respectively. We suppose that the two-dimensional measure of Γ_C^ϵ is strictly positive.

- $\Gamma_{N_1}^\epsilon$ corresponds to the region of the boundary in which the upper cylinder exerts a compression force with density $\mathbf{h}^\epsilon$ known.
- $\Gamma_{N_2}^\epsilon$ represents the remaining lateral boundary of the beam that is free of forces.

The ends of the beam are also assumed to be free of forces.

8.1.2 Equilibrium equations

Under the assumption of small displacements, the behaviour of the beam is governed by the usual equilibrium equations

$$-\mathrm{div}(\boldsymbol{\sigma}^\epsilon) = \mathbf{f}^\epsilon \text{ in } \Omega^\epsilon,$$

where the divergence operator is given by the expression

$$(\mathrm{div}^\epsilon(\boldsymbol{\tau}^\epsilon))_i = \frac{\partial \tau_{ij}^\epsilon}{\partial x_j^\epsilon},$$

and $\mathbf{f}^\epsilon$ denotes the volume density forces. In practice, we will only consider the gravitational forces.

8.1.3 Behaviour law

Let u_i^ϵ denote the i component of the displacement vector field $\mathbf{u}^\epsilon$; then the components of the infinitesimal strain field are given by

$$\varepsilon_{ij}^\epsilon(\mathbf{u}^\epsilon) = \frac{1}{2}\left(\frac{\partial u_i^\epsilon}{\partial x_j^\epsilon} + \frac{\partial u_j^\epsilon}{\partial x_i^\epsilon}\right), \tag{8.2}$$

where $\frac{\partial u_i^\epsilon}{\partial x_j^\epsilon}$ denotes the partial derivative of the component u_i^ϵ with respect to x_j^ϵ. We assume that $\boldsymbol{\varepsilon}^\epsilon(\mathbf{u}^\epsilon)$ is related to the stress tensor $\boldsymbol{\sigma}^\epsilon$ through Hooke's law (see [28] or [52]),

$$\boldsymbol{\sigma}^\epsilon = \boldsymbol{\Lambda}^\epsilon \boldsymbol{\varepsilon}^\epsilon(\mathbf{u}^\epsilon). \tag{8.3}$$

In the above expression, $\boldsymbol{\Lambda}^\epsilon$ is the fourth order linear elasticity tensor defined by

$$\boldsymbol{\Lambda}^\epsilon \boldsymbol{\tau} = \lambda^\epsilon \mathrm{tr}(\boldsymbol{\tau})\mathbf{I} + 2\mu^\epsilon \boldsymbol{\tau}, \tag{8.4}$$

where λ^ϵ and μ^ϵ are Lamé parameters of the material, related to Young's modulus E^ϵ and Poisson's ratio ν^ϵ by

$$\lambda^\epsilon = \frac{E^\epsilon \nu^\epsilon}{(1-2\nu^\epsilon)(1+\nu^\epsilon)}, \quad \mu^\epsilon = \frac{E^\epsilon}{2(1+\nu^\epsilon)}.$$

8.1.4 Problem (P^ϵ)

Summing up, the problem we must solve is the following:

Problem (P^ϵ):

Find the displacement vector field $\mathbf{u}(\mathbf{x})$ and the stress tensor field $\boldsymbol{\sigma}(\mathbf{x})$, at each point $\mathbf{x} \in \Omega$, satisfying:

$$-\mathrm{div}^\epsilon(\boldsymbol{\sigma}^\epsilon) = \mathbf{f}^\epsilon \text{ in } \Omega^\epsilon, \tag{8.5}$$

$$\boldsymbol{\sigma}^\epsilon \mathbf{n}^\epsilon = \mathbf{h}^\epsilon \text{ on } \Gamma^\epsilon_{N_1}, \tag{8.6}$$

$$\boldsymbol{\sigma}^\epsilon \mathbf{n}^\epsilon = \mathbf{0} \text{ on } \Gamma^\epsilon_{N_2} \cup \Gamma^\epsilon_{\pm}, \tag{8.7}$$

$$\boldsymbol{\sigma}^\epsilon_\tau = \mathbf{0},\ \sigma^\epsilon_n \le 0,\ u^\epsilon_n \le 0,\ \sigma^\epsilon_n u^\epsilon_n = 0 \text{ on } \Gamma^\epsilon_C, \tag{8.8}$$

$$\boldsymbol{\sigma}^\epsilon = \boldsymbol{\Lambda}^\epsilon \boldsymbol{\varepsilon}^\epsilon(\mathbf{u}^\epsilon) = \lambda^\epsilon \mathrm{tr}(\boldsymbol{\varepsilon}^\epsilon(\mathbf{u}^\epsilon))\mathbf{I} + 2\mu^\epsilon \boldsymbol{\varepsilon}^\epsilon(\mathbf{u}^\epsilon) \text{ in } \Omega^\epsilon. \tag{8.9}$$

8.2 Weak formulation

To carry out the mathematical analysis of Problem (P^ϵ), we introduce a weak formulation in a similar manner to those used in [40, 46, 54].

We consider the space of displacement vector fields $\mathbf{H}^1(\Omega^\epsilon) = [H^1(\Omega^\epsilon)]^3$ which is a Hilbert space with the norm

$$\|\mathbf{v}^\epsilon\|_{1,\Omega^\epsilon} = \left(\sum_{i=1}^{3} \|v_i^\epsilon\|^2_{0,\Omega^\epsilon} + \sum_{i,j=1}^{3} \|\varepsilon^\epsilon_{ij}(\mathbf{v}^\epsilon)\|^2_{0,\Omega^\epsilon} \right)^{1/2},$$

where $\|\cdot\|_{0,\Omega^\epsilon}$ denotes the usual norm in $L^2(\Omega^\epsilon)$. The subset of kinematically admissible displacements is the convex set (see [54])

$$\mathbf{K}(\Omega^\epsilon) = \{\mathbf{v}^\epsilon \in \mathbf{H}^1(\Omega^\epsilon); v^\epsilon_n \le 0 \text{ on } \Gamma^\epsilon_C\}.$$

Let us define the stress tensor space $\mathbf{X}(\Omega^\epsilon) = [L^2(\Omega^\epsilon)]^9_s$ where

$$[L^2(\Omega^\epsilon)]^9_s = \{\boldsymbol{\tau}^\epsilon = (\tau^\epsilon_{ij}) \in [L^2(\Omega^\epsilon)]^9; \tau^\epsilon_{ij} = \tau^\epsilon_{ji}\}.$$

$\mathbf{X}(\Omega^\epsilon)$ is a real Hilbert space endowed with the usual norm in $[L^2(\Omega^\epsilon)]^9$. Its subspace

$$\mathbf{H}(\mathrm{div}, \Omega^\epsilon) = \{\boldsymbol{\tau}^\epsilon \in \mathbf{X}(\Omega^\epsilon); \mathrm{div}^\epsilon(\boldsymbol{\tau}^\epsilon) \in \mathbf{L}^2(\Omega^\epsilon)\},$$

is also a Hilbert space with the norm

$$\|\boldsymbol{\tau}^\epsilon\|_{\mathbf{H}(\mathrm{div},\Omega^\epsilon)} = \left(\|\boldsymbol{\tau}^\epsilon\|^2_{0,\Omega^\epsilon} + \|\mathrm{div}^\epsilon(\boldsymbol{\tau}^\epsilon)\|^2_{0,\Omega^\epsilon}\right)^{1/2}.$$

We denote $\mathbf{H}^{1/2}(\Gamma^\epsilon) = [H^{1/2}(\Gamma^\epsilon)]^3$ as the image set of the trace application from $\mathbf{H}^1(\Omega^\epsilon)$. The following Green's formula holds:

$$\int_{\Omega^\epsilon} \boldsymbol{\tau}^\epsilon : \boldsymbol{\varepsilon}^\epsilon(\mathbf{v}^\epsilon) dx^\epsilon + \int_{\Omega^\epsilon} \mathrm{div}^\epsilon(\boldsymbol{\tau}^\epsilon) \cdot \mathbf{v}^\epsilon dx^\epsilon = \langle \boldsymbol{\tau}^\epsilon \mathbf{n}^\epsilon, \mathbf{v}^\epsilon \rangle_{\Gamma^\epsilon},$$

for all $\boldsymbol{\tau}^\epsilon \in \mathbf{H}(\mathrm{div}, \Omega^\epsilon)$ and $\mathbf{v}^\epsilon \in \mathbf{H}^1(\Omega^\epsilon)$, where $\langle \cdot, \cdot \rangle_{\Gamma^\epsilon}$ represents the duality between $\mathbf{H}^{-1/2}(\Gamma^\epsilon)$ and $\mathbf{H}^{1/2}(\Gamma^\epsilon)$.

8.2.1 Assumptions

From now on we consider the following hypotheses.

(H1$^\epsilon$) The volume forces satisfy $\mathbf{f}^\epsilon \in \mathbf{L}^2(\Omega^\epsilon)$ and the surface forces $\mathbf{h}^\epsilon \in \mathbf{L}^2(\Gamma^\epsilon_{N_1})$.

(H2$^\epsilon$) The material is homogeneous and isotropic; so, the elasticity tensor $\mathbf{\Lambda}^\epsilon$ defined in (8.9) is such that $\lambda^\epsilon, \mu^\epsilon \in \mathbb{R}$, $\lambda^\epsilon, \mu^\epsilon > 0$.

(H3$^\epsilon$) The applied forces verify the following compatibility condition

$$\int_{\Omega^\epsilon} \mathbf{f}^\epsilon \cdot \mathbf{w}^\epsilon dx^\epsilon + \int_{\Gamma^\epsilon_{N_1}} \mathbf{h}^\epsilon \cdot \mathbf{w}^\epsilon d\Gamma^\epsilon \leq 0,$$

for all $\mathbf{w}^\epsilon \in \mathbf{K}(\Omega^\epsilon) \cap \mathbf{R}(\Omega^\epsilon)$, where

$$\mathbf{R}(\Omega^\epsilon) = \{\mathbf{w}^\epsilon \in \mathbf{H}^1(\Omega^\epsilon) : \boldsymbol{\varepsilon}^\epsilon(\mathbf{w}^\epsilon) = \mathbf{0} \text{ in } [L^2(\Omega^\epsilon)]^9\},$$

is the set of rigid displacements. Moreover,

$$\int_{\Omega^\epsilon} \mathbf{f}^\epsilon \cdot \mathbf{w}^\epsilon dx^\epsilon + \int_{\Gamma^\epsilon_{N_1}} \mathbf{h}^\epsilon \cdot \mathbf{w}^\epsilon d\Gamma^\epsilon = 0,$$

if and only if $\mathbf{w}^\epsilon \in \mathbf{R}_n(\Omega^\epsilon)$, where

$$\mathbf{R}_n(\Omega^\epsilon) = \{\mathbf{w}^\epsilon \in \mathbf{R}(\Omega^\epsilon); w^\epsilon_n = 0 \ a.e. \text{ on } \Gamma^\epsilon_C\}.$$

(H4$^\epsilon$) The set $(\mathbf{K}(\Omega^\epsilon) \cap \mathbf{R}(\Omega^\epsilon)) \setminus \mathbf{R}_n(\Omega^\epsilon)$ is non-empty.

8.2.2 Weak formulation of the problem

To simplify the writing, the following notations are useful:

- The external virtual work for the applied forces over the virtual displacement $\mathbf{v}^\epsilon \in \mathbf{H}^1(\Omega^\epsilon)$ is defined as:
$$F^\epsilon(\mathbf{v}^\epsilon) = \int_{\Omega^\epsilon} \mathbf{f}^\epsilon \cdot \mathbf{v}^\epsilon dx^\epsilon + \int_{\Gamma^\epsilon_{N_1}} \mathbf{h}^\epsilon \cdot \mathbf{v}^\epsilon d\Gamma^\epsilon. \tag{8.10}$$

- The internal virtual work is related to the bilinear form a^ϵ defined by
$$a^\epsilon(\mathbf{v}^\epsilon, \mathbf{w}^\epsilon) = \int_{\Omega^\epsilon} \mathbf{\Lambda}^\epsilon \boldsymbol{\varepsilon}^\epsilon(\mathbf{v}^\epsilon) : \boldsymbol{\varepsilon}^\epsilon(\mathbf{w}^\epsilon) dx^\epsilon, \tag{8.11}$$
for all $\mathbf{v}^\epsilon, \mathbf{w}^\epsilon \in \mathbf{H}^1(\Omega^\epsilon)$.

With the above notation, we propose the following weak formulation:

Problem (VP^ϵ):

Find $(\mathbf{u}^\epsilon, \boldsymbol{\sigma}^\epsilon) \in \mathbf{K}(\Omega^\epsilon) \times \mathbf{X}(\Omega^\epsilon)$ such that

$$\begin{cases} a^\epsilon(\mathbf{u}^\epsilon, \mathbf{v}^\epsilon - \mathbf{u}^\epsilon) \geq F^\epsilon(\mathbf{v}^\epsilon - \mathbf{u}^\epsilon), \ \forall \mathbf{v}^\epsilon \in \mathbf{K}(\Omega^\epsilon), \\ \boldsymbol{\sigma}^\epsilon = \boldsymbol{\Lambda}^\epsilon \boldsymbol{\varepsilon}^\epsilon(\mathbf{u}^\epsilon). \end{cases} \tag{8.12}$$

It is easy to prove that every solution of the classic Problem (P^ϵ) is a solution of the weak Problem (VP^ϵ) and the reciprocal is also true (see [54]).

8.3 Existence of a solution of Problem (VP^ϵ)

Results of existence and uniqueness for Problem (VP^ϵ) when there exists a Dirichlet condition on a part of the boundary can be found in [61] or [58]. If there does not exist a Dirichlet condition, a result of existence was given by [40], rewritten Problem (VP^ϵ) as a minimization problem under the assumption of compatibility **(H3$^\epsilon$)**.

It is a classic result (see [37]) that Problem (VP^ϵ) admits the equivalent formulation:

Problem (MP^ϵ):

Find $\mathbf{u}^\epsilon \in \mathbf{K}(\Omega^\epsilon)$ such that

$$J^\epsilon(\mathbf{u}^\epsilon) \leq J^\epsilon(\mathbf{v}^\epsilon), \ \forall \mathbf{v}^\epsilon \in \mathbf{K}(\Omega^\epsilon),$$

where the minimization functional J^ϵ is defined by

$$J^\epsilon(\mathbf{v}^\epsilon) = \frac{1}{2} a^\epsilon(\mathbf{v}^\epsilon, \mathbf{v}^\epsilon) - F^\epsilon(\mathbf{v}^\epsilon), \quad \mathbf{v}^\epsilon \in \mathbf{H}^1(\Omega^\epsilon). \tag{8.13}$$

Consequently, we have the following result of existence:

Theorem 8.3.1. *Under assumptions* **(H1$^\epsilon$)-(H4$^\epsilon$)**, *there exists a solution* $\mathbf{u}^\epsilon$ *of Problem* (VP^ϵ).

Proof. The regularity properties of the domain Ω^ϵ, the assumptions **(H3$^\epsilon$) and (H4$^\epsilon$)** and that the bilinear form a^ϵ verifies

$$a^\epsilon(\mathbf{v}^\epsilon, \mathbf{v}^\epsilon) \geq 2\mu^\epsilon \|\boldsymbol{\varepsilon}^\epsilon(\mathbf{v}^\epsilon)\|^2_{0,\Omega^\epsilon}, \quad \forall \mathbf{v}^\epsilon \in \mathbf{H}^1(\Omega^\epsilon),$$

let us guarantee the hypotheses of theorem XVII of [40] so we can get the existence of a minimum of Problem (MP^ϵ) and consequently the existence of a solution of Problem (VP^ϵ). □

8.3.1 Properties of a solution of Problem (VP^ϵ)

In the following Lemma we are going to prove that, if there exists a gap between the beam and the lower cylinders, then the movement of the beam is free there.

Lemma 8.3.2. *Let* $(\mathbf{u}^\epsilon, \boldsymbol{\sigma}^\epsilon) \in \mathbf{K}(\Omega^\epsilon) \times \mathbf{X}(\Omega^\epsilon)$ *a solution for Problem* (VP^ϵ). *Let* $A \subset \Gamma_C^\epsilon$, $\text{meas}(A) > 0$, *such that* $u_n^\epsilon < 0$ *on* A. *Then* $\sigma_n^\epsilon = 0$ *on* A.

Proof. Since $(\mathbf{u}^\epsilon, \boldsymbol{\sigma}^\epsilon)$ is a solution of Problem (P^ϵ) in the sense of the distributions, we obtain that

$$\langle \boldsymbol{\sigma}^\epsilon \mathbf{n}^\epsilon, \mathbf{v}^\epsilon - \mathbf{u}^\epsilon \rangle_{\Gamma^\epsilon} \geq \int_{\Gamma_{N_1}^\epsilon} \mathbf{h}^\epsilon \cdot (\mathbf{v}^\epsilon - \mathbf{u}^\epsilon) d\Gamma^\epsilon,$$

for every $\mathbf{v}^\epsilon \in \mathbf{K}(\Omega^\epsilon)$. By choosing $\mathbf{v}^\epsilon = 2\mathbf{u}^\epsilon$ and $\mathbf{v}^\epsilon = \mathbf{u}^\epsilon/2$, we have that

$$\langle \boldsymbol{\sigma}^\epsilon \mathbf{n}^\epsilon, \mathbf{u}^\epsilon \rangle_{\Gamma^\epsilon} = \int_{\Gamma_{N_1}^\epsilon} \mathbf{h}^\epsilon \cdot \mathbf{u}^\epsilon d\Gamma^\epsilon. \tag{8.14}$$

Let us assume that $\sigma_n^\epsilon < 0$ on $B \subset A$, with $\text{meas}(B) > 0$. Since $\boldsymbol{\sigma}^\epsilon \mathbf{n}^\epsilon = \mathbf{h}^\epsilon$ on $\Gamma_{N_1}^\epsilon$, $\boldsymbol{\sigma}^\epsilon \mathbf{n}^\epsilon = \mathbf{0}$ on $\Gamma_{N_2}^\epsilon$, $\boldsymbol{\sigma}_\tau^\epsilon = \mathbf{0}$ on Γ_C^ϵ and $\sigma_n^\epsilon \leq 0$ on Γ_C^ϵ, we can deduce that

$$\langle \sigma_n^\epsilon, v_n^\epsilon \rangle_{\Gamma^\epsilon} > \int_{\Gamma_{N_1}^\epsilon} \mathbf{h}^\epsilon \cdot \mathbf{v}^\epsilon d\Gamma^\epsilon,$$

for every $\mathbf{v}^\epsilon \in \mathbf{K}(\Omega^\epsilon)$ such that $v_n^\epsilon < 0$ on B. This is a contradiction to (8.14) if we consider $\mathbf{v}^\epsilon = \mathbf{u}^\epsilon$. □

Lemma 8.3.3. *Under assumptions* **(H1$^\epsilon$)-(H4$^\epsilon$)**, *there exists a subset* $\Gamma_D^\epsilon \subset \Gamma_C^\epsilon$, $\text{meas}(\Gamma_D^\epsilon) > 0$, *such that the solution* $\mathbf{u}^\epsilon$ *of Problem* (VP^ϵ) *satisfies:*

$$u_n^\epsilon = 0 \text{ on } \Gamma_D^\epsilon.$$

Proof. Let us assume that there does not exist Γ_D^ϵ in those conditions. Then $u_n^\epsilon < 0$ on Γ_C^ϵ and, from Lemma 8.3.2, $\boldsymbol{\sigma}^\epsilon \mathbf{n}^\epsilon = \mathbf{0}$ on Γ_C^ϵ. Therefore, the tensor $\boldsymbol{\sigma}^\epsilon \mathbf{n}^\epsilon \in [L^2(\Gamma^\epsilon)]^3$ verifies

$$\boldsymbol{\sigma}^\epsilon \mathbf{n}^\epsilon = \begin{cases} \mathbf{h}^\epsilon & \text{on } \Gamma_{N_1}^\epsilon, \\ \mathbf{0} & \text{on } \Gamma_{N_2}^\epsilon \cup \Gamma_\pm^\epsilon \cup \Gamma_C^\epsilon. \end{cases} \tag{8.15}$$

Given that $\mathbf{u}^\epsilon$ is a solution of Problem (P^ϵ) in the sense of the distributions, we can replace boundary conditions (8.6)-(8.8) by (8.15) to conclude that

$$a^\epsilon(\mathbf{u}^\epsilon, \mathbf{w}^\epsilon) = F^\epsilon(\mathbf{w}^\epsilon), \, \forall \mathbf{w}^\epsilon \in \mathbf{H}^1(\Omega^\epsilon).$$

By choosing $\mathbf{w}^\epsilon \in (\mathbf{K}(\Omega^\epsilon) \cap \mathbf{R}(\Omega^\epsilon)) \setminus \mathbf{R}_n(\Omega^\epsilon)$, we find

$$0 = F^\epsilon(\mathbf{w}^\epsilon) = \int_{\Omega^\epsilon} \mathbf{f}^\epsilon \cdot \mathbf{w}^\epsilon dx^\epsilon + \int_{\Gamma_{N_1}^\epsilon} \mathbf{h}^\epsilon \cdot \mathbf{w}^\epsilon d\Gamma^\epsilon,$$

which is a contradiction with the assumption **(H3$^\epsilon$)**. □

Lemma 8.3.4. *Under assumptions* **(H1$^\epsilon$)-(H4$^\epsilon$)**, *if* $\mathbf{u}^\epsilon$ *is a solution of Problem* (VP^ϵ), *any other solution is given by* $\mathbf{u}^\epsilon + \mathbf{w}^\epsilon$, *where* $\mathbf{w}^\epsilon \in \mathbf{R}_n(\Omega^\epsilon)$.

Proof. Thanks to assumption **(H3$^\epsilon$)**, if $\mathbf{u}^\epsilon$ is a solution of Problem (VP^ϵ), then $\mathbf{u}^\epsilon + \mathbf{w}^\epsilon$ is also a solution for each $\mathbf{w}^\epsilon \in \mathbf{R}(\Omega^\epsilon)$ such that $w_n^\epsilon = 0$ on Γ_C^ϵ. Let us see the reciprocal.

Let us assume that $\mathbf{u}^\epsilon$ is a solution of Problem (VP^ϵ). By choosing as test functions $\mathbf{v}^\epsilon + \mathbf{u}^\epsilon$, with $\mathbf{v}^\epsilon = 2\mathbf{u}^\epsilon$ and $\mathbf{v}^\epsilon = \mathbf{u}^\epsilon/2$, we obtain

$$a^\epsilon(\mathbf{u}^\epsilon, \mathbf{v}^\epsilon) - F^\epsilon(\mathbf{v}^\epsilon) \geq 0, \quad \forall \mathbf{v}^\epsilon \in \mathbf{K}(\Omega^\epsilon), \tag{8.16}$$

$$a^\epsilon(\mathbf{u}^\epsilon, \mathbf{u}^\epsilon) - F^\epsilon(\mathbf{u}^\epsilon) = 0. \tag{8.17}$$

Expressions (8.16) and (8.17) allow us to prove the following inequality:

$$\begin{aligned} J^\epsilon(\mathbf{v}^\epsilon) - J^\epsilon(\mathbf{u}^\epsilon) &= \frac{1}{2}a^\epsilon(\mathbf{v}^\epsilon, \mathbf{v}^\epsilon) - F(\mathbf{v}^\epsilon) - \frac{1}{2}a^\epsilon(\mathbf{u}^\epsilon, \mathbf{u}^\epsilon) + F^\epsilon(\mathbf{u}^\epsilon) \\ &\geq \frac{1}{2}a^\epsilon(\mathbf{u}^\epsilon - \mathbf{v}^\epsilon, \mathbf{u}^\epsilon - \mathbf{v}^\epsilon) \geq 0, \, \forall \mathbf{v}^\epsilon \in \mathbf{K}(\Omega^\epsilon). \end{aligned}$$

If $\tilde{\mathbf{u}}^\epsilon \in \mathbf{K}(\Omega^\epsilon)$ is another solution of Problem (VP^ϵ) and equivalently of Problem (MP^ϵ), then

$$0 = J^\epsilon(\tilde{\mathbf{u}}^\epsilon) - J^\epsilon(\mathbf{u}^\epsilon) \geq \frac{1}{2}a^\epsilon(\mathbf{u}^\epsilon - \tilde{\mathbf{u}}^\epsilon, \mathbf{u}^\epsilon - \tilde{\mathbf{u}}^\epsilon) \geq 0,$$

that is, $\mathbf{u}^\epsilon - \tilde{\mathbf{u}}^\epsilon \in \mathbf{R}(\Omega^\epsilon)$. Therefore, we have

$$\tilde{\mathbf{u}}^\epsilon = \mathbf{u}^\epsilon + \mathbf{w}^\epsilon, \quad \mathbf{w}^\epsilon \in \mathbf{R}(\Omega^\epsilon).$$

In addition, given that $\mathbf{u}^\epsilon$ is also a solution of Problem (VP^ϵ), if we take $\mathbf{v}^\epsilon = \tilde{\mathbf{u}}^\epsilon$ in (8.12), we obtain

$$0 \geq F^\epsilon(\mathbf{w}^\epsilon) = \int_{\Omega^\epsilon} \mathbf{f}^\epsilon \cdot \mathbf{w}^\epsilon dx^\epsilon + \int_{\Gamma_{N_1}^\epsilon} \mathbf{h}^\epsilon \cdot \mathbf{w}^\epsilon d\Gamma^\epsilon.$$

Now, exchanging $\mathbf{u}^\epsilon$ and $\tilde{\mathbf{u}}^\epsilon$ in the above reasoning, we can conclude that $F^\epsilon(\mathbf{w}^\epsilon) = 0$. Therefore, from assumption **(H3$^\epsilon$)**, $w_n^\epsilon = 0$ on Γ_C^ϵ. This allows us to conclude the proof. □

8.4 Existence of a unique solution

In this section we are going to prove the uniqueness of solution of Problem (VP^ϵ) in the convex set $\mathbf{K}(\Omega^\epsilon)$. To do so, we assume the following assumptions of symmetry in the domain and in the applied forces.

(H5$^\epsilon$)

- Domain ω^ϵ is symmetrical with respect to the lines $x_1^\epsilon = 0$ and $x_2^\epsilon = 0$.
- Boundaries $\Gamma_{N_1}^\epsilon$ and Γ_C^ϵ are symmetrical with respect to the planes $x_1^\epsilon = 0$ and $x_3^\epsilon = 0$. Furthermore,

$$\begin{aligned} \Gamma_{N_1}^\epsilon &= \{\mathbf{x}^\epsilon \in \Gamma_l^\epsilon; |x_3^\epsilon| < \delta, \, (x_1^\epsilon, x_2^\epsilon) \in \gamma_{N_1}^\epsilon(x_3^\epsilon)\}, \\ \Gamma_C^\epsilon &= \{\mathbf{x}^\epsilon \in \Gamma_l^\epsilon; 0 < |x_3^\epsilon| - l < \hat{\delta}, \, (x_1^\epsilon, x_2^\epsilon) \in \gamma_C^\epsilon(x_3^\epsilon)\}, \end{aligned}$$

  where $2l$ is the distance between the two lower cylinders, $\gamma_{N_1}^\epsilon(x_3^\epsilon), \gamma_C^\epsilon(x_3^\epsilon) \subset \gamma^\epsilon$ and δ, $\hat{\delta}$ being small parameters, verifying $\delta < l - \hat{\delta}$.

- The second component of the outward normal vector to Γ^ϵ is not null on Γ_C^ϵ and with constant sign. Moreover, it is even with respect to x_1^ϵ.

(H6$^\epsilon$) Volume and surface forces verify that

- f_1^ϵ and h_1^ϵ are odd with respect to x_1^ϵ and even with respect to x_3^ϵ,
- f_2^ϵ and h_2^ϵ are even with respect to x_1^ϵ and x_3^ϵ,
- f_3^ϵ and h_3^ϵ are even with respect to x_1^ϵ and odd with respect to x_3^ϵ.

We consider the following subspace of $\mathbf{H}^1(\Omega^\epsilon)$:

$$\mathbf{H}_s^1(\Omega^\epsilon) = \left\{ \mathbf{v}^\epsilon \in \mathbf{H}^1(\Omega^\epsilon);\ \begin{array}{l} v_1^\epsilon \text{ is odd in } x_1^\epsilon \text{ and even in } x_3^\epsilon \\ v_2^\epsilon \text{ is even in } x_1^\epsilon \text{ and } x_3^\epsilon \\ v_3^\epsilon \text{ is even in } x_1^\epsilon \text{ and is odd in } x_3^\epsilon \end{array} \right\}.$$

Theorem 8.4.1. *Under assumptions* **(H1$^\epsilon$)-(H6$^\epsilon$)**, *there exists a unique solution* $\mathbf{u}^\epsilon \in \mathbf{H}_s^1(\Omega^\epsilon)$ *of Problem* (VP^ϵ)

Proof. Suppose that $\mathbf{u}^\epsilon \in \mathbf{H}^1(\Omega^\epsilon) \cap \mathbf{K}(\Omega^\epsilon)$ is a solution of Problem (VP^ϵ) and let $\hat{\mathbf{u}}^\epsilon$ be the vector field defined by:

$$\hat{\mathbf{u}}^\epsilon(x_1^\epsilon, x_2^\epsilon, x_3^\epsilon) = (-u_1^\epsilon(-x_1^\epsilon, x_2^\epsilon, x_3^\epsilon), u_2^\epsilon(-x_1^\epsilon, x_2^\epsilon, x_3^\epsilon), u_3^\epsilon(-x_1^\epsilon, x_2^\epsilon, x_3^\epsilon)).$$

Taking into account assumptions **(H5$^\epsilon$)** and **(H6$^\epsilon$)**, we can conclude that $\hat{\mathbf{u}}^\epsilon$ is also a solution of Problem (VP^ϵ). Moreover, it is easy to prove that $\hat{\hat{\mathbf{u}}}^\epsilon = 1/2(\mathbf{u}^\epsilon + \hat{\mathbf{u}}^\epsilon)$ is a solution of Problem (VP^ϵ) such that $\hat{u_1^\epsilon}$ is odd with respect to x_1^ϵ and $\hat{u_2^\epsilon}$ and $\hat{u_3^\epsilon}$ are even with respect to x_1^ϵ.

Analogously, if $\tilde{\mathbf{u}}^\epsilon$ is the vector field

$$\tilde{\mathbf{u}}^\epsilon(x_1^\epsilon, x_2^\epsilon, x_3^\epsilon) = (\hat{u}_1^\epsilon(x_1^\epsilon, x_2^\epsilon, -x_3^\epsilon), \hat{u}_2^\epsilon(x_1, x_2, -x_3), -\hat{u}_3^\epsilon(x_1^\epsilon, x_2^\epsilon, -x_3^\epsilon)),$$

both $\tilde{\mathbf{u}}^\epsilon$ and $\tilde{\tilde{\mathbf{u}}}^\epsilon = 1/2(\tilde{\mathbf{u}}^\epsilon + \hat{\tilde{\mathbf{u}}}^\epsilon)$ are solutions of Problem (VP^ϵ); moreover, $\tilde{u_3^\epsilon}$ is odd with respect to x_3^ϵ and $\tilde{u_1^\epsilon}$ and $\tilde{u_2^\epsilon}$ are even with respect to x_1^ϵ, that is, $\tilde{\tilde{\mathbf{u}}}^\epsilon \in \mathbf{H}_s^1(\Omega^\epsilon)$.

Finally, let $\bar{\mathbf{u}}^\epsilon \in \mathbf{H}_s^1(\Omega^\epsilon)$ be any solution of Problem (VP^ϵ). From Lemma 8.3.4, there exists $\mathbf{w}^\epsilon \in \mathbf{R}_n(\Omega^\epsilon)$ such that

$$\tilde{\tilde{\mathbf{u}}}^\epsilon = \bar{\mathbf{u}}^\epsilon + \mathbf{w}^\epsilon.$$

In addition, $\mathbf{w}^\epsilon$ must belong to $\mathbf{H}_s^1(\Omega^\epsilon)$, so we can conclude $\mathbf{w}^\epsilon = \mathbf{0}$ thanks to assumption **(H6$^\epsilon$)**. □

Remark 8.4.2. *Condition* **(H5$^\epsilon$)** *implies that the coordinates system* $0x_1^\epsilon x_2^\epsilon$ *is a principal system of inertia associated with the domain* ω^ϵ, *that is,*

$$\int_{\omega^\epsilon} x_\alpha^\epsilon dx_1^\epsilon dx_2^\epsilon = \int_{\omega^\epsilon} x_1^\epsilon x_2^\epsilon dx_1^\epsilon dx_2^\epsilon = 0. \tag{8.18}$$

Then, the 2×2 *geometrical inertia tensor of the cross section* w^ϵ *is just a diagonal matrix whose components are:*

$$I_1^\epsilon = \int_{\omega^\epsilon} (x_2^\epsilon)^2 dx_1^\epsilon dx_2^\epsilon,\ I_2^\epsilon = \int_{\omega^\epsilon} (x_1^\epsilon)^2 dx_1^\epsilon dx_2^\epsilon. \tag{8.19}$$

Chapter 9

Asymptotic analysis of three-point bending tests

In the previous chapter we have studied the existence of the unique solution for an elastic problem with a frictionless unilateral contact condition in displacements arising from the mathematical modeling of three-point bending tests. In order to find a mathematical justification of the classic theoretical expression for the MOR –arising from the classical theory of beams–, our next objective is to study the behaviour of the solution $(\mathbf{u}^\epsilon, \boldsymbol{\sigma}^\epsilon)$ of Problem (VP^ϵ) when ϵ tends to be smaller. To do this, we use the well known asymptotic expansion method (see [81, 18, 80]). This methodology allows us to obtain a one-dimensional limit model from the three-dimensional problem and to identify on it the relation between the rupture load and the corresponding MOR. By using this method, the classical theories of Bernouilli-Navier, Saint Venant, Timoshenko and Vlassov were studied and justified (see [18, 80]). Also beams in unilateral contact with a rigid foundation have already been studied in [82] when the rod is clamped at the ends.

The outline of the chapter is as follows: In Section 9.1, we redefine Problem (VP^ϵ) in a domain independent of the cross-section parameter ϵ by means of a variable change, and we introduce the fundamental scalings on the unknowns and the assumptions on the data. The application of the asymptotic expansion method is described in Section 9.2, giving a characterization of the terms of first order of the expansion through one-dimensional variational problems. In addition, we give results of existence and uniqueness of solution for the corresponding axial and bending displacements. Section 9.3 is devoted to study the strong convergences of displacements and stresses. In Section 9.4, we rewrite the limit problem over the original domain and, finally, in Section 9.5, we present the differential formulations associated with the one-dimensional models and we give some properties of the coincidence set as well as some regularity results for the bending problem.

9.1 Rescaling functions and changing variables

Following [80] and in order to simplify the calculations, we are going to introduce the mixed variational formulation of Problem (P^ϵ).

Problem (MVP^ϵ):

Find $\mathbf{u}^\epsilon \in \mathbf{K}(\Omega^\epsilon)$ and $\boldsymbol{\sigma}^\epsilon \in \mathbf{X}(\Omega^\epsilon)$ such that

$$\int_{\Omega^\epsilon} \left[\frac{1+\nu^\epsilon}{E^\epsilon} \boldsymbol{\sigma}^\epsilon - \frac{\nu^\epsilon}{E^\epsilon} \mathrm{tr}(\boldsymbol{\sigma}^\epsilon)\mathbf{I} \right] : \boldsymbol{\tau}^\epsilon dx^\epsilon = \int_{\Omega^\epsilon} \boldsymbol{\varepsilon}^\epsilon(\mathbf{u}^\epsilon) : \boldsymbol{\tau}^\epsilon dx^\epsilon, \ \forall \boldsymbol{\tau}^\epsilon \in \mathbf{X}(\Omega^\epsilon), \tag{9.1}$$

$$\int_{\Omega^\epsilon} \boldsymbol{\sigma}^\epsilon : \boldsymbol{\varepsilon}^\epsilon(\mathbf{v}^\epsilon - \mathbf{u}^\epsilon) dx^\epsilon \geq F^\epsilon(\mathbf{v}^\epsilon - \mathbf{u}^\epsilon), \ \forall \mathbf{v}^\epsilon \in \mathbf{K}(\Omega^\epsilon), \tag{9.2}$$

where E^ϵ and ν^ϵ are the Young's modulus and the Poisson's ratio of the material, respectively, related to the Lamé parameters by the usual relations.

Remark 9.1.1. *Under assumptions* **(H1$^\epsilon$)-(H6$^\epsilon$)**, *there exists a unique solution of Problem* (MVP^ϵ) *in* $(\mathbf{H}^1_s(\Omega^\epsilon) \cap \mathbf{K}(\Omega^\epsilon)) \times \mathbf{X}(\Omega^\epsilon)$ *thanks to Theorem 8.4.1.*

Given that the dependence of the solution $(\mathbf{u}^\epsilon, \boldsymbol{\sigma}^\epsilon)$ of Problem (MVP^ϵ) with respect to ϵ is very complex, we define an equivalent problem for which this dependence is explicit. To do so, we use a change of variable to a fixed domain and the subsequent rescaling of the displacements and stresses. The reference domain, independent of ϵ, is

$$\Omega = \omega \times (-L, L), \ \Omega = \Omega^1,$$
$$\gamma = \partial\omega = \gamma^1, \ \Gamma = \partial\Omega = \Gamma^1.$$

We associate each point $\mathbf{x} \in \overline{\Omega}$ with a point $\mathbf{x}^\epsilon \in \overline{\Omega}^\epsilon$ through the transformation (see [18])

$$\begin{aligned} \Pi^\epsilon : \overline{\Omega} &\to \overline{\Omega}^\epsilon \\ \mathbf{x} = (x_1, x_2, x_3) &\to \Pi^\epsilon(\mathbf{x}) = \mathbf{x}^\epsilon = (\epsilon x_1, \epsilon x_2, x_3), \end{aligned} \tag{9.3}$$

in such a way that

$$\Gamma^\epsilon = \Pi^\epsilon(\Gamma), \ \mathbf{n}^\epsilon(\mathbf{x}^\epsilon) = \mathbf{n}(\mathbf{x}),$$

where $\mathbf{n}$ is the outward unit normal vector to the surface Γ.

We associate the functions $\mathbf{v}^\epsilon \in \mathbf{H}^1(\Omega^\epsilon)$ with the scaled functions $\mathbf{v}(\epsilon) \in \mathbf{H}^1(\Omega)$ through

$$v_\alpha(\epsilon)(\mathbf{x}) = \epsilon v^\epsilon_\alpha(\mathbf{x}^\epsilon), \ v_3(\epsilon)(\mathbf{x}) = v^\epsilon_3(\mathbf{x}^\epsilon), \tag{9.4}$$

and the functions $\boldsymbol{\tau}^\epsilon \in \mathbf{X}(\Omega^\epsilon)$ with the scaled functions $\boldsymbol{\tau}(\epsilon) \in \mathbf{X}(\Omega)$ through

$$\tau_{\alpha\beta}(\epsilon)(\mathbf{x}) = \epsilon^{-2}\tau^\epsilon_{\alpha\beta}(\mathbf{x}^\epsilon), \ \tau_{3\beta}(\epsilon)(\mathbf{x}) = \epsilon^{-1}\tau^\epsilon_{3\beta}(\mathbf{x}^\epsilon), \ \tau_{33}(\epsilon)(\mathbf{x}) = \tau^\epsilon_{33}(\mathbf{x}^\epsilon). \tag{9.5}$$

Notice that (9.4)-(9.5) are not *a priori* assumptions on the order of magnitude of the displacements or stresses. It will be a result of the forthcoming analysis that the rescaled unknowns are actually bounded.

In what follows, we consider the following additional assumptions on the data:

(H7$^\epsilon$) The Lamé parameters are independent of ϵ: $\lambda^\epsilon = \lambda$, $\mu^\epsilon = \mu$. Consequently, Young's modulus and Poisson's coefficient are independent of ϵ.

(H8$^\epsilon$) There exist functions $\mathbf{f} \in [L^2(\Omega)]^3$ and $\mathbf{h} \in [L^2(\Gamma_{N_1})]^3$ independent of ϵ and such that

$$f_\alpha^\epsilon(\mathbf{x}^\epsilon) = \epsilon f_\alpha(\mathbf{x}),\ f_3^\epsilon(\mathbf{x}^\epsilon) = f_3(\mathbf{x}),\ \mathbf{x} \in \Omega,$$
$$h_\alpha^\epsilon(\mathbf{x}^\epsilon) = \epsilon^2 h_\alpha(\mathbf{x}),\ h_3^\epsilon(\mathbf{x}^\epsilon) = \epsilon h_3(\mathbf{x}),\ \mathbf{x} \in \Gamma_{N_1}.$$

In addition, $\mathbf{f}$ and $\mathbf{h}$ verify:

$$f_\alpha \in L^2(\Omega), \quad f_3 \in H^1((-L, L); L^2(\omega)),$$
$$h_\alpha \in L^2(\Gamma_{N_1}), \quad h_3 \in H^1((-\delta, \delta); L^2(\gamma_{N_1})).$$

Under the previous assumptions we obtain the following result:

Theorem 9.1.2. *Under assumptions* **(H1$^\epsilon$)-(H8$^\epsilon$)**, *the scaled displacement and stress fields* $(\mathbf{u}(\epsilon), \boldsymbol{\sigma}(\epsilon))$ *of the solution* $(\mathbf{u}^\epsilon, \boldsymbol{\sigma}^\epsilon) \in (\mathbf{H}_s^1(\Omega^\epsilon) \cap \mathbf{K}(\Omega^\epsilon)) \times \mathbf{X}(\Omega^\epsilon)$ *of Problem* (MVP^ϵ) *is the unique solution of the problem:*

Problem $(MVP(\epsilon))$*:*

Find $\mathbf{u}(\epsilon) \in \mathbf{H}_s^1(\Omega) \cap \mathbf{K}(\Omega)$ *and* $\boldsymbol{\sigma}(\epsilon) \in \mathbf{X}(\Omega)$ *such that*

$$a_0(\boldsymbol{\sigma}(\epsilon), \boldsymbol{\tau}) + \epsilon^2 a_2(\boldsymbol{\sigma}(\epsilon), \boldsymbol{\tau}) + \epsilon^4 a_4(\boldsymbol{\sigma}(\epsilon), \boldsymbol{\tau}) - b(\boldsymbol{\tau}, \mathbf{u}(\epsilon)) = 0,\ \forall \boldsymbol{\tau} \in \mathbf{X}(\Omega), \tag{9.6}$$
$$b(\boldsymbol{\sigma}(\epsilon), \mathbf{v} - \mathbf{u}(\epsilon)) \geq F(\mathbf{v} - \mathbf{u}(\epsilon)), \quad \forall \mathbf{v} \in \mathbf{H}_s^1(\Omega) \cap \mathbf{K}(\Omega), \tag{9.7}$$

where

$$a_0(\boldsymbol{\sigma}, \boldsymbol{\tau}) = \int_\Omega \frac{1}{E} \sigma_{33} \tau_{33} dx, \tag{9.8}$$
$$a_2(\boldsymbol{\sigma}, \boldsymbol{\tau}) = \int_\Omega \Big[\frac{2(1+\nu)}{E} \sigma_{3\beta} \tau_{3\beta} - \frac{\nu}{E}(\sigma_{33}\tau_{\mu\mu} + \sigma_{\mu\mu}\tau_{33})\Big] dx, \tag{9.9}$$
$$a_4(\boldsymbol{\sigma}, \boldsymbol{\tau}) = \int_\Omega \Big[\frac{1+\nu}{E} \sigma_{\alpha\beta} - \frac{\nu}{E} \sigma_{\mu\mu} \delta_{\alpha\beta}\Big] \tau_{\alpha\beta} dx, \tag{9.10}$$
$$b(\boldsymbol{\tau}, \mathbf{v}) = \int_\Omega \tau_{ij} \varepsilon_{ij}(\mathbf{v}) dx, \tag{9.11}$$
$$F(\mathbf{v}) = \int_\Omega f_i v_i dx + \int_{\Gamma_{N_1}} h_i v_i d\Gamma. \tag{9.12}$$

Proof. Taking into account expression (9.4), we obtain the following relation between the linearized strain tensor $\boldsymbol{\varepsilon}^\epsilon(\mathbf{v}^\epsilon)$ and the scaled linearized strain tensor $\boldsymbol{\varepsilon}(\mathbf{v})$:

$$\varepsilon_{\alpha\beta}(\mathbf{v}(\epsilon)) = \epsilon^2 \varepsilon_{\alpha\beta}^\epsilon(\mathbf{v}^\epsilon),\ \varepsilon_{3\beta}(\mathbf{v}(\epsilon)) = \epsilon\, \varepsilon_{3\beta}^\epsilon(\mathbf{v}^\epsilon),\ \varepsilon_{33}(\mathbf{v}(\epsilon)) = \varepsilon_{33}^\epsilon(\mathbf{v}^\epsilon).$$

So, we have that

$$\int_{\Omega^\epsilon} \mathbf{f}^\epsilon \cdot \mathbf{v}^\epsilon dx^\epsilon + \int_{\Gamma_{N_1}^\epsilon} \mathbf{h}^\epsilon \cdot \mathbf{v}^\epsilon d\Gamma^\epsilon = \epsilon^2 \left(\int_\Omega \mathbf{f} \cdot \mathbf{v}(\epsilon) dx + \int_{\Gamma_{N_1}} \mathbf{h} \cdot \mathbf{v}(\epsilon) d\Gamma \right),$$
$$\int_{\Omega^\epsilon} \boldsymbol{\sigma}^\epsilon : \boldsymbol{\varepsilon}^\epsilon(\mathbf{v}^\epsilon) dx^\epsilon = \epsilon^2 \left(\int_\Omega \boldsymbol{\sigma}(\epsilon) : \boldsymbol{\varepsilon}(\mathbf{v}(\epsilon)) dx \right),$$

thanks to (9.3)-(9.5). Consequently,

$$b(\boldsymbol{\sigma}(\epsilon), \mathbf{v} - \mathbf{u}(\epsilon)) \geq F(\mathbf{v} - \mathbf{u}(\epsilon)),\ \forall \mathbf{v} \in \mathbf{H}_s^1(\Omega) \cap \mathbf{K}(\Omega).$$

Analogously, substituting expressions (9.4), (9.5) and (9.8)-(9.12) in Problem (MVP^ϵ) and applying the change of variable theorem, we obtain expression (9.6). □

9.2 Asymptotic expansion method

From now on in Part II, unless otherwise stated, we assume hypotheses **(H1$^\epsilon$)-(H8$^\epsilon$)**. We suppose that the solution $(\mathbf{u}(\epsilon), \boldsymbol{\sigma}(\epsilon)) \in (\mathbf{H}_s^1(\Omega) \cap \mathbf{K}(\Omega)) \times \mathbf{X}(\Omega)$ of Problem $(MVP(\epsilon))$ can be written as a formal expansion

$$(\mathbf{u}(\epsilon), \boldsymbol{\sigma}(\epsilon)) = (\mathbf{u}^0, \boldsymbol{\sigma}^0) + \epsilon^2(\mathbf{u}^2, \boldsymbol{\sigma}^2) + \epsilon^4(\mathbf{u}^4, \boldsymbol{\sigma}^4) + o(\epsilon^4), \tag{9.13}$$

where $\mathbf{u}^i \in \mathbf{H}_s^1(\Omega) \cap \mathbf{K}(\Omega)$ and $\boldsymbol{\sigma}^i \in \mathbf{X}(\Omega)$ are independent of ϵ. Substituting expression (9.13) in Problem $(MVP(\epsilon))$ and identifying the coefficients of the same powers of ϵ, we obtain formally that the terms of order zero must be a solution of the problem:

Problem (MVP^0):

$$\begin{aligned} &\mathbf{u}^0 \in \mathbf{H}_s^1(\Omega) \cap \mathbf{K}(\Omega), \quad \boldsymbol{\sigma}^0 \in \mathbf{X}(\Omega), \\ &a_0(\boldsymbol{\sigma}^0, \boldsymbol{\tau}) - b(\boldsymbol{\tau}, \mathbf{u}^0) = 0, \quad \forall \boldsymbol{\tau} \in \mathbf{X}(\Omega), \\ &b(\boldsymbol{\sigma}^0, \mathbf{v} - \mathbf{u}^0) \geq F(\mathbf{v} - \mathbf{u}^0), \quad \forall \mathbf{v} \in \mathbf{H}_s^1(\Omega) \cap \mathbf{K}(\Omega). \end{aligned} \tag{9.14}$$

In order to characterize the element $(\mathbf{u}^0, \boldsymbol{\sigma}^0)$, solution of Problem (MVP^0), we consider the decomposition

$$\mathbf{H}_s^1(\Omega) = \mathbf{W}_{s2}(\Omega) \times H_s^1(\Omega),$$

where

$$\begin{aligned} \mathbf{W}_{s2}(\Omega) &= \{(v_1, v_2) \in [H^1(\Omega)]^2; (v_1, v_2, 0) \in \mathbf{H}_s^1(\Omega)\}, \\ H_s^1(\Omega) &= \{v \in H^1(\Omega); (0, 0, v) \in \mathbf{H}_s^1(\Omega)\}. \end{aligned}$$

Taking into account that in the contact boundary Γ_C the outward normal vector is given by $(n_1, n_2, 0)$, we have that

$$\mathbf{K}(\Omega) = \mathbf{K}_2(\Omega) \times H^1(\Omega),$$

where

$$\mathbf{K}_2(\Omega) = \{(v_1, v_2) \in [H^1(\Omega)]^2; v_\alpha n_\alpha \leq 0 \text{ on } \Gamma_C\}.$$

Consequently, Problem (MVP^0) can be rewritten in the equivalent form:

$$(u_1^0, u_2^0) \in \mathbf{W}_{s2}(\Omega) \cap \mathbf{K}_2(\Omega),\ u_3^0 \in H_s^1(\Omega), \boldsymbol{\sigma}^0 \in \mathbf{X}(\Omega), \tag{9.15}$$

$$\int_\Omega \frac{1}{E}\sigma_{33}^0 \tau_{33} dx - \int_\Omega \partial_3 u_3^0 \tau_{33} dx = 0, \forall \tau_{33} \in L^2(\Omega), \tag{9.16}$$

$$\int_\Omega \varepsilon_{3\beta}(\mathbf{u}^0)\tau_{3\beta} dx = 0, \forall (\tau_{3\beta}) \in [L^2(\Omega)]^2, \tag{9.17}$$

$$\int_\Omega \varepsilon_{\alpha\beta}(\mathbf{u}^0)\tau_{\alpha\beta} dx = 0, \forall (\tau_{\alpha\beta}) \in [L^2(\Omega)]_s^4, \tag{9.18}$$

$$\int_\Omega (\sigma_{33}^0 \partial_3 v_3 + \sigma_{3\beta}^0 \partial_\beta v_3) dx = \int_\Omega f_3 v_3 dx + \int_{\Gamma_{N_1}} h_3 v_3 d\Gamma, \forall v_3 \in H_s^1(\Omega), \tag{9.19}$$

$$\int_\Omega [\sigma_{\alpha\beta}^0 \partial_\alpha (v_\beta - u_\beta^0) + \sigma_{3\beta}^0 \partial_3 (v_\beta - u_\beta^0)] dx \geq \int_\Omega f_\beta (v_\beta - u_\beta^0) dx + \int_{\Gamma_{N_1}} h_\beta (v_\beta - u_\beta^0) d\Gamma, \tag{9.20}$$
$$\forall (v_\beta) \in \mathbf{W}_{s2}(\Omega) \cap \mathbf{K}_2(\Omega).$$

To characterize the solutions of Problem (9.15)-(9.20), we introduce the following notations:

- The total force per unit of length is

$$q_i(x_3) = \int_\omega f_i(x_1, x_2, x_3) dx_1 dx_2 + \chi_{[-\delta,\delta]}(x_3) \int_{\gamma_{N_1}(x_3)} h_i(x_1, x_2, x_3) d\gamma. \tag{9.21}$$

- The total moment about the origin of the cross-section per unit of length is defined as

$$\mathbf{M}(x_3) = \int_\omega (x_2 f_3, -x_1 f_3, x_1 f_2 - x_2 f_1) dx_1 dx_2 + \chi_{[-\delta,\delta]}(x_3) \int_{\gamma_{N_1}(x_3)} (x_2 h_3, -x_1 h_3, x_1 h_2 - x_2 h_1) d\gamma. \tag{9.22}$$

We also introduce the subspace of $\mathbf{H}^1(\Omega)$ corresponding to Bernouilli-Navier displacements (see [80]):

$$\mathbf{V}_{BN}(\Omega) = \{\mathbf{v} \in \mathbf{H}_s^1(\Omega); v_\alpha \in H^2(-L, L), v_3 = \underline{v}_3 - x_\alpha \partial_3 v_\alpha, \underline{v}_3 \in H^1(-L, L)\}.$$

Moreover, to take into account the hypotheses of symmetry, we consider the subspace of $H^m(-L, L)$, $H_e^m(-L, L)$ and $H_o^m(-L, L)$, $m = 1, 2$, corresponding to its even and odd functions, respectively.

The following theorem characterizes the solutions of Problem (9.15)-(9.20):

Theorem 9.2.1. *Every solution of Problem (9.15)-(9.20) verifies:*

(i) The displacement field $\mathbf{u}^0 \in \mathbf{V}_{BN}(\Omega)$*;* u_3^0 *being given by*

$$u_3^0(x_1, x_2, x_3) = \underline{u}_3^0(x_3) - x_2 \partial_3 u_2^0(x_3),\ \forall (x_1, x_2, x_3) \in \Omega, \tag{9.23}$$

with $\underline{u}_3^0 \in H_o^1(-L, L)$*. Moreover,* u_1^0 *is null and* $u_2^0 \in H_e^2(-L, L)$*.*

(ii) The axial stress σ_{33}^0 *is given by*

$$\sigma_{33}^0 = E\partial_3 u_3^0 = E(\partial_3 \underline{u}_3^0 - x_2 \partial_{33} u_2^0), \tag{9.24}$$

and the corresponding component of the bending moment is

$$m_2^0 = \int_\omega x_2 \sigma_{33}^0 dx_1 dx_2 = -EI_1 \partial_{33} u_2^0.$$

(iii) The stretch component $\underline{u}_3^0$ *is a solution of the axial problem:*

Problem $(\mathbf{P_3^0})$*: Find* $\underline{u}_3^0 \in H_o^1(-L, L)$ *such that*

$$\int_{-L}^{L} EA\partial_3 \underline{u}_3^0 \partial_3 v_3^0 dx_3 = \int_{-L}^{L} q_3 v_3^0 dx_3, \tag{9.25}$$

for all $v_3^0 \in H_o^1(-L, L)$.

(iv) The displacement u_2^0 *is a solution of the bending problem:*

Problem $(\mathbf{P_2^0})$*: Find* $u_2^0 \in H_e^2(-L, L)$, $(0, u_2^0) \in \mathbf{K}_2(\Omega)$, *such that*

$$\int_{-L}^{L} EI_1 \partial_{33} u_2^0 \partial_{33}(v_2^0 - u_2^0) dx_3 \geq \int_{-L}^{L} q_2(v_2^0 - u_2^0) dx_3 - \int_{-L}^{L} M_1 \partial_3 (v_2^0 - u_2^0) dx_3, \tag{9.26}$$

for all $v_2^0 \in H_e^2(-L, L)$, $(0, v_2^0) \in \mathbf{K}_2(\Omega)$.

Proof. *(i)* By expression (9.18) we obtain that

$$\partial_1 u_1^0 = \partial_2 u_2^0 = 0, \quad \partial_1 u_2^0 + \partial_2 u_1^0 = 0.$$

Then, we deduce

$$u_1^0(x_1, x_2, x_3) = \phi_1^0(x_2, x_3),\ u_2^0(x_1, x_2, x_3) = \phi_2^0(x_1, x_3),$$
$$\partial_2 \phi_1^0(x_2, x_3) + \partial_1 \phi_2^0(x_1, x_3) = 0.$$

Given that the variables x_1, x_2 and x_3 are independent, we find that

$$\partial_2 \phi_1^0(x_2, x_3) = -\partial_1 \phi_2^0(x_1, x_3) = z^0(x_3)$$

and consequently,

$$u_1^0(x_1, x_2, x_3) = z_1^0(x_3) + x_2 z^0(x_3),$$
$$u_2^0(x_1, x_2, x_3) = z_2^0(x_3) - x_1 z^0(x_3).$$

In addition, u_1^0 must be odd with respect to x_1, so $z_1^0 = z^0 \equiv 0$. Therefore, $u_1^0 = 0$ and $u_2^0 = z_2^0(x_3)$. Moreover, $(u_1^0, u_2^0) \in \mathbf{W}_{s2}(\Omega)$ and consequently, $z_2^0 \in H_e^1(-L, L)$.

Furthermore, from (9.17), $\varepsilon_{3\beta}(\mathbf{u}^0) = 0$, thus

$$\partial_1 u_3^0 = -\partial_3 u_1^0 = 0,\ \partial_2 u_3^0 = -\partial_3 u_2^0 = -\partial_3 z_2^0.$$

Integrating, we obtain that

$$u_3^0(x_1,x_2,x_3) = \underline{u}_3^0(x_3) - x_2\partial_3 z_2^0(x_3) = \underline{u}_3^0(x_3) - x_2\partial_3 u_2^0(x_3). \tag{9.27}$$

Summing up, we have proved that:

$$\mathbf{u}^0(x_1,x_2,x_3) = (0, u_2^0(x_3), \underline{u}_3^0(x_3) - x_2\partial_3 u_2^0(x_3)) \in \mathbf{H}_s^1(\Omega)\cap\mathbf{K}(\Omega). \tag{9.28}$$

In particular, $\partial_3 u_3^0 = \partial_3\underline{u}_3^0 - x_2\partial_{33}u_2^0 \in L^2(\Omega)$, from which we infer that:

$$\int_\Omega (\partial_3 u_3^0)^2 dx = A\int_{-L}^{L}(\partial_3\underline{u}_3^0(x_3))^2 dx_3 + I_1\int_{-L}^{L}(\partial_{33}u_2^0(x_3))^2 dx_3 < \infty;$$

so $u_2^0 \in H_e^2(-L,L)$ and $\underline{u}_3^0 \in H_o^1(-L,L)$.

(ii) It is easy to prove (9.24) substituting expression (9.27) in equation (9.16).

(iii) Substituting expression (9.24) in (9.19), we deduce that

$$\int_\Omega [E(\partial_3\underline{u}_3^0 - x_2\partial_{33}u_2^0)\partial_3 v_3 + \sigma_{3\beta}^0\partial_\beta v_3]dx = \int_\Omega f_3 v_3 dx + \int_{\Gamma_{N_1}} h_3 v_3 d\Gamma,\ \forall v_3 \in H_s^1(\Omega).$$

Choosing $v_3(x_1,x_2,x_3) = v_3^0(x_3) \in H_o^1(-L,L)$ as a test function, we have that

$$\int_\Omega E(\partial_3\underline{u}_3^0 - x_2\partial_{33}u_2^0)\partial_3 v_3^0 dx = \int_\Omega f_3 v_3^0 dx + \int_{\Gamma_{N_1}} h_3 v_3^0 d\Gamma.$$

Taking into account (8.18), we conclude that

$$\int_{-L}^{L} EA\partial_3\underline{u}_3^0\partial_3 v_3^0 dx_3 = \int_{-L}^{L}\left(\int_\omega f_3 dx_1 dx_2\right) v_3^0 dx_3 + \int_{-\delta}^{\delta}\left(\int_{\gamma_{N_1}(x_3)} h_3 d\gamma\right) v_3^0 dx_3,$$

for all $v_3^0 \in H_o^1(-L,L)$. Therefore, from expression (9.21), $\underline{u}_3^0$ is a solution of Problem $(\mathbf{P_3^0})$.

(iv) By choosing $(v_1,v_2)(x_1,x_2,x_3) = (0, v_2^0(x_3)) \in \mathbf{W}_{s2}(\Omega)\cap\mathbf{K}_2(\Omega)$, with $v_2^0 \in H_e^2(-L,L)$, as a test function in inequality (9.20), we obtain that

$$\int_\Omega \sigma_{32}^0\partial_3(v_2^0 - u_2^0)dx \geq \int_\Omega f_2(v_2^0 - u_2^0)dx + \int_{\Gamma_{N_1}} h_2(v_2^0 - u_2^0)d\Gamma. \tag{9.29}$$

Moreover, choosing $v_3(x_1,x_2,x_3) = x_2\partial_3(v_2^0 - u_2^0)(x_3) \in H_s^1(\Omega)$ in expression (9.19), we deduce that

$$\begin{aligned}&\int_\Omega [\sigma_{33}^0\partial_3(x_2\partial_3(v_2^0 - u_2^0)) + \sigma_{32}^0\partial_2(x_2\partial_3(v_2^0 - u_2^0))]dx\\ &= \int_\Omega f_3 x_2\partial_3(v_2^0 - u_2^0)dx + \int_{\Gamma_{N_1}} h_3 x_2\partial_3(v_2^0 - u_2^0)d\Gamma,\end{aligned}$$

and, consequently,

$$\int_\Omega [\sigma^0_{33} x_2 \partial_{33}(v^0_2 - u^0_2) + \sigma^0_{32} \partial_3 (v^0_2 - u^0_2)] dx$$
$$= \int_\Omega f_3 x_2 \partial_3 (v^0_2 - u^0_2) dx + \int_{\Gamma_{N_1}} h_3 x_2 \partial_3 (v^0_2 - u^0_2) d\Gamma. \tag{9.30}$$

Now, taking into account expression (9.24), we have that

$$\int_\Omega \sigma^0_{33} x_2 \partial_{33}(v^0_2 - u^0_2) dx = \int_{-L}^{L} \partial_{33}(v^0_2 - u^0_2) \left(\int_\omega x_2 E(\partial_3 \underline{u}^0_3 - x_2 \partial_{33} u^0_2) dx_1 dx_2 \right) dx_3 =$$
$$- \int_{-L}^{L} EI_1 \partial_{33} u^0_2 \partial_{33}(v^0_2 - u^0_2) dx_3. \tag{9.31}$$

From (9.29)-(9.31) we infer that:

$$\int_\Omega \sigma^0_{32} \partial_3 (v^0_2 - u^0_2) dx = \int_{-L}^{L} EI_1 \partial_{33} u^0_2 \partial_{33}(v^0_2 - u^0_2) dx_3 +$$
$$\int_\Omega x_2 f_3 \partial_3 (v^0_2 - u^0_2) dx + \int_{\Gamma_{N_1}} x_2 h_3 \partial_3 (v^0_2 - u^0_2) d\Gamma,$$
$$\int_\Omega \sigma^0_{32} \partial_3 (v^0_2 - u^0_2) dx \geq \int_\Omega f_2 (v^0_2 - u^0_2) dx + \int_{\Gamma_{N_1}} h_2 (v^0_2 - u^0_2) d\Gamma.$$

Finally, from expressions (9.21) and (9.22), we deduce inequality (9.26) and then (iv).

□

Theorem 9.2.2. *Under assumptions* **(H1$^\epsilon$), (H2$^\epsilon$), (H7$^\epsilon$)** *and* **(H8$^\epsilon$)**, *there exists a unique solution of Problem* $(\mathbf{P^0_3})$.

Proof. Since $\underline{u}^0_3$ must be an odd function, the bilinear form associated to Problem $(\mathbf{P^0_3})$ is coercive on $H^1_o(-L, L) \subset \mathcal{C}([-L, L])$ and the uniqueness is proved. □

Theorem 9.2.3. *Under assumptions* **(H1$^\epsilon$)-(H3$^\epsilon$)**, **(H7$^\epsilon$)** *and* **(H8$^\epsilon$)**, *there exists a unique solution of Problem* $(\mathbf{P^0_2})$.

Proof. It can be proved by applying a well-known result of Lions and Stampacchia [58]. Then, we consider $V = H^2_e(-L, L)$ which is a dense subspace of $H^1_e(-L, L) \subset C^0([-L, L])$.

We denote by p_0 the usual norm in $H^1(-L, L)$ which gives a pre-Hilbert structure to V and by p_1 the seminorm in V:

$$p_1(v) = \left\| \frac{d^2 v}{dx_3^2} \right\|_{0,(-L,L)}.$$

The subspace $Y = \{v \in V; p_1(v) = 0\}$ is finite-dimensional since

$$Y = \{v \in V; v(x_3) = c, c \in \mathbb{R}\}.$$

Moreover, due to the compact injection $V \hookrightarrow H_e^1(-L, L)$, we have that (see [74])

$$\inf_{y \in Y} p_0(v - y) \leq c_1 p_1(v), \, \forall v \in V. \tag{9.32}$$

If we denote by a the bilinear form in (9.26), we obtain that a is continuous on V and semicoercive, i.e.,

$$a(v, v) \geq c_2 p_1^2(v), \, \forall v \in V, \quad c_2 > 0. \tag{9.33}$$

In addition, the right-hand side of equation (9.26) can be identified as an element of V'

$$(F^0, v) = \int_{-L}^{L} q_2 v dx_3 - \int_{-L}^{L} M_1 \partial_3 v dx_3,$$

and, thanks to hypothesis ($\mathbf{H3}^\epsilon$) for $\varepsilon = 1$, it is easy to prove that

$$(F^0, y) < 0, \quad \forall y \in Y, \, y \neq 0, \, (0, y) \in \mathbf{K}_2(\Omega). \tag{9.34}$$

Relations (9.32)-(9.34) allow us to apply Theorem 5.1 of Lions and Stampacchia [58] and obtain the existence of, at least, one solution of Problem ($\mathbf{P_2^0}$).

Now, let us assume that u and $\tilde{u}$ are two different solutions of Problem ($\mathbf{P_2^0}$). Then, we can prove that there exists $y \in Y$such that $\tilde{u} = u + y$. Indeed, given that u and $\tilde{u}$ are solutions, we can write

$$\begin{aligned} a(u, \tilde{u} - u) &\geq (F^0, \tilde{u} - u) = (F^0, y), \\ a(\tilde{u}, \tilde{u} - u) &\leq (F^0, \tilde{u} - u) = (F^0, y), \end{aligned}$$

that is,

$$a(\tilde{u} - u, \tilde{u} - u) \leq 0.$$

Consequently, from (9.33), $y \in Y$ and $(F^0, y) = 0$; so, from (9.34), $y = 0$. In conclusion, there exists a unique solution of Problem ($\mathbf{P_2^0}$). □

9.3 Convergence of scaled displacements and stresses

In order to complete the asymptotic analysis of the problem, we are going to carry out a convergence analysis of the solution of Problem $(MVP(\varepsilon))$, $(\mathbf{u}(\epsilon), \boldsymbol{\sigma}(\epsilon))_{\varepsilon > 0}$, when ϵ goes to 0. For all $\mathbf{v} \in \mathbf{H}^1(\Omega)$, we denote

$$|\mathbf{v}|_{1,\Omega} = \|\mathbf{v}\|_{0,\Omega} + \|\boldsymbol{\varepsilon}(\mathbf{v})\|_{0,\Omega},$$

which is an equivalent norm to $\|\cdot\|_{1,\Omega}$ in $\mathbf{H}^1(\Omega)$; the first addend gives a pre-Hilbert structure to $\mathbf{H}^1(\Omega)$ and the second addend is a seminorm in $\mathbf{H}^1(\Omega)$.

Definition 9.3.1. *We define the subspace* $\mathbf{Y}(\Omega) = \mathbf{H}_s^1(\Omega) \cap \mathbf{R}(\Omega)$

$$\mathbf{Y}(\Omega) = \{\mathbf{w} \in \mathbf{H}_s^1(\Omega); \|\boldsymbol{\varepsilon}(\mathbf{w})\|_{0,\Omega} = 0\} = \{\mathbf{w} = (0, c, 0); c \in \mathbb{R}\}.$$

Lemma 9.3.2. *Let* P *be the projection of* $\mathbf{H}^1_s(\Omega)$ *onto* $\mathbf{Y}(\Omega)$*, with respect to the pre-Hilbert structure on* $\mathbf{H}^1_s(\Omega)$ *defined by* $\|\cdot\|_{0,\Omega}$*. Then,*

$$\mathrm{P}\mathbf{v} = (0, \mathcal{M}_\Omega(v_2), 0)\,,\ \forall \mathbf{v} \in \mathbf{H}^1_s(\Omega),$$
$$\mathcal{M}_\Omega(v_2) = \frac{1}{\mathrm{meas}(\Omega)} \int_\Omega v_2 dx.$$

Furthermore,

$$\inf_{\mathbf{w}\in\mathbf{Y}(\Omega)} \|\mathbf{v}-\mathbf{w}\|_{0,\Omega} = \|\mathbf{v}-\mathrm{P}\mathbf{v}\|_{0,\Omega} \le \tilde{C}\|\boldsymbol{\varepsilon}(\mathbf{v})\|_{0,\Omega},\ \forall \mathbf{v} \in \mathbf{H}^1_s(\Omega),\ \tilde{C} > 0, \tag{9.35}$$

$\tilde{C}$ *depending only on* Ω*.*

Proof. The projection $\mathbf{P}$ is well defined because $\mathbf{Y}(\Omega)$ is a finite-dimensional space. In addition, given that $\mathbf{Y}(\Omega)$ is a closed subspace, we have for each $\mathbf{v} \in \mathbf{H}^1_s(\Omega)$ (see [26])

$$(\mathbf{v} - \mathrm{P}\mathbf{v}, \mathbf{w}) = 0,\ \forall \mathbf{w} \in \mathbf{Y},$$

that is,

$$0 = (\mathbf{v} - \mathrm{P}\mathbf{v}, (0, c, 0)) = c \int_\Omega (v_2 - (\mathrm{P}\mathbf{v})_2)\, dx,\ \forall c \in \mathbb{R},\ c \neq 0.$$

Taking into account that $(Pv)_2$ is a constant, we can deduce

$$(\mathrm{P}\mathbf{v})_2 = \frac{1}{\mathrm{meas}(\Omega)} \int_\Omega v_2 dx = \mathcal{M}_\Omega(v_2).$$

Finally, $\mathcal{M}_\Omega(v_1) = \mathcal{M}_\Omega(v_3) = 0$ since $\mathbf{v} \in \mathbf{H}^1_s(\Omega)$ and from Poincaré-Wirtinger inequality, we obtain (9.35). □

From now on, we will use an auxiliary stress tensor $\tilde{\boldsymbol{\sigma}}(\epsilon)$ defined by

$$\tilde{\sigma}_{33}(\epsilon) = \sigma_{33}(\epsilon), \quad \tilde{\sigma}_{3\beta}(\epsilon) = \epsilon\sigma_{3\beta}(\epsilon), \quad \tilde{\sigma}_{\alpha\beta}(\epsilon) = \epsilon^2\sigma_{\alpha\beta}(\epsilon). \tag{9.36}$$

Lemma 9.3.3. *The following estimates hold:*

$$\|\tilde{\boldsymbol{\sigma}}(\epsilon)\|^2_{0,\Omega} \le C_1 \left(\|\mathbf{f}\|_{0,\Omega} + \|\mathbf{h}\|_{0,\Gamma_{N_1}}\right) \|\mathbf{u}(\epsilon)\|_{1,\Omega}, \tag{9.37}$$
$$C_2\|\boldsymbol{\varepsilon}(\mathbf{u}(\epsilon))\|^2_{0,\Omega} \le F(\mathbf{u}(\epsilon)), \tag{9.38}$$
$$\|\boldsymbol{\varepsilon}(\mathbf{u}(\epsilon))\|^2_{0,\Omega} \le C_3 \left(\|\mathbf{f}\|_{0,\Omega} + \|\mathbf{h}\|_{0,\Gamma_{N_1}}\right) \|\mathbf{u}(\epsilon)\|_{1,\Omega}. \tag{9.39}$$

Proof. If we consider $\mathbf{v} = \mathbf{0}$ and $\mathbf{v} = 2\mathbf{u}(\epsilon)$ in (9.7) and $\boldsymbol{\tau} = \boldsymbol{\sigma}(\epsilon)$ in (9.6) we obtain that

$$a_0(\boldsymbol{\sigma}(\epsilon), \boldsymbol{\sigma}(\epsilon)) + \epsilon^2 a_2(\boldsymbol{\sigma}(\epsilon), \boldsymbol{\sigma}(\epsilon)) + \epsilon^4 a_4(\boldsymbol{\sigma}(\epsilon), \boldsymbol{\sigma}(\epsilon)) = b(\boldsymbol{\sigma}(\epsilon), \mathbf{u}(\epsilon)) = F(\mathbf{u}(\epsilon)). \tag{9.40}$$

From (9.8)-(9.12) and (9.40) and taking into account expressions (9.36), it is easy to prove that

$$\int_\Omega \left(\frac{1+\nu}{E}\tilde{\sigma}_{ij}(\epsilon) - \frac{\nu}{E}\tilde{\sigma}_{pp}(\epsilon)\delta_{ij}\right)\tilde{\sigma}_{ij}(\epsilon)dx = \int_\Omega f_i u_i(\epsilon)dx + \int_{\Gamma_{N_1}} h_i u_i(\epsilon)d\Gamma.$$

Thanks to the properties of the Lamé coefficients and the assumptions on the volume and surface forces, we have that

$$C_4\|\tilde{\boldsymbol{\sigma}}(\epsilon)\|_{0,\Omega}^2 \leq \int_\Omega \left(\frac{1+\nu}{E}\tilde{\sigma}_{ij}(\epsilon) - \frac{\nu}{E}\tilde{\sigma}_{pp}(\epsilon)\delta_{ij}\right)\tilde{\sigma}_{ij}(\epsilon)dx =$$
$$\int_\Omega f_i u_i(\epsilon)dx + \int_{\Gamma_{N_1}} h_i u_i(\epsilon)d\Gamma \leq C_5\left(\|\mathbf{f}\|_{0,\Omega} + \|\mathbf{h}\|_{0,\Gamma_{N_1}}\right)\|\mathbf{u}(\epsilon)\|_{1,\Omega},$$

and consequently,

$$C_4\|\tilde{\boldsymbol{\sigma}}(\epsilon)\|_{0,\Omega}^2 \leq \int_\Omega \mathbf{f}\cdot\mathbf{u}(\epsilon)dx + \int_{\Gamma_{N_1}} \mathbf{h}\cdot\mathbf{u}(\epsilon)d\Gamma = F(\mathbf{u}(\epsilon)), \tag{9.41}$$
$$\|\tilde{\boldsymbol{\sigma}}(\epsilon)\|_{0,\Omega}^2 \leq C_1\left(\|\mathbf{f}\|_{0,\Omega} + \|\mathbf{h}\|_{0,\Gamma_{N_1}}\right)\|\mathbf{u}(\epsilon)\|_{1,\Omega},$$

where C_1 and C_4 are positive constants depending on Ω, E and ν. So, we have proved estimate (9.37).

From (9.6) and taking into account the definition of bilinear forms a_0, a_2 and a_4, we obtain that

$$\left|\int_\Omega \boldsymbol{\tau} : \boldsymbol{\varepsilon}(\mathbf{u}(\epsilon))dx\right| \leq C_6\|\tilde{\boldsymbol{\sigma}}(\epsilon)\|_{0,\Omega}\|\boldsymbol{\tau}\|_{0,\Omega},\ \forall\boldsymbol{\tau}\in\mathbf{X}(\Omega),\ C_6>0,$$

since $0<\epsilon\leq 1$. By choosing $\boldsymbol{\tau} = \boldsymbol{\varepsilon}(\mathbf{u}(\epsilon))$, we deduce that

$$\|\boldsymbol{\varepsilon}(\mathbf{u}(\epsilon))\|_{0,\Omega} \leq C_6\|\tilde{\boldsymbol{\sigma}}(\epsilon)\|_{0,\Omega}. \tag{9.42}$$

From inequalities (9.41) and (9.42), we have that

$$C_2\|\boldsymbol{\varepsilon}(\mathbf{u}(\epsilon))\|_{0,\Omega}^2 \leq \int_\Omega \mathbf{f}\cdot\mathbf{u}(\epsilon)dx + \int_{\Gamma_{N_1}} \mathbf{h}\cdot\mathbf{u}(\epsilon)d\Gamma = F(\mathbf{u}(\epsilon)),\ C_2>0,$$

therefore,

$$\|\boldsymbol{\varepsilon}(\mathbf{u}(\epsilon))\|_{0,\Omega}^2 \leq C_3\left(\|\mathbf{f}\|_{0,\Omega} + \|\mathbf{h}\|_{0,\Gamma_{N_1}}\right)\|\mathbf{u}(\epsilon)\|_{1,\Omega},$$

and hence estimates (9.38) and (9.39) are verified. □

Theorem 9.3.4. *There exist constants C_7 and C_8, independent of ϵ, such that for all $0<\epsilon\leq 1$ the solution $(\mathbf{u}(\epsilon),\boldsymbol{\sigma}(\epsilon))\in(\mathbf{H}_s^1(\Omega)\cap\mathbf{K}(\Omega))\times\mathbf{X}(\Omega)$ of Problem $(MVP(\varepsilon))$ verifies*

$$\|\mathbf{u}(\epsilon)\|_{1,\Omega} \leq C_7, \tag{9.43}$$

$$\|\sigma_{33}(\epsilon)\|_{0,\Omega} \leq C_8,\quad \epsilon\|\sigma_{3\beta}(\epsilon)\|_{0,\Omega} \leq C_8,\quad \epsilon^2\|\sigma_{\alpha\beta}(\epsilon)\|_{0,\Omega} \leq C_8. \tag{9.44}$$

Proof. Let us assume that (9.43) is false, so there exists a sequence $R_n\to+\infty$ as $n\to+\infty$ such that for all $n>0$ there exists ϵ_n satisfying

$$\|\mathbf{u}(\epsilon_n)\|_{1,\Omega} = R_n. \tag{9.45}$$

We define the sequence

$$\mathbf{w}_n = \frac{1}{R_n}\mathbf{u}(\epsilon_n), \tag{9.46}$$

that verifies $\mathbf{w}_n \in \mathbf{H}^1_s(\Omega) \cap \mathbf{K}(\Omega)$ and obviously $\|\mathbf{w}_n\|_{1,\Omega} = 1$. Therefore, there exists a subsequence, still denoted by $(\mathbf{w}_n)_{n\geq 0}$, such that $\mathbf{w}_n \rightharpoonup \mathbf{w}$ in $\mathbf{H}^1(\Omega)$ as $n \to +\infty$ and $\mathbf{w} \in \mathbf{H}^1_s(\Omega) \cap \mathbf{K}(\Omega)$.

From inequality (9.39), it is verified

$$\|\boldsymbol{\varepsilon}(\mathbf{u}(\epsilon_n))\|^2_{0,\Omega} \leq C_3 \left(\|\mathbf{f}\|_{0,\Omega} + \|\mathbf{h}\|_{0,\Gamma_{N_1}} \right) R_n, \tag{9.47}$$

and consequently,

$$\|\boldsymbol{\varepsilon}(\mathbf{w}_n)\|_{0,\Omega} = O(1/\sqrt{R_n}), \tag{9.48}$$

thanks to (9.46); so

$$\|\boldsymbol{\varepsilon}(\mathbf{w})\|_{0,\Omega} = 0, \tag{9.49}$$

that is, $\mathbf{w} \in \mathbf{K}(\Omega) \cap \mathbf{Y}(\Omega)$.

Let P be the projection of $\mathbf{H}^1_s(\Omega)$ onto $\mathbf{Y}(\Omega)$ given by Lemma 9.3.1. Then,

$$\|\mathrm{P}\mathbf{w}_n\|_{0,\Omega} \geq C_9 > 0, \text{ as } n \to \infty. \tag{9.50}$$

Indeed, if the subsequence $(\mathbf{w}_n)_{n\geq 0}$ verifies

$$\|\mathrm{P}\mathbf{w}_n\|_{0,\Omega} \to 0,$$

then, from (9.35) and (9.48),

$$\|\mathbf{w}_n\|_{0,\Omega} \leq \|\mathbf{w}_n - \mathrm{P}\mathbf{w}_n\|_{0,\Omega} + \|\mathrm{P}\mathbf{w}_n\|_{0,\Omega} \leq \tilde{C}\|\boldsymbol{\varepsilon}(\mathbf{w}_n)\|_{0,\Omega} + \|\mathrm{P}\mathbf{w}_n\|_{0,\Omega} \to 0,$$

and consequently,

$$\|\mathbf{w}_n\|_{1,\Omega} = O(\|\boldsymbol{\varepsilon}(\mathbf{w}_n)\|_{0,\Omega} + \|\mathrm{P}\mathbf{w}_n\|_{0,\Omega}) \to 0,$$

while $\|\mathbf{w}_n\|_{1,\Omega} = 1$ by construction; so (9.50) is true.

Since $\dim\mathbf{Y}(\Omega) < +\infty$, the projection of $\mathbf{H}^1_s(\Omega)$ onto $\mathbf{Y}(\Omega)$ is compact (see [71]), so $\mathrm{P}\mathbf{w}_n \to \mathrm{P}\mathbf{w}$ and hence, from (9.50),

$$\|\mathrm{P}\mathbf{w}\|_{0,\Omega} \geq C_9 > 0.$$

Moreover, from (9.49), $\mathrm{P}\mathbf{w} = \mathbf{w}$, so we can deduce that $\mathbf{w} \in \mathbf{Y}(\Omega) \cap \mathbf{K}(\Omega)$ is not null.

If $\mathbf{Y}(\Omega) \cap \mathbf{K}(\Omega) = \{\mathbf{0}\}$, we obtain a contradiction. If $\mathbf{Y}(\Omega) \cap \mathbf{K}(\Omega) \neq \{\mathbf{0}\}$, from assumptions $(\mathbf{H3}^\epsilon)$ and $(\mathbf{H5}^\epsilon)$ for $\epsilon = 1$, and since $w_n = cn_2$, $c \neq 0$, we have that

$$\int_\Omega \mathbf{f} \cdot \mathbf{w} dx + \int_{\Gamma_{N_1}} \mathbf{h} \cdot \mathbf{w} d\Gamma = F(\mathbf{w}) = -r^* < 0.$$

So, for each r fixed, $r \in (r^*/2, 3r^*/2)$, there exists n_r such that

$$F(\mathrm{P}\mathbf{w}_n) = \int_\Omega \mathbf{f} \cdot \mathrm{P}\mathbf{w}_n dx + \int_{\Gamma_{N_1}} \mathbf{h} \cdot \mathrm{P}\mathbf{w}_n d\Gamma \leq -r < 0, \, \forall n \geq n_r. \tag{9.51}$$

From inequality (9.38),

$$C_2\|\boldsymbol{\varepsilon}(\mathbf{u}(\epsilon_n))\|^2_{0,\Omega} \leq F(\mathbf{u}(\epsilon_n)) = F(\mathbf{u}(\epsilon_n) - \mathrm{P}\mathbf{u}(\epsilon_n)) + F(\mathrm{P}\mathbf{u}(\epsilon_n)),\ C_2 > 0,$$

and we obtain that

$$C_2\|\boldsymbol{\varepsilon}(\mathbf{u}(\epsilon_n))\|^2_{0,\Omega} - R_n F(\mathrm{P}\mathbf{w}(\epsilon_n)) \leq \left(\|\mathbf{f}\|_{0,\Omega} + \|\mathbf{h}\|_{0,\Gamma_{N_1}}\right)\|\mathbf{u}(\epsilon_n) - \mathrm{P}\mathbf{u}(\epsilon_n)\|_{0,\Omega} \leq$$
$$\tilde{C}\left(\|\mathbf{f}\|_{0,\Omega} + \|\mathbf{h}\|_{0,\Gamma_{N_1}}\right)\|\boldsymbol{\varepsilon}(\mathbf{u}(\epsilon_n))\|_{0,\Omega} \leq C_{10}\|\boldsymbol{\varepsilon}(\mathbf{u}(\epsilon_n))\|_{0,\Omega},$$

thanks to (9.35) with $C_{10} > 0$. Finally, from (9.47),

$$-R_n F(\mathrm{P}\mathbf{w}(\epsilon_n)) \leq C_{10}\sqrt{R_n},$$

and taking into account expression (9.51), we conclude

$$rR_n \leq C_{10}\sqrt{R_n},\ n > n_r,$$

which is obviously absurd since $R_n \to +\infty$. So, expression (9.45) cannot be true and, consequently, estimate (9.43) is verified. Therefore, from Lemma (9.3.3), bounds (9.44) are obtained and the proof of Theorem 9.3.4 is complete. □

Corollary 9.3.5. *The auxiliary stress tensor $\tilde{\boldsymbol{\sigma}}(\epsilon)$ defined by (9.36) and the auxiliary strain tensor $\tilde{\boldsymbol{\varepsilon}}(\epsilon)$ given by*

$$\tilde{\varepsilon}_{33}(\epsilon) = \varepsilon_{33}(\mathbf{u}(\epsilon)),\ \tilde{\varepsilon}_{3\beta}(\epsilon) = \epsilon^{-1}\varepsilon_{3\beta}(\mathbf{u}(\epsilon)),\ \tilde{\varepsilon}_{\alpha\beta}(\epsilon) = \epsilon^{-2}\varepsilon_{\alpha\beta}(\mathbf{u}(\epsilon)), \tag{9.52}$$

verifies that

$$\tilde{\sigma}_{ij}(\epsilon) = \frac{E}{1+\nu}\tilde{\varepsilon}_{ij}(\epsilon) + \frac{\nu E}{(1+\nu)(1-2\nu)}\tilde{\varepsilon}_{pp}(\epsilon)\delta_{ij} = \Lambda_{ijkl}\tilde{\varepsilon}_{kl}(\epsilon),$$
$$\tilde{\varepsilon}_{ij}(\epsilon) = \frac{1+\nu}{E}\tilde{\sigma}_{ij}(\epsilon) - \frac{\nu}{E}\tilde{\sigma}_{pp}(\epsilon)\delta_{ij} = \Lambda^{-1}_{ijkl}\tilde{\sigma}_{kl}(\epsilon).$$

Moreover, there exists $C_{11} > 0$ such that for all ϵ, $0 < \epsilon \leq 1$,

$$\|\tilde{\varepsilon}_{33}(\epsilon)\|_{0,\Omega} \leq C_{11},\quad \|\tilde{\varepsilon}_{3\beta}(\epsilon)\|_{0,\Omega} \leq C_{11},\quad \|\tilde{\varepsilon}_{\alpha\beta}(\epsilon)\|_{0,\Omega} \leq C_{11}. \tag{9.53}$$

Theorem 9.3.6. *There exists a subsequence of $(\mathbf{u}(\epsilon), \boldsymbol{\sigma}(\epsilon))$, also denoted with ϵ, and there exists an element $\boldsymbol{\Psi} = (\Psi_{ij}) \in \mathbf{X}(\Omega)$ such that*

$$\mathbf{u}(\epsilon) \rightharpoonup \tilde{\mathbf{u}},\ \ \textit{in } \mathbf{H}^1_s(\Omega), \tag{9.54}$$
$$\sigma_{33}(\epsilon) \rightharpoonup \Psi_{33},\ \epsilon\sigma_{3\beta}(\epsilon) \rightharpoonup \Psi_{3\beta},\ \epsilon^2\sigma_{\alpha\beta}(\epsilon) \rightharpoonup \Psi_{\alpha\beta},\ \ \textit{in } L^2(\Omega), \tag{9.55}$$

when ϵ goes to zero. In addition, the following symmetry properties hold:

- *Ψ_{ii}, $i = 1, 2, 3$, are even with respect to x_1 and x_3,*
- *Ψ_{12} is odd with respect to x_1 and even with respect to x_3,*

- Ψ_{13} *is odd with respect to* x_1 *and* x_3,
- Ψ_{23} *is even with respect to* x_1 *and odd with respect to* x_3.

Moreover,

$$\int_\Omega \Psi_{3\beta}\partial_\beta v dx = 0,\ \forall v \in H^1_s(\Omega), \tag{9.56}$$

$$\int_\Omega \Psi_{\alpha\beta}\partial_\alpha v_\beta dx \geq 0,\ \forall (v_1, v_2) \in \mathbf{W}_{s2}(\Omega) \cap \mathbf{K}_2(\Omega). \tag{9.57}$$

Proof. From Theorem 9.3.4 and Corollary 9.3.5, there exists a subsequence of $(\mathbf{u}(\epsilon), \boldsymbol{\sigma}(\epsilon))_{\epsilon>0}$ such that $(\mathbf{u}(\epsilon), \tilde{\boldsymbol{\sigma}}(\epsilon))$ converges weakly in $\mathbf{H}^1_s(\Omega) \times \mathbf{X}(\Omega)$ when ϵ goes to zero, i.e.:

$$\mathbf{u}(\epsilon) \rightharpoonup \tilde{\mathbf{u}}, \text{ in } \mathbf{H}^1_s(\Omega),$$
$$\sigma_{33}(\epsilon) \rightharpoonup \Psi_{33},\ \epsilon\sigma_{3\beta}(\epsilon) \rightharpoonup \Psi_{3\beta},\ \epsilon^2\sigma_{\alpha\beta}(\epsilon) \rightharpoonup \Psi_{\alpha\beta} \text{ in } L^2(\Omega).$$

The symmetry properties are a direct consequence from $\mathbf{u}(\epsilon) \in \mathbf{H}^1_s(\Omega)$.

By choosing $(v_1+u_1(\epsilon), v_2+u_2(\epsilon), u_3(\epsilon))$, with $\mathbf{v} = (v_1, v_2, 0) \in \mathbf{H}^1_s(\Omega) \cap \mathbf{K}(\Omega)$ as a test function in (9.7) and multiplying by ϵ^2, we have that

$$\epsilon^2 \int_\Omega \sigma_{\alpha\beta}(\epsilon)\varepsilon_{\alpha\beta}(\mathbf{v})dx + 2\epsilon^2 \int_\Omega \sigma_{3\beta}(\epsilon)\varepsilon_{3\beta}(\mathbf{v})dx \geq \epsilon^2 \left[\int_\Omega f_\beta v_\beta dx + \int_{\Gamma_{N_1}} h_\beta v_\beta d\Gamma\right].$$

Taking limits when ϵ goes to zero, we obtain

$$\int_\Omega \Psi_{\alpha\beta}\varepsilon_{\alpha\beta}(\mathbf{v})dx \geq 0, \quad \forall\, \mathbf{v} = (v_1, v_2, 0) \in \mathbf{H}^1_s(\Omega) \cap \mathbf{K}(\Omega),$$

and thanks to the symmetry properties of $\Psi_{\alpha\beta}$ we deduce that

$$\int_\Omega \Psi_{\alpha\beta}\partial_\alpha v_\beta dx \geq 0, \quad \forall\, (v_1, v_2) \in \mathbf{W}_{s2}(\Omega) \cap \mathbf{K}_2(\Omega).$$

With the same procedure, by choosing $\mathbf{u}(\epsilon) \pm (0, 0, v)$, with $v \in H^1_s(\Omega)$, as test functions in (9.7) and multiplying by ϵ, we have that

$$\epsilon \int_\Omega \sigma_{3\beta}(\epsilon)\partial_\beta v dx + \epsilon \int_\Omega \sigma_{33}(\epsilon)\partial_3 v dx = \epsilon \left[\int_\Omega f_3 v dx + \int_{\Gamma_{N_1}} h_3 v d\Gamma\right].$$

Taking again limits when ϵ goes to zero, we find that

$$\int_\Omega \Psi_{3\beta}\partial_\beta v dx = 0, \quad \forall\, v \in H^1_s(\Omega).$$

□

Corollary 9.3.7. *The limit stress components $\Psi_{\alpha\beta}$ verify*

$$\int_\Omega \Psi_{\alpha\beta}\partial_\alpha v_\beta dx = 0,\ \forall (v_1, v_2) \in \mathbf{W}_{s2}(\Omega). \tag{9.58}$$

Moreover,

$$\int_\omega \Psi_{\alpha\alpha} dx_1 dx_2 = \int_\omega x_2 \Psi_{\alpha\alpha} dx_1 dx_2 = 0. \tag{9.59}$$

Proof. The three-dimensional stress tensor

$$\tilde{\mathbf{\Psi}} = \begin{pmatrix} \Psi_{11} & \Psi_{12} & 0 \\ \Psi_{21} & \Psi_{22} & 0 \\ 0 & 0 & 0 \end{pmatrix},$$

verifies variational problem (9.57), which can be written in differential form as

$$\begin{aligned} -\mathrm{div}\tilde{\mathbf{\Psi}} = -\partial_\alpha \Psi_{\alpha\beta} = \mathbf{0} \text{ in } \Omega, \\ \tilde{\mathbf{\Psi}}\mathbf{n} = \mathbf{0} \text{ on } \partial\Omega \backslash \Gamma_C, \\ \tilde{\mathbf{\Psi}}_\tau = \mathbf{0} \text{ on } \Gamma_C, \\ \tilde{\Psi}_n \leq 0 \text{ on } \Gamma_C, \end{aligned}$$

where the boundary conditions must be understood as described in [13]. Consequently,

$$\mathbf{0} = -\int_\Omega \mathrm{div}\tilde{\mathbf{\Psi}} dx = \int_{\partial\Omega} \tilde{\mathbf{\Psi}}\mathbf{n} d\Gamma = \int_{\Gamma_C} \tilde{\Psi}_n \mathbf{n} d\Gamma. \tag{9.60}$$

Given that $\tilde{\Psi}_n$ has constant sign on Γ_C and thanks to hypothesis ($\mathbf{H5}^\epsilon$) concerning to n_2, we deduce that $\tilde{\Psi}_n = 0$ on Γ_C. Therefore, components $\Psi_{\alpha\beta}$ are a weak solution of variational problem (9.58).

Choosing $(v_1, v_2) = (x_1 v^0, x_2 v^0)$, with $v^0 \in H^1_e(-L, L)$ as a test function in (9.58), we have that

$$\int_{-L}^{L} v^0 \int_\omega \Psi_{\alpha\alpha} dx_1 dx_2 dx_3 = 0,\ \forall v^0 \in H^1_e(-L, L),$$

so, since $\Psi_{\alpha\alpha}$ is also even with respect to x_3, we conclude

$$\int_\omega \Psi_{\alpha\alpha} dx_1 dx_2 = 0.$$

Analogously, choosing as test functions in (9.58) $(v_1, v_2) = (0, \frac{1}{2}x_1^2 v^0)$ and $(v_1, v_2) = (x_1 x_2 v^0, \frac{1}{2}x_2^2 v^0)$, with $v^0 \in H^1_e(-L, L)$, we obtain

$$\int_{-L}^{L} v^0 \int_\omega x_1 \Psi_{12} dx_1 dx_2 dx_3 = 0,$$

$$\int_{-L}^{L} v^0 \int_\omega (x_2 \Psi_{\alpha\alpha} dx_1 dx_2 + x_1 \Psi_{12} dx_1 dx_2) dx_3 = 0,$$

for all $v^0 \in H^1_e(-L,L)$; then,

$$\int_\omega x_2 \Psi_{\alpha\alpha} dx_1 dx_2 = 0.$$

So, components $\Psi_{\alpha\alpha}$ verify expression (9.59). □

Corollary 9.3.8. *There exists a subsequence of* $(\boldsymbol{\sigma}(\epsilon))_{\epsilon>0}$ *such that*

$$\sigma_{33}(\epsilon) \rightharpoonup \Psi_{33}, \quad \epsilon\sigma_{3\beta}(\epsilon) \rightharpoonup \Psi_{3\beta}, \quad \epsilon^2\sigma_{\alpha\beta}(\epsilon) \rightharpoonup \Psi_{\alpha\beta},$$

in $L^2(\Omega)$ *and there exist a subsequence of* $(\mathbf{u}(\epsilon))_{\epsilon>0}$ *and* $\boldsymbol{\varsigma} \in \mathbf{X}(\Omega)$ *such that*

$$\varepsilon_{33}(\mathbf{u}(\epsilon)) \rightharpoonup \varsigma_{33}, \quad \epsilon^{-1}\varepsilon_{3\beta}(\mathbf{u}(\epsilon)) \rightharpoonup \varsigma_{3\beta}, \quad \epsilon^{-2}\varepsilon_{\alpha\beta}(\mathbf{u}(\epsilon)) \rightharpoonup \varsigma_{\alpha\beta},$$

in $L^2(\Omega)$. *Moreover,*

$$\Psi_{ij} = \frac{E}{1+\nu}\varsigma_{ij} + \frac{\nu E}{(1+\nu)(1-2\nu)}\varsigma_{pp}\delta_{ij} = \Lambda_{ijkl}\varsigma_{kl},$$
$$\varsigma_{ij} = \frac{1+\nu}{E}\Psi_{ij} - \frac{\nu}{E}\Psi_{pp}\delta_{ij} = \Lambda^{-1}_{ijkl}\Psi_{kl}.$$

Proof. The result is a direct consequence of (9.52), (9.53) and (9.55). □

Theorem 9.3.9. *The sequence* $(\mathbf{u}(\epsilon))_{\epsilon>0}$ *verifies*

$$\mathbf{u}(\epsilon) \rightharpoonup \mathbf{u}^0 \ \text{ in } \mathbf{H}^1(\Omega), \tag{9.61}$$

where $\mathbf{u}^0 \in \mathbf{V}_{BN}(\Omega)$ *is the first term in the asymptotic expansion* (9.13).

Proof. There exists a subsequence, still denoted by $(\mathbf{u}(\epsilon))_{\epsilon>0}$, in $\mathbf{H}^1_s(\Omega)$ that converges weakly in $\mathbf{H}^1(\Omega)$ thanks to Theorem 9.3.6; let $\tilde{\mathbf{u}} \in \mathbf{H}^1_s(\Omega)$ be its limit. We will prove that $\tilde{\mathbf{u}} = \mathbf{u}^0$.

Taking limits when ϵ goes to zero in (9.6) and taking into account expressions (9.8)-(9.12), we have that

$$\frac{1}{E}\int_\Omega \Psi_{33}\tau_{33}dx - \frac{\nu}{E}\int_\Omega \Psi_{\mu\mu}\tau_{33}dx = \int_\Omega \varepsilon_{ij}(\tilde{\mathbf{u}})\tau_{ij}dx, \quad \forall \boldsymbol{\tau} \in \mathbf{X}(\Omega),$$

thanks to (9.55). From this relation we obtain:

$$\begin{aligned} &\varepsilon_{\alpha\beta}(\tilde{\mathbf{u}}) = \varepsilon_{3\beta}(\tilde{\mathbf{u}}) = 0, \\ &\Psi_{33} = E\varepsilon_{33}(\tilde{\mathbf{u}}) + \nu\Psi_{\mu\mu}. \end{aligned} \tag{9.62}$$

So, a similar methodology to that used in proof of Item (i) in Theorem 9.2.1, allow us to deduce

$$\left.\begin{aligned} &\tilde{\mathbf{u}} \in \mathbf{V}_{BN}(\Omega), \\ &\tilde{u}_1 = 0, \\ &\tilde{u}_2 \in H^2_e(-L,L),\ (0,\tilde{u}_2) \in \mathbf{K}_2(\Omega), \\ &\tilde{u}_3 = \underline{\tilde{u}}_3 - x_2\partial_3\tilde{u}_2,\ \underline{\tilde{u}}_3 \in H^1_o(-L,L). \end{aligned}\right\} \tag{9.63}$$

Consequently, replacing these results on (9.62), we find that

$$\Psi_{33} = E(\partial_3\underline{\tilde{u}}_3 - x_2\partial_{33}\tilde{u}_2) + \nu\Psi_{\mu\mu}. \tag{9.64}$$

If we consider $\mathbf{v} \in \mathbf{V}_{BN}(\Omega) \cap \mathbf{K}(\Omega)$ as a test function in (9.7), we obtain

$$\int_\Omega \sigma_{33}(\epsilon)\varepsilon_{33}(\mathbf{v})dx - \int_\Omega \sigma_{ij}(\epsilon)\varepsilon_{ij}(\mathbf{u}(\epsilon))dx \geq \int_\Omega f_i(v_i - u_i(\epsilon))dx + \int_{\Gamma_{N_1}} h_i(v_i - u_i(\epsilon))d\Gamma. \quad (9.65)$$

Moreover, taking into account expression (9.36) and Corollary 9.3.5, we have

$$\int_\Omega \sigma_{ij}(\epsilon)\varepsilon_{ij}(\mathbf{u}(\epsilon))dx = \int_\Omega \tilde{\boldsymbol{\sigma}}(\epsilon):\tilde{\boldsymbol{\varepsilon}}(\epsilon)dx = \int_\Omega \boldsymbol{\Lambda}\tilde{\boldsymbol{\varepsilon}}(\epsilon):\tilde{\boldsymbol{\varepsilon}}(\epsilon)dx,$$

and, from Corollary 9.3.8,

$$\liminf_{\epsilon\to 0} \int_\Omega \sigma_{ij}(\epsilon)\varepsilon_{ij}(\mathbf{u}(\epsilon))dx \geq \int_\Omega \boldsymbol{\Lambda}\boldsymbol{\varsigma}:\boldsymbol{\varsigma}dx = \int_\Omega \boldsymbol{\Psi}:\boldsymbol{\varsigma}dx = \int_\Omega \Psi_{ij}\varsigma_{ij}dx, \quad (9.66)$$

since Λ is a weakly lower-semicontinuous function (see [54]). So, taking lower limits when ϵ goes to zero in (9.65), we have for each $\mathbf{v} \in \mathbf{V}_{BN}(\Omega) \cap \mathbf{K}(\Omega)$,

$$\begin{aligned}\int_\Omega \Psi_{33}\varepsilon_{33}(\mathbf{v})dx - \int_\Omega \Psi_{ij}\varsigma_{ij}dx &\geq \liminf_{\epsilon\to 0} \int_\Omega \sigma_{33}(\epsilon)\varepsilon_{33}(\mathbf{v})dx - \liminf_{\epsilon\to 0} \int_\Omega \sigma_{ij}(\epsilon)\varepsilon_{ij}(\mathbf{u}(\epsilon))dx \geq \\ &\liminf_{\epsilon\to 0} \left(\int_\Omega \sigma_{33}(\epsilon)\varepsilon_{33}(\mathbf{v})dx - \int_\Omega \sigma_{ij}(\epsilon)\varepsilon_{ij}(\mathbf{u}(\epsilon))dx \right) \geq \\ &\liminf_{\epsilon\to 0} \left(\int_\Omega f_i(v_i - u_i(\epsilon))dx + \int_{\Gamma_{N_1}} h_i(v_i - u_i(\epsilon))d\Gamma \right) = \\ &\int_\Omega f_i(v_i - \tilde{u}_i)dx + \int_{\Gamma_{N_1}} h_i(v_i - \tilde{u}_i)d\Gamma.\end{aligned}$$

Therefore,

$$\begin{aligned}\int_\Omega \Psi_{33}\varepsilon_{33}(\mathbf{v} - \tilde{\mathbf{u}})dx \geq \int_\Omega f_i(v_i - \tilde{u}_i)dx + \int_{\Gamma_{N_1}} h_i(v_i - \tilde{u}_i)d\Gamma + \\ \int_\Omega \Psi_{3\beta}\varsigma_{3\beta}dx + \int_\Omega \Psi_{\alpha\beta}\varsigma_{\alpha\beta}dx, \ \forall \mathbf{v} \in \mathbf{V}_{BN}(\Omega) \cap \mathbf{K}(\Omega). \quad (9.67)\end{aligned}$$

Moreover, choosing $v = u_3(\epsilon) \in H^1_s(\Omega)$ in expression (9.56), we find that

$$\int_\Omega \Psi_{3\beta}\partial_\beta u_3(\epsilon)dx = 0.$$

Multiplying by ϵ^{-1} and taking limits when $\epsilon \to 0$, we deduce

$$\int_\Omega \Psi_{3\beta}\varsigma_{3\beta}dx = 0. \quad (9.68)$$

Furthermore, choosing $(v_1, v_2) = (u_1(\epsilon), u_2(\epsilon)) \in \mathbf{W}_{s2}(\Omega) \cap \mathbf{K}_2(\Omega)$ in expression (9.58), we have that

$$\int_\Omega \Psi_{\alpha\beta}\partial_\alpha u_\beta(\epsilon)dx = 0.$$

Multiplying by ϵ^{-2} and taking limits, we see that

$$\int_\Omega \Psi_{\alpha\beta}\varsigma_{\alpha\beta}dx = 0. \tag{9.69}$$

Therefore, from (9.67)-(9.69) we obtain

$$\int_\Omega \Psi_{33}\varepsilon_{33}(\mathbf{v}-\tilde{\mathbf{u}})dx \geq \int_\Omega \mathbf{f}\cdot(\mathbf{v}-\tilde{\mathbf{u}})dx + \int_{\Gamma_{N_1}} \mathbf{h}\cdot(\mathbf{v}-\tilde{\mathbf{u}})d\Gamma,\ \forall \mathbf{v}\in \mathbf{V}_{BN}(\Omega)\cap\mathbf{K}(\Omega).$$

Taking into account the expression for Ψ_{33} obtained in (9.64), we can write:

$$\int_\Omega [E(\partial_3\underline{\tilde{u}}_3 - x_2\partial_{33}\tilde{u}_2)+\nu\Psi_{\mu\mu}]\varepsilon_{33}(\mathbf{v}-\tilde{\mathbf{u}})dx \geq \int_\Omega \mathbf{f}\cdot(\mathbf{v}-\tilde{\mathbf{u}})dx + \int_{\Gamma_{N_1}} \mathbf{h}\cdot(\mathbf{v}-\tilde{\mathbf{u}})d\Gamma,$$

for all $\mathbf{v}\in\mathbf{V}_{BN}(\Omega)\cap\mathbf{K}(\Omega)$. Then,

$$\begin{aligned}\int_\Omega E\partial_3\underline{\tilde{u}}_3\varepsilon_{33}(\mathbf{v}-\tilde{\mathbf{u}})dx - \int_\Omega Ex_2\partial_{33}\tilde{u}_2\varepsilon_{33}(\mathbf{v}-\tilde{\mathbf{u}})dx + \int_\Omega \nu\Psi_{\mu\mu}\varepsilon_{33}(\mathbf{v}-\tilde{\mathbf{u}})dx \geq \\ \int_\Omega \mathbf{f}\cdot(\mathbf{v}-\tilde{\mathbf{u}})dx + \int_{\Gamma_{N_1}} \mathbf{h}\cdot(\mathbf{v}-\tilde{\mathbf{u}})d\Gamma,\ \forall \mathbf{v}\in \mathbf{V}_{BN}(\Omega)\cap\mathbf{K}(\Omega).\end{aligned} \tag{9.70}$$

In particular, considering in equation (9.70) $\mathbf{v}\in\mathbf{V}_{BN}(\Omega)\cap\mathbf{K}(\Omega)$ such that $v_1=0$, v_2 depending only on x_3 and even with $(0,v_2)\in\mathbf{K}_2(\Omega)$ and $v_3=\underline{\tilde{u}}_3 - x_2\partial_3 v_2$, we obtain

$$\begin{aligned}\int_\Omega Ex_2^2\partial_{33}\tilde{u}_2\partial_{33}(v_2-\tilde{u}_2)dx \geq \int_\Omega f_2(v_2-\tilde{u}_2)dx + \int_{\Gamma_{N_1}} h_2(v_2-\tilde{u}_2)d\Gamma - \\ \int_\Omega x_2 f_3\partial_3(v_2-\tilde{u}_2)dx - \int_{\Gamma_{N_1}} x_2h_3\partial_3(v_2-\tilde{u}_2)d\Gamma + \int_\Omega \nu x_2\Psi_{\mu\mu}\partial_{33}(v_2-\tilde{u}_2)dx,\end{aligned}$$

thanks to (9.63). Taking into account (9.59), we conclude that

$$\int_{-L}^{L} EI_1\partial_{33}\tilde{u}_2\partial_{33}(v_2-\tilde{u}_2)dx_3 \geq \int_{-L}^{L} q_2(v_2-\tilde{u}_2)dx_3 - \int_{-L}^{L} M_1\partial_3(v_2-\tilde{u}_2)dx_3,$$

for all $v_2\in H_e^2(-L,L)$, $(0,v_2)\in\mathbf{K}_2(\Omega)$; so, $\tilde{u}_2=u_2^0$ thanks to Theorem 9.2.3.

Similarly, choosing $\mathbf{v}\in\mathbf{V}_{BN}(\Omega)\cap\mathbf{K}(\Omega)$ as a test function in (9.70), such that $v_\alpha=\tilde{u}_\alpha$ and $v_3=\tilde{u}_3\pm\underline{v}_3$, with $\underline{v}_3\in H_o^1(-L,L)$, we find that

$$\int_{-L}^{L} EA\partial_3\underline{\tilde{u}}_3\partial_3\underline{v}_3dx_3 + \int_\Omega \nu\Psi_{\mu\mu}\partial_3\underline{v}_3dx = \int_{-L}^{L} q_3\underline{v}_3dx_3,$$

and from (9.59), $\underline{\tilde{u}}_3=\underline{u}_3^0$ thanks to Theorem 9.2.2, which proves (9.61) for the subsequence $\mathbf{u}(\epsilon)$. We can repeat this procedure for each subsequence of $(\mathbf{u}(\epsilon))_{\epsilon>0}$ converging weakly in $\mathbf{H}_s^1(\Omega)$; then, the uniqueness of the limit implies that the entire sequence $(\mathbf{u}(\epsilon))_{\epsilon>0}$ converges weakly to $\mathbf{u}^0$. □

Remark 9.3.10. *From previous Theorem and Corollary 9.3.8,*

$$\varepsilon_{\alpha\beta}(\mathbf{u}(\epsilon)) \rightharpoonup \varepsilon_{\alpha\beta}(\mathbf{u}^0) = 0, \quad \frac{1}{\epsilon^2}\varepsilon_{\alpha\beta}(\mathbf{u}(\epsilon)) \rightharpoonup \varsigma_{\alpha\beta}, \tag{9.71}$$

$$\varepsilon_{3\beta}(\mathbf{u}(\epsilon)) \rightharpoonup \varepsilon_{3\beta}(\mathbf{u}^0) = 0, \quad \frac{1}{\epsilon}\varepsilon_{3\beta}(\mathbf{u}(\epsilon)) \rightharpoonup \varsigma_{3\beta}, \tag{9.72}$$

$$\varepsilon_{33}(\mathbf{u}(\epsilon)) \rightharpoonup \varepsilon_{33}(\mathbf{u}^0) = \varsigma_{33}, \tag{9.73}$$

weakly in $L^2(\Omega)$.

Theorem 9.3.11. *For each* $0 < \epsilon \leq 1$, *let* $(\mathbf{u}(\epsilon), \boldsymbol{\sigma}(\epsilon))_{\epsilon>0} \in (\mathbf{H}^1_s(\Omega) \cap \mathbf{K}(\Omega)) \times \mathbf{X}(\Omega)$ *be the solution of problem (9.6)-(9.7). Let* $\mathbf{u}^0 \in \mathbf{H}^1_s(\Omega) \cap \mathbf{K}(\Omega)$, $\sigma^0_{33} \in L^2(\Omega)$ *be the first term of the asymptotic expansion (9.13). Then, when* $\epsilon \to 0$, *the following convergences are obtained:*

$$\|\mathbf{u}(\epsilon) - \mathbf{u}^0\|_{1,\Omega} \to 0, \tag{9.74}$$

$$\|\sigma_{33}(\epsilon) - \sigma^0_{33}\|_{0,\Omega} \to 0, \tag{9.75}$$

$$\epsilon\|\sigma_{3\beta}\|_{0,\Omega} \to 0, \tag{9.76}$$

$$\epsilon^2\|\sigma_{\alpha\beta}\|_{0,\Omega} \to 0. \tag{9.77}$$

Proof. Convergences (9.75)-(9.77) are obtained by applying the same methodology given in Proof of Theorem 10.4 in [80].

In order to prove (9.74), since $\mathbf{u}(\epsilon)$ converges weakly in $\mathbf{H}^1(\Omega)$, there exists a subsequence, still denoted $\mathbf{u}(\epsilon)$, such that converges strongly in $[L^2(\Omega)]^3$,

$$\|\mathbf{u}(\epsilon) - \mathbf{u}^0\|_{0,\Omega} \to 0. \tag{9.78}$$

From (9.6) and (9.14), we obtain the following identity:

$$b(\boldsymbol{\tau}, \mathbf{u}(\epsilon) - \mathbf{u}^0) = a_0(\boldsymbol{\sigma}(\epsilon) - \boldsymbol{\sigma}^0, \boldsymbol{\tau}) + \epsilon^2 a_2(\boldsymbol{\sigma}(\epsilon), \boldsymbol{\tau}) + \epsilon^4 a_4(\boldsymbol{\sigma}(\epsilon), \boldsymbol{\tau}). \tag{9.79}$$

Moreover, for each $\boldsymbol{\tau} \in \mathbf{X}(\Omega)$

$$\begin{gathered}|a_0(\boldsymbol{\sigma}(\epsilon) - \boldsymbol{\sigma}^0, \boldsymbol{\tau}) + \epsilon^2 a_2(\boldsymbol{\sigma}(\epsilon), \boldsymbol{\tau}) + \epsilon^4 a_4(\boldsymbol{\sigma}(\epsilon), \boldsymbol{\tau})| \leq \\ C_{12}\left[\|\sigma_{33}(\epsilon) - \sigma^0_{33}\|_{0,\Omega} + \epsilon\|\sigma_{3\beta}(\epsilon)\|_{0,\Omega} + \epsilon^2\|\sigma_{\alpha\beta}(\epsilon)\|_{0,\Omega}\right]\|\boldsymbol{\tau}\|_{0,\Omega},\end{gathered} \tag{9.80}$$

taking into account that $0 \leq \epsilon < 1$ and then ϵ^2, ϵ^4 can be bounded by ϵ and ϵ^2, respectively, when necessary.

Choosing $\boldsymbol{\tau} = \boldsymbol{\varepsilon}(\mathbf{u}(\epsilon) - \mathbf{u}^0)$ in relations (9.79) and (9.80), we have that

$$\begin{gathered}C_{17}\|\boldsymbol{\varepsilon}(\mathbf{u}(\epsilon) - \mathbf{u}^0)\|^2_{0,\Omega} \leq a_0(\boldsymbol{\sigma}(\epsilon) - \boldsymbol{\sigma}^0, \boldsymbol{\varepsilon}(\mathbf{u}(\epsilon) - \mathbf{u}^0)) + \\ \epsilon^2 a_2(\boldsymbol{\sigma}(\epsilon), \boldsymbol{\varepsilon}(\mathbf{u}(\epsilon) - \mathbf{u}^0)) + \epsilon^4 a_4(\boldsymbol{\sigma}(\epsilon), \boldsymbol{\varepsilon}(\mathbf{u}(\epsilon) - \mathbf{u}^0)) \leq \\ C_{12}\left(\|\sigma_{33}(\epsilon) - \sigma^0_{33}\|_{0,\Omega} + \epsilon\|\sigma_{3\beta}(\epsilon)\|_{0,\Omega} + \epsilon^2\|\sigma_{\alpha\beta}(\epsilon)\|_{0,\Omega}\right)\|\boldsymbol{\varepsilon}(\mathbf{u}(\epsilon) - \mathbf{u}^0)\|_{0,\Omega},\end{gathered}$$

therefore,

$$\|\boldsymbol{\varepsilon}(\mathbf{u}(\epsilon)-\mathbf{u}^0)\|_{0,\Omega}\to 0,$$

and taking into account (9.78) we conclude (9.74) for the subsequence $\mathbf{u}(\epsilon)$. This procedure may be applied to any weakly convergent subsequence of $(\mathbf{u}(\epsilon))_{\epsilon>0}$ in $\mathbf{H}^1(\Omega)$; so, the whole sequence converges strongly. □

9.4 Returning to domain Ω^ϵ

In previous section, we have proved that the first term of the asymptotic expansion $(\mathbf{u}^0,\boldsymbol{\sigma}^0)$ is a good approximation of the scaled displacements and stresses $(\mathbf{u}(\epsilon),\boldsymbol{\sigma}(\epsilon))$ when the cross-section parameter ϵ is small. Then, by applying the inverse transformations of (9.3)-(9.5), we obtain an approximation of $(\mathbf{u}^\epsilon,\boldsymbol{\sigma}^\epsilon)$, denoted by $(\mathbf{u}^{0\epsilon},\boldsymbol{\sigma}^{0\epsilon})$, such that

$$u_\alpha^{0\epsilon}(\mathbf{x}^\epsilon)=\frac{1}{\epsilon}u_\alpha^0(\mathbf{x}),\ u_3^{0\epsilon}(\mathbf{x}^\epsilon)=u_3^0(\mathbf{x}),$$

$$\sigma_{\alpha\beta}^{0\epsilon}(\mathbf{x}^\epsilon)=\epsilon^2\sigma_{\alpha\beta}^0(\mathbf{x}),\ \sigma_{3\beta}^{0\epsilon}(\mathbf{x}^\epsilon)=\epsilon\sigma_{3\beta}^0(\mathbf{x}),\ \sigma_{33}^{0\epsilon}(\mathbf{x}^\epsilon)=\sigma_{33}^0(\mathbf{x}),$$

The following theorem gives a characterization of this approximation:

Theorem 9.4.1. *The terms $\mathbf{u}^{0\epsilon}$, $\sigma_{33}^{0\epsilon}$ are determined as follows:*

(i) The displacement field $\mathbf{u}^{0\epsilon}$ belongs to the subspace $\mathbf{V}_{BN}(\Omega^\epsilon)$, where $u_1^{0\epsilon}$ is null, $u_2^{0\epsilon}\in H_e^2(-L,L)$ and

$$u_3^{0\epsilon}=\underline{u}_3^{0\epsilon}-x_2^\epsilon\partial_3u_2^{0\epsilon},\ \underline{u}_3^{0\epsilon}\in H_o^1(-L,L). \tag{9.81}$$

(ii) The stress component $\sigma_{33}^{0\epsilon}$ is given by

$$\sigma_{33}^{0\epsilon}=E(\partial_3\underline{u}_3^{0\epsilon}-x_2^\epsilon\partial_{33}u_2^{0\epsilon}). \tag{9.82}$$

(iii) The axial displacement $\underline{u}_3^{0\epsilon}$ is the unique solution of the problem:

Problem ($\mathbf{P_3^{0\epsilon}}$):

Find $\underline{u}_3^{0\epsilon}\in H_o^1(-L,L)$ such that

$$\int_{-L}^{L}EA^\epsilon\partial_3\underline{u}_3^{0\epsilon}\ \partial_3v_3^0dx_3=\int_{-L}^{L}q_3^\epsilon v_3^0dx_3,\ \forall v_3^0\in H_o^1(-L,L), \tag{9.83}$$

(iv) The displacement $u_2^{0\epsilon}$ is the unique solution of the bending problem:

Problem ($\mathbf{P_2^{0\epsilon}}$):

Find $u_2^{0\epsilon}\in H_e^2(-L,L)$, $(0,u_2^{0\epsilon})\in\mathbf{K}_2(\Omega^\epsilon)$, such that

$$\int_{-L}^{L}EI_1^\epsilon\partial_{33}u_2^{0\epsilon}\partial_{33}(v_2^0-u_2^{0\epsilon})dx_3\geq\int_{-L}^{L}q_2^\epsilon(v_2^0-u_2^{0\epsilon})dx_3-\int_{-L}^{L}M_1^\epsilon\partial_3(v_2^0-u_2^{0\epsilon})dx_3, \tag{9.84}$$

for all $v_2^0\in H_e^2(-L,L)$, $(0,v_2^0)\in\mathbf{K}_2(\Omega^\epsilon)$.

9.5 Some properties of the limit models

In the axis of the beam, we distinguish:

- $\Gamma^0_{N_1} = (-\delta, \delta)$, the part of the axis corresponding to the beam slice in which some surface forces are applied.
- $\Gamma^0_C = (-l-\hat{\delta}, -l) \cup (l, l+\hat{\delta})$, the parts of the beam axis under sections where their boundaries intersect with Γ^ϵ_C.

From now on and without loss of generality, we consider that the second component of the normal vector is negative, $n^\epsilon_2 < 0$, on the contact boundary Γ^ϵ_C.

Theorem 9.5.1. *The unique solution $\underline{u}^{0\epsilon}_3 \in H^1_o(-L, L)$ of Problem $(\mathbf{P^{0\epsilon}_3})$ verifies the following differential formulation:*

$$EA^\epsilon \Delta \underline{u}^{0\epsilon}_3 = q^\epsilon_3, \tag{9.85}$$

$$EA^\epsilon \partial_3 \underline{u}^{0\epsilon}_3(\pm L) = 0. \tag{9.86}$$

In addition, $\underline{u}^{0\epsilon}_3 \in H^2_o(-L, L)$.

Proof. Firstly, choosing an odd function $\phi \in \mathcal{D}(-L, L) \subset H^1(-L, L)$, as test function in (9.83), and applying integration by parts, we obtain

$$-\int_{-L}^{L} EA^\epsilon \Delta \underline{u}^{0\epsilon}_3 \phi dx_3 = \int_{-L}^{L} q^\epsilon_3 \phi dx_3.$$

So, expression (9.85) is obtained in the sense of distributions. Moreover, since q^ϵ_3 is smooth,

$$\underline{u}^{0^\epsilon}_3 \in H^2_o(-L, L).$$

Multiplying (9.85) by $v \in H^1_o(L, L)$ and applying again Green's theorem, we have

$$\int_{-L}^{L} q^\epsilon_3 v dx_3 = \int_{-L}^{L} EA^\epsilon \partial_3 \underline{u}^{0\epsilon}_3 \partial_3 v dx_3 - EA^\epsilon \partial_3 \underline{u}^{0\epsilon}_3(L) v(L) + EA^\epsilon \partial_3 \underline{u}^{0\epsilon}_3(-L) v(-L) =$$
$$\int_{-L}^{L} q^\epsilon_3 v dx_3 - 2EA^\epsilon \partial_3 \underline{u}^{0\epsilon}_3(L) v(L),$$

taking into account expression (9.83), so we deduce (9.86). □

Theorem 9.5.2. *Let $u^{0\epsilon}_2 \in H^2_e(-L, L)$ be the unique solution of Problem $(\mathbf{P^{0\epsilon}_2})$ and let denote the coincidence set $I = \{x_3 \in \bar{\Gamma}^0_C; u^{0\epsilon}_2(x_3) = 0\}$. Then there exists a nonnegative Radon measure μ such that*

$$EI^\epsilon_1 \Delta^2 u^{0\epsilon}_2 = q^\epsilon_2 + \partial_3 M^\epsilon_1 + \mu \text{ in } (-L, L), \tag{9.87}$$

$$\partial_3 \Delta u^{0\epsilon}_2(\pm L) = \Delta u^{0\epsilon}_2(\pm L) = 0, \tag{9.88}$$

with $\text{supp}(\mu) \subset I$.

Proof. Firstly, let $\phi \in \mathcal{D}(\mathcal{J}) \subset H^2(-L,L)$ be an even function, with $\mathcal{J} = (-L,L)\backslash\bar{\Gamma}_C^0$; taking $v_2^0 = u_2^{0\epsilon} \pm \phi$, as test function in (9.84), and applying integration by parts, we find that

$$\int_{\mathcal{J}} EI_1^\epsilon \Delta u_2^{0\epsilon} \Delta\phi dx_3 = \int_{\mathcal{J}} q_2^\epsilon \phi dx_3 + \int_{\mathcal{J}} \partial_3 M_1^\epsilon \phi dx_3.$$

So, we obtain in the sense of distributions

$$EI_1^\epsilon \Delta^2 u_2^{0\epsilon} = q_2^\epsilon + \partial_3 M_1^\epsilon \text{ in } \mathcal{D}'(\mathcal{J}). \tag{9.89}$$

Therefore, multiplying (9.89) by a test function v, taking into account that $H_e^2(L,L) \subset \mathcal{C}^1(-L,L)$ and since $q_2^\epsilon + \partial_3 M_1 \in L^2(-L,L)$, applying again integration by parts, we deduce that

$$\begin{aligned}\int_{\mathcal{J}} EI_1^\epsilon \Delta^2 u_2^{0\epsilon} v dx_3 = &\int_{\mathcal{J}} EI_1^\epsilon \Delta u_2^{0\epsilon} \Delta v dx_3 - EI_1^\epsilon \partial_3 \Delta u_2^{0\epsilon}(-L)v(-L) + \\ &EI_1^\epsilon \partial_3 \Delta u_2^{0\epsilon}(L)v(L) + EI_1^\epsilon \Delta u_2^{0\epsilon}(-L)\partial_3 v(-L) - EI_1^\epsilon \Delta u_2^{0\epsilon}(L)\partial_3 v(L) = \\ &\int_{\mathcal{J}} q_2^\epsilon v dx_3 + \int_{\mathcal{J}} \partial_3 M_1^\epsilon v dx_3,\end{aligned}$$

for all $v \in H_e^2(-L,L)$ such that $v = 0$ in $\bar{\Gamma}_C^0$ and hence, using variational formulation (9.84), we deduce (9.88).

Next, let $x_3^0 \in \Gamma_C^0\backslash I$, $x_3^0 > 0$, be arbitrary and $B_r(\pm x_3^0) = B_r(x_3^0) \cup B_r(-x_3^0)$. Because $(0, u_2^{0\epsilon}) \in \mathbf{K}_2(\Omega^\epsilon)$, there exist $r > 0$ and $\phi \in \mathcal{D}(B_r(\pm x_3^0))$ such that

$$\begin{aligned}\phi(x) > 0 \text{ in } B_r(\pm x_3^0),\\ u_2^{0\epsilon} \geq \phi \text{ in } H^2(B_r(\pm x_3^0)).\end{aligned}$$

Then, for all $\xi \in \mathcal{D}(B_{r/2}(\pm x_3^0))$, there exists $\nu > 0$ such that

$$u_2^{0\epsilon} + \nu\xi \geq \frac{\phi}{2} \text{ in } H^2(B_{r/2}(\pm x_3^0)).$$

Choosing $v_2^0 = u_2^{0\epsilon} + \nu\xi$ in (9.84) and dividing by ν, we have that

$$\int_{B_{r/2}(\pm x_3^0)} EI_1^\epsilon \Delta u_2^{0\epsilon} \Delta\xi dx_3 \geq \int_{B_{r/2}(\pm x_3^0)} q_2^\epsilon \xi dx_3 + \int_{B_{r/2}(\pm x_3^0)} M_1^\epsilon \partial_3 \xi dx_3.$$

Analogously, applying the same procedure to $-\xi$, we obtain the equality

$$\int_{B_{r/2}(\pm x_3^0)} EI_1^\epsilon \Delta u_2^{0\epsilon} \Delta\xi dx_3 = \int_{B_{r/2}(\pm x_3^0)} q_2^\epsilon \xi dx_3 + \int_{B_{r/2}(\pm x_3^0)} M_1^\epsilon \partial_3 \xi dx_3,$$

for all $\xi \in \mathcal{D}(B_{r/2}(\pm x_3^0))$, and then,

$$EI_1^\epsilon \Delta^2 u_2^{0\epsilon} = q_2^\epsilon + \partial_3 M_1^\epsilon \text{ in } \mathcal{D}'(\Gamma_C^0\backslash I). \tag{9.90}$$

Now, we notice that from (9.84),

$$\int_{-L}^{L} EI_1^\epsilon \Delta u_2^{0\epsilon} \Delta v dx_3 \geq \int_{-L}^{L} q_2^\epsilon v dx_3 - \int_{-L}^{L} M_1^\epsilon \partial_3 v dx_3,$$

for all $v \in H_e^2(-L,L)$ with $v \geq 0$ in Γ_C^0; in particular,

$$a(u_2^{0\epsilon}, v) - (f_0^\epsilon, v) \geq 0, \forall v \in H_e^2(-L,L) \cap H_0^1(-L,L),\ v \geq 0 \text{ in } \Gamma_C^0,$$

where a is the bilinear form

$$a(u,v) = \int_{-L}^{L} EI_1^\epsilon \Delta u \Delta v dx_3,\ \forall v \in H_e^2(-L,L),$$

and $f_0^\epsilon \in [H_e^2(-L,L)]'$ is given by

$$(f_0^\epsilon, v) = \int_{-L}^{L} q_2^\epsilon v dx_3 + \int_{-L}^{L} \partial_3 M_1^\epsilon v dx_3,\ \forall v \in H_e^2(-L,L) \cap H_0^1(-L,L).$$

Therefore, by Riesz-Schwartz theorem (see [76]), there exists a positive Radon measure μ in $(-L,L)$ such that

$$a(u_2^{0\epsilon}, v_2^0) - (f_0^\epsilon, v_2^0) = \int_{-L}^{L} v_2^0 d\mu, \forall v_2^0 \in H_e^2(-L,L) \cap H_0^1(-L,L),\ v_2^0 \geq 0 \text{ in } \Gamma_C^0.$$

Finally, from (9.89) and (9.90), $supp(\mu) \subset I$ and we deduce (9.87). □

Remark 9.5.3. *The problem defined by equations (9.87) and (9.88) constitutes a generalization of the Euler-Bernouilli theory for the case of beams in contact with a rigid foundation, in which becomes into a singularity in the resultant of the applied loads. Other generalizations of Bernouilli-Euler models with singularities are shown in [21] and [80].*

Proposition 9.5.4. *The limit vertical displacement satisfies the following regularity properties:*

$$u_2^{0\epsilon} \in \mathcal{C}^2(-L,L) \cap \mathcal{C}^3((-L,L)\backslash I).$$

Moreover, the lateral limits $\partial_3 \Delta u_2^{0\epsilon}(x_3^\pm)$ exist for all $x_3 \in I$ and

$$\partial_3 \Delta u_2^{0\epsilon}(x_3^+) \geq \partial_3 \Delta u_2^{0\epsilon}(x_3^-), \forall x_3 \in I. \tag{9.91}$$

Proof. From previous Theorem it is clear that $\Delta^2 u_2^{0\epsilon} \in L^2((-L,L)\backslash I)$. Since I is a closed interval, $u_2^{0\epsilon} \in H^4((-L,L)\backslash I)$, and then, $u_2^{0\epsilon} \in \mathcal{C}^3((-L,L)\backslash I)$.

Moreover, from (9.87) and given that μ is a positive Radon measure, and hence it can be considered as the derivative of an increasing function φ (see [76]), we can write

$$EI_1^\epsilon \partial_3 \Delta u_2^{0\epsilon} = G^\epsilon + \varphi \text{ in } (-L,L), \tag{9.92}$$

thanks to (9.88), where G^ϵ is the continuous function in $(-L,L)$ given by

$$G^\epsilon(x_3) = \int_{-L}^{x_3} (q_2^\epsilon(s) + \partial_3 M_1^\epsilon(s)) ds, \tag{9.93}$$

and φ is defined by:

$$\varphi(x_3) = \int_{-L}^{x_3} d\mu. \tag{9.94}$$

By integrating (9.92) and thanks again to (9.88), we obtain

$$EI_1^\epsilon \Delta u_2^{0\epsilon}(x_3) = \int_{-L}^{x_3} (G^\epsilon + \varphi) ds,\ x_3 \in (-L, L), \tag{9.95}$$

where the right-side term is a continuous function in $(-L, L)$; therefore, $\Delta u_2^{0\epsilon}$ is continuous in $(-L, L)$ and, consequently, $u_2^{0\epsilon} \in \mathcal{C}^2(-L, L)$.

Finally, we know that φ defined by (9.94) is a function of bounded variation in all closed interval; hence the discontinuities of φ are only jump discontinuities (see [3]) and hence, from (9.92), the lateral limits $\partial_3 \Delta u_2^{0\epsilon}(x_3^\pm)$ exist and verify (9.91) thanks to φ is growing. □

Proposition 9.5.5. *i) If the axial forces F_3 and H_3 are null, the axial stress component $\sigma_{33}^{0\epsilon}$ is null on* $\mathrm{int}(I)$.

ii) If $I \subset (-L, L)$, the measure μ verifies:

$$\mu(I) = -\int_{-L}^{L} q_2^\epsilon dx_3, \tag{9.96}$$

$$\mu = -q_2^\epsilon - \partial_3 M_1^\epsilon \ \textit{in}\ \mathcal{D}'(\mathrm{int}(I)). \tag{9.97}$$

iii) The jump discontinuities of $\partial_3 \Delta u_2^{0\epsilon}$ lie in ∂I.

Proof. i) It is easy to prove that $\underline{u}_3^{0\epsilon} = 0$.

Then, let $x_3 \in \mathrm{int}(I)$; there exists $\alpha > 0$ such that

$$u_2^{0\epsilon}(y) = 0,\ \forall y \in B_\alpha(x_3) \subset \mathrm{int}(I),$$

which implies that

$$u_2^{0\epsilon}(y) = \partial_3 u_2^{0\epsilon}(y) = \partial_{33} u_2^{0\epsilon}(y) = \partial_{333} u_2^{0\epsilon}(y) = 0,\ \forall y \in B_\alpha(x_3). \tag{9.98}$$

So, thanks to (9.82), $\sigma_{33}^{0\epsilon}$ is null in $B_\alpha(x_3)$, and therefore, $\sigma_{33}^{0\epsilon}$ is null in $\mathrm{int}(I)$.

ii) Multiplying expression (9.92) by $\partial_3 v$, with $v \in H_e^2(-L, L)$, such that $v \geq 0$ in Γ_C^0 and integrating in $(-L, L)$, we find that:

$$\int_{-L}^{L} EI_1^\epsilon \partial_3 \Delta u_2^{0\epsilon} \partial_3 v dx_3 = \int_{-L}^{L} G^\epsilon \partial_3 v dx_3 + \int_{-L}^{L} \varphi \partial_3 v dx_3.$$

By applying Green's identity and the even character of v, we can write

$$-\int_{-L}^{L} EI_1^\epsilon \Delta u_2^{0\epsilon} \Delta v dx_3 = -\int_{-L}^{L} q_2^\epsilon v dx_3 + \left(\int_{-L}^{L} q_2^\epsilon dx_3 \right) v(L) + \int_{-L}^{L} M_1^\epsilon \partial_3 v dx_3 + \int_{-L}^{L} \varphi \partial_3 v dx_3. \tag{9.99}$$

Besides, from the variational formulation (9.84) we obtain that

$$\int_{-L}^{L} EI_1^\epsilon \Delta u_2^{0\epsilon} \Delta v dx_3 \geq \int_{-L}^{L} q_2^\epsilon v dx_3 - \int_{-L}^{L} M_1^\epsilon \partial_3 v dx_3, \tag{9.100}$$

By term-by-term addition of (9.99) and (9.100), we have that

$$0 \geq \left(\int_{-L}^{L} q_2^\epsilon dx_3 \right) v(L) + \int_{-L}^{L} \varphi \partial_3 v dx_3, \, \forall v \in H_e^2(-L,L); v \geq 0 \text{ in } \Gamma_C^0. \tag{9.101}$$

Let us choose v such that $\text{supp}(v) \cap \text{supp}(\mu) = \emptyset$ and let us consider $\bar{v} = v - v(L) \in H_e^2(-L,L) \cap H_0^1(-L,L)$; by using the definition of derivative in the sense of distributions,

$$\int_{-L}^{L} \varphi \partial_3 v dx_3 = \int_{-L}^{L} \varphi \partial_3 \bar{v} dx_3 = -\int_{-L}^{L} \bar{v} d\mu = -\int_{-L}^{L} v d\mu + v(L)\mu(I) = v(L)\mu(I). \tag{9.102}$$

So, substituting (9.102) in expression (9.101), we deduce that

$$v(L) \left(\int_{-L}^{L} q_2^\epsilon dx_3 + \mu(I) \right) \leq 0, \forall v \in H_e^2(-L,L); v \geq 0 \text{ in } \Gamma_C^0.$$

Then, we conclude (9.96) considering test functions v such that $v(L) = \pm 1$.

Finally, if $v \in \mathcal{D}(\text{int}(I))$ is an even function, from (9.99) we obtain that

$$0 = \int_I EI_1^\epsilon \Delta u_2^{0\epsilon} \Delta v dx_3 = \int_I q_2^\epsilon v dx_3 + \int_I \partial_3 M_1^\epsilon v dx_3 + \int_I v d\mu,$$

and so (9.97).

iii) From the demonstration of Proposition 9.5.4, we know that $\partial_3 \Delta u_2^{0\epsilon}$ has only jump discontinuities that are in the coincidence set I. Due to (9.98), $\partial_3 \Delta u_2^{0\epsilon}$ is continuous in $\text{int}(I)$ (identically zero) and, therefore, the discontinuities must appear on ∂I.

□

Proposition 9.5.6. *Let $u_2^{0\epsilon}$ be a smooth solution of the differential problem (9.87)-(9.88). If $u_2^{0\epsilon} \geq 0$ in Γ_C^0, then $u_2^{0\epsilon}$ is the solution of Problem $(\mathbf{P_2^{0\epsilon}})$.*

Proof. Following the same reasoning that in Proposition 9.5.5, we can write:

$$\begin{aligned} \int_{-L}^{L} EI_1^\epsilon \partial_3 \Delta u_2^{0\epsilon} \partial_3 v dx_3 = &- \int_{-L}^{L} q_2^\epsilon v dx_3 + v(L) \int_{-L}^{L} q_2^\epsilon dx_3 + \int_{-L}^{L} M_1^\epsilon \partial_3 v dx_3 - \\ &- \int_{-L}^{L} v d\mu - v(L) \int_{-L}^{L} q_2^\epsilon dx_3 = \\ &- \int_{-L}^{L} q_2^\epsilon v dx_3 + \int_{-L}^{L} M_1^\epsilon \partial_3 v dx_3 - \int_{-L}^{L} v d\mu, \end{aligned}$$

for all $v \in H_e^2(-L,L)$ such that $v \geq 0$ in Γ_C^0.

Besides, by applying integration by parts to the first term in the previous expression and taking into account (9.88), we have that

$$\int_{-L}^{L} EI_1^\epsilon \Delta u_2^{0\epsilon} \Delta v dx_3 = \int_{-L}^{L} q_2^\epsilon v dx_3 - \int_{-L}^{L} M_1^\epsilon \partial_3 v dx_3 + \int_{-L}^{L} v d\mu \geq \int_{-L}^{L} q_2^\epsilon v dx_3 - \int_{-L}^{L} M_1^\epsilon \partial_3 v dx_3,$$

since μ is a nonnegative measure and, therefore, the theorem is proved. □

Chapter 10

An improved formula for the MOR

As we have mentioned in the introduction of Part II, the relative simplicity of the three-point bending tests has permitted its popularization for measuring the MOR of brittle materials; nevertheless, the fact that samples of same material can lead to different values for the MOR is something quite common. Our guess is that this effect is due to the classic theoretical formula generally used in engineering to compute the MOR which, from our point of wiev, should be completed with some three-dimensional effects.

By taking advantage of all the theoretical results collected in Chapters 8 and 9, in this chapter we are going to obtain a new formula for the MOR. This new expression takes into account not only the rupture load and the total length of the beam but also the distance between the two lower cylinders, the effect of the gravity and the distance between the ends of the beam and the lower cylinders.

The outline of this chapter is as follows: In Section 10.1, we introduce the classic formula for the MOR of brittle materials. Section 10.2 is devoted to recall the mathematical model associated with this experiment: an elastic problem with a frictionless unilateral contact condition. We summarize the assumptions of compatibility on the forces needed to obtain the existence of a unique solution of the associated variational problem. Several examples for laboratory tests for cylindrical and rectangular beams are detailed in Section 10.3: The Experiments I and II. We show that the previous compatibility assumptions are satisfied for these real experiments. In Section 10.4, we obtain, from the differential formulation of the bending and axial displacements obtained in Section 9.5 by using the asymptotic analysis, analytical solutions for Experiments I and II. Moreover, we introduce the new theoretical expression for the MOR.

10.1 The theoretical MOR

In the classical theory of beams, the MOR is given by an explicit expression which involves the value of the load of failure, H, the distance, $2l$, between the two lower cylinders, and the second moment of inertia, I_1, of the transversal section of the beam (see [5]).

In particular, the theoretical MOR of a cylindrical beam with radius R subjected to a failure

load with modulus H is

$$\sigma_{ft} = \frac{2Hl}{\pi R^3}; \tag{10.1}$$

analogously, if the beam is rectangular with width $2a$ and height $2b$, the theoretical MOR is

$$\sigma_{ft} = \frac{3Hl}{8ab^2}. \tag{10.2}$$

An explanation on the classic expression for the MOR will be presented later in Appendix A.

10.2 Mathematical model for the real experiments

We recall in this section the mathematical problem arising from the three-point bending test already introduced in Chapter 8 and, from now on, we omit the index ϵ to simplify the notation, that is, $\epsilon = 1$.

Let ω be a bounded, open, connected domain in $\mathbb{R}^2$; we consider a beam which occupies at rest the domain $\overline{\Omega} = \overline{\omega} \times [-L, L], L > 0$, and we refer the motion of the beam to a fixed Cartesian system $Ox_1x_2x_3$ whose origin is situated at the center of gravity of the beam (see Fig. 10.1).

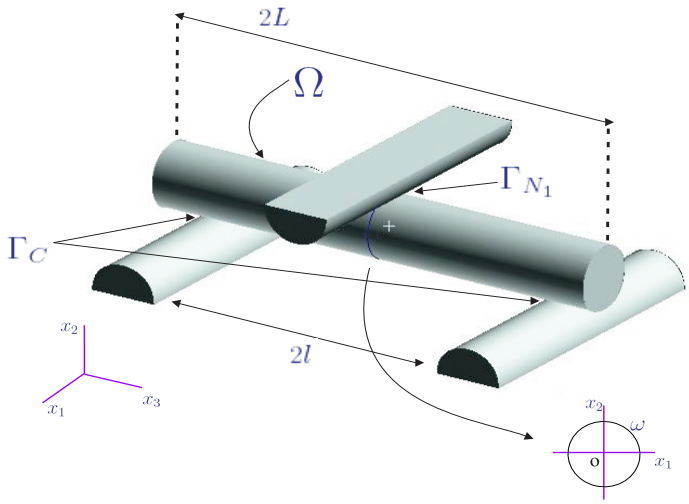

Figure 10.1: Sketch of three-point bending test.

The physical problem consists of determining the displacement vector field, $\mathbf{u}$, and the stress tensor field, $\boldsymbol{\sigma}$, that the beam $\bar{\Omega}$ suffers when it is subjected to a three-point bending test.

Let Γ be the boundary of the beam which is the union of the lateral boundary Γ_l and the ends $\Gamma_\pm = \omega \times \{\pm L\}$, $\mathbf{n}$ being the outward unit normal vector to Γ. Γ_l is partitioned into three non-empty, open and disjointed parts Γ_C, Γ_{N_1} and Γ_{N_2}, where Γ_C is the region of the beam resting on the two lower cylinders for which we impose a Signorini frictionless contact condition (see [54]); Γ_{N_1} corresponds to the region of the boundary in which the upper cylinder exerts a compression

force of known resultant, H, and Γ_{N_2} represents the remaining lateral boundary of the beam that is free of forces. The ends of the beam are also assumed to be free of forces.

The most used materials in three-point bending tests are brittle materials that break suddenly, being its response, until the moment of failure, almost elastic and linear. Then, we assume that the infinitesimal strain field, $\boldsymbol{\varepsilon}(\mathbf{u})$, is related to the stress tensor, $\boldsymbol{\sigma}$, through Hooke's law and that the material is homogeneous and isotropic.

Under the assumption of small displacements, the behavior of the beam is governed by the usual equilibrium equations:

Problem *(P)*:

Find the displacement vector field, $\mathbf{u}(\mathbf{x})$, and the stress tensor field, $\boldsymbol{\sigma}(\mathbf{x})$, at each point $\mathbf{x} \in \Omega$, satisfying:

$$-\mathrm{div}(\boldsymbol{\sigma}) = \mathbf{f} \text{ in } \Omega, \tag{10.3}$$

$$\boldsymbol{\sigma}\mathbf{n} = \mathbf{h} \text{ on } \Gamma_{N_1}, \tag{10.4}$$

$$\boldsymbol{\sigma}\mathbf{n} = \mathbf{0} \text{ on } \Gamma_{N_2} \cup \Gamma_{\pm}, \tag{10.5}$$

$$\boldsymbol{\sigma}_\tau = \mathbf{0},\ \sigma_n \leq 0,\ u_n \leq 0,\ \sigma_n u_n = 0 \text{ on } \Gamma_C, \tag{10.6}$$

$$\boldsymbol{\sigma} = \boldsymbol{\Lambda}\boldsymbol{\varepsilon}(\mathbf{u}) = \lambda \mathrm{tr}(\boldsymbol{\varepsilon}(\mathbf{u}))\mathbf{I} + 2\mu\boldsymbol{\varepsilon}(\mathbf{u}) \text{ in } \Omega, \tag{10.7}$$

where u_n is the normal component of $\mathbf{u}$ and σ_n and $\boldsymbol{\sigma}_\tau$ are the normal and tangential components of $\boldsymbol{\sigma}\mathbf{n}$, respectively. In (8.9), λ and μ are the Lamé parameters of the material, related with Young's modulus, E, and Poisson's ratio, ν, by the usual expressions.

In order to carry out a mathematical analysis of Problem (P), associated with the three-point bending test, we consider the space of displacement vector fields $\mathbf{H}^1(\Omega) = [H^1(\Omega)]^3$ and the convex subset of kinematically admissible displacements

$$\mathbf{K}(\Omega) = \{\mathbf{v} \in \mathbf{H}^1(\Omega); v_n \leq 0 \text{ on } \Gamma_C\}.$$

The corresponding space of stress fields is defined by

$$\mathbf{X}(\Omega) = \{\boldsymbol{\tau} = (\tau_{ij}); \boldsymbol{\tau} \in [L^2(\Omega)]^9, \tau_{ij} = \tau_{ji}\}.$$

From now on in this Part II, we consider the following hypotheses.

(H1) The volume forces satisfy $\mathbf{f} \in \mathbf{L}^2(\Omega)$ and the surface forces $\mathbf{h} \in \mathbf{L}^2(\Gamma_{N_1})$.

(H2) The material is homogeneous and isotropic; so, the elasticity tensor $\boldsymbol{\Lambda}$ defined in (8.9) is such that $\lambda, \mu \in \mathbb{R}$, $\lambda, \mu > 0$.

(H3) The applied forces verify the compatibility condition

$$\int_\Omega \mathbf{f} \cdot \mathbf{w} d\mathbf{x} + \int_{\Gamma_{N_1}} \mathbf{h} \cdot \mathbf{w} d\Gamma \leq 0,$$

for all $\mathbf{w} \in \mathbf{K}(\Omega) \cap \mathbf{R}(\Omega)$, where

$$\mathbf{R}(\Omega) = \{\mathbf{w} \in \mathbf{H}^1(\Omega) : \boldsymbol{\varepsilon}(\mathbf{w}) = \mathbf{0} \text{ in } [L^2(\Omega)]^9\}, \tag{10.8}$$

is the set of rigid displacements. Moreover,

$$\int_\Omega \mathbf{f}\cdot\mathbf{w}d\mathbf{x}+\int_{\Gamma_{N_1}}\mathbf{h}\cdot\mathbf{w}d\Gamma=0,$$

if and only if $\mathbf{w}\in\mathbf{R}_n(\Omega)$, where

$$\mathbf{R}_n(\Omega)=\{\mathbf{w}\in\mathbf{R}(\Omega); w_n=0 \ a.e. \text{ on } \Gamma_C\}.$$

(H4) The set $(\mathbf{K}(\Omega)\cap\mathbf{R}(\Omega))\setminus\mathbf{R}_n(\Omega)$ is non-empty.

(H5)
- Domain ω is symmetrical with respect to the lines $x_1=0$ and $x_2=0$.
- Boundaries Γ_{N_1} and Γ_C are symmetrical with respect to the planes $x_1=0$ and $x_3=0$. Furthermore,

$$\Gamma_{N_1}=\{\mathbf{x}\in\Gamma_l;|x_3|<\delta,\,(x_1,x_2)\in\gamma_{N_1}(x_3)\},$$
$$\Gamma_C=\{\mathbf{x}\in\Gamma_l;0<|x_3|-l<\hat{\delta},\,(x_1,x_2)\in\gamma_C(x_3)\},$$

  with $\gamma_{N_1}(x_3),\gamma_C(x_3)\subset\gamma$, and δ, $\hat{\delta}$ being small parameters, verifying $\delta<l-\hat{\delta}$.
- The second component of the outward normal vector to Γ is not null on Γ_C and with constant sign. Moreover, it is even with respect to x_1.

(H6) Volume and surface forces verify that

- f_1 and h_1 are odd with respect to x_1 and even with respect to x_3,
- f_2 and h_2 are even with respect to x_1 and x_3,
- f_3 and h_3 are even with respect to x_1 and odd with respect to x_3.

The weak formulation corresponding to Problem (P) is the following:

Problem *(VP)*:

Find $\mathbf{u}\in\mathbf{K}(\Omega)$ such that:

$$\int_\Omega \mathbf{\Lambda}\boldsymbol{\varepsilon}(\mathbf{u}):\boldsymbol{\varepsilon}(\mathbf{v}-\mathbf{u})d\mathbf{x}\geq\int_\Omega\mathbf{f}\cdot(\mathbf{v}-\mathbf{u})d\mathbf{x}+\int_{\Gamma_{N_1}}\mathbf{h}\cdot(\mathbf{v}-\mathbf{u})d\Gamma,\quad\forall\mathbf{v}\in\mathbf{K}(\Omega).$$

By using a well-known result of Fichera (see [40]), in Section 8.4 we have established the existence of a unique solution of Problem (PV) (see [69]):

Theorem 10.2.1. *i) Under assumptions* **(H1)-(H4)**, *there exists a solution of Problem* (VP).

ii) Under assumptions **(H1)-(H6)**, *there exists a unique solution* $\mathbf{u}\in\mathbf{H}^1_s(\Omega)\cap\mathbf{K}(\Omega)$ *of Problem* (VP), $\mathbf{H}^1_s(\Omega)$ *being the set:*

$$\mathbf{H}^1_s(\Omega)=\left\{\mathbf{v}\in\mathbf{H}^1(\Omega);\ \begin{array}{l} v_1 \text{ is odd in } x_1 \text{ and even in } x_3\\ v_2 \text{ is even in } x_1 \text{ and } x_3\\ v_3 \text{ is even in } x_1 \text{ and is odd in } x_3\end{array}\right\}.$$

10.3 Verifying hypotheses for two laboratory experiences

In this section, we are going to describe in detail the two real cases of bending tests carried out in laboratory and to prove that the assumptions of compatibility introduced in previous Chapters are satisfied. These experiments have been carried out in collaboration with the Institute of Ceramics of the Universidade de Santiago de Compostela where porcelain is used as the brittle material and cylindrical and rectangular beams are considered. For both, numerical results will be presented in Chapter 11.

10.3.1 Description of data of the experiments

In the following, we present a description of the geometry of the samples, of the different regions considered at the boundary and of the applied forces. In three-point bending tests, the boundary Γ_{N_1} corresponds to the region of contact between the beam and the upper cylinder, which is assumed to be known in advance. In this region, the force is applied vertically to the beam and its resultant, $\mathbf{H} = -H\mathbf{e}_2$, $H > 0$, is measured in laboratory. In practice (see Figure 7.1), this force is very close to a "Dirac's delta" distribution, which can be approached in numerical simulations as top hat functions defined on small areas and with the same resultant. In effect, according to Saint Venant's principle (see [35]), if a body is submitted to a system of forces acting over a bounded region of its surface, stresses and strains induced away from this region do not depend on the particular form of the applied force, but rather on its resultant. Taking into account that our objective is to compute the MOR, which depends only on the stresses induced in the region opposite to Γ_{N_1}, in order to simplify the computations, we assume that the applied force is a top hat function with constant density, h,

$$\mathbf{h} = -h\mathbf{e}_2,\ h = \frac{H}{\text{area}(\Gamma_{N_1})}.$$

The contact boundary, Γ_C, corresponds to the region where the beam may come into contact with the two lower cylinders; while Γ_C is fixed in advance, the actual contact area is, of course, a priori unknown.

The only volume force acting on the beam is due to the action of the gravity and its expression is

$$\mathbf{f} = -\rho g\mathbf{e}_2,$$

where ρ is the density of the material and g is the gravitational acceleration. In both experiments we consider, as brittle material, the porcelain.

We detail below the two considered experiments.

Experiment I: Cylindrical beams.

In this first case, we are going to use a system of cylindrical coordinates $\{r, \theta, z\}$. We consider a beam of length $2L$ whose section is a circle of radius R and we assume that there

is a distance $2l$ between the two lower cylinders. The geometry of the beam can be expressed by

$$\Omega = \{(r, \theta, z); r \in [0, R), \theta \in [0, 2\pi), z \in (-L, L)\}. \tag{10.9}$$

The expression for the boundary Γ_{N_1} is

$$\Gamma_{N_1} = \{(R, \theta, z); \theta \in \left(\frac{\pi}{2} - \delta, \frac{\pi}{2} + \delta\right), z \in (-\delta, \delta)\}, \tag{10.10}$$

where δ is a positive parameter and small enough to assure that the resultant force on Γ_{N_1} is $\mathbf{H}$; therefore,

$$\delta = \left(\frac{H}{4hR}\right)^{1/2}.$$

The contact boundary, Γ_C, is given by the expression

$$\Gamma_C = \{(R, \theta, z); \theta \in \left(\frac{3\pi}{2} - \frac{\hat{\delta}}{2}, \frac{3\pi}{2} + \frac{\hat{\delta}}{2}\right), z \in (-l - \hat{\delta}, -l) \cup (l, l + \hat{\delta})\}, \tag{10.11}$$

where $\hat{\delta}$ is the thickness of the contact zone between the beam and each lower cylinder; $\hat{\delta}$ is a positive parameter and small.

Experiment II: Rectangular beams.

In the second experiment, we use rectangular beams of length $2L$, width $2a$ and height $2b$, so their geometry is described as

$$\Omega = (-a, a) \times (-b, b) \times (-L, L).$$

The expression of the boundary Γ_{N_1} is

$$\Gamma_{N_1} = \{(x_1, b, x_3); x_1 \in (-a, a), x_3 \in (-\delta, \delta)\}, \tag{10.12}$$

where, again, 2δ is chosen such that the resultant force on Γ_{N_1} is $\mathbf{H}$:

$$\delta = \frac{H}{4ha}.$$

The contact boundary, Γ_C, is given by the expression

$$\Gamma_C = \{(x_1, -b, x_3); x_1 \in (-a, a), x_3 \in (-l - \hat{\delta}, -l) \cup (l, l + \hat{\delta})\}, \tag{10.13}$$

where, again, $\hat{\delta}$ is the thickness of the contact zone between the beam and each lower cylinder.

10.3.2 Behaviour of applied forces

As we have recalled in Section 10.2, there exists a unique solution of Problem (VP) if assumptions **(H1)-(H6)** are verified. In this section, we focus on prove that the assumption **(H3)** is satisfied for both experiments I and II. For this, first, we are going to characterize the expression of rigid displacements.

Characterization of rigid displacements

The following lemma identifies the elements of $\mathbf{R}(\Omega)$ defined by (10.8).

Lemma 10.3.1. *The following conditions are equivalent:*

(i) $\mathbf{w} \in \mathbf{R}(\Omega)$,

(ii) $\mathbf{w}(\mathbf{x}) = \mathbf{c} + \mathbf{d} \times \mathbf{x}$, *a.e. in* Ω, *with* $\mathbf{c}, \mathbf{d} \in \mathbb{R}^3$,

(iii) $\mathbf{w}(r, \theta, z) = w_r \mathbf{e}_r + w_\theta \mathbf{e}_\theta + w_z \mathbf{e}_z$, *where*

$$\begin{aligned} w_r &= (A \sin\theta + B\cos\theta) + z(C \sin\theta + D\cos\theta), \\ w_\theta &= (A\cos\theta - B \sin\theta) + z(C\cos\theta - D \sin\theta) + Er, \\ w_z &= F - r(C \sin\theta + D\cos\theta), \end{aligned}$$

a.e. in Ω, *with* $A, B, C, D, E, F \in \mathbb{R}$,

where $\times$ *denotes the vectorial product,* $\mathbf{x}$ *is the position vector of the point* (x_1, x_2, x_3) *and* (r, θ, z) *are the cylindrical coordinates of* $\mathbf{x}$ *in* Ω.

Proof. Equivalence between *(i)* and *(ii)* can be seen in Theorem 3.2 of Chapter 6 in [61]. Implication *(iii)*$\rightarrow$ *(i)* is obvious if we take into account the expression of the infinitesimal strain field in cylindrical coordinates (see [53]).

We are going to prove the implication *(i)*$\rightarrow$ *(iii)*. We have that $\mathbf{w} \in \mathbf{R}(\Omega)$, so it means in cylindrical coordinates

$$0 = \varepsilon_{rr}(\mathbf{w}) = w_{r,r}, \tag{10.14}$$

$$0 = \varepsilon_{\theta\theta}(\mathbf{w}) = \frac{1}{r} w_{\theta,\theta} + \frac{w_r}{r}, \tag{10.15}$$

$$0 = \varepsilon_{zz}(\mathbf{w}) = w_{z,z}, \tag{10.16}$$

$$0 = 2\varepsilon_{r\theta}(\mathbf{w}) = w_{\theta,r} + \frac{1}{r} w_{r,\theta} - \frac{w_\theta}{r}, \tag{10.17}$$

$$0 = 2\varepsilon_{\theta z}(\mathbf{w}) = \frac{1}{r} w_{z,\theta} + w_{\theta,z}, \tag{10.18}$$

$$0 = 2\varepsilon_{rz}(\mathbf{w}) = w_{r,z} + w_{z,r}. \tag{10.19}$$

By using (10.14), (10.16) and (10.19) we have

$$w_r = f_1(\theta) + f_2(\theta) z, \tag{10.20}$$

$$w_z = \hat{f}_1(\theta) + \hat{f}_2(\theta) r, \tag{10.21}$$

with

$$f_2(\theta) = -\hat{f}_2(\theta). \tag{10.22}$$

Deriving with respect to z in (10.18) and by using (10.16) we have that $w_{\theta,zz} = 0$. Again, deriving with respect to r in (10.18) and by using (10.21), we obtain

$$w_{\theta,zr} = \frac{1}{r^2}\hat{f}_1'(\theta). \tag{10.23}$$

Deriving with respect to z in (10.17) and by using (10.20) and (10.23) we can write

$$w_{\theta,z} = \frac{1}{r}\hat{f}_1'(\theta) + f_2'(\theta), \tag{10.24}$$

and deriving now with respect to r

$$w_{\theta,zr} = -\frac{1}{r^2}\hat{f}_1'(\theta). \tag{10.25}$$

Expressions (10.23) and (10.25) lead to the condition

$$\hat{f}_1'(\theta) = 0 \quad \forall\theta \in [0, 2\pi) \Rightarrow \hat{f}_1(\theta) = \hat{f}_1 \in \mathbb{R} \quad \forall\theta \in [0, 2\pi). \tag{10.26}$$

Therefore, from (10.21), (10.22), (10.24) and (10.26) we have the expressions

$$w_\theta = f_2'(\theta)z + f_3(r, \theta), \tag{10.27}$$

$$w_z = \hat{f}_1 - f_2(\theta)r. \tag{10.28}$$

Substituting (10.20), (10.27) and (10.28) in (10.15) and (10.17), we obtain

$$0 = (f_2''(\theta) + f_2(\theta))z + f_1(\theta) + f_{3,\theta}, \tag{10.29}$$

$$0 = f_{3,r} - \frac{1}{r}f_3(r, \theta) + \frac{1}{r}f_1'(\theta). \tag{10.30}$$

Deriving with respect to r in (10.29) and with respect to θ in (10.30), we deduce

$$0 = f_{3,r\theta},$$
$$0 = -\frac{1}{r}f_{3,\theta} + \frac{1}{r}f_1''(\theta),$$

and then

$$f_{3,\theta} = f_1''(\theta).$$

Therefore, we have

$$f_3(r, \theta) = f_1'(\theta) + f_4(r). \tag{10.31}$$

In addition, substituting (10.31) in (10.30), we obtain that f_4 must verify the ordinary differential equation:

$$f_4'(r) = \frac{1}{r}f_4(r),$$

whose general solution is

$$f_4(r) = f_4 r, \quad f_4 \in \mathbb{R};$$

this leads to the following expression for f_3:

$$f_3(r, \theta) = f_1'(\theta) + f_4 r. \tag{10.32}$$

Finally, substituting the previous expression in (10.29), we have

$$0 = (f_2''(\theta) + f_2(\theta))z + (f_1''(\theta) + f_1(\theta)), \quad \forall(\theta, z) \in [0, 2\pi) \times (-L, L), \tag{10.33}$$

so we obtain the homogeneous ordinary differential equations for f_1 and f_2:

$$f_1''(\theta) + f_1(\theta) = 0,$$
$$f_2''(\theta) + f_2(\theta) = 0,$$

whose general solutions are:

$$f_1(\theta) = A \sin\theta + B\cos\theta, \quad A, B \in \mathbb{R}, \tag{10.34}$$
$$f_2(\theta) = C \sin\theta + D\cos\theta, \quad C, D \in \mathbb{R}. \tag{10.35}$$

In conclusion, from (10.20), (10.27), (10.28), (10.32) and (10.34)-(10.35) we have that $\mathbf{w}$ verifies *(iii)*. □

10.3.3 Verification of assumption (H3)

In three-point bending tests, volume and surface forces are given by the following expressions in cartesian and cylindrical coordinates:

$$\mathbf{f} = -\rho g \mathbf{e_2} = -\rho g(\sin\theta \mathbf{e}_r + \cos\theta \mathbf{e}_\theta), \tag{10.36}$$
$$\mathbf{h} = -h\mathbf{e_2} = -h(\sin\theta \mathbf{e}_r + \cos\theta \mathbf{e}_\theta), \quad h > 0. \tag{10.37}$$

We are going to prove that these forces satisfy assumption **(H3)** in order to obtain the existence of a unique solution of Problem (VP).

Lemma 10.3.2. *In experiment I, volume and surface forces verify assumption **(H3)**.*

Proof. Taking into account expression (10.9) and by using (10.36) and (10.37), we have

$$\int_\Omega \mathbf{f}\cdot\mathbf{w}d\mathbf{x} + \int_{\Gamma_{N_1}} \mathbf{h}\cdot\mathbf{w}d\Gamma = -2R(\pi LR\rho g + 2\delta^2 h)A, \tag{10.38}$$

for every $\mathbf{w} \in \mathbf{R}(\Omega)$ given by *(iii)* of Lemma 10.3.1.

Then, hypothesis **(H3)** is verified if we prove that $A \geq 0$, for every $\mathbf{w} \in \mathbf{K}(\Omega) \cap \mathbf{R}(\Omega)$ and $A = 0$ if and only if $w_n = 0$ on Γ_C.

Let us assume that $\mathbf{w} \in \mathbf{K}(\Omega) \cap \mathbf{R}(\Omega)$; since $\mathbf{n} = \mathbf{e}_r$ on Γ_C, we can write

$$w_n = \mathbf{w}\cdot\mathbf{n} = A\sin\theta + B\cos\theta + z(C\sin\theta + D\cos\theta) \leq 0 \ \textit{a.e.} \text{ on } \Gamma_C.$$

Consequently:

$$0 \geq \int_{\Gamma_C} \mathbf{w}\cdot\mathbf{n}d\Gamma = -4\hat{\delta}\cos\left(\frac{3\pi}{2} + \frac{\hat{\delta}}{2}\right)RA, \tag{10.39}$$

and so $A \geq 0$.

In order to complete the proof of **(H3)**, from (10.39), $A = 0$ if and only if

$$\int_{\Gamma_C} \mathbf{w} \cdot \mathbf{n} d\Gamma = 0.$$

Since $w_n \leq 0$ on Γ_C, we can conclude that $A = 0$ if and only if $w_n = 0$ on Γ_C. □

Lemma 10.3.3. *In experiment II, volume and surface forces verify assumption **(H3)**.*

Proof. In this case we consider a rectangular domain, where $x_1 \in (-a, a)$, $x_2 \in (-b, b)$ and $x_3 \in (-L, L)$. Let $\mathbf{w} \in \mathbf{K}(\Omega) \cap \mathbf{R}(\Omega)$, we have that

$$\int_{\Omega} \mathbf{f} \cdot \mathbf{w} d\mathbf{x} + \int_{\Gamma_{N_1}} \mathbf{h} \cdot \mathbf{w} d\Gamma = -(8abL\rho g + 4a\delta h)c_2, \tag{10.40}$$

for every $\mathbf{w} \in \mathbf{R}(\Omega)$ given by *(ii)* of Lemma 10.3.1.

Then, hypothesis **(H3)** is verified if we prove that $c_2 \geq 0$, for every $\mathbf{w} \in \mathbf{K}(\Omega) \cap \mathbf{R}(\Omega)$ and $c_2 = 0$ if and only if $\mathbf{w} \in \mathbf{R}_n(\Omega)$.

Let us assume that $\mathbf{w} \in \mathbf{K}(\Omega) \cap \mathbf{R}(\Omega)$; because $\mathbf{w} \cdot \mathbf{n} \leq 0$ *a.e.* on Γ_C, we have that

$$0 \geq \int_{\Gamma_C} \mathbf{w} \cdot \mathbf{n} d\Gamma = -4a\hat{\delta}c_2, \tag{10.41}$$

and so $c_2 \geq 0$. Moreover, $c_2 = 0$ if and only if

$$\int_{\Gamma_C} \mathbf{w} \cdot \mathbf{n} d\mathbf{x} = 0,$$

and, since the sign of w_n is constant on Γ_C, we conclude that $c_2 = 0$ if and only if $w_n = 0$ on Γ_C. □

10.3.4 Existence and uniqueness of solution for experiments I and II

Proposition 10.3.4. *There exists a unique weak solution $\mathbf{u} \in \mathbf{H}_s^1(\Omega)$ of Problem (P), defined by (10.3)-(10.7), corresponding to experiments I and II for a porcelain beam.*

Proof. Assumptions **(H1)** and **(H6)** are satisfied thanks to expressions (10.36) and (10.37). As porcelain is a homogeneous and isotropic material, with positive and constant Lamé parameters, assumption **(H2)** is also verified. Lemmas 10.3.2 and 10.3.3 guarantee that assumption **(H3)** is satisfied for experiments I and II, respectively. Assumption (H5) is also verified due to the sample geometries.

Furthermore, it is easy to verify assumption **(H4)**. Indeed, if we consider $\mathbf{w} \in \mathbf{K}(\Omega) \cap \mathbf{R}(\Omega)$,

$$\mathbf{w} \cdot \mathbf{n} = (c_1 + d_2 x_3 - d_3 x_2)n_1 + (c_2 + d_3 x_1 - d_1 x_3)n_2 \leq 0 \text{ on } \Gamma_C.$$

Finally, since n_2 is non null, choosing $c_1 = d_2 = d_3 = 0$ and $c_2, d_1 \neq 0$, we obtain that there exists $\mathbf{w} \in (\mathbf{K}(\Omega) \cap \mathbf{R}(\Omega)) \setminus \mathbf{R}_n(\Omega)$, $\mathbf{w} \neq \mathbf{0}$, such that

$$\mathbf{w} \cdot \mathbf{n} = (c_2 - d_1 x_3) n_2 \neq 0.$$

So the result is obtained from Theorem 10.2.1. □

10.4 Obtaining a new formula for the MOR

In Section 9.4 we have obtained the one-dimensional variational problems associated to the bending and axial displacements in three-point bending tests by applying the well-known method of asymptotic expansions. We have proved that a good approximation of the solution of the three-dimensional Problem (VP) is the limit displacement $\mathbf{u}^0 = (u_1^0, u_2^0, u_3^0)$, where the transversal displacement, u_1^0, is null, the bending displacement, u_2^0, only depends on x_3, and the axial displacement, u_3^0, is given by:

$$u_3^0 = \underline{u}_3^0 - x_2 \partial_3 u_2^0.$$

In particular, in the scenario of experiments I and II introduced in Section 10.3, the limit bending and axial displacements are the solution of the following variational problems:

Problem $(\mathbf{P_2^0})$:
Find $u_2^0 \in H_e^2(-L, L)$, such that $u_2^0 \geq 0$ in $\Gamma_C^0 = (-l - \hat{\delta}, -l) \cup (l, l + \hat{\delta})$ and

$$\int_{-L}^{L} EI_1 \Delta u_2^0 \Delta(v_2^0 - u_2^0) dx_3 \geq \int_{-L}^{L} q_2 (v_2^0 - u_2^0) dx_3, \tag{10.42}$$

for all $v_2^0 \in H_e^2(-L, L)$ such that $v_2^0 \geq 0$ in Γ_C^0. Here, q_2 is the total vertical force per unit of length:

$$q_2(x_3) = -\rho g \beta - \chi_{(-\delta,\delta)}(x_3) \alpha h,$$

where:

$$\beta = \begin{cases} \pi R^2 & \text{for experiment I,} \\ 4ab & \text{for experiment II,} \end{cases} \qquad \alpha = \begin{cases} 2\delta R & \text{for experiment I,} \\ 2a & \text{for experiment II.} \end{cases}$$

Problem $(\mathbf{P_3^0})$:
Find $\underline{u}_3^0 \in H_o^1(-L, L)$, such that

$$\int_{-L}^{L} \partial_3 \underline{u}_3^0 \, \partial_3 v_3^0 dx_3 = 0, \, \forall v_3^0 \in H_o^1(-L, L). \tag{10.43}$$

Moreover, in Section 9.5, we establish some properties of the bending and axial displacements which are collected in the following propositions (see [69]).

Proposition 10.4.1. *In the scenario of experiments I and II, the bending and axial problems* $(\mathbf{P_2^0})$ *and* $(\mathbf{P_3^0})$ *have unique solutions. Furthermore,* $\underline{u}_3^0$ *is null and the axial normal stress is given by the expression*

$$\sigma_{33}^0(\mathbf{x}) = -E x_2 \Delta u_2^0(x_3), \, \forall \mathbf{x} \in \Omega. \tag{10.44}$$

Proposition 10.4.2. *Let denote the coincidence set*

$$I = \{x_3 \in \bar{\Gamma}_C^0; u_2^0(x_3) = 0\}.$$

i) The bending displacement u_2^0 satisfies the following differential problem:

$$EI_1\Delta^2 u_2^0 = q_2 + \mu \text{ in } (-L, L), \tag{10.45}$$

$$\partial_3\Delta u_2^0(\pm L) = \Delta u_2^0(\pm L) = 0, \tag{10.46}$$

where μ is a nonnegative Radon measure μ such that $\text{supp}(\mu) \subset I$.

ii) u_2^0 verifies the regularity properties:

$$u_2^0 \in \mathcal{C}^2(-L, L) \cap \mathcal{C}^3((-L, L)\backslash I).$$

iii) The lateral limits $\partial_3\Delta u_2^0(x_3^{\pm})$ exist for all $x_3 \in I$ and

$$\partial_3\Delta u_2^0(x_3^+) \geq \partial_3\Delta u_2^0(x_3^-), \forall x_3 \in I.$$

iv) The measure μ verifies:

$$\mu(I) = -\int_{-L}^{L} q_2 dx_3.$$

v) The reciprocal of i) is also true if $u_2^0 \geq 0$ in Γ_C^0.

In the particular case of the experiments I and II, we can demonstrate that the effective support on each lower cylinder will be a point or an interval.

Proposition 10.4.3. *Let u_2^0 be the solution of Problem $(\mathbf{P_2^0})$. If x_0, $x_1 \in I$ with $0 < x_0 < x_1$, therefore $[-x_1, -x_0] \cup [x_0, x_1] \subset I$.*

Proof. The proof is very close to that given in [29]. From now on, we denote $\tilde{I} = [-x_1, -x_0] \cup [x_0, x_1]$. We define the following function:

$$v = u_2^0(1 - \chi_{\tilde{I}})$$

which satisfies $v \in H_e^2(-L, L)$ as a straightforward consequence of the fact that $u_2^0 \in H_e^2(-L, L) \subset \mathcal{C}^1(-L, L)$ and $u_2^0 \geq 0$ on Γ_C^0. Moreover, $v \geq 0$ in Γ_C^0.

We consider $w = u_2^0 - v \in H_e^2(-L, L)$ that verifies $w \geq 0$ on $\tilde{I}$ and $w = 0$ on $(-L, L)\backslash\tilde{I}$. Then, choosing $v_2^0 = w + u_2^0$ as test function in expression (10.42), we have that

$$\int_{-L}^{L} EI_1\Delta u_2^0\Delta w dx_3 \geq \int_{-L}^{L} q_2 w dx_3,$$

and from the definition of w,

$$\int_{\tilde{I}} EI_1\Delta u_2^0\Delta u_2^0 dx_3 \geq \int_{\tilde{I}} q_2 u_2^0 dx_3.$$

Now, choosing $v_2^0 = v$ as test function in expression (10.42), we have that

$$\int_{-L}^{L} EI_1 \Delta u_2^0 \Delta(v - u_2^0) dx_3 \geq \int_{-L}^{L} q_2 (v - u_2^0) dx_3,$$

and taking into account the definition of v,

$$\int_{\tilde{I}} EI_1 \Delta u_2^0 \Delta u_2^0 dx_3 \leq \int_{\tilde{I}} q_2 u_2^0 dx_3.$$

Therefore, we deduce that

$$0 \leq \int_{\tilde{I}} EI_1 \Delta u_2^0 \Delta u_2^0 dx_3 = \int_{\tilde{I}} q_2 u_2^0 dx_3 \leq 0, \tag{10.47}$$

since q_2 is negative and u_2^0 positive. Relation (10.47) implies that $\Delta u_2^0 = 0$ in $\tilde{I}$ and as $u_2^0 = 0$ in $\partial\tilde{I}$, then $u_2^0 = 0$ on $\tilde{I}$ and we conclude the proof. □

Corollary 10.4.4. *The coincidence set I is either two isolated points or two closed intervals.*

10.4.1 Analytical solution. A new formula for MOR

It is easy to obtain an analytical solution of differential problem (10.45)-(10.46):

Proposition 10.4.5. *An analytical solution of differential problem (10.45)-(10.46) is given by:*

$$u_2^0(x_3) = \frac{1}{24EI_1} \begin{cases} -(\alpha h + \rho g \beta) x_3^4 + b_3 x_3^2 + d_3 \ \textit{in}\ (-\delta, \delta), \\ -\rho g \beta (x_3^4 - l^4) + b_2 (x_3^3 - l^3) + c_2 (x_3^2 - l^2) + d_2 (x_3 - l) \ \textit{in}\ [\delta, l), \\ -\rho g \beta (x_3^4 - l^4) + b_1 (x_3^3 - l^3) + c_1 (x_3^2 - l^2) + d_1 (x_3 - l) \ \textit{in}\ [l, L), \end{cases}$$

and by its even extension in $[-L, -\delta)$, where

$$\begin{aligned} &b_1 = 4\rho g \beta L, \quad b_2 = -4\alpha h \delta, \quad b_3 = 6\rho g \beta L(2l - L) - 6\alpha h \delta(\delta - 2l), \\ &c_1 = -6\rho g \beta L^2, \quad c_2 = 6\rho g \beta L(2l - L) + 12\alpha h \delta l, \\ &d_1 = 12\rho g \beta L l^2 - 4\alpha h \delta(\delta^2 - 3l^2), \quad d_2 = -4\alpha h \delta^3, \\ &d_3 = \rho g \beta l^2 \left(l^2 - 6L(2l - L)\right) - \alpha h \delta(8l^3 + \delta^3 - 4\delta^2 l). \end{aligned}$$

The Radon measure μ is given by:

$$\mu = (\alpha h \delta + \rho g \beta L)(\delta_{\{x_3 = -l\}} + \delta_{\{x_3 = l\}}), \tag{10.48}$$

and $I = \text{supp}(\mu) = \{-l, l\}$.

Moreover, the axial normal stress σ_{33}^0 on each transversal section of the beam is expressed by:

$$\sigma_{33}^0(\mathbf{x}) = \frac{x_2}{2I_1} \begin{cases} \rho g \beta (x_3^2 + L^2 - 2Ll) + \alpha h (x_3^2 + \delta^2 - 2\delta l), & \textit{if } x_3 \in (-\delta, \delta), \\ \rho g \beta (x_3^2 + L^2 - 2Ll) + 2\alpha h \delta (x_3 - l), & \textit{if } x_3 \in (\delta, l) \\ \rho g \beta (L - x_3)^2, & \textit{if } x_3 \in (l, L). \end{cases} \tag{10.49}$$

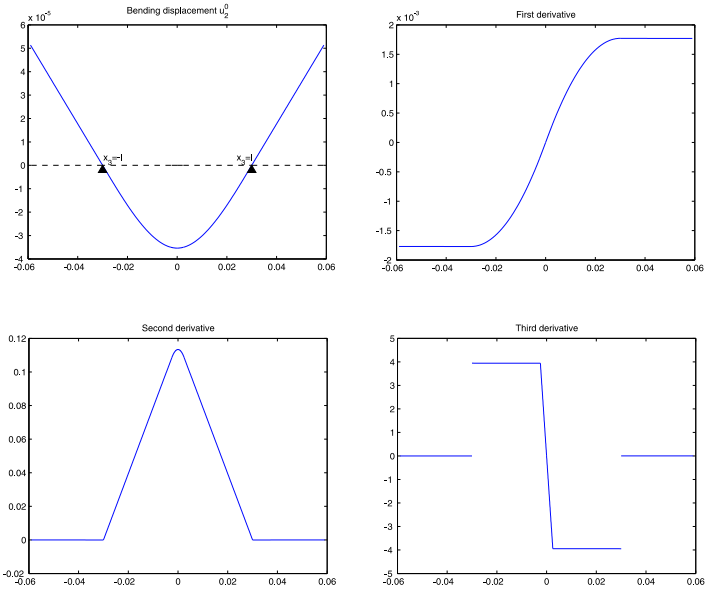

Figure 10.2: Analytical solution of Problem (10.45)-(10.46) and its derivatives.

Proof. It is easy to check that u_2^0 is a solution of equation (10.45) with μ given by expression (10.48). So, the proof is a straightforward consequence from Proposition 10.4.2. □

Figures 10.2 and 10.3 show a graphical representation of the analytical solution of Problem (10.45)-(10.46) for the experiment II with the following data:

$$2L = 0.118\text{m},\ 2a = 2b = 0.0085\text{m},\ 2l = 0.06\text{m},\ \delta = 0.0025\text{m},$$
$$E = 6.9975 \times 10^{10}\text{N/m}^2,\ \rho = 2340\text{kg/m}^3,\ h = 5649412\text{N/m}^2.$$

These values will be used both in the experiments in laboratory and in the numerical simulations. Notice that the second derivative of u_2^0 is still continuous while in the third derivative there exist two discontinuities in the support points, $\pm l$, which conform the coincidence set I.

Corollary 10.4.6. *i) If the following condition is satisfied:*

$$\rho g\beta l\left(3(L-l)^2 - 2l^2\right) - \alpha h\delta(3l^2 - \delta^2) < 0, \tag{10.50}$$

then, there exists $\hat{\delta}_0 > 0$ such that for all $\hat{\delta} < \hat{\delta}_0$ the analytical solution given in Proposition 10.4.5 is the unique solution of variational problem $(\mathbf{P_2^0})$.

ii) If condition (10.50) is satisfied and $\hat{\delta}$ verifies

$$\rho g\beta\left[(2l+\hat{\delta})((l+\hat{\delta})^2 + l^2 + 6L^2) - 4L((2l+\hat{\delta})(l+\hat{\delta}) + 4l^2)\right] - 4\alpha h\delta(3l^2 - \delta^2) < 0. \tag{10.51}$$

then, u_2^0 is the unique solution of variational problem $(\mathbf{P_2^0})$.

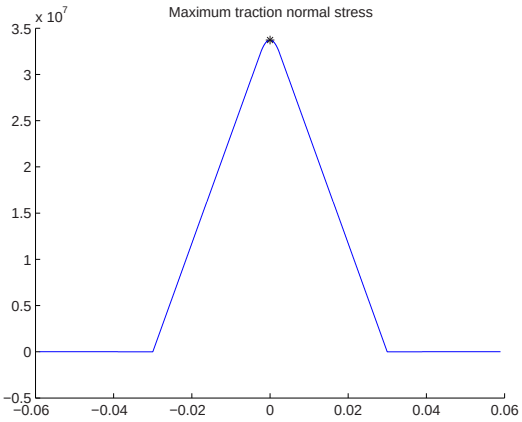

Figure 10.3: Axial normal stress obtained in the fiber $x_2 = -b$.

Proof. i) Condition (10.50) guarantees that $\partial_3 u_2^0(l) > 0$, so there exists $\hat{\delta}_1 > 0$ such that u_2^0 is increasing in $(l, l+\hat{\delta}_1)$. Moreover, since $u_2^0(l) = 0$, we deduce that u_2^0 is positive in the interval $(l, l+\hat{\delta})$, with $\hat{\delta} < \hat{\delta}_0 = \min(\hat{\delta}_1, L-l)$. A similar argument can be used at $x_3 = -l$. Therefore, u_2^0 is the solution of Problem $(\mathbf{P_2^0})$.

ii) Condition (10.51) guarantees that the solution is positive at $x_3 = l + \hat{\delta}$. Thanks to condition (10.50) and taking into account that u_2^0 is a concave function in the interval (l, L), we can state that u_2^0 is positive in the interval $(l, l+\hat{\delta})$.

□

From expression (10.49), we can deduce a new formula for the MOR. Recall that the MOR corresponds with the maximum surface stress of the bent beam at the instant of failure. As we will see, the maximum stress occurs in the opposite zone to the load application zone, which coincides with the results found in the classic literature.

Proposition 10.4.7. *If $2l > L$, then the maximum fiber normal stresses are achieved at $(0, \pm d, 0)$ and their values are:*

$$\sigma_{mt} = \frac{d}{2I_1}\left[\alpha h\delta\left(2l-\delta\right) - \rho g\beta L(L-2l)\right], \tag{10.52}$$

for the maximum in traction and

$$\sigma_{mc} = -\sigma_{mt},$$

for the maximum in compression, where d is the farthest distance in the x_2-direction from the axis of the beam.

Proof. Let us suppose that x_2 is fixed and let us define

$$f(x_3) = \sigma_{33}^0(x_2, x_3),$$

with σ_{33}^0 defined by (10.49). Then,

$$\frac{df}{dx_3}(x_3) = \frac{x_2}{I_1}\begin{cases} x_3(\rho g\beta + \alpha h), & \text{if } x_3 \in (-\delta, \delta), \\ \rho g\beta x_3 + \alpha h\delta, & \text{if } x_3 \in [\delta, l) \\ -\rho g\beta(L - x_3), & \text{if } x_3 \in (l, L], \end{cases}$$

In order to study the extrema of f we have to analyze its critical points $x_3 = 0$, $x_3 = \pm L$ and also the jump discontinuities of its derivative $x_3 = \pm l$. So, we can distinguish two situations:

i) If $x_2 < 0$, we have that $x_3 = 0$ is a local maximum that verifies:

$$f(0) > 0 = f(\pm L),$$

if $2l > L$. Furthermore, $f(\pm l) \leq 0$, so the maximum traction normal stress is achieved at $(0, -d, 0)$.

ii) Analogously if $x_2 > 0$, we have that $x_3 = 0$ is a local minimum that verifies:

$$f(0) < 0 = f(\pm L),$$

if $2l > L$. Furthermore, $f(\pm l) \geq 0$, so the maximum compression normal stress is achieved at $(0, d, 0)$.

□

Corollary 10.4.8. *The MOR for the experiment I is given by*

$$\sigma_{ft}^0 = \frac{H}{\pi R^3}(2l - \delta) - \frac{F}{\pi R^3}(L - 2l). \tag{10.53}$$

where F and H are the modulus of the total gravity forces and the load of failure, respectively. Analogously, the MOR for the experiment II is given by

$$\sigma_{ft}^0 = \frac{3H}{16ab^2}(2l - \delta) - \frac{3F}{16ab^2}(L - 2l). \tag{10.54}$$

Proof. From expression (10.52) and taking into account that

$$I_1 = \frac{\pi R^4}{4},\ I_1 = \frac{4}{3}ab^3,$$

for experiments I and II, respectively, we have that

$$\sigma_{mt} = \frac{2}{\pi R^3}\left[\alpha h\delta\,(2l - \delta) - \rho g\beta L(L - 2l)\right] \text{ for experiment I,}$$
$$\sigma_{mt} = \frac{3}{8ab^2}\left[\alpha h\delta\,(2l - \delta) - \rho g\beta L(L - 2l)\right] \text{ for experiment II.}$$

Then, since the total gravity forces and the load of failure are given by

$$F = 2L\rho g\beta,\ H = 2\delta\alpha h,$$

we conclude the proof. □

Notice that if the total gravity forces, F, can be neglected and the upper cylinder exerts really a punctual force, that is $\delta = 0$, expressions (10.53) and (10.54) are in line with classic formulas (10.1) and (10.2).

Chapter 11

Computing the MOR

In this chapter we are going to show the results from numerical simulations of experiments I and II described in Section 10.3. These experiments have been carried out in collaboration with the Institute of Ceramics of the Universidade de Santiago de Compostela.

In this section, the methodology to compute the MOR is as follows:

- Firstly, we have carried out various laboratory tests on porcelain beams in order to determine the experimental force of rupture, $\mathbf{H}$.
- Secondly, we calculate a theoretical value for the modulus of rupture, σ_{ft}, by using the classic formulas of the MOR (10.1) and (10.2).
- Thirdly, considering the experimental force of rupture, $\mathbf{H}$, we compute numerically the corresponding three-dimensional stresses and so, we compute its 3d numerical MOR, σ_{fn}.
- Fourthly, we compute numerically the displacements and stresses by using the one-dimensional model and, therefore, we compute its 1d numerical MOR, σ^0_{fn}.
- Finally, we also compute a new value for the MOR, the 1d analytical MOR, denoted by σ^0_{ft}, by using expressions (10.53) and (10.54) obtained in Section 10.4.

These all experiences are repeated for different sizes of samples and for different distances between the two lower cylinders.

In order to carrying out the three-dimensional numerical simulations that we present below we use the finite element software package MSC.MARC[1], that let us make simulations in solids mechanics when there exist contact conditions with a foundation or a deformable body. We show below figures corresponding to the computed stresses and displacements, and tables with computed values for the MOR, by using hexahedrical meshes with a characteristic size of $e = 0.0025\,\mathrm{m}$. Besides, for the one-dimensional numerical simulation, a MATLAB code has been developed which uses a generalized Newton technique to deal with the nonlinearity due to the contact conditions (see [7]).

[1]MSC.MARC is a registered trademark of MSC.Software Corporation.

In our experiments, the beams are made of porcelain, a brittle material which breaks suddenly, when the response is still substantially elastic and linear. In material databases, the characteristic parameters of porcelain range between the following values:

$$\begin{aligned} E &= 6.82 \times 10^{10} - 7.175 \times 10^{10}\,\mathrm{N/m^2}, \\ \nu &= 0.17 - 0.18, \\ \rho &= 2260 - 2420\,\mathrm{kg/m^3}. \end{aligned}$$

The characteristic parameters of porcelain we use in the numerical simulations are the following:

$$E = 6.9975 \times 10^{10}\,\mathrm{N/m^2}, \nu = 0.175,\ \rho = 2340\,\mathrm{kg/m^3}.$$

11.1 Numerical results for Experiment I

As we have said above, in experiment I we use cylindrical beams of radius $R = 0.009\,\mathrm{m}$ and we consider two lengths:

$$2L_1 = 0.125\,\mathrm{m},\ 2L_2 = 0.18\,\mathrm{m}.$$

For each fixed length, three different distances between the two lower cylinders are considered:

$$2l_1 = 0.06\,\mathrm{m},\ 2l_2 = 0.1\,\mathrm{m},\ 2l_3 = 0.15\,\mathrm{m}.$$

The parameters δ and $\hat{\delta}$ are taken as 0.0025.

Table 11.1 shows the modulus of the maximum surface stress of the bent beams at the instant of failure. These values were obtained by making several laboratory tests, and taking the arithmetic mean of the corresponding rupture loads. Notice that the experimental rupture load varies substantially with the dimensions of the beam, depending on the relation between the total length and the distance between the two lower cylinders.

Table 11.1: Experimental load of failure for cylindrical beams.

$2L$ / $2l$	$2l_1 = 0.06\,\mathrm{m}$	$2l_2 = 0.1\,\mathrm{m}$	$2l_3 = 0.15\,\mathrm{m}$
$2L_1 = 0.125\,\mathrm{m}$	$H = 2054\,\mathrm{N}$	$H = 1312\,\mathrm{N}$	-
$2L_1 = 0.18\,\mathrm{m}$	$H = 2007.5\,\mathrm{N}$	$H = 1394\,\mathrm{N}$	$H = 845\,\mathrm{N}$

With the values for the rupture loads of Table 11.1 and by using the classic formula (10.1), we obtain theoretical values for the MOR, denoted by σ_{ft}, which are different with each sample (see Table 11.2).

Next, we are going to compute the MOR by means of three-dimensional numerical simulations and by using again the values of the experimental rupture loads, we solve the problem numerically. Figure 11.1 shows the vertical displacement and the x_3x_3 component of the stress tensor for a particular sample. Notice that the greatest deflection appears in the center of the beam, while the smallest displacements occur in the contact boundary. Moreover, it is also important to notice

Table 11.2: Theoretical MOR for cylindrical beams.

	$2l_1 = 0.06\,\mathrm{m}$		$2l_2 = 0.1\,\mathrm{m}$		$2l_3 = 0.15\,\mathrm{m}$	
	$H\,(\mathrm{N})$	$\sigma_{ft}\,(\mathrm{N/m^2})$	$H\,(\mathrm{N})$	$\sigma_{ft}\,(\mathrm{N/m^2})$	$H\,(\mathrm{N})$	$\sigma_{ft}\,(\mathrm{N/m^2})$
$2L_1 = 0.125\,\mathrm{m}$	2054	5.38×10^7	1312	5.73×10^7	-	-
$2L_2 = 0.18\,\mathrm{m}$	2007.5	5.26×10^7	1394	6.09×10^7	845	5.53×10^7

that the behaviour of the beam is almost constant at each cross section. We can also observe that the greatest value of the stresses in compression is reached in the force application zone, while the greatest value in bending appears in the opposite zone, in which the beam collapses. Table 11.3 shows the maximum value of the x_3x_3 component of the stresses at this zone for each sample. This value is denoted in the following by σ_{fn}, the 3d numerical value for the MOR.

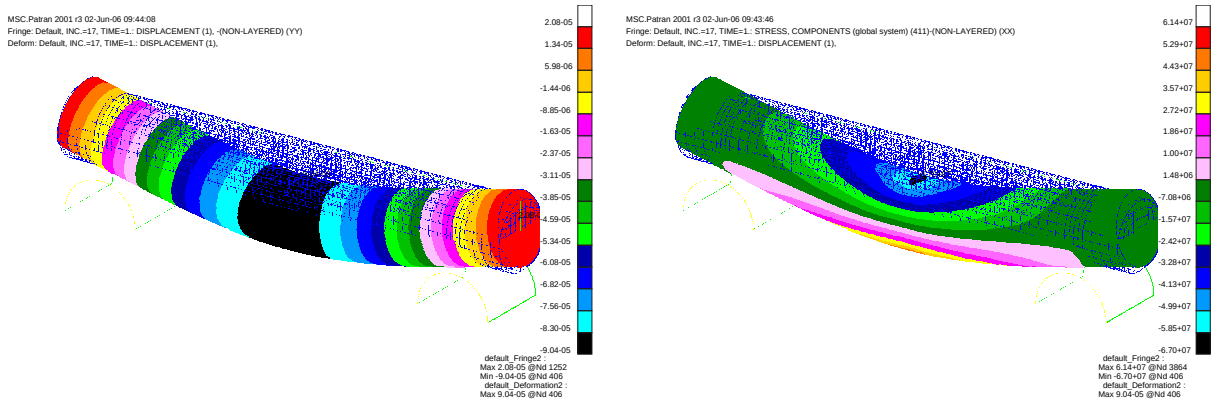

Figure 11.1: Vertical displacement and x_3x_3 component of stresses for a cylindrical beam with $2L_1 = 0.125$m and $2l_2 = 0.1$m.

Table 11.3: 3d numerical MOR for cylindrical beams

	$2l_1 = 0.06\,\mathrm{m}$		$2l_2 = 0.1\,\mathrm{m}$		$2l_3 = 0.15\,\mathrm{m}$	
	$H\,(\mathrm{N})$	$\sigma_{fn}\,(\mathrm{N/m^2})$	$H\,(\mathrm{N})$	$\sigma_{fn}\,(\mathrm{N/m^2})$	$H\,(\mathrm{N})$	$\sigma_{fn}\,(\mathrm{N/m^2})$
$2L_1 = 0.125\,\mathrm{m}$	2054	4.76×10^7	1312	5.32×10^7	-	-
$2L_2 = 0.18\,\mathrm{m}$	2007.5	4.66×10^7	1394	5.65×10^7	845	5.25×10^7

By using the one-dimensional bending problem (10.42) we carry out a new numerical simulation of the three-point bending test, obtaining in this way a 1d numerical approach for the MOR, denoted by σ^0_{fn}. This new value for the MOR has a great importance to compute the MOR for brittle materials, because the three-dimensional simulations can be inaccurate when the ratio between the area of the cross-section and the length of the beam is very small.

In Figures 11.2 and 11.3, the bending displacement u_2 and the axial normal stress σ_{33} for a

porcelain beam obtained from the one and three-dimensional numerical simulations are shown as well as the 1d analytical solution obtained in Section 10.4.1. In these figures, the plots on the right represent a zoom of the axial normal stress in order to better appreciate the behaviour in the loading area; moreover, the theoretical MOR and the 3d and 1d numerical MOR are also depicted. These values are computed in the maximum deflection line, that is, in $x_2 = -R$.

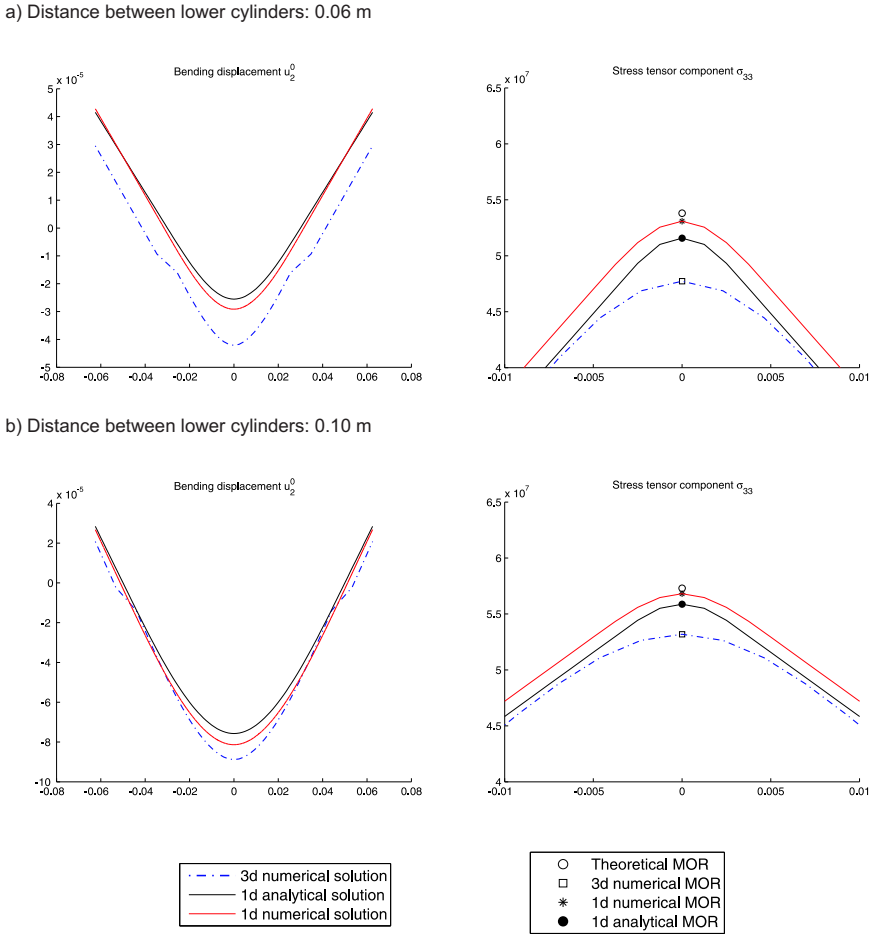

Figure 11.2: Bending displacement and axial normal stress for a cylindrical beam with $2L_1 = 0.125$m.

Notice that when comparing Figures 11.2.b) and 11.3.b) for the same distance between the two lower cylinders, the smaller the ratio between the area of the cross-section and the length of the beam is, the better the 1d numerical MOR approaches the theoretical MOR. Furthermore, we can observe that the 1d numerical MOR comes closer to the theoretical MOR when the distance between the two lower cylinders becomes larger, while the approach is worse when the two lower cylinders are nearer.

Finally, the last approach for the MOR is obtained by using the new expression (10.53) arising from the analytical solution we have calculated from the asymptotic analysis of the problem, called the 1d analytical MOR and denoted by σ_{ft}^0 (this value is also shown in Figures 11.2 and 11.3).

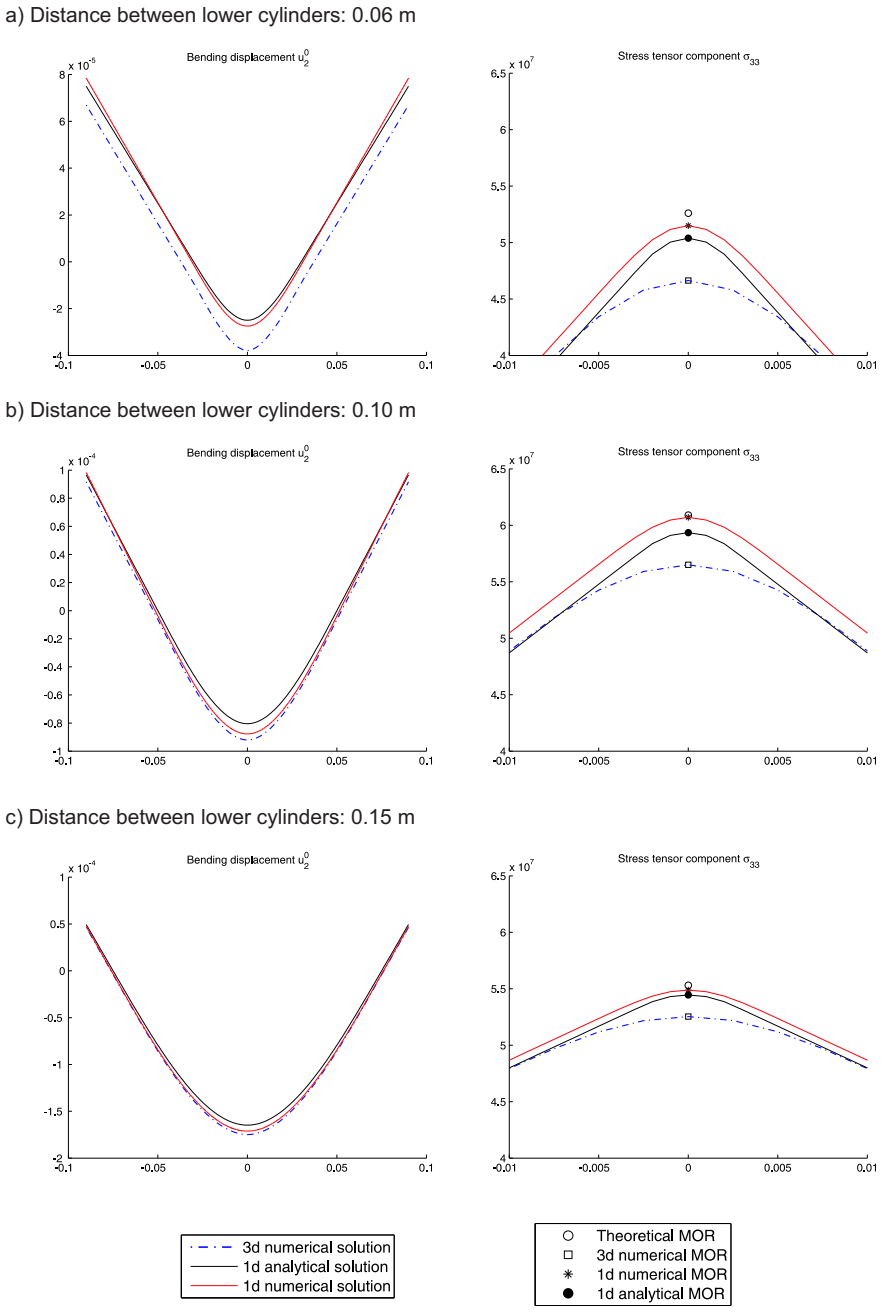

Figure 11.3: Bending displacement and axial normal stress for a cylindrical beam with $2L_1 = 0.18$m.

Tables 11.4 and 11.5 gather the different values obtained for the MOR of a cylindrical beam of porcelain. Notice that, the differences decrease when the two lower cylinders are close to the ends of the beam; so, the theoretical expression (10.1) gives a good approach when the beam is supported at its ends.

Table 11.4: Theoretical and numerical MOR for a cylindrical beam of length $2L_1 = 0.125\,\mathrm{m}$.

	σ_{ft} (Pa)	σ_{fn} (Pa)	σ^0_{fn} (Pa)	σ^0_{ft} (Pa)
$2l_1 = 0.06\,\mathrm{m}$	5.38×10^7	4.77×10^7	5.31×10^7	5.16×10^7
$2l_1 = 0.1\,\mathrm{m}$	5.73×10^7	5.32×10^7	5.68×10^7	5.59×10^7

Table 11.5: Theoretical and numerical MOR for a cylindrical beam of length $2L_2 = 0.18\,\mathrm{m}$.

	σ_{ft} (Pa)	σ_{fn} (Pa)	σ^0_{fn} (Pa)	σ^0_{ft} (Pa)
$2l_1 = 0.06\,\mathrm{m}$	5.26×10^7	4.66×10^7	5.15×10^7	5.04×10^7
$2l_1 = 0.1\,\mathrm{m}$	6.09×10^7	5.65×10^7	6.07×10^7	5.94×10^7
$2l_1 = 0.15\,\mathrm{m}$	5.53×10^7	5.25×10^7	5.49×10^7	5.45×10^7

11.2 Numerical results for Experiment II

In experiment II, we use beams of square section, of height and width $2a = 2b = 0.0085\,\mathrm{m}$ and of length $2L = 0.118\,\mathrm{m}$. The distances between the two lower cylinders considered are $2l_1 = 0.06\,\mathrm{m}$ or $2l_2 = 0.1\,\mathrm{m}$. Again, the parameters δ and $\hat{\delta}$ have the same value, that is, 0.0025.

Table 11.6 shows the modulus of the experimental load at the instant of failure and the corresponding theoretical MOR, σ_{ft}, obtained from the classic formula (10.2).

Table 11.6: Experimental load of failure and theoretical MOR for beams of square section.

	$2l_1 = 0.06\,\mathrm{m}$		$2l_2 = 0.1\,\mathrm{m}$	
	H	σ_{ft}	H	σ_{ft}
$2L_1 = 0.118\,\mathrm{m}$	$240.1\,\mathrm{N}$	$3.52 \times 10^7 \mathrm{N/m^2}$	$156.8\,\mathrm{N}$	$3.83 \times 10^7 \mathrm{N/m^2}$

Following the same procedure as in the cylindrical case, firstly, we carried out the three-dimensional numerical simulations corresponding to the experimental rupture loads obtained in laboratory. Figure 11.4 shows the vertical displacement and the x_3x_3 component of the stress tensor for a particular sample. In column 3 in Table 11.7 we show the 3d numerical MOR of porcelain, σ_{fn}.

Again, by using the one-dimensional bending problem (10.42) we carry out a new numerical simulation of the three-point bending test, to obtain the 1d numerical MOR, σ^0_{fn} (see Column 4 in Table 11.7).

In Figure 11.5 the bending displacement, u_2, and the axial normal stress, σ_{33}, for a porcelain beam, obtained from the one and three-dimensional numerical simulations are shown as well as the 1d analytical solution obtained in Section 10.4.1. As we have done above, the plots on the

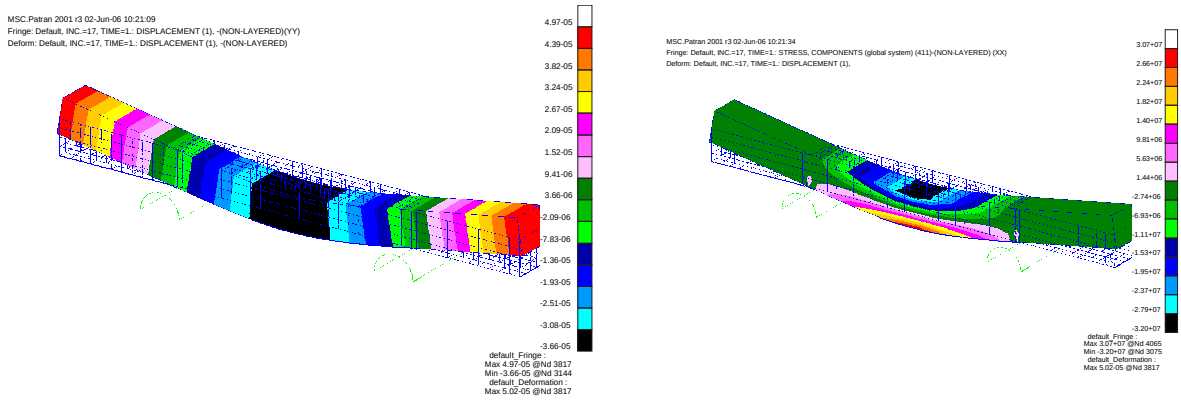

Figure 11.4: Vertical displacement and x_3x_3 component of stresses for a beam of square section with $2L = 0.118$m and $2l = 0.06$m.

right represent a zoom of the axial normal stress to better appreciate the behaviour in the loading area. Moreover, the theoretical and the 1d and 3d numerical MOR are depicted. These values are computed in the maximum deflection line, that is, in $x_2 = -b$.

Finally, the 1d analytical MOR, σ^0_{ft}, is obtained by using the expression (10.54) arising from the asymptotic analysis of the problem (this value is also shown in Figure 11.5). Table 11.7 gathers the different values obtained for the MOR of a porcelain beam of square section. Notice that, as in the experiment I, the differences are smaller when the two lower cylinders are close to the ends of the beam, showing that the theoretical expression (10.2) gives a good approach when the beam is supported at its ends.

Table 11.7: Theoretical and numerical MOR for a beam of square section of length $2L = 0.118\,\mathrm{m}$.

	σ_{ft} (Pa)	σ_{fn} (Pa)	σ^0_{fn} (Pa)	σ^0_{ft} (Pa)
$2l_1 = 0.06\,\mathrm{m}$	3.52×10^7	3.27×10^7	3.45×10^7	3.37×10^7
$2l_1 = 0.1\,\mathrm{m}$	3.83×10^7	3.63×10^7	3.75×10^7	3.74×10^7

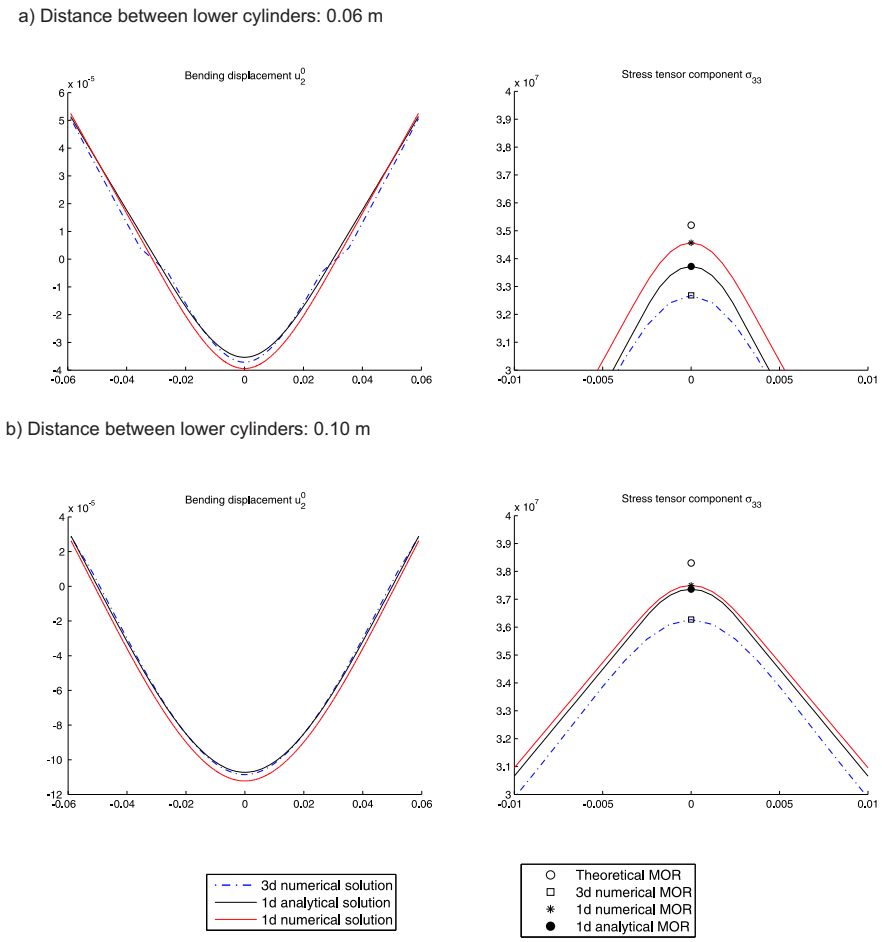

Figure 11.5: Bending displacement and axial normal stress for a beam of square section with $2L_1 = 0.118$m.

Chapter 12

Conclusions

In Part II of this manuscript we have carried out a complete mathematical study for the three-point bending test and a complete analysis of the MOR for brittle materials, comparing four different methodologies to obtain an approach of its value.

Firstly, under suitable assumptions of compatibility on the applied forces and on the geometry of the beam, we have proved the existence of a unique solution for the three-dimensional elastic model with contact constraints associated to the three-point bending test. These hypotheses are necessary to guarantee the existence of a unique solution of the problem due to the absence of Dirichlet conditions.

Moreover, we have studied the asymptotic behaviour of the beam if the area of its cross-section goes to zero. Using the asymptotic expansion method, we have obtained the one-dimensional models associated both with the bending problem and that of axial traction as well as the corresponding results of existence and uniqueness of solution. In particular, we have obtained the axial normal stresses associated to the MOR; its expression is given in terms of the derivatives of the vertical and axial displacements. The variational formulation corresponding to the limit problem of bending involves an inequality due to the contact condition between the beam and the two lower cylinders. Furthermore, the admissible test functions for the axial and bending problems are even and odd, respectively, which is a consequence of the assumptions needed to obtain the existence of a unique solution for the three-dimensional problem of departure. Finally, we have obtained the differential formulations of the problems associated with the one-dimensional models and we have presented a characterization of the zone of effective contact.

Secondly, in order to carry out a complete analysis of the MOR for brittle materials, we have proved that the assumptions of compatibility on the forces are satisfied for laboratory three-point bending tests with cylindrical and square beams. Moreover, thanks to the one-dimensional problems obtained using the asymptotic expansion method, we have deduced a new expression for the MOR, which involves not only the rupture load and the distance between the two lower cylinders but also the gravitational effects and the distance between the supports and the ends of the beam.

In order to find an effective method to compute the MOR of brittle materials, we have carried

out a comparison between four methodologies applied to cylindrical and square beams: Firstly, we have experimentally measured the rupture load at the instant of failure at laboratory. By using the classical formulas (10.1) and (10.2), we have computed the corresponding theoretical MOR. Secondly, from the numerical simulations we have obtained the 3d and 1d numerical MOR. Finally, by using the new expressions obtained in this work by means of the one-dimensional analytical solution, we have computed a new 1d analytical MOR. After comparing all the values obtained, we conclude that formulas (10.53) and (10.54) give a better approach of the MOR for brittle materials than the classical ones. Moreover, we want to remark that the MOR for brittle materials is a mechanical property strongly sensitive to variations in the dimensions of the beam; due to this, we have found that there exist great differences between the values for the MOR obtained in this work and the range of values found in databases in which the dimensions or the geometries of the samples are not indicated.

Appendix A

Appendix: Modulus of rupture

This appendix offers a basic explanation of the expression for the MOR of a material obtained by using habitual procedures in solid mechanics. In addition, using physical hypotheses, we will deduce the classical formula for the MOR. A more detailed description of this can be found in [15, 44, 74].

In engineering science, three-point bending tests are generally used to determine the MOR of materials: The value corresponding to the maximum surface stress that the beam supports until breaking. Compressive stresses are generated on the upper surface while bending stresses occur on the lower surface. The fracture generally starts on the lower surface, and the maximum bending stress is produced on the region opposite to the loading area, where the upper cylinder applies surface forces.

The classical formula for the MOR we consider in this article is obtained from the stresses generated in a beam subjected to pure bending, that is, when the bending moment is constant. A clear example of pure bending is a beam subjected to two pairs M of the same direction and magnitude but acting on opposite directions at the ends of the beam. This configuration produces a constant bending moment M over the entire length of the beam. A three-point bending test, however, is an example of non uniform bending: the bending moment varies along the length of the beam. Despite this difference between bending moments, the classic mechanical bibliography, based on Saint Venant's principle, considers that the experimental results obtained for pure bending can also be used for non uniform bending.

In pure bending, the following bending stress formula is obtained (see [15]):

$$\sigma_{33} = -\frac{M x_2}{I_1}, \tag{A.1}$$

which shows that stresses are directly proportional to the bending moment M and to the coordinate x_2, and inversely proportional to the second moment of inertia, I_1, of the transversal section of the beam. The maximum bending or compression stresses are produced at points placed at the farthest distance from the axis of the beam denoted by d_1 and d_2, above and below the beam,

respectively. The corresponding maximum stresses are

$$\sigma_{33_1} = -\frac{Md_1}{I_1}, \quad \sigma_{33_2} = \frac{Md_2}{I_1}.$$

The second expression is the classical formula for the MOR when the bending moment is constant.

In three-point bending tests there exists non uniform bending moment, that is, M is not constant. Therefore, in order to give the classical expression for the MOR when a beam is subjected to this test, we must determine the maximum bending moment, M_{max}. Consequently, the MOR would be given by the expression

$$\sigma_f = \frac{M_{max}d_2}{I_1}, \tag{A.2}$$

where $d_2 > 0$ denotes the distance from the axis of the beam to its boundary in the negative direction x_2.

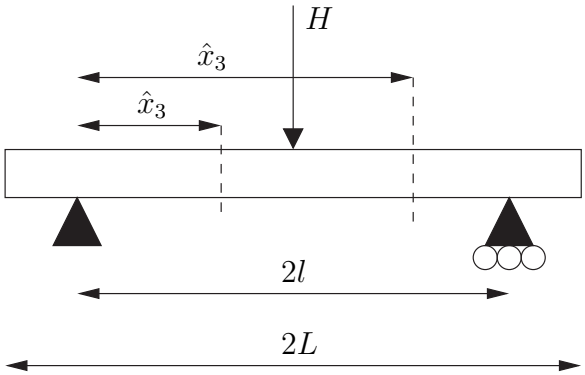

Figure A.1: Simply supported beam subjected to a concentrated force H.

To compute M_{max}, we consider a beam of length $2L$, that is simply supported at points placed at a distance $2l$ and is subjected to a concentrated load H in its center (see Figure A.1). If we consider this beam like a free body, we can determine easily the reactions in the beam from the moment equilibrium equation, that is:

$$R_{-l} = R_l = \frac{H}{2}.$$

We cut the beam in a section to the left of the load H and at a distance $\hat{x}_3$ from the support in $x_3 = -l$. From the equilibrium equation for this free body, we obtain that the bending moment at a distance $\hat{x}_3$ from the left support is

$$M = R_{-l}\hat{x}_3 = \frac{H\hat{x}_3}{2}, \quad 0 < \hat{x}_3 < l.$$

Analogously, if we cut the beam in a section to the right of the load H and at a distance $\hat{x}_3$ from the support in $x_3 = -l$, we obtain that the bending moment is

$$M = R_{-l}\hat{x}_3 - H(\hat{x}_3 - l) = \frac{H\hat{x}_3}{2} - H(\frac{\hat{x}_3}{2} - l) = \frac{H}{2}(2l - \hat{x}_3), \quad l < \hat{x}_3 < 2l.$$

Therefore, the bending moment for a simply supported beam in a point placed at a distance $\hat{x}_3$ from the left support is

$$M = \begin{cases} \frac{H\hat{x}_3}{2}, & 0 < \hat{x}_3 < l, \\ \frac{H}{2}(2l - \hat{x}_3), & l < \hat{x}_3 < 2l. \end{cases}$$

The maximum bending moment is

$$M_{max} = \frac{Hl}{2}, \tag{A.3}$$

and is produced under the concentrated load H in $\hat{x}_3 = l$.

Substituting (A.3) in (A.2), we obtain that the classical expression for the MOR of a material is

$$\sigma_f = \frac{M_{max} d_2}{I_1} = \frac{Hld_2}{2I_1}.$$

Part III

An elasticity problem for catalyst supports: Unfolding method

Table of Contents

Chapter 13

Introduction

A catalytic converter in an automobile's exhaust system provides an environment for a chemical reaction where unburned hydrocarbons completely combust, in such a way that the pollution is reduced. An enormous effort is being made with the purpose of developing appropriate supports and the catalyst itself. In some cases the correct support is what makes all the difference to the viability of a process. A catalyst support should allow the catalyst to be highly dispersed on the surface of the support. The support needs to be stable under the reaction conditions and it must not be affected by the reactants or products.

The objective of Part III of this manuscript is to model the catalyst process which occurs in an automobile's exhaust system. Due to the great difficulty of the problem, the first step is to study the asymptotic behaviour of the supports in a linear elasticity problem. The catalyst support we consider in this work is a structure made of rods with thickness $e\varepsilon$ and inner holes of size $e\varepsilon\delta$ (see Figure 13.1).

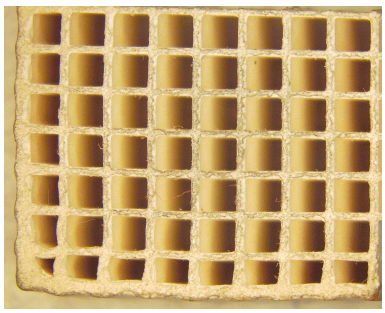

Figure 13.1: Cross-section of a catalyst support.

A new procedure, called the unfolding method, developed by Cioranescu, Damlamian and Griso (see [30]), is applied to solve this first approach. This method is a generalization of the notion of two-scale convergence introduced by G. Nguetseng [62] and further developed by G. Allaire [1]. The method is based onthe unfolding operator $\mathcal{T}_\varepsilon^{\mathbf{h}}$, similar to the dilation operator. If Ω is a bounded open set and Y a reference cell in $\mathbb{R}^n$, the operator $\mathcal{T}_\varepsilon^{\mathbf{h}}$ associates to any function $v \in L^p(\Omega)$, a function $\mathcal{T}_\varepsilon^{\mathbf{h}}(v) \in L^p(\Omega \times Y)$. An immediate property of $\mathcal{T}_\varepsilon^{\mathbf{h}}$ is that it enables to

transform any integral over Ω in an integral over $\Omega \times Y$. Moreover, $\mathcal{T}_\varepsilon^{\mathbf{h}}$ allows to show that the two-scale convergence in the $L^p(\Omega)$-sense of a sequence of functions v_ε is equivalent to the weak convergence of the sequence of unfolded functions $\mathcal{T}_\varepsilon^{\mathbf{h}} v_\varepsilon$ in $L^p(\Omega \times Y)$.

One of the most important results of the unfolding method is the following: For any weakly convergent sequence w^ε in $H^1(\Omega)$, one can extract a subsequence (still denoted ε) such that

$$
\begin{aligned}
&w^\varepsilon \rightharpoonup w \text{ weakly in } H^1(\Omega),\\
&\mathcal{T}_\varepsilon^{\mathbf{h}}(w^\varepsilon) \rightharpoonup w \text{ weakly in } L^2(\Omega; H^1(Y)),\\
&\mathcal{T}_\varepsilon^{\mathbf{h}}(\nabla w^\varepsilon) \rightharpoonup \nabla w + \nabla_Y \hat{w} \text{ weakly in } L^2(\Omega; H^1(Y))^n,
\end{aligned}
$$

where $\hat{w}$ belongs to $L^2(\Omega; H^1_{per}(\mathbf{Y}))$.

Besides, a new approach of linear elasticity problems in thin domains (such as rods or plates) is obtained by means of the unfolding method. The method consists of decomposing a displacement in a cross-section displacement (an elementary displacement) and a warping associated to the cross-section deformation. An elementary displacement is a displacement of the middle-line of the beam and a small rotation of the cross-section. This new technique has been introduced in [47] to study curved rods. The same methodology has been developed to study plates and structures made of plates (see [48, 49]) and to study problems with junctions rods-plates (see [22, 23]). The results presented in this part of the manuscript are published in [50].

The outline of Part III is as follows:

In Chapter 14 we introduce the computational domain and the notation we will use in the sequel. Moreover, the three-dimensional elasticity problem for structures used as a catalyst support is formulated. These structures are made of a periodic family of elastic rods with thickness $e\varepsilon$ and inner holes of size $e\varepsilon\delta$.

In Chapter 15 we present some tools used when applying the unfolding method. We define the elementary displacements associated to a beam and we give some estimates for this kind of displacement. Firstly, we introduce the unfolding operator related to the elasticity parameter e, obtaining some weak convergences. Secondly, we define the unfolding operator related to the periodicity parameter ε and we study the limit of a bounded sequence of displacements in a structure when the elasticity and periodicity parameters, e and ε, go to zero.

In Chapter 16, under suitable hypotheses on the applied forces, we give the limit problem of the three-dimensional elasticity problem when e, ε go to zero, obtaining three uncoupled problems: The first problem defines the longitudinal displacement and the second one gives the transversal bending of the structure, while the third one defines the torsion angle.

Part III of this manuscript is the result of the research stays of the author in the Laboratoire Jacques-Louis Lions in the University Pierre et Mary Curie (Paris VI), France, funded by the Spanish Ministry of Education and Science (Spain) by means of the FPU program.

Chapter 14

Position of the elasticity problem

In this chapter we present the elasticity problem associated to catalyst supports. These supports are structures made of beams, placed periodically and with inner holes. We consider a static problem for an elastic structure fixed on a part of the boundary and subjected only to volume forces.

In Section 14.1 we introduce the notation we will use in the sequel and in Section 14.2 the linear elasticity problem for structures used as catalyst supports together with its variational formulation is formulated.

14.1 Computational domain and notations

Let introduce some notations we will use later on. We denote

$$\omega = \left(-\frac{1}{2}, \frac{1}{2}\right)^2,$$
$$\omega_l = \left(-\frac{l}{2}, \frac{l}{2}\right)^2, \, l > 0.$$

From now on, $\omega = \omega_1$.

Let denote the unit cells

$$\mathbf{Y} = (0,1)^2,$$
$$\mathbf{Y}^* = \mathbf{Y} \backslash [\delta, 1-\delta]^2,$$

with $\delta > 0$ a fixed parameter (see Figure 14.1).

Let e, ε be real positive numbers such that $e = M\varepsilon$, with $M \in \mathbb{N}^*$. We consider $L > 0$ fixed such that $L = (2N+1)e\varepsilon$, with $N \in \mathbb{N}^*$. Notice that the ratio height of the beam over $e\varepsilon$ is an odd number in order to simplify the calculations but the procedure can be extended to the general case.

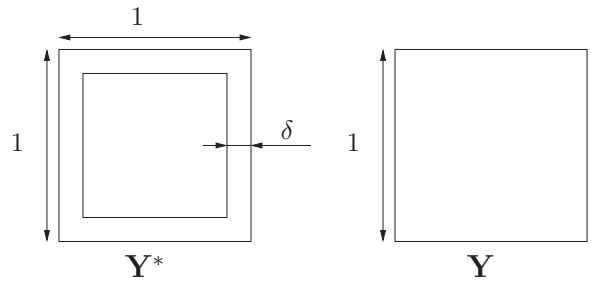

Figure 14.1: Unit cells $\mathbf{Y}^*$ and $\mathbf{Y}$.

We denote the periodic union of cells

$$\Xi_\varepsilon = \{\xi \in \mathbb{Z}^2; \varepsilon\xi + \varepsilon\mathbf{Y} \subset \omega\}.$$

Let consider $\Omega_e = \omega_e \times (0, L)$ a three-dimensional domain with cross-section ω_e. We denote the perforated cross-section (see Figure 14.2)

$$\omega^*_{e,\varepsilon} = \bigcup_{\xi \in \Xi_\varepsilon} e\varepsilon(\xi + \mathbf{Y}^*),$$

and the structure we are interested in is $\Omega^*_{e,\varepsilon} = \omega^*_{e,\varepsilon} \times (0, L)$. Again,

$$\Omega = \Omega_1 = \omega \times (0, L),$$
$$\omega^*_\varepsilon = \omega^*_{1,\varepsilon} = \bigcup_{\xi \in \Xi_\varepsilon} \varepsilon(\xi + \mathbf{Y}^*).$$

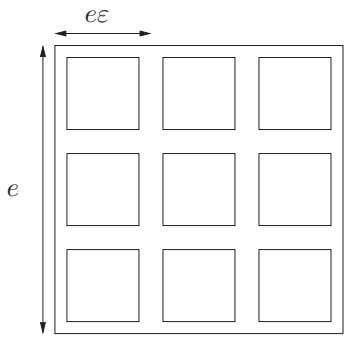

Figure 14.2: Domain $\omega^*_{e,\varepsilon}$.

Furthermore, structures $\Omega^*_{e,\varepsilon}$ and Ω_e can be expressed as the union of the following domains, respectively (see Figure 14.3):

$$\Theta^*_{e,\varepsilon} = e\varepsilon\mathbf{Y}^* \times (0, L),$$
$$\Theta_{e,\varepsilon} = e\varepsilon\mathbf{Y} \times (0, L).$$

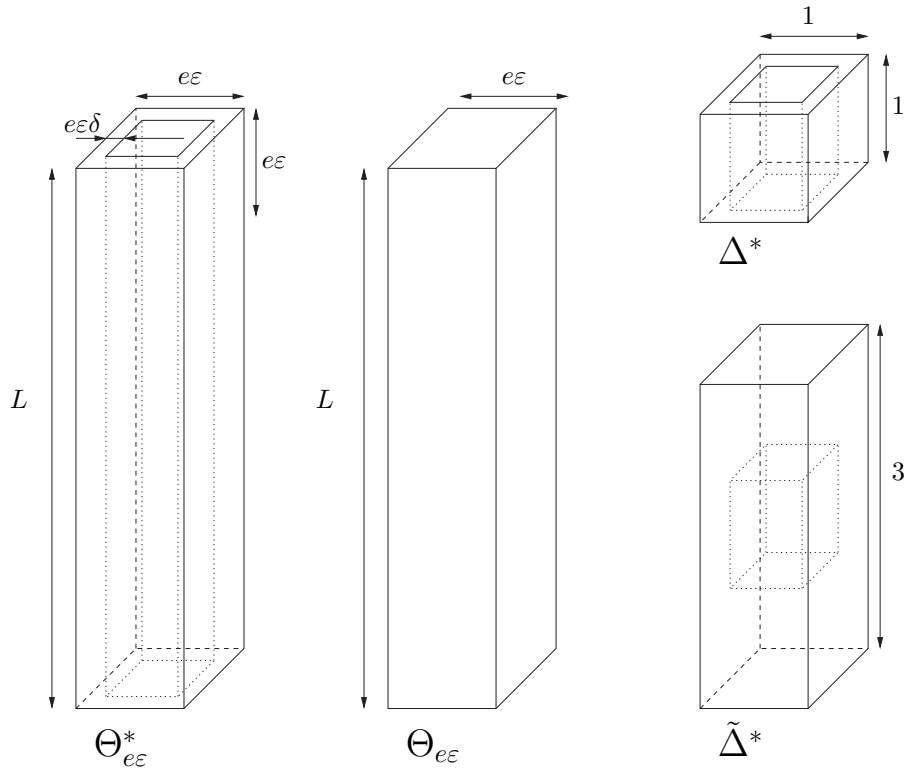

Figure 14.3: Domains $\Theta^*_{e,\varepsilon}$, $\Theta_{e,\varepsilon}$, Δ^* and $\tilde{\Delta}^*$.

Finally, let introduce other notations of three-dimensional cells used in this paper:

$$\Delta^* = \mathbf{Y}^* \times (0,1),\ \Delta = \mathbf{Y} \times (0,1), \tag{14.1}$$

$$\tilde{\Delta}^* = \{\mathbf{Y} \times (0,1)\} \cup \{\mathbf{Y}^* \times [1,2]\} \cup \{\mathbf{Y} \times (2,3)\},\ \tilde{\Delta} = \mathbf{Y} \times (0,3). \tag{14.2}$$

Hereafter, Latin subscripts are understood to range over the integers $\{1,2,3\}$ and Greek subscripts over the integers $\{1,2\}$. Moreover, summation over repeated subscripts is implied. Finally, for any open subset $\mathcal{O} \subset \mathbb{R}^3$, and any displacement $\mathbf{v} \in H^1(\mathcal{O};\mathbb{R}^3)$, we denote

$$\mathcal{E}(\mathbf{v},\mathcal{O}) = \int_{\mathcal{O}} \gamma_{ij}(\mathbf{v})\gamma_{ij}(\mathbf{v})dx,\ ,$$
$$\mathcal{D}(\mathbf{v},\mathcal{O}) = \int_{\mathcal{O}} \frac{\partial v_i}{\partial x_j}\frac{\partial v_i}{\partial x_j}dx,$$

where $\boldsymbol{\gamma}(\mathbf{v})$ is the tensor given by

$$\gamma_{ij}(\mathbf{v}) = \frac{1}{2}\left(\frac{\partial v_i}{\partial x_j} + \frac{\partial v_j}{\partial x_i}\right).$$

14.2 Elasticity problem

The physical problem we want to solve consists of determining the displacement vector field $\mathbf{u}^{e\varepsilon}$ and the stress tensor field $\boldsymbol{\sigma}^{e\varepsilon}$ that the structure $\Omega^*_{e,\varepsilon}$ suffers when it is submitted to the action of volume forces.

Let $\Gamma^*_{e,\varepsilon} = \partial\Omega^*_{e,\varepsilon}$ be the boundary of $\Omega^*_{e,\varepsilon}$ and $\Gamma^*_D = \omega^*_{e,\varepsilon} \times \{0\}$ the bottom surface. We assume that the structure is fixed on Γ^*_D and the remaining boundary $\Gamma^*_N = \Gamma^*_{e,\varepsilon} \backslash \Gamma^*_D$ is free of forces.

Under small deformations assumption, the behaviour of the structure is governed by the usual equilibrium equation

$$-\mathrm{div}\boldsymbol{\sigma}^{e\varepsilon} = \mathbf{f}^{e\varepsilon} \text{ in } \Omega^*_{e,\varepsilon},$$

where $\mathbf{f}^{e\varepsilon}$ denotes the volume forces acting on the structure.

We assume that $\Omega^*_{e,\varepsilon}$ is made of an isotropic and homogeneous material. So, the infinitesimal strain field $\boldsymbol{\gamma}(\mathbf{u})$ is related to the stress tensor $\boldsymbol{\sigma}$ trough Hooke's law (see [28])

$$\boldsymbol{\sigma}^{e\varepsilon} = \boldsymbol{\Lambda}\boldsymbol{\gamma}(\mathbf{u}).$$

In the above expression, $\boldsymbol{\Lambda}$ is the fourth order linear elasticity tensor defined by

$$\boldsymbol{\Lambda}\boldsymbol{\tau} = \lambda \mathrm{tr}(\boldsymbol{\tau})\mathbf{I} + 2\mu\boldsymbol{\tau},$$

where λ and μ are the Lamé parameters of the material, $\lambda, \mu > 0$.

Summing up, the problem we must solve is the following:

Problem $(P^{e\varepsilon})$:

Find the displacement vector field $\mathbf{u}^{e\varepsilon}(\mathbf{x})$ and the stress tensor field $\boldsymbol{\sigma}^{e\varepsilon}(\mathbf{x})$, at each point $\mathbf{x} \in \Omega^*_{e,\varepsilon}$, satisfying:

$$\begin{aligned} -\mathrm{div}(\boldsymbol{\sigma}^{e\varepsilon}) &= \mathbf{f}^{e\varepsilon} \text{ in } \Omega^*_{e,\varepsilon}, \\ \boldsymbol{\sigma}^{e\varepsilon}\mathbf{n} &= \mathbf{0} \text{ on } \Gamma^*_N, \\ \mathbf{u}^{e\varepsilon} &= \mathbf{0} \text{ on } \Gamma^*_D, \\ \boldsymbol{\sigma}^{e\varepsilon} = \lambda \mathrm{tr}(\boldsymbol{\gamma}(\mathbf{u}^{e\varepsilon}))\mathbf{I} + 2\mu\boldsymbol{\gamma}(\mathbf{u}^{e\varepsilon}) &\text{ in } \Omega^*_{e,\varepsilon}. \end{aligned}$$

Moreover, the associated variational problem is the following:

Problem $(VP^{e\varepsilon})$:

Find $\mathbf{u}^{e\varepsilon} \in H^1_{\Gamma_D}(\Omega^*_{e,\varepsilon}; \mathbb{R}^3)$ such that

$$\int_{\Omega^*_{e,\varepsilon}} \boldsymbol{\Lambda}\boldsymbol{\gamma}(\mathbf{u}^{e\varepsilon}) : \boldsymbol{\gamma}(\mathbf{v}) dx = \int_{\Omega^*_{e,\varepsilon}} \mathbf{f}^{e\varepsilon} \cdot \mathbf{v} dx, \quad \forall \mathbf{v} \in H^1_{\Gamma_D}(\Omega^*_{e,\varepsilon}; \mathbb{R}^3),$$

where

$$H^1_{\Gamma_D}(\Omega^*_{e,\varepsilon}; \mathbb{R}^3) = \{\mathbf{v} \in H^1(\Omega^*_{e,\varepsilon}; \mathbb{R}^3) : \mathbf{v} = \mathbf{0} \text{ on } \Gamma^*_D\}.$$

Our objective is to study the asymptotic behaviour of a sequence of displacement fields $\mathbf{u}^{e\varepsilon} \in H^1(\Omega^*_{e,\varepsilon}; \mathbb{R}^3)$, solutions of Problem $(VP^{e\varepsilon})$, when thickness parameter e and periodicity parameter ε go to zero. To do so, we use the unfolding methods in elasticity and periodic homogenization. The volume forces will be described in Section 16.1.

Chapter 15

Tools of the unfolding method

In this chapter we introduce some tools used in the application of the unfolding method. Firstly, we extend the computational domain to the whole structure without considering the inner holes. To do this, we use some classical results. Secondly, we define the two unfolding operators we are going to use and we obtain some estimates.

The outline of this chapter is as follows: In Section 15.1 we recall some classical results and we obtain some extension operators. In Section 15.2 we define the elementary displacements associated to a beam and we give some estimates for this kind of displacement. In Section 15.3 we introduce the unfolding operator $\mathcal{T}_e^{\mathbf{e}}$ related to the elasticity parameter e and we obtain some weak convergences. Finally, in Section 15.4 we define the unfolding operator $\mathcal{T}_\varepsilon^{\mathbf{h}}$ related to the periodicity parameter ε and we study the limit of a bounded sequence of displacements in a structure when the elasticity and periodicity parameters go to zero.

15.1 Extension of a displacement field

We recall some classical results:

- Let $\mathcal{O} \subset \mathbb{R}^3$ be an open bounded subset with Lipschitz-continuous boundary. Then, there exists a linear and bounded extension operator $\mathcal{P}$ from $H^1(\mathcal{O})$ to $H^1(\mathbb{R}^3)$ such that

$$\|\mathcal{P}(v)\|_{H^1(\mathbb{R}^3)} \leq C\|v\|_{H^1(\mathcal{O})}, \forall v \in H^1(\mathcal{O}),$$

  where $C > 0$ (see [44]).

- For each $\mathbf{u} \in H^1(\mathcal{O}, \mathbb{R}^3)$, there exists a rigid displacement $\mathbf{r}$ such that

$$\|\mathbf{u} - \mathbf{r}\|^2_{H^1(\mathcal{O};\mathbb{R}^3)} \leq C\mathcal{E}(\mathbf{u}, \mathcal{O}),\ C > 0.$$

We have two consequences from these results:

Remark 15.1.1. *There exists an extension operator from $H^1(\Delta^*;\mathbb{R}^3)$ to $H^1(\Delta;\mathbb{R}^3)$ such that for all $\mathbf{u}\in H^1(\Delta^*;\mathbb{R}^3)$, its extended displacement $\tilde{\mathbf{u}}$ to Δ verifies*

$$\tilde{\mathbf{u}}\in H^1(\Delta;\mathbb{R}^3),$$
$$\mathcal{E}(\tilde{\mathbf{u}},\Delta)\leq C\mathcal{E}(\mathbf{u},\Delta^*),\ C>0.$$

Remark 15.1.2. *There exists an extension operator from $H^1(\tilde{\Delta}^*;\mathbb{R}^3)$ to $H^1(\tilde{\Delta};\mathbb{R}^3)$ such that for all $\mathbf{u}\in H^1(\tilde{\Delta}^*;\mathbb{R}^3)$, its extended displacement $\tilde{\mathbf{u}}$ to $\tilde{\Delta}$ verifies*

$$\tilde{\mathbf{u}}\in H^1(\tilde{\Delta};\mathbb{R}^3),$$
$$\mathcal{E}(\tilde{\mathbf{u}},\tilde{\Delta})\leq C\mathcal{E}(\mathbf{u},\tilde{\Delta}^*),\ C>0.$$

By using the above remarks, we are going to obtain an extension operator from $H^1(\Omega^*_{e,\varepsilon};\mathbb{R}^3)$ to $H^1(\Omega_e;\mathbb{R}^3)$. To do so, we will use an intermediate result. We recall that Δ, Δ^* and $\tilde{\Delta}^*$ are defined by expressions (14.1) and (14.2).

Lemma 15.1.3. *There exists an extension operator from $H^1(\Theta^*_{e,\varepsilon};\mathbb{R}^3)$ to $H^1(\Theta_{e,\varepsilon};\mathbb{R}^3)$ such that for each displacement $\mathbf{u}\in H^1(\Theta^*_{e,\varepsilon};\mathbb{R}^3)$, its extended displacement, still denoted by $\mathbf{u}$, belongs to $H^1(\Theta_{e,\varepsilon};\mathbb{R}^3)$ and verifies*

$$\mathcal{E}(\mathbf{u},\Theta_{e,\varepsilon})\leq C\mathcal{E}(\mathbf{u},\Theta^*_{e,\varepsilon}),$$

where $C>0$ independent of e and ε.

Proof. Let $\mathbf{u}\in H^1(\Theta^*_{e\varepsilon};\mathbb{R}^3)$ be an arbitrary displacement and we define $\mathbf{v}_p\in H^1(\Delta^*;\mathbb{R}^3)$ as follows (by using a homotecy):

$$\mathbf{v}_p(y_1,y_2,y_3)=\mathbf{u}(e\varepsilon y_1,e\varepsilon y_2,e\varepsilon p+e\varepsilon y_3),$$
$$(y_1,y_2,y_3)\in\Delta^*,\ p\in\{0,2,\dots,2N\}.$$

From Remark 15.1.1, the extended displacement $\tilde{\mathbf{v}}_p$ of $\mathbf{v}_p$ to Δ verifies

$$\mathcal{E}(\tilde{\mathbf{v}}_p,\Delta)\leq C\mathcal{E}(\mathbf{v}_p,\Delta^*).$$

Then, by inverse homotecy, $\mathbf{u}$ is extended to $e\varepsilon\mathbf{Y}\times\,]e\varepsilon p,e\varepsilon(p+1)[$, with $p\in\{0,2,\dots,2N\}$ (still denoted by $\mathbf{u}$) and

$$\mathcal{E}\left(\mathbf{u},e\varepsilon\mathbf{Y}\times\,]e\varepsilon p,e\varepsilon(p+1)[\right)\leq C\mathcal{E}\left(\mathbf{u},e\varepsilon\mathbf{Y}^*\times\,]e\varepsilon p,e\varepsilon(p+1)[\right),$$

with $C>0$ independent of e and ε.

Analogously, we define $\tilde{\mathbf{v}}_p\in H^1(\tilde{\Delta}^*;\mathbb{R}^3)$ as follows (by using a homotecy):

$$\tilde{\mathbf{v}}_p(y_1,y_2,y_3)=\mathbf{u}(e\varepsilon y_1,e\varepsilon y_2,e\varepsilon p+e\varepsilon y_3),$$
$$(y_1,y_2,y_3)\in\tilde{\Delta}^*,\ p\in\{0,2,\dots,2N\}.$$

Thanks to Remark 15.1.2 and by inverse homotecy, $\mathbf{u}$ is extended to $e\varepsilon\mathbf{Y}\times(e\varepsilon p,e\varepsilon(p+3))$, with $p\in\{0,2,\dots,2N-2\}$ (still denoted by $\mathbf{u}$) and

$$\mathcal{E}\left(\mathbf{u},e\varepsilon\mathbf{Y}\times\,]e\varepsilon p,e\varepsilon(p+3)[\right)\leq C\mathcal{E}\left(\mathbf{u},(0,0,e\varepsilon)+e\varepsilon\tilde{\Delta}^*\right),$$

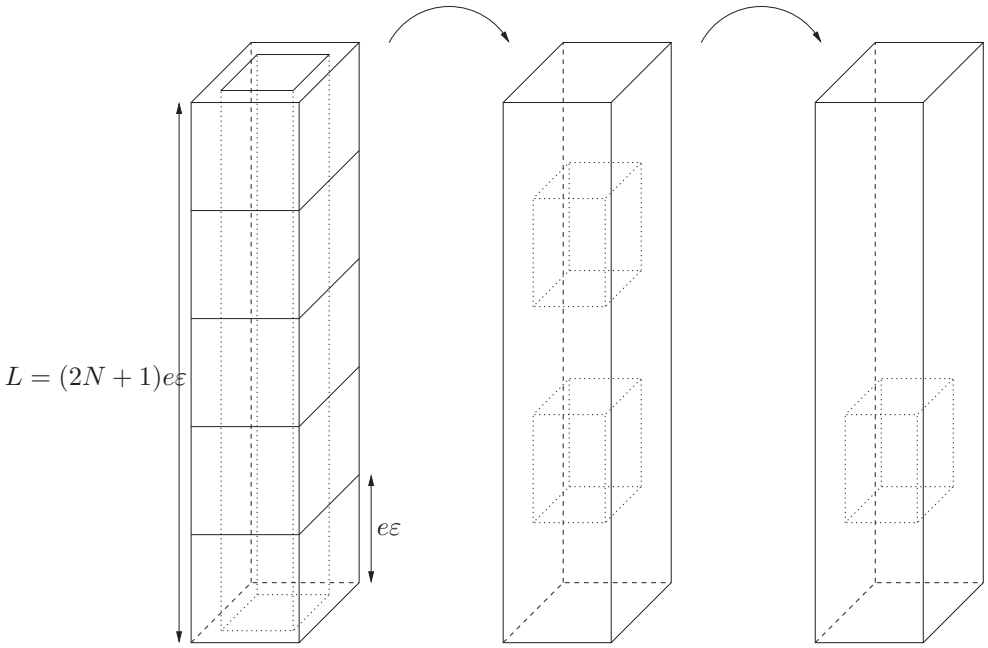

Figure 15.1: Extending displacement fields.

with $C > 0$ independent of e and ε.

Since $\Theta^*_{e,\varepsilon}$ is a union of an odd number of domains $e\varepsilon\Delta^*$ and combining the previous results we have finished the proof (see Figure 15.1). □

Theorem 15.1.4. *There exists an extension operator from $H^1(\Omega^*_{e,\varepsilon};\mathbb{R}^3)$ to $H^1(\Omega_e;\mathbb{R}^3)$ such that for each displacement $\mathbf{u} \in H^1(\Omega^*_{e,\varepsilon};\mathbb{R}^3)$, its extended displacement (still denoted by $\mathbf{u}$) belongs to $H^1(\Omega_e;\mathbb{R}^3)$ and verifies*

$$\mathcal{E}(\mathbf{u},\Omega_e) \leq C\mathcal{E}(\mathbf{u},\Omega^*_{e,\varepsilon}), \tag{15.1}$$

with $C > 0$ independent of e and ε.

Proof. The result is obtained by applying Lemma 15.1.3 on $(e\varepsilon\xi + e\varepsilon\mathbf{Y}^*) \times (0, L)$, $\xi \in \Xi_\varepsilon$. □

Remark 15.1.5. *If $\mathbf{u} \in H^1(\Omega^*_{e,\varepsilon};\mathbb{R}^3)$ is null on $\omega^*_{e,\varepsilon} \times \{0\}$, then we can choose its extended displacement $\mathbf{u} \in H^1(\Omega_e;\mathbb{R}^3)$ also null on $\omega_e \times \{0\}$ and verifying (15.1).*

Now, it will be easier to obtain estimates and convergences by using the extension operator.

15.2 Elementary displacements in a beam

As we have mentioned at the beginning, in a catalyst support, under the action of any displacement $\mathbf{u}$, the structure is submitted to a translation and a rotation, called elementary displacement, and to a displacement which deforms the cross-sections, called residual displacement or warping (see

[47]). *A priori* estimates are obtained by using some results due to Griso (see [47]), which are based on the method used by Kondratiev and Oleinik [54] and by Cioranescu *et al.* [31] to establish Korn inequalities for frame-type structures and junctions. Once *a priori* estimates are established, we study the convergence of displacements and strains of the structure when thickness parameter e goes to zero.

We recall here the definition given in [47].

Definition 15.2.1. *An elementary displacement in the beam Ω_e is defined in the form*

$$\mathbf{U}_e(x_1, x_2, x_3) = \mathcal{U}(x_3) + \mathcal{R}(x_3) \wedge (x_1\mathbf{e_1} + x_2\mathbf{e_2}),$$

where $\mathcal{U}, \mathcal{R} \in L^1(0, L; \mathbb{R}^3)$.

Definition 15.2.2. *Each $\mathbf{u} \in L^1(\Omega_e; \mathbb{R}^3)$ is written in the form $\mathbf{u} = \mathbf{U}_e + \bar{\mathbf{u}}$,*

$$\begin{aligned} u_1(x_1, x_2, x_3) &= \mathcal{U}_1(x_3) - x_2\mathcal{R}_3(x_3) + \overline{u}_1(x_1, x_2, x_3), \\ u_2(x_1, x_2, x_3) &= \mathcal{U}_2(x_3) + x_1\mathcal{R}_3(x_3) + \overline{u}_2(x_1, x_2, x_3), \\ u_3(x_1, x_2, x_3) &= \mathcal{U}_3(x_3) - x_1\mathcal{R}_2(x_3) + x_2\mathcal{R}_1(x_3) + \overline{u}_3(x_1, x_2, x_3), \end{aligned} \tag{15.2}$$

where $\mathbf{U}_e$ is an elementary displacement and $\bar{\mathbf{u}} \in H^1(\Omega_e; \mathbb{R}^3)$ verifies

$$\begin{aligned} &\int_{\omega_e} \bar{u}_i dx_1 dx_2 = 0, \\ &\int_{\omega_e} x_\alpha \bar{u}_3 dx_1 dx_2 = 0, \\ &\int_{\omega_e} (x_1\bar{u}_2 - x_2\bar{u}_1) dx_1 dx_2 = 0. \end{aligned}$$

Remark 15.2.3. *For each $\mathbf{u} \in L^1(\Omega_e; \mathbb{R}^3)$, its elementary displacement $\mathbf{U}_e$ is given by*

$$\begin{aligned} \mathcal{U}_i(x_3) &= \frac{1}{e^2} \int_{\omega_e} u_i(x_1, x_2, x_3) dx_1 dx_2, \\ \mathcal{R}_1(x_3) &= \frac{1}{e^4 I_2} \int_{\omega_e} x_2 \mathbf{u}_3(x_1, x_2, x_3) dx_1 dx_2, \\ \mathcal{R}_2(x_3) &= -\frac{1}{e^4 I_1} \int_{\omega_e} x_1 \mathbf{u}_3(x_1, x_2, x_3) dx_1 dx_2, \\ \mathcal{R}_3(x_3) &= \frac{1}{e^4(I_1 + I_2)} \int_{\omega_e} (x_1 \mathbf{u}_2(x_1, x_2, x_3) - x_2 \mathbf{u}_1(x_1, x_2, x_3)) dx_1 dx_2, \end{aligned}$$

where

$$I_\alpha = \int_\omega X_\alpha^2 dX_1 dX_2.$$

The following result gives us some estimates of displacements in $H^1(\Omega_e)$ related with its elementary displacement:

Theorem 15.2.4. *For each displacement* $\mathbf{u} \in H^1(\Omega_e;\mathbb{R}^3)$*, we have* $\bar{\mathbf{u}} \in H^1(\Omega_e;\mathbb{R}^3)$*,* $\mathcal{U},\mathcal{R} \in H^1(0,L;\mathbb{R}^3)$ *verifying the following estimates:*

$$\mathcal{D}(\bar{\mathbf{u}},\Omega_e) \leq C\mathcal{E}(\mathbf{u},\Omega_e), \tag{15.3}$$

$$\|\bar{\mathbf{u}}\|^2_{L^2(\Omega_e;\mathbb{R}^3)} \leq Ce^2\mathcal{E}(\mathbf{u},\Omega_e), \tag{15.4}$$

$$e^2\|\frac{d\mathcal{R}}{dx_3}\|^2_{L^2(0,L;\mathbb{R}^3)} + \|\frac{d\mathcal{U}}{dx_3} - \mathcal{R}\wedge\mathbf{e}_3\|^2_{L^2(0,L;\mathbb{R}^3)} \leq \frac{C}{e^2}\mathcal{E}(\mathbf{u},\Omega_e). \tag{15.5}$$

If the structure is fixed at the bottom $\omega_e\times\{0\}$*, we have* $\mathcal{U}(\mathbf{0}) = \mathcal{R}(\mathbf{0}) = \mathbf{0}$ *and moreover,*

$$\|\mathcal{R}\|^2_{H^1(0,L;\mathbb{R}^3)} \leq \frac{C}{e^4}\mathcal{E}(\mathbf{u},\Omega_e), \tag{15.6}$$

$$\|\mathcal{U}_\alpha\|^2_{H^1(0,L)} \leq \frac{C}{e^4}\mathcal{E}(\mathbf{u},\Omega_e), \tag{15.7}$$

$$\|\mathcal{U}_3\|^2_{H^1(0,L)} \leq \frac{C}{e^2}\mathcal{E}(\mathbf{u},\Omega_e). \tag{15.8}$$

Constants C *are independent of* e*.*

Proof. The proof is given in [47]. □

Corollary 15.2.5. *For each displacement* $\mathbf{u}\in H^1(\Omega_e;\mathbb{R}^3)$*,*

$$\|u_3\|^2_{L^2(\Omega_e)} + e^2\|\mathbf{u}_\alpha\|^2_{L^2(\Omega_e)} + e^2\mathcal{D}(\mathbf{u},\Omega_e) \leq C\mathcal{E}(\mathbf{u},\Omega_e).$$

Proof. Let $\mathbf{u}\in H^1(\Omega_e;\mathbb{R}^3)$ be arbitrary. Thanks to expression (15.2), we have that

$$\|u_3\|_{L^2(\Omega_e)} \leq e\|\mathcal{U}_3\|_{L^2(0,L)} + e^2\|\mathcal{R}_2\|_{L^2(0,L)} + e^2\|\mathcal{R}_1\|_{L^2(0,L)} + \|\bar{u}_3\|_{L^2(\Omega_e)},$$

and by using estimates (15.4), (15.6) and (15.8), we obtain that

$$\|u_3\|^2_{L^2(\Omega_e)} \leq C\mathcal{E}(\mathbf{u},\Omega_e).$$

The remaining estimates are obtained analogously. □

15.3 The unfolding operator $\mathcal{T}_e^{\mathbf{e}}$

We are going to define the unfolding operator we will use in the following results:

Definition 15.3.1. *The unfolding operator* $\mathcal{T}_e^{\mathbf{e}}$ *from* $L^2(\Omega_e)$ *to* $L^2(\Omega)$ *is defined by*

$$\mathcal{T}_e^{\mathbf{e}}(w)(X_1,X_2,x_3) = w(eX_1,eX_2,x_3),$$
$$w\in L^2(\Omega_e),\ (X_1,X_2,x_3)\in\Omega.$$

Proposition 15.3.2. *The unfolding operator $\mathcal{T}_e^{\mathbf{e}}$ verifies the following properties for all $w \in H^1(\Omega_e)$:*

$$
\begin{aligned}
&i)\ \frac{\partial \mathcal{T}_e^{\mathbf{e}}(w)}{\partial X_\alpha} = e\mathcal{T}_e^{\mathbf{e}}\left(\frac{\partial w}{\partial x_\alpha}\right),\\
&ii)\ \frac{\partial \mathcal{T}_e^{\mathbf{e}}(w)}{\partial x_3} = \mathcal{T}_e^{\mathbf{e}}\left(\frac{\partial w}{\partial x_3}\right),\\
&iii)\ \|\mathcal{T}_e^{\mathbf{e}}(w)\|_{L^2(\Omega)} = \frac{1}{e}\|w\|_{L^2(\Omega_e)},\\
&iv)\ \int_{\Omega_e} w dx = e^2 \int_{\Omega} \mathcal{T}_e^{\mathbf{e}}(w) dX_1 dX_2 dx_3.
\end{aligned}
$$

Definition 15.3.3. *For each displacement $\mathbf{u} \in H^1(\Omega_e;\mathbb{R}^3)$, we define the formal warping displacement $\overline{\mathbf{U}} \in L^2(0,L;H^1(\omega;\mathbb{R}^3))$*

$$
\overline{U}_\alpha = \frac{1}{e}\mathcal{T}_e^{\mathbf{e}}(\overline{u}_\alpha), \quad \overline{U}_3 = \frac{1}{e}\mathcal{T}_e^{\mathbf{e}}(\overline{u}_3) + X_1\left(\frac{d\mathcal{U}_1}{dx_3} - \mathcal{R}_2\right) + X_2\left(\frac{d\mathcal{U}_2}{dx_3} + \mathcal{R}_1\right). \tag{15.9}
$$

Proposition 15.3.4. *The formal warping displacement $\overline{\mathbf{U}}$ verifies the estimates*

$$
\|\overline{\mathbf{U}}\|^2_{L^2(0,L;H^1(\omega;\mathbb{R}^3))} \leq C\frac{\mathcal{E}(\mathbf{u},\Omega_e)}{e^2}, \tag{15.10}
$$

$$
\left\|\frac{\partial \overline{U}_\alpha}{\partial x_3}\right\|^2_{L^2(\Omega)} \leq C\frac{\mathcal{E}(\mathbf{u},\Omega_e)}{e^4}, \tag{15.11}
$$

with $C > 0$ independent of e.

Proof. These estimates are a direct consequence of estimates (15.3)-(15.8) by taking into account properties of Proposition 15.3.2. □

Let consider

$$
H^1_D(\Omega_e;\mathbb{R}^3) = \{\mathbf{v} \in H^1(\Omega_e;\mathbb{R}^3); \mathbf{v} = \mathbf{0} \text{ on } \omega_e \times \{0\}\}.
$$

Theorem 15.3.5. *Let $\{\mathbf{u}^e\}_{e\geq 0}$ be a sequence in $H^1_D(\Omega_e;\mathbb{R}^3)$ such that*

$$
\mathcal{E}(\mathbf{u}^e,\Omega_e) \leq Ce^2. \tag{15.12}
$$

Then the following convergences (up to a subsequence) are obtained:

$$
e\,\mathcal{U}^e_\alpha \rightharpoonup \mathcal{U}_\alpha \quad \textit{weakly in } H^1(0,L), \tag{15.13}
$$

$$
\mathcal{U}^e_3 \rightharpoonup \mathcal{U}_3 \quad \textit{weakly in } H^1(0,L), \tag{15.14}
$$

$$
e\,\mathcal{R}^e \rightharpoonup \mathcal{R} \quad \textit{weakly in } H^1(0,L;\mathbb{R}^3), \tag{15.15}
$$

$$
\overline{\mathbf{U}}^e \rightharpoonup \overline{\mathbf{U}} \quad \textit{weakly in } L^2(0,L;H^1(\omega;\mathbb{R}^3)), \tag{15.16}
$$

where $\mathcal{U}_\alpha \in H^2(0,L)$, $\mathcal{U}_3 \in H^1(0,L)$, $\mathcal{R} \in H^1(0,L;\mathbb{R}^3)$ and

$$
\frac{d\mathcal{U}_1}{dx_3} = \mathcal{R}_2,\ \frac{d\mathcal{U}_2}{dx_3} = -\mathcal{R}_1,
$$

$$
\mathcal{U}_\alpha(0) = \frac{d\mathcal{U}_\alpha}{dx_3}(0) = 0,\ \mathcal{U}_3(0) = 0,\ \mathcal{R}_i(0) = 0.
$$

The formal warping displacement $\overline{\mathbf{U}} \in L^2(0,L;H^1(\omega;\mathbb{R}^3))$ *verifies*

$$\int_\omega \overline{U}_i dX_1 dX_2 = \int_\omega (X_1\overline{U}_2 - X_2\overline{U}_1) dX_1 dX_2 = 0. \tag{15.17}$$

Moreover, the following convergences of the unfolded strain tensor (up to a subsequence) are hold:

$$\mathcal{T}_e^{\mathbf{e}}(\gamma_{\alpha\alpha}(\mathbf{u}^e)) \rightharpoonup \frac{\partial \overline{U}_\alpha}{\partial X_\alpha}, \tag{15.18}$$

$$\mathcal{T}_e^{\mathbf{e}}(\gamma_{12}(\mathbf{u}^e)) \rightharpoonup \frac{1}{2}\left(\frac{\partial \overline{U}_1}{\partial X_2} + \frac{\partial \overline{U}_2}{\partial X_1}\right), \tag{15.19}$$

$$\mathcal{T}_e^{\mathbf{e}}(\gamma_{33}(\mathbf{u}^e)) \rightharpoonup \frac{d\mathcal{U}_3}{dx_3} - X_1\frac{d^2\mathcal{U}_1}{dx_3^2} - X_2\frac{d^2\mathcal{U}_2}{dx_3^2}, \tag{15.20}$$

$$\mathcal{T}_e^{\mathbf{e}}(\gamma_{13}(\mathbf{u}^e)) \rightharpoonup \frac{1}{2}\left(-X_2\frac{d\mathcal{R}_3}{dx_3} + \frac{\partial \overline{U}_3}{\partial X_1}\right), \tag{15.21}$$

$$\mathcal{T}_e^{\mathbf{e}}(\gamma_{23}(\mathbf{u}^e)) \rightharpoonup \frac{1}{2}\left(X_1\frac{d\mathcal{R}_3}{dx_3} + \frac{\partial \overline{U}_3}{\partial X_2}\right), \tag{15.22}$$

weakly in $L^2(\Omega)$.

Proof. For each $\mathbf{u}^e \in H^1(\Omega_e;\mathbb{R}^3)$ we have that

$$\begin{aligned}
u_1^e(x_1,x_2,x_3) &= \mathcal{U}_1^e(x_3) - x_2\mathcal{R}_3^e(x_3) + \overline{u}_1^e(x_1,x_2,x_3),\\
u_2^e(x_1,x_2,x_3) &= \mathcal{U}_2^e(x_3) + x_1\mathcal{R}_3^e(x_3) + \overline{u}_2^e(x_1,x_2,x_3),\\
u_3^e(x_1,x_2,x_3) &= \mathcal{U}_3^e(x_3) - x_1\mathcal{R}_2^e(x_3) + x_2\mathcal{R}_1^e(x_3) + \overline{u}_3^e(x_1,x_2,x_3).
\end{aligned}$$

From estimates (15.6)-(15.8) we obtain weak convergences (15.13)-(15.15) on $\mathcal{U}^e$ and $\mathcal{R}^e$. From (15.5) and (15.12) we have that

$$\left|\left|\frac{d\mathcal{U}_1^{e\varepsilon}}{dx_3} - \mathcal{R}_2^{e\varepsilon}\right|\right|_{L^2(0,L)} + \left|\left|\frac{d\mathcal{U}_2^{e\varepsilon}}{dx_3} + \mathcal{R}_1^{e\varepsilon}\right|\right|_{L^2(0,L)} \leq C,$$

and then, from (15.13)-(15.15), we obtain that

$$\frac{d\mathcal{U}_1}{dx_3} = \mathcal{R}_2, \quad \frac{d\mathcal{U}_2}{dx_3} = -\mathcal{R}_1.$$

Thanks to estimate (15.10), we conclude weak convergence (15.16) on $\overline{\mathbf{U}}^e$. Moreover, from Definition 15.2.2, expression (15.9) and property *iv*) of Proposition 15.3.2, we prove that $\overline{\mathbf{U}}$ verifies (15.17).

By doing some easy calculations, we obtain that

$$\begin{aligned}
\gamma_{\alpha\beta}(\mathbf{u}^e) &= \gamma_{\alpha\beta}(\overline{\mathbf{u}}^e),\\
\gamma_{33}(\mathbf{u}^e) &= \frac{d\mathcal{U}_3^e}{dx_3} - x_1\frac{d\mathcal{R}_2^e}{dx_3} + x_2\frac{d\mathcal{R}_1^e}{dx_3} + \frac{\partial \overline{\mathbf{u}}_3^e}{\partial x_3},\\
\gamma_{13}(\mathbf{u}^e) &= \frac{1}{2}\left[\left(\frac{d\mathcal{U}_1^e}{dx_3} - \mathcal{R}_2^e\right) - x_2\frac{d\mathcal{R}_3^e}{dx_3} + \frac{\partial \overline{u}_1^e}{\partial x_3} + \frac{\partial \overline{u}_3^e}{\partial x_1}\right],\\
\gamma_{23}(\mathbf{u}^e) &= \frac{1}{2}\left[\left(\frac{d\mathcal{U}_2^e}{dx_3} + \mathcal{R}_1^e\right) + x_1\frac{d\mathcal{R}_3^e}{dx_3} + \frac{\partial \overline{u}_2^e}{\partial x_3} + \frac{\partial \overline{u}_3^e}{\partial x_2}\right],
\end{aligned}$$

and transforming these equalities by applying $\mathcal{T}_e^{\mathbf{e}}$, we have that

$$\mathcal{T}_e^{\mathbf{e}}(\gamma_{\alpha\alpha}(\mathbf{u}^e)) = \frac{\partial \overline{U}_\alpha^e}{\partial X_\alpha},\ \mathcal{T}_e^{\mathbf{e}}(\gamma_{12}(\mathbf{u}^e)) = \frac{1}{2}\left(\frac{\partial \overline{U}_1^e}{\partial X_2} + \frac{\partial \overline{U}_2^e}{\partial X_1}\right),$$
$$\mathcal{T}_e^{\mathbf{e}}(\gamma_{33}(\mathbf{u}^e)) = \frac{d\mathcal{U}_3^e}{dx_3} - eX_1\frac{d\mathcal{R}_2^e}{dx_3} + eX_2\frac{d\mathcal{R}_1^e}{dx_3} + \frac{\partial \mathcal{T}_e^{\mathbf{e}}(\overline{\mathbf{u}}_3^e)}{\partial x_3},$$
$$\mathcal{T}_e^{\mathbf{e}}(\gamma_{13}(\mathbf{u}^e)) = \frac{1}{2}\left(-eX_2\frac{d\mathcal{R}_3^e}{dx_3} + e\frac{\partial \overline{U}_1^e}{\partial x_3} + \frac{\partial \overline{U}_3^e}{\partial X_1}\right),$$
$$\mathcal{T}_e^{\mathbf{e}}(\gamma_{23}(\mathbf{u}^e)) = \frac{1}{2}\left(eX_1\frac{d\mathcal{R}_3^e}{dx_3} + e\frac{\partial \overline{U}_2^e}{\partial x_3} + \frac{\partial \overline{U}_3^e}{\partial X_2}\right).$$

Passing to the limit when e goes to zero, weak convergence (15.16) gives weak convergences (15.18) and (15.19).

In order to obtain convergence (15.20), we must prove that

$$\frac{\partial \mathcal{T}_e^{\mathbf{e}}(\overline{\mathbf{u}}_3^e)}{\partial x_3} \rightharpoonup 0,$$

in $L^2(\Omega)$. In fact, thanks to estimate (15.3) and properties $i) - iii)$ of Proposition 15.3.2,

$$\left\|\frac{\partial \mathcal{T}_e^{\mathbf{e}}(\overline{\mathbf{u}}_3^e)}{\partial X_\alpha}\right\|^2_{L^2(\Omega)} = e^2\left\|\mathcal{T}_e^{\mathbf{e}}\left(\frac{\partial \overline{\mathbf{u}}_3^e}{\partial x_\alpha}\right)\right\|^2_{L^2(\Omega)} = \left\|\frac{\partial \overline{\mathbf{u}}_3^e}{\partial x_\alpha}\right\|^2_{L^2(\Omega_e)} \le C\mathcal{E}(\mathbf{u},\Omega_e) \le Ce^2,$$
$$\left\|\frac{\partial \mathcal{T}_e^{\mathbf{e}}(\overline{\mathbf{u}}_3^e)}{\partial x_3}\right\|^2_{L^2(\Omega)} = \left\|\mathcal{T}_e^{\mathbf{e}}\left(\frac{\partial \overline{\mathbf{u}}_3^e}{\partial x_3}\right)\right\|^2_{L^2(\Omega)} = \frac{1}{e^2}\left\|\frac{\partial \overline{\mathbf{u}}_3^e}{\partial x_3}\right\|^2_{L^2(\Omega_e)} \le \frac{1}{e^2}C\mathcal{E}(\mathbf{u},\Omega_e) \le C.$$

Besides, from estimate (15.4),

$$\|\mathcal{T}_e^{\mathbf{e}}(\overline{\mathbf{u}}_3^e)\|^2_{L^2(\Omega)} = \frac{1}{e^2}\|\overline{\mathbf{u}}_3^e\|^2_{L^2(\Omega_e)} \le C\mathcal{E}(\mathbf{u},\Omega_e) \le Ce^2,$$

so, $\mathcal{T}_e^{\mathbf{e}}(\overline{\mathbf{u}}_3^e)$ is bounded in $H^1(\Omega)$ and $\mathcal{T}_e^{\mathbf{e}}(\overline{\mathbf{u}}_3^e) \to 0$ in $L^2(\Omega)$, from where we deduce the result. Then, convergence (15.20) is obtained by taking into account convergences (15.13)-(15.15).

Analogously, we obtain convergences (15.21) and (15.22). □

15.4 The unfolding operator $\mathcal{T}_\varepsilon^{\mathbf{h}}$

Definition 15.4.1. *The unfolding operator $\mathcal{T}_\varepsilon^{\mathbf{h}}$ from $L^2(\Omega)$ to $L^2(\mathbf{Y}\times\Omega)$ is defined by*

$$\mathcal{T}_\varepsilon^{\mathbf{h}}(\mathbf{w})(Y,X,x_3) = \mathbf{w}\left(\varepsilon\left[\frac{X}{\varepsilon}\right] + \varepsilon Y, x_3\right), \quad (Y,X,x_3) \in \mathbf{Y}\times\omega\times(0,L),$$
$$\mathbf{w} \in L^2(\Omega), \quad Y = (Y_1,Y_2),\ X = (X_1,X_2),$$

where $[X] = ([X_1],[X_2])$, $[X_i]$ denotes the integer part of $X_i \in \mathbb{R}$.

The next result contains the main properties of $\mathcal{T}_\varepsilon^{\mathbf{h}}$ (see [30]).

Proposition 15.4.2. *The unfolding operator $\mathcal{T}_\varepsilon^{\mathbf{h}}$ verifies the following properties:*

i) For all $v, w \in L^1(\Omega)$,

$$\mathcal{T}_\varepsilon^{\mathbf{h}}(vw) = \mathcal{T}_\varepsilon^{\mathbf{h}}(v)\mathcal{T}_\varepsilon^{\mathbf{h}}(w).$$

ii) For all $w \in L^1(\Omega)$,

$$\int_{\omega\times(0,L)} w dX_1 dX_2 dx_3 = \int_{\mathbf{Y}\times\Omega} \mathcal{T}_\varepsilon^{\mathbf{h}}(w) dY_1 dY_2 dX_1 dX_2 dx_3.$$

iii) For all $w \in L^1(\Omega)$,

$$\int_{\omega\times(0,L)} |w|\, dX_1 dX_2 dx_3 = \int_{\mathbf{Y}\times\Omega} |\mathcal{T}_\varepsilon^{\mathbf{h}}(w)|\, dY_1 dY_2 dX_1 dX_2 dx_3.$$

iv) Let $1 \le p < \infty$. Let $\{w^\varepsilon\}_{\varepsilon>0} \subset L^p(\Omega)$ such that $w^\varepsilon \to w$ strongly in $L^p(\Omega)$. Then

$$\mathcal{T}_\varepsilon^{\mathbf{h}}(w^\varepsilon) \to w,$$

strongly in $L^p(\mathbf{Y}\times\Omega)$.

v) Let $\{w^\varepsilon\}_{\varepsilon>0} \subset L^2(0,L;H^1(\omega))$ such that $w^\varepsilon \rightharpoonup w$ weakly in $L^2(0,L;H^1(\omega))$. Then there exists a subsequence, still denoted by w^ε, and $\hat{w} \in L^2(\Omega; H^1_{per}(\mathbf{Y}))$ such that

$$\mathcal{T}_\varepsilon^{\mathbf{h}}(w^\varepsilon) \rightharpoonup w,$$
$$\mathcal{T}_\varepsilon^{\mathbf{h}}(\nabla_X w^\varepsilon) \rightharpoonup \nabla_X w + \nabla_Y \hat{w},$$

weakly in $L^2(\mathbf{Y}\times\Omega)$. The function $\hat{w} \in L^2(\Omega; H^1_{per}(\mathbf{Y}))$ is determined up to a function belonging to $L^2(\Omega)$.

vi) Let $w \in H^1(\Omega)$,

$$\frac{\partial \mathcal{T}_\varepsilon^{\mathbf{h}}(w)}{\partial x_3} = \mathcal{T}_\varepsilon^{\mathbf{h}}\left(\frac{\partial w}{\partial x_3}\right).$$

Theorem 15.4.3. *Let $\{\mathbf{u}^{e\varepsilon}\}_{e\ge0}$ be a sequence in $H^1_{\Gamma_D}(\Omega^*_{e,\varepsilon};\mathbb{R}^3)$ such that*

$$\mathcal{E}(\mathbf{u}^{e\varepsilon}, \Omega^*_{e,\varepsilon}) \le Ce^2. \tag{15.23}$$

There exist $\mathcal{U}_\alpha \in H^2(0,L)$, $\mathcal{U}_3 \in H^1(0,L)$, $\mathcal{R}_3 \in H^1(0,L)$, $\overline{\mathbf{U}} \in L^2(\mathbf{Y}^*\times\Omega;\mathbb{R}^3)$ and $\hat{\mathbf{u}} \in L^2(\Omega; H^1_{per}(\mathbf{Y}^*;\mathbb{R}^3))$ such that

$$\mathcal{U}_\alpha(0) = \frac{d\mathcal{U}_\alpha}{dx_3}(0) = 0,\ \mathcal{U}_3(0) = 0,\ \mathcal{R}_3(0) = 0,$$
$$\int_\omega \overline{U}_i dX_1 dX_2 = \int_\omega (X_1\overline{U}_2 - X_2\overline{U}_1) dX_1 dX_2 = 0,$$
$$\int_{\mathbf{Y}^*} \hat{v}_i dY_1 dY_2 = 0,$$

and the following convergences are hold:

$$e\mathcal{T}_e^{\mathbf{e}}(u_1^{e\varepsilon}) \rightharpoonup \mathcal{U}_1, \tag{15.24}$$

$$\mathcal{T}_e^{\mathbf{e}}(u_1^{e\varepsilon}) - \mathcal{U}_1^{e\varepsilon} \rightharpoonup -X_2\mathcal{R}_3, \tag{15.25}$$

$$e\mathcal{T}_e^{\mathbf{e}}(u_2^{e\varepsilon}) \rightharpoonup \mathcal{U}_2, \tag{15.26}$$

$$\mathcal{T}_e^{\mathbf{e}}(u_2^{e\varepsilon}) - \mathcal{U}_2^{e\varepsilon} \rightharpoonup X_1\mathcal{R}_3, \tag{15.27}$$

$$\mathcal{T}_e^{\mathbf{e}}(u_3^{e\varepsilon}) \rightharpoonup \mathcal{U}_3 - X_1\frac{d\mathcal{U}_1}{dx_3} - X_2\frac{d\mathcal{U}_2}{dx_3}, \tag{15.28}$$

weakly in $H^1(\Omega)$.

Moreover, the following convergences of the unfolded strain tensor (up to a subsequence) hold:

$$\mathcal{T}_\varepsilon^{\mathbf{h}}(\mathcal{T}_e^{\mathbf{e}}(\gamma_{\alpha\beta}(\mathbf{u}^{e\varepsilon}))) \rightharpoonup \frac{1}{2}\left(\frac{\partial\overline{U}_\alpha}{\partial X_\beta} + \frac{\partial\overline{U}_\beta}{\partial X_\alpha}\right) + \frac{1}{2}\left(\frac{\partial\hat{u}_\alpha}{\partial Y_\beta} + \frac{\partial\hat{u}_\beta}{\partial Y_\alpha}\right), \tag{15.29}$$

$$\mathcal{T}_\varepsilon^{\mathbf{h}}(\mathcal{T}_e^{\mathbf{e}}(\gamma_{33}(\mathbf{u}^{e\varepsilon}))) \rightharpoonup \frac{d\mathcal{U}_3}{dx_3} - X_1\frac{d^2\mathcal{U}_1}{dx_3^2} - X_2\frac{d^2\mathcal{U}_2}{dx_3^2}, \tag{15.30}$$

$$\mathcal{T}_\varepsilon^{\mathbf{h}}(\mathcal{T}_e^{\mathbf{e}}(\gamma_{13}(\mathbf{u}^{e\varepsilon}))) \rightharpoonup \frac{1}{2}\left(-X_2\frac{d\mathcal{R}_3}{dx_3} + \frac{\partial\overline{U}_3}{\partial X_1} + \frac{\partial\hat{u}_3}{\partial Y_1}\right), \tag{15.31}$$

$$\mathcal{T}_\varepsilon^{h}(\mathcal{T}_e^{\mathbf{e}}(\gamma_{23}(\mathbf{u}^{e\varepsilon}))) \rightharpoonup \frac{1}{2}\left(X_1\frac{d\mathcal{R}_3}{dx_3} + \frac{\partial\overline{U}_3}{\partial X_2} + \frac{\partial\hat{u}_3}{\partial Y_2}\right), \tag{15.32}$$

weakly in $L^2(\mathbf{Y}^* \times \Omega)$.

Proof. Thanks to Theorem 15.1.4, we obtain an extended displacement of $\mathbf{u}^{e\varepsilon}$ to Ω_e, still denoted by $\mathbf{u}^{e\varepsilon}$, verifying (15.12) by Remark 15.1.5 and $\mathbf{u}^{e\varepsilon} \in H^1_{\Gamma_D}(\Omega_e;\mathbb{R}^3)$. By applying Theorem 15.3.5 and using properties of Proposition 15.4.2, we have proved Theorem 15.4.3. □

Chapter 16

The unfolded elasticity problem

The objective of Part III of this manuscript is to study the asymptotic behaviour of catalyst supports in a linear elasticity problem. By means of the unfolding method and from the estimates obtained in Chapter 15 we obtain the limit problem when the thickness of the structure beams, e, and the periodicity parameter ε go to zero.

The outline of this chapter is as follows: In section 16.1 we introduce suitable applied forces such that its associated displacements in the structure are bounded. In Section 16.2 the complete characterization of the limit problem is given and in Section 16.3 strong convergences are obtained.

16.1 Determination of applied forces

Recall that we are interested in studying the asymptotic behaviour, when e, ε go to zero, of the variational problem we have introduced before:

Problem $(VP^{e\varepsilon})$:

Find $\mathbf{u}^{e\varepsilon} \in H^1_{\Gamma_D}(\Omega^*_{e,\varepsilon};\mathbb{R}^3)$ such that

$$\int_{\Omega^*_{e,\varepsilon}} \mathbf{\Lambda}\boldsymbol{\gamma}(\mathbf{u}^{e\varepsilon}) : \boldsymbol{\gamma}(\mathbf{v})dx = \int_{\Omega^*_{e,\varepsilon}} \mathbf{f}^{e\varepsilon}\cdot\mathbf{v}dx, \quad \forall \mathbf{v} \in H^1_{\Gamma_D}(\Omega^*_{e,\varepsilon};\mathbb{R}^3), \tag{16.1}$$

where

$$H^1_{\Gamma_D}(\Omega^*_{e,\varepsilon};\mathbb{R}^3) = \{\mathbf{v} \in H^1(\Omega^*_{e,\varepsilon};\mathbb{R}^3) : \mathbf{v} = \mathbf{0} \text{ on } \Gamma^*_D\}.$$

In order to use results given in Theorem 15.4.3, we have to obtain some suitable volume forces $\mathbf{f}^{e\varepsilon}$ such that its related displacement field verifies estimate (15.23).

Proposition 16.1.1. *Let* $\mathbf{f}^{e\varepsilon} \in L^2(\Omega^*_{e,\varepsilon};\mathbb{R}^3)$ *be the volume forces given by*

$$\mathbf{f}^{e\varepsilon}(x_1,x_2,x_3) = \begin{pmatrix} ef_1(x_3) - \frac{x_2}{e}f_T(x_3) \\ ef_2(x_3) + \frac{x_1}{e}f_T(x_3) \\ f_3(x_3) \end{pmatrix}, \tag{16.2}$$

where $f_1, f_2, f_3, f_T \in L^2(0,L)$. The displacement field corresponding to volume forces $\mathbf{f}^{e\varepsilon}$ verifies the estimate

$$\mathcal{E}(\mathbf{u}^{e\varepsilon}, \Omega^*_{e,\varepsilon}) \leq Ce^2. \tag{16.3}$$

Proof. Using the decomposition (15.2) of $\mathbf{u}^{e\varepsilon}$, the estimates (15.4), (15.6), (15.7) and (15.8) in Theorem 15.2.4, we immediately obtain the following inequality:

$$\left| \int_{\Omega^*_{e,\varepsilon}} \mathbf{f}^{e\varepsilon} \cdot \mathbf{u}^{e\varepsilon} dx \right| \leq Ce\mathcal{E}(\mathbf{u}^{e\varepsilon}, \Omega^*_{e,\varepsilon})^{1/2},$$

and, thanks to the coercivity of the problem, we can conclude the result. □

16.2 Obtaining the limit unfolded problem and displacements

The displacement field $\mathbf{u}^{e\varepsilon}$ which is the solution of Problem $(VP^{e\varepsilon})$ can be written as in expression (15.2). Our objective is to find some limit problems for the elementary displacements $\mathcal{U}$, $\mathcal{R}_3$ and $\overline{\mathbf{U}}$ in order to obtain simpler problems or expressions for our solution. To do this, we will use Theorem 15.4.3 which will give us the weak limits of our elementary displacements.

First of all, we will obtain the unfolded problem, limit of the variational problem (16.1). Formally, motivated by weak convergences (15.24)-(15.28), we can write the solution of Problem $(VP^{e\varepsilon})$ in the form

$$\begin{aligned}\mathbf{u}^{e\varepsilon}(x_1,x_2,x_3) \approx & \left(\frac{1}{e}\mathcal{U}_1(x_3) - \frac{x_2}{e}\mathcal{R}_3(x_3)\right)\mathbf{e}_1 + \left(\frac{1}{e}\mathcal{U}_2(x_3) + \frac{x_1}{e}\mathcal{R}_3(x_3)\right)\mathbf{e}_2 + \\ & \left(\mathcal{U}_3(x_3) - \frac{x_1}{e}\frac{d\mathcal{U}_1}{dx_3} - \frac{x_2}{e}\frac{d\mathcal{U}_2}{dx_3}\right)\mathbf{e}_3 + \\ & e\overline{\mathbf{U}}\left(\frac{x_1}{e}, \frac{x_2}{e}, x_3\right) + e\varepsilon\hat{\mathbf{u}}\left(\frac{x_1}{e}, \frac{x_2}{e}, x_3, \frac{x_1}{e\varepsilon}, \frac{x_2}{e\varepsilon}\right).\end{aligned} \tag{16.4}$$

We define the following displacements space $\mathcal{D}$:

$$\begin{aligned}\mathcal{D} = \Bigg\{ & \mathbf{V} = (\mathcal{V}_1, \mathcal{V}_2, \mathcal{V}_3, \mathcal{A}_3, \overline{\mathbf{V}}, \hat{\mathbf{v}}); \mathcal{V}_1, \mathcal{V}_2 \in H^2(0,L), \mathcal{V}_1(0) = \mathcal{V}_2(0) = \frac{d\mathcal{V}_1}{dx_3}(0) = \frac{d\mathcal{V}_2}{dx_3}(0) = 0, \\ & \mathcal{V}_3, \mathcal{A}_3 \in H^1(0,L), \mathcal{V}_3(0) = \mathcal{A}_3(0) = 0, \\ & (\overline{\mathbf{V}}, \hat{\mathbf{v}}) \in L^2(0,L; H^1(\omega;\mathbb{R}^3)) \times L^2(\Omega; H^1_{per}(\mathbf{Y}^*;\mathbb{R}^3)), \\ & \int_\omega \overline{V}_i dX_1 dX_2 = \int_\omega (X_1\overline{V}_2 - X_2\overline{V}_1) dX_1 dX_2 = 0, \quad \int_{\mathbf{Y}^*} \hat{v}_i dY_1 dY_2 = 0 \Bigg\}.\end{aligned} \tag{16.5}$$

We associate to any element $\mathbf{V}$ in $\mathcal{D}$ a formal displacement $\mathbf{v}$ as in (16.4):

$$\begin{aligned}\mathbf{v}(x_1,x_2,x_3) = & \left(\frac{1}{e}\mathcal{V}_1(x_3) - \frac{x_2}{e}\mathcal{A}_3(x_3)\right)\mathbf{e}_1 + \left(\frac{1}{e}\mathcal{V}_2(x_3) + \frac{x_1}{e}\mathcal{A}_3(x_3)\right)\mathbf{e}_2 + \\ & \left(\mathcal{V}_3(x_3) - \frac{x_1}{e}\frac{d\mathcal{V}_1}{dx_3} - \frac{x_2}{e}\frac{d\mathcal{V}_2}{dx_3}\right)\mathbf{e}_3 + \\ & e\overline{\mathbf{V}}\left(\frac{x_1}{e}, \frac{x_2}{e}, x_3\right) + e\varepsilon\hat{\mathbf{v}}\left(\frac{x_1}{e}, \frac{x_2}{e}, x_3, \frac{x_1}{e\varepsilon}, \frac{x_2}{e\varepsilon}\right).\end{aligned}$$

Analogously, motivated by weak convergences (15.29)-(15.32), for any element $\mathbf{V} \in \mathcal{D}$, we define a formal strain tensor $\Gamma_{ij}(\mathbf{V})$ expressed in $\mathbf{Y}^* \times \Omega$. To do that, we calculate the strain tensor of $\mathbf{v}$ and we omit some partial derivatives (those which do not make sense):

$$\Gamma_{\alpha\beta}(\mathbf{V}) = \frac{1}{2}\left(\frac{\partial \overline{V}_\alpha}{\partial X_\beta} + \frac{\partial \overline{V}_\beta}{\partial X_\alpha}\right) + \frac{1}{2}\left(\frac{\partial \hat{v}_\alpha}{\partial Y_\beta} + \frac{\partial \hat{v}_\beta}{\partial Y_\alpha}\right), \tag{16.6}$$

$$\Gamma_{33}(\mathbf{V}) = \frac{d\,\mathcal{V}_3}{dx_3} - X_1\frac{d^2\mathcal{V}_1}{dx_3^2} - X_2\frac{d^2\mathcal{V}_2}{dx_3^2}, \tag{16.7}$$

$$\Gamma_{13}(\mathbf{V}) = \frac{1}{2}\left(-X_2\frac{d\mathcal{A}_3}{dx_3} + \frac{\partial \overline{V}_3}{\partial X_1} + \frac{\partial \hat{v}_3}{\partial Y_1}\right), \tag{16.8}$$

$$\Gamma_{23}(\mathbf{V}) = \frac{1}{2}\left(X_1\frac{d\mathcal{A}_3}{dx_3} + \frac{\partial \overline{V}_3}{\partial X_2} + \frac{\partial \hat{v}_3}{\partial Y_2}\right). \tag{16.9}$$

Finally, we define the following inner product:

$$< \mathbf{U}, \mathbf{V} >= \int_0^L \int_\omega \int_{\mathbf{Y}^*} \Gamma_{ij}(\mathbf{U})\Gamma_{ij}(\mathbf{V}) dY_1 dY_2 dX_1 dX_2 dx_3, \quad \forall\, \mathbf{U}, \mathbf{V} \in \mathcal{D}. \tag{16.10}$$

Proposition 16.2.1. *The associated norm to the inner product in $\mathcal{D}$ is equivalent to the norm $\|\cdot\|$ of the product space*

$$[H^2(0,L)]^2 \times [H^1(0,L)]^2 \times L^2(0,L;H^1(\omega;\mathbb{R}^3)) \times L^2(\Omega; H^1_{per}(\mathbf{Y}^*;\mathbb{R}^3)).$$

Lemma 16.2.2. *Let $\mathbf{V} \in \mathcal{D}$. The following estimates are verified:*

$$\int_0^L \|\bar{V}_\alpha\|^2_{H^1(\omega)} dx_3 + \int_0^L \int_\omega \|\hat{v}_\alpha\|^2_{H^1_{per}(\mathbf{Y}^*)} dX dx_3 \leq C \int_0^L \int_\omega \int_{\mathbf{Y}^*} (\Gamma_{\alpha\beta}(\mathbf{V}))^2 dY dX dx_3, \tag{16.11}$$

$$\|\mathcal{A}_3\|^2_{H^1(0,L)} + \int_0^L \|\bar{V}_3\|^2_{H^1(\omega)} dx_3 + \int_0^L \int_\omega \|\hat{v}_3\|^2_{H^1_{per}(\mathbf{Y}^*)} dX dx_3 \leq C \int_0^L \int_\omega \int_{\mathbf{Y}^*} (\Gamma_{3\alpha}(\mathbf{V}))^2 dY dX dx_3, \tag{16.12}$$

$$\|\mathcal{V}_\alpha\|^2_{H^2(0,L)} + \|\mathcal{V}_3\|^2_{H^1(0,L)} \leq C \int_0^L \int_\omega \int_{\mathbf{Y}^*} (\Gamma_{33}(\mathbf{V}))^2 dY dX dx_3. \tag{16.13}$$

The constants depend only on $\mathbf{Y}^*$ and L.

Proof. The proof is made in three steps.

Step 1: We recall that $\hat{\mathbf{v}} \in L^2(\Omega; H^1_{per}(\mathbf{Y}^*;\mathbb{R}^3))$. We define $\hat{\hat{\mathbf{v}}} \in L^2(\Omega; H^1(\mathbf{Y}^*;\mathbb{R}^2))$ in the following form:

$$\hat{\hat{v}}_1(Y_1,Y_2,\cdot) = \hat{v}_1(Y_1,Y_2,\cdot) + \frac{\partial \bar{V}_1}{\partial X_1}Y_1 + \frac{1}{2}\left(\frac{\partial \bar{V}_1}{\partial X_2} + \frac{\partial \bar{V}_2}{\partial X_1}\right)Y_2,$$

$$\hat{\hat{v}}_2(Y_1,Y_2,\cdot) = \hat{v}_2(Y_1,Y_2,\cdot) + \frac{1}{2}\left(\frac{\partial \bar{V}_1}{\partial X_2} + \frac{\partial \bar{V}_2}{\partial X_1}\right)Y_1 + \frac{\partial \bar{V}_2}{\partial X_2}Y_2.$$

Thanks to Korn inequality for displacements in $H^1(\mathbf{Y}^*;\mathbb{R}^2)$, there exists a rigid body displacement $\mathbf{r} \in L^2(\Omega; H^1(\mathbf{Y}^*;\mathbb{R}^2))$,

$$r_1(Y_1,Y_2,\cdot) = a_1(\cdot) + b(\cdot)Y_2,$$
$$r_2(Y_1,Y_2,\cdot) = a_2(\cdot) - b(\cdot)Y_1,$$
$$a_1, a_2, b \in L^2(\Omega),$$

such that

$$\|\hat{\hat{\mathbf{v}}} - \mathbf{r}\|^2_{L^2(\mathbf{Y}^*\times\Omega;\mathbb{R}^2)} + \|\nabla_Y(\hat{\hat{\mathbf{v}}} - \mathbf{r})\|^2_{L^2(\mathbf{Y}^*\times\Omega;\mathbb{R}^2)} \leq$$
$$C\int_0^L \int_\omega \int_{\mathbf{Y}^*} |\Gamma_{\alpha\beta}(\mathbf{V})|^2 dY dX dx_3.$$

Moreover,

$$\|\hat{\hat{\mathbf{v}}} - \mathbf{r}\|^2_{L^2(\partial\mathbf{Y}^*\times\Omega;\mathbb{R}^2)} \leq C\int_0^L \int_\omega \int_{\mathbf{Y}^*} |\Gamma_{\alpha\beta}(\mathbf{V})|^2 dY dX dx_3,$$

due to the continuous injection from $H^1(\mathbf{Y}^*)$ in $L^2(\partial\mathbf{Y})$. By considering the trace of $\hat{\hat{\mathbf{v}}} - \mathbf{r}$ on $\partial\mathbf{Y}$, we have that

$$\hat{\hat{v}}_1(0,Y_2,\cdot) - r_1(0,Y_2,\cdot) = \hat{v}_1(0,Y_2,\cdot) + \left[\frac{1}{2}\left(\frac{\partial\bar{V}_1}{\partial X_2} + \frac{\partial\bar{V}_2}{\partial X_1}\right) - b(\cdot)\right] Y_2 - a_1(\cdot),$$
$$\hat{\hat{v}}_1(1,Y_2,\cdot) - r_1(1,Y_2,\cdot) = \hat{v}_1(1,Y_2,\cdot) + \frac{\partial\bar{V}_1}{\partial X_1} + \left[\frac{1}{2}\left(\frac{\partial\bar{V}_1}{\partial X_2} + \frac{\partial\bar{V}_2}{\partial X_1}\right) - b(\cdot)\right] Y_2 - a_1(\cdot),$$
$$\hat{\hat{v}}_2(0,Y_2,\cdot) - r_2(0,Y_2,\cdot) = \hat{v}_2(0,Y_2,\cdot) + \frac{\partial\bar{V}_2}{\partial X_2} Y_2 - a_2(\cdot),$$
$$\hat{\hat{v}}_2(0,Y_2,\cdot) - r_2(1,Y_2,\cdot) = \hat{v}_2(1,Y_2,\cdot) + \left[\frac{1}{2}\left(\frac{\partial\bar{V}_1}{\partial X_2} + \frac{\partial\bar{V}_2}{\partial X_1}\right) + b(\cdot)\right] + \frac{\partial\bar{V}_2}{\partial X_2} Y_2 - a_2(\cdot),$$

and due to the periodicity of $\hat{\mathbf{v}}$, we obtain that

$$\|(\hat{\hat{v}} - r)_1(0,Y_2,\cdot) - (\hat{\hat{v}} - r)_1(1,Y_2,\cdot)\|^2_{L^2((0,1)\times\Omega)} = \left\|\frac{\partial\bar{V}_1}{\partial X_1}\right\|^2_{L^2(\Omega)} \leq$$
$$\|\hat{\hat{\mathbf{v}}} - \mathbf{r}\|^2_{L^2(\partial\mathbf{Y}\times\Omega;\mathbb{R}^2)} \leq C\int_0^L \int_\omega \int_{\mathbf{Y}^*} |\Gamma_{\alpha\beta}(\mathbf{V})|^2 dY dX dx_3,$$
$$\|(\hat{\hat{v}} - r)_2(0,Y_2,\cdot) - (\hat{\hat{v}} - r)_2(1,Y_2,\cdot)\|_{L^2((0,1)\times\Omega)} = \left\|\frac{1}{2}\left(\frac{\partial\bar{V}_1}{\partial X_2} + \frac{\partial\bar{V}_2}{\partial X_1}\right) + b\right\|_{L^2(\Omega)} \leq$$
$$\|\hat{\hat{\mathbf{v}}} - \mathbf{r}\|^2_{L^2(\partial\mathbf{Y}\times\Omega;\mathbb{R}^2)} \leq C\int_0^L \int_\omega \int_{\mathbf{Y}^*} |\Gamma_{\alpha\beta}(\mathbf{V})|^2 dY dX dx_3. \tag{16.14}$$

Analogously,

$$\left\|\frac{1}{2}\left(\frac{\partial\bar{V}_1}{\partial X_2} + \frac{\partial\bar{V}_2}{\partial X_1}\right) - b\right\|^2_{L^2(\Omega)} \leq C\int_0^L \int_\omega \int_{\mathbf{Y}^*} |\Gamma_{\alpha\beta}(\mathbf{V})|^2 dY dX dx_3,$$
$$\left\|\frac{\partial\bar{V}_2}{\partial X_2}\right\|_{L^2(\Omega)} \leq C\int_0^L \int_\omega \int_{\mathbf{Y}^*} |\Gamma_{\alpha\beta}(\mathbf{V})|^2 dY dX dx_3, \tag{16.15}$$

and from estimates (16.14) and (16.15),

$$\left\| \frac{\partial \bar{V}_1}{\partial X_2} + \frac{\partial \bar{V}_2}{\partial X_1} \right\|^2_{L^2(\Omega)} \leq C \int_0^L \int_\omega \int_{\mathbf{Y}^*} |\Gamma_{\alpha\beta}(\mathbf{V})|^2 dY dX dx_3,$$

$$\|b\|^2_{L^2(\Omega)} \leq C \int_0^L \int_\omega \int_{\mathbf{Y}^*} |\Gamma_{\alpha\beta}(\mathbf{V})|^2 dY dX dx_3.$$

Then, we obtain (16.11) thanks to (16.14), (16.15) and the 2d-Korn's inequality applied to the displacement $\bar{V}_1 \mathbf{e}_1 + \bar{V}_2 \mathbf{e}_2$ and remembering that:

$$\nabla_Y \hat{v}_1 = \nabla_Y \hat{\hat{v}}_1 - \begin{pmatrix} \frac{\partial \bar{V}_1}{\partial X_1} \\ \frac{1}{2}\left(\frac{\partial \bar{V}_1}{\partial X_2} + \frac{\partial \bar{V}_2}{\partial X_1} \right) \end{pmatrix},$$

$$\nabla_Y \hat{v}_2 = \nabla_Y \hat{\hat{v}}_2 - \begin{pmatrix} \frac{1}{2}\left(\frac{\partial \bar{V}_1}{\partial X_2} + \frac{\partial \bar{V}_2}{\partial X_1} \right) \\ \frac{\partial \bar{V}_2}{\partial X_2} \end{pmatrix}.$$

Step 2: We define $\hat{\hat{v}}_3 \in L^2(\Omega; H^1(\mathbf{Y}^*))$ in the following form:

$$\hat{\hat{v}}_3(Y_1, Y_2) = \hat{v}_3(Y_1, Y_2) + \left(-X_2 \frac{d\mathcal{A}_3}{dx_3} + \frac{\partial \bar{V}_3}{\partial X_1} \right) Y_1 + \left(X_1 \frac{d\mathcal{A}_3}{dx_3} + \frac{\partial \bar{V}_3}{\partial X_2} \right) Y_2.$$

Thanks to Poincaré-Wirtinger inequality, there exists a function $m \in L^2(\Omega)$ such that

$$\|\hat{\hat{v}}_3 - m\|^2_{L^2(\mathbf{Y}^* \times \Omega)} + \|\hat{\hat{v}}_3 - m\|^2_{L^2(\partial \mathbf{Y}^* \times \Omega)} \leq C \|\nabla_Y \hat{\hat{v}}_3\|^2_{L^2(\mathbf{Y}^* \times \Omega; \mathbb{R}^2)} \leq$$
$$C \int_0^L \int_\omega \int_{\mathbf{Y}^*} |\Gamma_{3\alpha}(\mathbf{V})|^2 dY dX dx_3.$$

Then, taking into account that $\frac{\partial \hat{\hat{v}}_3}{\partial Y_\alpha} = 2\Gamma_{3\alpha}(\mathbf{V})$, we have that

$$\left\| -X_2 \frac{d\mathcal{A}_3}{dx_3} + \frac{\partial \bar{V}_3}{\partial X_1} \right\|^2_{L^2(\Omega)} + \left\| X_1 \frac{d\mathcal{A}_3}{dx_3} + \frac{\partial \bar{V}_3}{\partial X_2} \right\|^2_{L^2(\Omega)} \leq$$
$$C \int_0^L \int_\omega \int_{\mathbf{Y}^*} |\Gamma_{3\alpha}(\mathbf{V})|^2 dY dX.$$

In order to obtain estimate (16.12), we use the fact that

$$\nabla_Y \hat{v}_3 = \nabla_Y \hat{\hat{v}}_3 - \begin{pmatrix} -X_2 \frac{d\mathcal{A}_3}{dx_3} + \frac{\partial \bar{V}_3}{\partial X_1} \\ X_1 \frac{d\mathcal{A}_3}{dx_3} + \frac{\partial \bar{V}_3}{\partial X_2} \end{pmatrix}.$$

Step 3: Estimates of $\mathcal{V}_\alpha, \mathcal{V}_3$ are immediate. □

Lemma 16.2.3. *Let $\mathcal{V}(\omega)$ be the subspace*

$$\mathcal{V}(\omega) = \left\{ V \in H^1(\omega); \int_\omega V dX = 0 \right\}.$$

Then, in $\mathcal{V}(\omega)+\mathbb{R}$ the following norms are equivalent:

$$\|V+a\|_{\mathcal{V}(\omega)+\mathbb{R}} = \left(|a|^2 + \|\nabla V\|^2_{L^2(\omega)}\right)^{1/2}$$
$$|V+a|_{\mathcal{V}(\omega)+\mathbb{R}} = \left(\left\|-X_2 a + \frac{\partial V}{\partial X_1}\right\|^2_{L^2(\omega)} + \left\|X_1 a + \frac{\partial V}{\partial X_2}\right\|^2_{L^2(\omega)}\right)^{1/2}.$$

Therefore, there exists a positive constant C such that

$$|a|^2 + \|\nabla V\|^2_{L^2(\omega)} \leq C\left(\left\|-X_2 a + \frac{\partial V}{\partial X_1}\right\|^2_{L^2(\omega)} + \left\|X_1 a + \frac{\partial V}{\partial X_2}\right\|^2_{L^2(\omega)}\right), \tag{16.16}$$

for all $V + a \in \mathcal{V}(\omega)+\mathbb{R}$.

Proof. Let us assume that estimate (16.16) is not verified. Then, there exist sequences $\{V_n\}_{n\in\mathbb{N}}$, $\{a_n\}_{n\in\mathbb{N}}$ such that

$$\|\nabla V_n\|_{L^2(\omega)} + |a_n| = 1, \tag{16.17}$$
$$\left\|-X_2 a_n + \frac{\partial V_n}{\partial X_1}\right\|_{L^2(\omega)} + \left\|X_1 a_n + \frac{\partial V_n}{\partial X_2}\right\|_{L^2(\omega)} \leq \frac{1}{n}. \tag{16.18}$$

The sequences V_n and a_n are bounded and there exist subsequences (denoted in the same way) such that

$$V_n \rightharpoonup V \text{ in } H^1(\omega) \text{ weakly},$$
$$a_n \to a.$$

Moreover, thanks to (16.18) we have

$$-X_2 a_n + \frac{\partial V_n}{\partial X_1} \to -X_2 a + \frac{\partial V}{\partial X_1} = 0,$$
$$X_1 a_n + \frac{\partial V_n}{\partial X_2} \to X_1 a + \frac{\partial V}{\partial X_2} = 0,$$

strongly in $L^2(\omega)$, and we obtain that $\mathbf{V} = 0$, $a = 0$. Then,

$$\nabla V_n \to 0 \text{ in } L^2(\omega) \text{ strongly},$$

which leads us to a contradiction when we pass to the limit in (16.17). □

Proof. (*Of Proposition 16.2.1*) Obviously, the associated norm to the inner product in $\mathcal{D}$ is a seminorm in the product space. Thanks to estimates of Lemma 16.2.2 the seminorm is a norm.

It remains to prove that both norms are equivalent. Thanks to the definition (16.5), we have that

$$< \mathbf{V}, \mathbf{V} > \leq \alpha \|\mathbf{V}\|^2, \ \forall\, \mathbf{V} \in \mathcal{D},\ \alpha > 0.$$

We can conclude that both norms are equivalent using estimates given in Lemma 16.2.2. □

Theorem 16.2.4. *The limit problem of Problem $(VP^{e\varepsilon})$ is given by the following unfolded variational problem:*

Problem (UP)*:*

Find $\mathbf{U} \in \mathcal{D}$ *such that*

$$\int_0^L \int_\omega \int_{\mathbf{Y}^*} a_{ijkl}\Gamma_{ij}(\mathbf{U})\Gamma_{kl}(\mathbf{V})dY_1dY_2dX_1dX_2dx_3 =$$
$$\int_0^L \int_\omega \int_{\mathbf{Y}^*} \{f_\alpha \mathcal{V}_\alpha + f_3\mathcal{V}_3 + (X_1^2+X_2^2)f_T\mathcal{A}_3\}dY_1dY_2dX_1dX_2dx_3, \quad \forall \mathbf{V} \in \mathcal{D}, \tag{16.19}$$

where a_{ijkl} are the usual elasticity coefficients

$$a_{ijkl} = \lambda\delta_{ij}\delta_{kl} + \mu(\delta_{ik}\delta_{jl} + \delta_{il}\delta_{jk}).$$

Proof. Firstly, we choose as a test function v in (16.1)

$$\mathbf{v}(x_1,x_2,x_3) = \begin{pmatrix} \frac{1}{e}\mathcal{V}_1(x_3) - \frac{x_2}{e}\mathcal{A}_3(x_3) \\ \frac{1}{e}\mathcal{V}_2(x_3) + \frac{x_1}{e}\mathcal{A}_3(x_3) \\ \mathcal{V}_3(x_3) - \frac{x_1}{e}\frac{d\mathcal{V}_1}{dx_3}(x_3) - \frac{x_2}{e}\frac{d\mathcal{V}_2}{dx_3}(x_3) \end{pmatrix} \in H^1(\Omega^*_{e,\varepsilon};\mathbb{R}^3),$$

where $\mathcal{V}_1, \mathcal{V}_2 \in H^2(0,L)$, $\mathcal{V}_3, \mathcal{A}_3 \in H^1(0,L)$, with

$$\mathcal{V}_1(0) = \mathcal{V}_2(0) = \mathcal{V}_3(0) = \mathcal{A}_3(0) = \frac{d\mathcal{V}_1}{dx_3}(0) = \frac{d\mathcal{V}_2}{dx_3}(0) = 0.$$

By applying $\mathcal{T}_e^{\mathbf{e}}$ to the strain tensor $\gamma_{ij}(\mathbf{v})$, we obtain that

$$\begin{aligned}
&\mathcal{T}_e^{\mathbf{e}}(\gamma_{\alpha\beta}(\mathbf{v})) = 0,\\
&\mathcal{T}_e^{\mathbf{e}}(\gamma_{13}(\mathbf{v})) = -\frac{1}{2}X_2\frac{d\mathcal{A}_3}{dx_3} = \Gamma_{13}(\mathbf{V}),\\
&\mathcal{T}_e^{\mathbf{e}}(\gamma_{23}(\mathbf{v})) = \frac{1}{2}X_1\frac{d\mathcal{A}_3}{dx_3} = \Gamma_{23}(\mathbf{V}),\\
&\mathcal{T}_e^{\mathbf{e}}(\gamma_{33}(\mathbf{v})) = \frac{d\mathcal{V}_3}{dx_3} - X_1\frac{d^2\mathcal{V}_1}{dx_3^2} - X_2\frac{d^2\mathcal{V}_2}{dx_3^2} = \Gamma_{33}(\mathbf{V}),
\end{aligned}$$

where $\mathbf{V} = \mathbf{V}_e$. We transform the left-hand term in (16.1) by applying $\mathcal{T}_e^{\mathbf{e}}$ and $\mathcal{T}_\varepsilon^{\mathbf{h}}$ and we obtain that

$$\int_{\Omega^*_{e,\varepsilon}} \mathbf{\Lambda}\boldsymbol{\gamma}(\mathbf{u}^{e\varepsilon}) : \boldsymbol{\gamma}(\mathbf{v})dx_1dx_2dx_3 =$$
$$e^2\int_0^L \int_{\omega^*_\varepsilon} \{[(\lambda+2\mu)\mathcal{T}_e^{\mathbf{e}}(\gamma_{33}(\mathbf{u}^{e\varepsilon})) + \lambda(\mathcal{T}_e^{\mathbf{e}}(\gamma_{11}(\mathbf{u}^{e\varepsilon})) + \mathcal{T}_e^{\mathbf{e}}(\gamma_{22}(\mathbf{u}^{e\varepsilon})))]\,\Gamma_{33}(\mathbf{V})$$
$$+2\mu\mathcal{T}_e^{\mathbf{e}}(\gamma_{13}(\mathbf{u}^{e\varepsilon}))\Gamma_{13}(\mathbf{V}) + 2\mu\mathcal{T}_e^{\mathbf{e}}(\gamma_{23}(\mathbf{u}^{e\varepsilon}))\Gamma_{13}(\mathbf{V})\}\,dX_1dX_2dx_3 =$$
$$\frac{e^2}{|\mathbf{Y}^*|}\int_{\Omega\times\mathbf{Y}^*} \Big\{\Big[(\lambda+2\mu)\mathcal{T}_\varepsilon^{\mathbf{h}}(\mathcal{T}_e^{\mathbf{e}}(\gamma_{33}(\mathbf{u}^{e\varepsilon}))) + \lambda(\mathcal{T}_\varepsilon^{\mathbf{h}}(\mathcal{T}_e^{\mathbf{e}}(\gamma_{11}(\mathbf{u}^{e\varepsilon}))) + \mathcal{T}_\varepsilon^{\mathbf{h}}(\mathcal{T}_e^{\mathbf{e}}(\gamma_{22}(\mathbf{u}^{e\varepsilon}))))\Big]\,\Gamma_{33}(\mathbf{V})$$
$$+2\mu\mathcal{T}_\varepsilon^{\mathbf{h}}(\mathcal{T}_e^{\mathbf{e}}(\gamma_{13}(\mathbf{u}^{e\varepsilon})))\Gamma_{13}(\mathbf{V}) + 2\mu\mathcal{T}_\varepsilon^{\mathbf{h}}(\mathcal{T}_e^{\mathbf{e}}(\gamma_{23}(\mathbf{u}^{e\varepsilon})))\Gamma_{13}(\mathbf{V})\Big\}\,dY_1dY_2dX_1dX_2dx_3,$$

and the right-hand term is given by

$$\int_{\Omega^*_{e,\varepsilon}} \mathbf{f}^{e\varepsilon}\cdot\mathbf{v}dx = \frac{e^2}{|\mathbf{Y}^*|}\int_{\Omega\times\mathbf{Y}^*}\left(f_\alpha\mathcal{V}_\alpha + f_3\mathcal{V}_3 + (X_1^2+X_2^2)f_T\mathcal{A}_3\right)dY_1dY_2dX_1dX_2dx_3.$$

Then, by passing to the limit when e,ε go to zero, we obtain the unfolded problem

$$\int_{\Omega\times\mathbf{Y}^*}\{[(\lambda+2\mu)\Gamma_{33}(\mathbf{U})+\lambda(\Gamma_{11}(\mathbf{U})+\Gamma_{22}(\mathbf{U}))]\,\Gamma_{33}(\mathbf{V})$$
$$+2\mu\Gamma_{13}(\mathbf{U})\Gamma_{13}(\mathbf{V})+2\mu\Gamma_{23}(\mathbf{U})\Gamma_{13}(\mathbf{V})\}\,dY_1dY_2dX_1dX_2dx_3 =$$
$$\int_{\Omega\times\mathbf{Y}^*}\left(f_1\mathcal{V}_1+f_2\mathcal{V}_2+(X_1^2+X_2^2)f_T\mathcal{A}_3\right)dY_1dY_2dX_1dX_2dx_3,$$

where

$$\mathbf{U} = \begin{pmatrix} \mathcal{U}_1 - X_2\mathcal{R}_3 \\ \mathcal{U}_2 + X_1\mathcal{R}_3 \\ \mathcal{U}_3 - X_1\frac{d\mathcal{U}_1}{dx_3} - X_2\frac{d\mathcal{U}_2}{dx_3}\end{pmatrix} + \overline{\mathbf{U}} + \hat{\mathbf{u}} = \mathbf{U}_e + \overline{\mathbf{U}} + \hat{\mathbf{u}}. \tag{16.20}$$

Then, we obtain the unfolded problem

$$\int_{\Omega\times\mathbf{Y}^*} a_{ijkl}\Gamma_{kl}(\mathbf{U})\Gamma_{ij}(\mathbf{V}_e)dY_1dY_2dX_1dX_2dx_3 =$$
$$\int_{\Omega\times\mathbf{Y}^*}\left(f_1\mathcal{V}_1+f_2\mathcal{V}_2+(X_1^2+X_2^2)f_T\mathcal{A}_3\right)dY_1dY_2dX_1dX_2dx_3,\ \forall\mathbf{V}_e. \tag{16.21}$$

Next, we choose as test function in (16.1)

$$\mathbf{v}(x_1,x_2,x_3) = e\overline{\mathbf{V}}(\frac{x_1}{e},\frac{x_2}{e},x_3),$$

where $\overline{\mathbf{V}}\in H^1(\Omega;\mathbb{R}^3)$. So, we have that

$$\mathcal{T}_e^{\mathbf{e}}(\gamma_{\alpha\alpha}(\mathbf{v})) = \frac{\partial\overline{V}_\alpha}{\partial X_\alpha} = \Gamma_{\alpha\alpha}(\overline{\mathbf{V}}),$$
$$\mathcal{T}_e^{\mathbf{e}}(\gamma_{\alpha\beta}(\mathbf{v})) = \frac{1}{2}\left(\frac{\partial\overline{V}_\alpha}{\partial X_\beta}+\frac{\partial\overline{V}_\beta}{\partial X_\alpha}\right) = \Gamma_{\alpha\beta}(\overline{\mathbf{V}}),$$
$$\mathcal{T}_e^{\mathbf{e}}(\gamma_{13}(\mathbf{v})) = \frac{1}{2}\left(e\frac{\partial\overline{V}_1}{\partial x_3}+\frac{\partial\overline{V}_3}{\partial X_1}\right)\longrightarrow\Gamma_{13}(\overline{\mathbf{V}}),$$
$$\mathcal{T}_e^{\mathbf{e}}(\gamma_{23}(\mathbf{v})) = \frac{1}{2}\left(e\frac{\partial\overline{V}_2}{\partial x_3}+\frac{\partial\overline{V}_3}{\partial X_2}\right)\longrightarrow\Gamma_{23}(\overline{\mathbf{V}}),$$
$$\mathcal{T}_e^{\mathbf{e}}(\gamma_{33}(\mathbf{v})) = e\frac{\partial\overline{V}_3}{\partial x_3}\longrightarrow\Gamma_{33}(\overline{\mathbf{V}}) = 0,$$

strongly in $L^2(\Omega)$ when e goes to zero. Moreover, by property $iv)$ of Proposition 15.4.2, $\mathcal{T}_\varepsilon^{\mathbf{h}}(\mathcal{T}_e^{\mathbf{e}}(\gamma_{ij}(\mathbf{v})))$ converge strongly in $L^2(\mathbf{Y}^*\times\Omega)$. Then, we obtain that the left-hand term in (16.1) can be written

$$\int_{\Omega^*_{e,\varepsilon}}\mathbf{\Lambda}\boldsymbol{\gamma}(\mathbf{u}^{e\varepsilon}):\boldsymbol{\gamma}(\mathbf{v})dx_1dx_2dx_3 = e^2\int_0^L\int_{\omega^*_\varepsilon}a_{ijkl}\mathcal{T}_e^{\mathbf{e}}(\gamma_{kl}(\mathbf{u}^{e\varepsilon}))\mathcal{T}_e^{\mathbf{e}}(\gamma_{ij}(\overline{\mathbf{V}}))dX_1dX_2dx_3 =$$
$$\frac{e^2}{|\mathbf{Y}^*|}\int_{\Omega\times\mathbf{Y}^*}a_{ijkl}\mathcal{T}_\varepsilon^{\mathbf{h}}\mathcal{T}_e^{\mathbf{e}}(\gamma_{kl}(\mathbf{u}^{e\varepsilon}))\mathcal{T}_\varepsilon^{\mathbf{h}}\mathcal{T}_e^{\mathbf{e}}(\gamma_{ij}(\overline{\mathbf{V}}))dY_1dY_2dX_1dX_2dx_3,$$

and the right-hand term is given by

$$\int_{\Omega_e^*} \mathbf{f}^{e\varepsilon} \cdot \mathbf{v} dx = \frac{e^2}{|\mathbf{Y}^*|} \int_{\Omega \times \mathbf{Y}^*} e \left(e f_1 \overline{V}_1 + e f_2 \overline{V}_2 + f_3 \overline{V}_3 \right.$$
$$\left. - X_2 f_T \overline{V}_1 + X_1 f_T \overline{V}_2 \right) dY_1 dY_2 dX_1 dX_2 dx_3.$$

So, by passing to the limit when e, ε go to zero and taking into account that $H^1(\Omega; \mathbb{R}^3)$ is dense in $L^2(0, L; H^1(\omega; \mathbb{R}^3))$, we obtain the unfolded problem

$$\int_{\Omega \times \mathbf{Y}^*} a_{ijkl} \Gamma_{kl}(\mathbf{U}) \Gamma_{ij}(\bar{\mathbf{V}}) dY_1 dY_2 dX_1 dX_2 dx_3 = 0, \tag{16.22}$$
$$\forall\, \bar{\mathbf{V}} \in L^2(0, L; H^1(\omega; \mathbb{R}^3)).$$

Similarly, we choose as a test function in (16.1)

$$\mathbf{v}(x_1, x_2, x_3) = e\varepsilon \psi \left(\frac{x_1}{e}, \frac{x_2}{e}, x_3 \right) \hat{\mathbf{v}} \left(\frac{x_1}{e\varepsilon}, \frac{x_2}{e\varepsilon} \right),$$

where $\psi \in \mathcal{D}(\Omega)$, $\hat{\mathbf{v}} \in H^1_{per}(\mathbf{Y}^*; \mathbb{R}^3)$. So, we have that

$$\mathcal{T}_e^{\mathbf{e}}(\gamma_{\alpha\alpha}(\mathbf{v})) = \varepsilon \frac{\partial \psi}{\partial X_\alpha} \hat{v}_\alpha + \psi \frac{\partial \hat{v}_\alpha}{\partial Y_\alpha} \longrightarrow \psi \Gamma_{\alpha\alpha}(\hat{\mathbf{v}}),$$
$$\mathcal{T}_e^{\mathbf{e}}(\gamma_{\alpha\beta}(\mathbf{v})) = \frac{1}{2} \left(\varepsilon \frac{\partial \psi}{\partial X_\beta} \hat{v}_\alpha + \psi \frac{\partial \hat{v}_\alpha}{\partial Y_\beta} + \varepsilon \frac{\partial \psi}{\partial X_\alpha} \hat{v}_\beta + \psi \frac{\partial \hat{v}_\beta}{\partial Y_\alpha} \right) \longrightarrow \psi \Gamma_{\alpha\beta}(\hat{\mathbf{v}}),$$
$$\mathcal{T}_e^{\mathbf{e}}(\gamma_{13}(\mathbf{v})) = \frac{1}{2} \left(e\varepsilon \frac{\partial \psi}{\partial x_3} \hat{v}_1 + \varepsilon \frac{\partial \psi}{\partial X_1} \hat{v}_3 + \psi \frac{\partial \hat{v}_3}{\partial Y_1} \right) \longrightarrow \psi \Gamma_{13}(\mathbf{V}),$$
$$\mathcal{T}_e^{\mathbf{e}}(\gamma_{23}(\mathbf{V})) = \frac{1}{2} \left(e\varepsilon \frac{\partial \psi}{\partial x_3} \hat{v}_2 + \varepsilon \frac{\partial \psi}{\partial X_2} \hat{v}_3 + \psi \frac{\partial \hat{v}_3}{\partial Y_2} \right) \longrightarrow \psi \Gamma_{23}(\mathbf{V}),$$
$$\mathcal{T}_e^{\mathbf{e}}(\gamma_{33}(\mathbf{V})) = e\varepsilon \frac{\partial \psi}{\partial x_3} \hat{v}_3 \longrightarrow 0,$$

strongly in $L^2(\Omega)$ when e, ε goes to zero. Again, thanks to property $iv)$ of Proposition 15.4.2, $\mathcal{T}_\varepsilon^{\mathbf{h}}(\mathcal{T}_e^{\mathbf{e}}(\gamma_{ij}(\mathbf{v})))$ converge strongly in $L^2(\mathbf{Y}^* \times \Omega)$. By passing to the limit and taking into account that $\mathcal{D}(\Omega) \oplus H^1_{per}(\mathbf{Y}^*; \mathbb{R}^3)$ is dense in $L^2(\Omega; H^1_{per}(\mathbf{Y}^*; \mathbb{R}^3))$, we obtain the unfolded problem

$$\int_{\Omega \times \mathbf{Y}^*} a_{ijkl} \Gamma_{kl}(\mathbf{U}) \Gamma_{ij}(\hat{\mathbf{v}}) dY_1 dY_2 dX_1 dX_2 dx_3 = 0, \tag{16.23}$$
$$\forall\, \hat{\mathbf{v}} \in L^2(\Omega; H^1_{per}(\mathbf{Y}^*; \mathbb{R}^3)).$$

Consequently, from unfolded problems (16.21)-(16.23) we have obtained expression (16.19) for any $\mathbf{V} \in \mathcal{D}$. □

Remark 16.2.5. *Problem (UP) has a unique solution in $\mathcal{D}$.*

Our next aim will be to obtain the limit problems associated to limit elementary displacements $\mathcal{U}$ and $\mathcal{R}_3$.

16.2.1 Determinating $\hat{u}_3$, $\overline{U}_3$ and $\mathcal{R}_3$

Firstly, we are going to obtain an expression for $\hat{u}_3$ in terms of $\overline{U}_3$ and $\mathcal{R}_3$. Let $\phi \in L^2(\Omega)$, $\psi \in H^1_{per}(\mathbf{Y}^*)$ and we choose in expression (16.19) test functions in the form

$$\mathbf{V}(Y_1, Y_2, X_1, X_2, x_3) = \hat{\mathbf{v}}(Y_1, Y_2, X_1, X_2, x_3) = \psi(Y_1, Y_2)\phi(X_1, X_2, x_3)\mathbf{e}_3;$$

so,

$$\begin{aligned}
&\Gamma_{\alpha\alpha}(\mathbf{V}) = \Gamma_{12}(\mathbf{V}) = 0,\\
&\Gamma_{33}(\mathbf{V}) = 0,\\
&\Gamma_{13}(\mathbf{V}) = \frac{1}{2}\phi\frac{\partial\psi}{\partial Y_1},\ \Gamma_{23}(\mathbf{V}) = \frac{1}{2}\phi\frac{\partial\psi}{\partial Y_2}.
\end{aligned}$$

Then, we have that

$$\begin{aligned}
&\int_{\mathbf{Y}^*\times\Omega} 2\mu\Gamma_{13}(\mathbf{U})\phi\frac{\partial\psi}{\partial Y_1}dY_1dY_2dx_3dX_1dX_2 +\\
&\int_{\mathbf{Y}^*\times\Omega} 2\mu\Gamma_{23}(\mathbf{U})\phi\frac{\partial\psi}{\partial Y_2}dY_1dY_2dx_3dX_1dX_2 = 0,
\end{aligned}$$

and we can supress the integral over Ω, obtaining that

$$\int_{\mathbf{Y}^*} \nabla_Y\hat{u}_3 : \nabla_Y\psi dY = -\int_{\mathbf{Y}^*} 2\Gamma_{\alpha 3}(\mathbf{U}_e + \overline{\mathbf{U}})\frac{\partial\psi}{\partial Y_\alpha}dY_1dY_2,\ \forall\psi \in H^1_{per}(\mathbf{Y}^*).$$

In order to simplify the previous limit problem, we define some suitable correctors

$$\begin{aligned}
&\hat{\chi}_\alpha \in H^1_{per}(\mathbf{Y}^*),\\
&\int_{\mathbf{Y}^*} \nabla_Y\hat{\chi}_\alpha : \nabla_Y\psi dY = -\int_{\mathbf{Y}^*} \frac{\partial\psi}{\partial Y_\alpha}dY, \quad \forall\psi \in H^1_{per}(\mathbf{Y}^*).
\end{aligned} \tag{16.24}$$

Consequently,

$$\hat{u}_3 = \left(-X_2\frac{d\mathcal{R}_3}{dx_3} + \frac{\partial\bar{U}_3}{\partial X_1}\right)\hat{\chi}_1 + \left(X_1\frac{d\mathcal{R}_3}{dx_3} + \frac{\partial\bar{U}_3}{\partial X_2}\right)\hat{\chi}_2. \tag{16.25}$$

Remark 16.2.6. *By choosing suitable test functions and by using some very simple changes of variable like*

$$\begin{aligned}
&\tilde{Y}_1 = Y_1,\ \tilde{Y}_2 = 1 - Y_2,\\
&\tilde{Y}_1 = 1 - Y_1,\ \tilde{Y}_2 = Y_2,
\end{aligned}$$

it is easy to prove that correctors $\hat{\chi}_\alpha$ verify

$$\begin{aligned}
&\hat{\chi}_1(Y_1, Y_2) = \hat{\chi}_1(Y_1, 1 - Y_2) = -\hat{\chi}_1(1 - Y_1, Y_2),\\
&\hat{\chi}_2(Y_1, Y_2) = -\hat{\chi}_2(Y_1, 1 - Y_2) = \hat{\chi}_2(1 - Y_1, Y_2),
\end{aligned}$$

Consequently,

$$\int_{\mathbf{Y}^*} \frac{\partial \hat{\chi}_\alpha}{\partial Y_\beta} dY_1 dY_2 = 0.$$

Similarly, if we consider the change of variable $\tilde{Y}_1 = Y_2$, $\tilde{Y}_2 = Y_1$, *we obtain the following relations:*

$$\hat{\chi}_1(Y_1, Y_2) = \hat{\chi}_2(Y_2, Y_1),$$

and, consequently,

$$\int_{\mathbf{Y}^*} \frac{\partial \hat{\chi}_1}{\partial Y_1} dY_1 dY_2 = \int_{\mathbf{Y}^*} \frac{\partial \hat{\chi}_2}{\partial Y_2} dY_1 dY_2.$$

Secondly, we are going to obtain an expression for $\overline{U}_3$ in terms of $\mathcal{R}_3$. By choosing in expression (16.19)

$$\mathbf{V}(Y_1, Y_2, X_1, X_2, x_3) = \overline{\mathbf{V}}(X_1, X_2, x_3) = \phi(x_3)\overline{V}(X_1, X_2)\mathbf{e}_3,$$

where $\phi \in L^2(0, L)$, $\overline{V} \in H^1(\omega)$, we have that

$$\int_{\mathbf{Y}^* \times \Omega} \mu \left(-X_2 \frac{d\mathcal{R}_3}{dx_3} + \frac{\partial \overline{U}_3}{\partial X_1} + \frac{\partial \hat{u}_3}{\partial Y_1} \right) \phi \frac{\partial \overline{V}}{\partial X_1} dY_1 dY_2 dX_1 dX_2 dx_3 +$$
$$\int_{\mathbf{Y}^* \times \Omega} \mu \left(X_1 \frac{d\mathcal{R}_3}{dx_3} + \frac{\partial \overline{U}_3}{\partial X_2} + \frac{\partial \hat{u}_3}{\partial Y_2} \right) \phi \frac{\partial \overline{V}}{\partial X_2} dY_1 dY_2 dX_1 dX_2 dx_3 = 0,$$

for all $\phi \in L^2(0, L)$, $\overline{V} \in H^1(\omega)$. Again, we can suppress the integral over $(0, L)$. By taking into account expression (16.25),

$$\int_{\mathbf{Y}^* \times \omega} \mu \left[-X_2 \frac{d\mathcal{R}_3}{dx_3} + \frac{\partial \overline{U}_3}{\partial X_1} + \left(-X_2 \frac{d\mathcal{R}_3}{dx_3} + \frac{\partial \bar{U}_3}{\partial X_1} \right) \frac{\partial \hat{\chi}_1}{\partial Y_1} + \left(X_1 \frac{d\mathcal{R}_3}{dx_3} + \frac{\partial \bar{U}_3}{\partial X_2} \right) \frac{\hat{\chi}_2}{\partial Y_1} \right] \frac{\partial \overline{V}}{\partial X_1} dY dX +$$
$$\int_{\mathbf{Y}^* \times \omega} \mu \left[X_1 \frac{d\mathcal{R}_3}{dx_3} + \frac{\partial \overline{U}_3}{\partial X_2} + \left(-X_2 \frac{d\mathcal{R}_3}{dx_3} + \frac{\partial \bar{U}_3}{\partial X_1} \right) \frac{\partial \hat{\chi}_1}{\partial Y_2} + \left(X_1 \frac{d\mathcal{R}_3}{dx_3} + \frac{\partial \bar{U}_3}{\partial X_2} \right) \frac{\hat{\chi}_2}{\partial Y_2} \right] \frac{\partial \overline{V}}{\partial X_2} dY dX = 0,$$

and thanks to Remark 16.2.6,

$$\int_\omega \int_{\mathbf{Y}^*} \left(1 + \frac{\partial \hat{\chi}_1}{\partial Y_1} \right) \left(-X_2 \frac{d\mathcal{R}_3}{dx_3} + \frac{\partial \overline{U}_3}{\partial X_1} \right) \frac{\partial \overline{V}}{\partial X_1} dY dX +$$
$$\int_\omega \int_{\mathbf{Y}^*} \left(1 + \frac{\partial \hat{\chi}_2}{\partial Y_2} \right) \left(X_1 \frac{d\mathcal{R}_3}{dx_3} + \frac{\partial \overline{U}_3}{\partial X_2} \right) \frac{\partial \overline{V}}{\partial X_2} dY dX = 0, \, \forall \overline{V} \in H^1(\omega).$$

Therefore, we define

$$b^* = \int_{\mathbf{Y}^*} \left(1 + \frac{\partial \hat{\chi}_1}{\partial Y_1} \right) dY = \int_{\mathbf{Y}^*} \left(1 + \frac{\partial \hat{\chi}_2}{\partial Y_2} \right) dY,$$

thanks to symmetry properties of Remark 16.2.6, and the previous problem remains

$$\int_\omega b^* \left(-X_2 \frac{d\mathcal{R}_3}{dx_3} + \frac{\partial \overline{U}_3}{\partial X_1} \right) \frac{\partial \overline{V}}{\partial X_1} dX_1 dX_2 +$$
$$\int_\omega b^* \left(X_1 \frac{d\mathcal{R}_3}{dx_3} + \frac{\partial \overline{U}_3}{\partial X_2} \right) \frac{\partial \overline{V}}{\partial X_2} dX_1 dX_2 = 0, \, \forall \overline{V} \in H^1(\omega).$$

Moreover,

$$b^* = \int_{\mathbf{Y}^*} \left(1 + \frac{\partial \hat{\chi}_1}{\partial Y_1}\right) dY > 0.$$

In fact, by using definition of corrector $\hat{\chi}_\alpha$,

$$\int_{\mathbf{Y}^*} |\nabla_Y(\hat{\chi}_1 + Y_1)|^2 dY = \int_{\mathbf{Y}^*} \left[\left(\frac{\partial \hat{\chi}_1}{\partial Y_1} + 1\right)^2 + \left(\frac{\partial \hat{\chi}_1}{\partial Y_2}\right)\right]^2 dY =$$
$$\int_{\mathbf{Y}^*} \left(\frac{\partial \hat{\chi}_1}{\partial Y_1}\frac{\partial \hat{\chi}_1}{\partial Y_1} + \frac{\partial \hat{\chi}_1}{\partial Y_2}\frac{\partial \hat{\chi}_1}{\partial Y_2} + 1 + 2\frac{\partial \hat{\chi}_1}{\partial Y_1}\right) dY = \int_{\mathbf{Y}^*} \left(-\frac{\partial \hat{\chi}_1}{\partial Y_1} + 1 + 2\frac{\partial \hat{\chi}_1}{\partial Y_1}\right) dY =$$
$$\int_{\mathbf{Y}^*} \left(1 + \frac{\partial \hat{\chi}_1}{\partial Y_1}\right) dY = b^* \geq 0.$$

If $b^* = 0$, then $\hat{\chi}_1 + Y_1 = C$, which is impossible, since $\hat{\chi}_1 \in H^1_{per}(\mathbf{Y}^*)$.

Therefore,

$$b^* = \int_{\mathbf{Y}^*} \left(1 + \frac{\partial \hat{\chi}_\alpha}{\partial Y_\alpha}\right) dY = \int_{\mathbf{Y}^*} |\nabla_Y(\hat{\chi}_\alpha + Y_\alpha)|^2 dY, \tag{16.26}$$

and we obtain the problem

$$\int_\omega \nabla_X \overline{U}_3 : \nabla_X \overline{V} dX_1 dX_2 =$$
$$-\int_\omega \left(-X_2 \frac{d\mathcal{R}_3}{dx_3}\frac{\partial \overline{V}}{\partial X_1} + X_1 \frac{d\mathcal{R}_3}{dx_3}\frac{\partial \overline{V}}{\partial X_2}\right) dX_1 dX_2, \, \forall \overline{V} \in H^1(\omega).$$

We introduce the corrector $\overline{\chi}$ which is the solution of the problem

$$\overline{\chi} \in H^1(\omega),$$
$$\int_\omega \nabla_X \overline{\chi} : \nabla_X \bar{\psi} dX = -\int_\omega \left(X_1 \frac{\partial \bar{\psi}}{\partial X_2} - X_2 \frac{\partial \bar{\psi}}{\partial X_1}\right) dX, \, \forall \bar{\psi} \in H^1(\omega). \tag{16.27}$$

Consequently,

$$\overline{U}_3(X_1, X_2, x_3) = \frac{d\mathcal{R}_3}{dx_3}(x_3)\overline{\chi}(X_1, X_2). \tag{16.28}$$

Thirdly, we are going to obtain the problem associated to $\mathcal{R}_3$. By choosing in expression (16.19)

$$\mathbf{V}(Y_1, Y_2, X_1, X_2, x_3) = \begin{pmatrix} -X_2 \mathcal{A}_3 \\ X_1 \mathcal{A}_3 \\ 0 \end{pmatrix},$$

where $\mathcal{A}_3 \in H^1(0, L)$, we have that

$$-\int_{\mathbf{Y}^* \times \Omega} \mu \left(-X_2 \frac{d\mathcal{R}_3}{dx_3} + \frac{\partial \overline{U}_3}{\partial X_1} + \frac{\partial \hat{u}_3}{\partial Y_1}\right) X_2 \frac{d\mathcal{A}_3}{dx_3} dY_1 dY_2 dX_1 dX_2 dx_3 +$$
$$\int_{\mathbf{Y}^* \times \Omega} \mu \left(X_1 \frac{d\mathcal{R}_3}{dx_3} + \frac{\partial \overline{U}_3}{\partial X_2} + \frac{\partial \hat{u}_3}{\partial Y_2}\right) X_1 \frac{d\mathcal{A}_3}{dx_3} dY_1 dY_2 dX_1 dX_2 dx_3 =$$
$$\int_0^L \int_\omega \int_{\mathbf{Y}^*} (X_1^2 + X_2^2) f_T \mathcal{A}_3 dY_1 dY_2 dX_1 dX_2 dx_3.$$

Taking into account expression (16.25) and Remark 16.2.6,

$$-\int_{\mathbf{Y}^*\times\Omega}\mu\left(-X_2\frac{d\mathcal{R}_3}{dx_3}+\frac{\partial\overline{U}_3}{\partial X_1}+\left(-X_2\frac{d\mathcal{R}_3}{dx_3}+\frac{\partial\bar{U}_3}{\partial X_1}\right)\frac{\partial\hat{\chi}_1}{\partial Y_1}\right)X_2\frac{d\mathcal{A}_3}{dx_3}dYdXdx_3+$$
$$\int_{\mathbf{Y}^*\times\Omega}\mu\left(X_1\frac{d\mathcal{R}_3}{dx_3}+\frac{\partial\overline{U}_3}{\partial X_2}+\left(X_1\frac{d\mathcal{R}_3}{dx_3}+\frac{\partial\bar{U}_3}{\partial X_2}\right)\frac{\partial\hat{\chi}_2}{\partial Y_2}\right)X_1\frac{d\mathcal{A}_3}{dx_3}dYdXdx_3=$$
$$\int_0^L\int_\omega(X_1^2+X_2^2)f_T\mathcal{A}_3dYdXdx_3,$$

that is,

$$-\int_{\mathbf{Y}^*\times\Omega}\mu b^*\left(-X_2\frac{d\mathcal{R}_3}{dx_3}+\frac{\partial\overline{U}_3}{\partial X_1}\right)X_2\frac{d\mathcal{A}_3}{dx_3}dX_1dX_2dx_3+$$
$$\int_{\mathbf{Y}^*\times\Omega}\mu b^*\left(X_1\frac{d\mathcal{R}_3}{dx_3}+\frac{\partial\overline{U}_3}{\partial X_2}\right)X_1\frac{d\mathcal{A}_3}{dx_3}dX_1dX_2dx_3=$$
$$\int_0^L\int_\omega(X_1^2+X_2^2)f_T\mathcal{A}_3dX_1dX_2dx_3.$$

Taking into account expression (16.28), the previous problem is written

$$-\int_\Omega\mu b^*\left(-X_2+\frac{\partial\overline{\chi}}{\partial X_1}\right)X_2\frac{d\mathcal{R}_3}{dx_3}\frac{d\mathcal{A}_3}{dx_3}dX_1dX_2dx_3+$$
$$\int_\Omega\mu b^*\left(X_1+\frac{\partial\overline{\chi}}{\partial X_2}\right)X_1\frac{d\mathcal{R}_3}{dx_3}\frac{d\mathcal{A}_3}{dx_3}dX_1dX_2dx_3=$$
$$\int_0^L\int_\omega(X_1^2+X_2^2)f_T\mathcal{A}_3dX_1dX_2dx_3.$$

Then,

$$\int_0^L\mu b^*b_\omega\frac{d\mathcal{R}_3}{dx_3}\frac{d\mathcal{A}_3}{dx_3}dx_3=\int_0^L\int_\omega(X_1^2+X_2^2)f_T\mathcal{A}_3dX_1dX_2dx_3,$$

where

$$b_\omega=\int_\omega\left[X_2\left(X_2-\frac{\partial\overline{\chi}}{\partial X_1}\right)+X_1\left(X_1+\frac{\partial\overline{\chi}}{\partial X_2}\right)\right]dX_1dX_2.$$

It is easy to prove that the coefficient b_ω is strictly positive. In fact, taking into account definition of corrector $\overline{\chi}$, we have that

$$\int_\omega\left[\left(\frac{\partial\overline{\chi}}{\partial X_1}-X_2\right)^2+\left(\frac{\partial\overline{\chi}}{\partial X_2}+X_1\right)^2\right]dX=$$
$$\int_\omega\left(\frac{\partial\overline{\chi}}{\partial X_1}\frac{\partial\overline{\chi}}{\partial X_1}+\frac{\partial\overline{\chi}}{\partial X_2}\frac{\partial\overline{\chi}}{\partial X_2}-2X_2\frac{\partial\overline{\chi}}{\partial X_1}+2X_1\frac{\partial\overline{\chi}}{\partial X_2}+X_2^2+X_1^2\right)dX=$$
$$\int_\omega\left(-X_1\frac{\partial\overline{\chi}}{\partial X_2}+X_2\frac{\partial\overline{\chi}}{\partial X_1}-2X_2\frac{\partial\overline{\chi}}{\partial X_1}+2X_1\frac{\partial\overline{\chi}}{\partial X_2}+X_2^2+X_1^2\right)dX=$$
$$\int_\omega\left(-X_2\frac{\partial\overline{\chi}}{\partial X_1}+X_1\frac{\partial\overline{\chi}}{\partial X_2}+X_2^2+X_1^2\right)dX=b_\omega\geq0.$$

If $b_\omega = 0$, then

$$\frac{\partial \overline{\chi}}{\partial X_1} = X_2,\ \frac{\partial \overline{\chi}}{\partial X_2} = -X_1,$$

which leads to

$$\frac{\partial^2 \overline{\chi}}{\partial X_2 X_1} = 1,\ \frac{\partial^2 \overline{\chi}}{\partial X_1 X_2} = -1,$$

which is impossible.

Therefore,

$$b_\omega = \int_\omega \left[X_2 \left(X_2 - \frac{\partial \overline{\chi}}{\partial X_1} \right) + X_1 \left(X_1 + \frac{\partial \overline{\chi}}{\partial X_2} \right) \right] dX = \int_\omega \left[\left(\frac{\partial \overline{\chi}}{\partial X_1} - X_2 \right)^2 + \left(\frac{\partial \overline{\chi}}{\partial X_2} + X_1 \right)^2 \right] dX. \tag{16.29}$$

In conclusion, we have obtained a problem for $\mathcal{R}_3$

$$\int_0^L K^* \frac{d\mathcal{R}_3}{dx_3} \frac{d\mathcal{A}_3}{dx_3} dx_3 = \int_0^L \frac{1}{6} f_T \mathcal{A}_3 dx_3, \quad \forall \mathcal{A}_3 \in H^1(0, L),$$

where

$$K^* = \mu b^* b_\omega = \mu \int_\omega \int_{\mathbf{Y}^*} |\nabla_Y (\hat{\chi}_\alpha + Y_\alpha)|^2 \left[\left(\frac{\partial \overline{\chi}}{\partial X_1} - X_2 \right)^2 + \left(\frac{\partial \overline{\chi}}{\partial X_2} + X_1 \right)^2 \right] dY dX.$$

16.2.2 Determinating $\hat{u}_\alpha$, $\overline{U}_\alpha$, $\mathcal{U}_\alpha$ and $\mathcal{U}_3$

Firstly, we are going to obtain an expression for $\hat{u}_\alpha$ in terms of $\overline{U}_\alpha$, $\mathcal{U}_\alpha$ and $\mathcal{U}_3$. Let introduce some notation we will use in this paragraph:

$$\gamma_{\alpha\beta,Y}(\hat{\mathbf{v}}) = \frac{1}{2} \left(\frac{\partial \hat{v}_\alpha}{\partial Y_\beta} + \frac{\partial \hat{v}_\beta}{\partial Y_\alpha} \right),\ \forall \overline{\mathbf{V}} \in H^1_{per}(\mathbf{Y}^*; \mathbb{R}^2),$$
$$\gamma_{\alpha\beta,X}(\overline{\mathbf{V}}) = \frac{1}{2} \left(\frac{\partial \overline{U}_\alpha}{\partial X_\beta} + \frac{\partial \overline{U}_\beta}{\partial X_\alpha} \right),\ \forall \overline{\mathbf{V}} \in H^1(\omega; \mathbb{R}^2).$$

Let $\phi \in L^2(\Omega)$, $\boldsymbol{\psi} \in H^1_{per}(\mathbf{Y}; \mathbb{R}^2)$ and we choose in expression (16.19) test functions in the form

$$\mathbf{V}(Y_1, Y_2, X_1, X_2, x_3) = \psi_1(Y_1, Y_2)\phi(X_1, X_2, x_3)\mathbf{e}_1 + \psi_2(Y_1, Y_2)\phi(X_1, X_2, x_3)\mathbf{e}_2;$$

so,

$$\Gamma_{\alpha\beta}(\mathbf{V}) = \phi \gamma_{\alpha\beta,Y}(\boldsymbol{\psi}),$$
$$\Gamma_{13}(\mathbf{V}) = \Gamma_{23}(\mathbf{V}) = \Gamma_{33}(\mathbf{V}) = 0.$$

Then, we obtain the problem

$$\int_{\mathbf{Y}^*} a_{\alpha\beta\alpha'\beta'} \Gamma_{\alpha\beta}(\mathbf{U}) \gamma_{\alpha'\beta',Y}(\boldsymbol{\psi}) dY_1 dY_2 = 0,$$

that is,

$$\int_{\mathbf{Y}^*}\left[(\lambda+2\mu)\frac{\partial\hat{u}_1}{\partial Y_1}+\lambda\frac{\partial\hat{u}_2}{\partial Y_2}\right]\frac{\partial\psi_1}{\partial Y_1}dY_1dY_2+\int_{\mathbf{Y}^*}\left[(\lambda+2\mu)\frac{\partial\hat{u}_2}{\partial Y_2}+\lambda\frac{\partial\hat{u}_1}{\partial Y_1}\right]\frac{\partial\psi_2}{\partial Y_2}dY_1dY_2+$$
$$\int_{\mathbf{Y}^*}\mu\left(\frac{\partial\hat{u}_1}{\partial Y_2}+\frac{\partial\hat{u}_2}{\partial Y_1}\right)\left(\frac{\partial\psi_1}{\partial Y_2}+\frac{\partial\psi_2}{\partial Y_1}\right)dY_1dY_2=$$
$$-\left\{\int_{\mathbf{Y}^*}\left[(\lambda+2\mu)\Gamma_{11}(\mathbf{U}_e+\overline{\mathbf{U}})+\lambda\left(\Gamma_{22}(\mathbf{U}_e+\overline{\mathbf{U}})+\Gamma_{33}(\mathbf{U}_e+\overline{\mathbf{U}})\right)\right]\frac{\partial\psi_1}{\partial Y_1}dY_1dY_2+\right.$$
$$\int_{\mathbf{Y}^*}\left[(\lambda+2\mu)\Gamma_{22}(\mathbf{U}_e+\overline{\mathbf{U}})+\lambda\left(\Gamma_{11}(\mathbf{U}_e+\overline{\mathbf{U}})+\Gamma_{33}(\mathbf{U}_e+\overline{\mathbf{U}})\right)\right]\frac{\partial\psi_2}{\partial Y_2}dY_1dY_2+$$
$$\left.\int_{\mathbf{Y}^*}\mu\left(\Gamma_{12}(\mathbf{U}_e+\overline{\mathbf{U}})+\Gamma_{21}(\mathbf{U}_e+\overline{\mathbf{U}})\right)\left(\frac{\partial\psi_1}{\partial Y_2}+\frac{\partial\psi_2}{\partial Y_1}\right)dY_1dY_2\right\}.$$

In order to simplify the previous limit problem, we are going to define some suitable correctors:

$$\hat{\boldsymbol{\chi}}_{11}\in H^1_{per}(\mathbf{Y}^*;\mathbb{R}^2),$$
$$\int_{\mathbf{Y}^*}a_{\alpha\beta\alpha'\beta'}\gamma_{\alpha\beta,Y}(\hat{\boldsymbol{\chi}}_{11})\gamma_{\alpha'\beta',Y}(\boldsymbol{\psi})dY=-\int_{\mathbf{Y}^*}a_{\alpha\beta\alpha'\beta'}\gamma_{\alpha\beta,Y}(\mathbb{U}_{11})\gamma_{\alpha'\beta',Y}(\boldsymbol{\psi})dY,$$
$$\forall\boldsymbol{\psi}\in H^1_{per}(\mathbf{Y}^*;\mathbb{R}^2),$$

$$\hat{\boldsymbol{\chi}}_{22}\in H^1_{per}(\mathbf{Y}^*;\mathbb{R}^2),$$
$$\int_{\mathbf{Y}^*}a_{\alpha\beta\alpha'\beta'}\gamma_{\alpha\beta,Y}(\hat{\boldsymbol{\chi}}_{22})\gamma_{\alpha'\beta',Y}(\boldsymbol{\psi})dY=-\int_{\mathbf{Y}^*}a_{\alpha\beta\alpha'\beta'}\gamma_{\alpha\beta,Y}(\mathbb{U}_{22})\gamma_{\alpha'\beta',Y}(\boldsymbol{\psi})dY,$$
$$\forall\boldsymbol{\psi}\in H^1_{per}(\mathbf{Y}^*;\mathbb{R}^2),$$

$$\hat{\boldsymbol{\chi}}_{12}\in H^1_{per}(\mathbf{Y}^*;\mathbb{R}^2),$$
$$\int_{\mathbf{Y}^*}a_{\alpha\beta\alpha'\beta'}\gamma_{\alpha\beta,Y}(\hat{\boldsymbol{\chi}}_{12})\gamma_{\alpha'\beta',Y}(\boldsymbol{\psi})dY=-\int_{\mathbf{Y}^*}a_{\alpha\beta\alpha'\beta'}\gamma_{\alpha\beta,Y}(\mathbb{U}_{12})\gamma_{\alpha'\beta',Y}(\boldsymbol{\psi})dY,$$
$$\forall\boldsymbol{\psi}\in H^1_{per}(\mathbf{Y}^*;\mathbb{R}^2),$$

where

$$\mathbb{U}_{11}=Y_1\mathbf{e}_1,\ \mathbb{U}_{22}=Y_2\mathbf{e}_2,\ \mathbb{U}_{12}=Y_2\mathbf{e}_1+Y_1\mathbf{e}_2.$$

Consequently,

$$(\hat{u}_1,\hat{u}_2)=\left(\gamma_{11,X}(\overline{\mathbf{U}})+\nu\frac{d\tilde{\mathcal{U}}}{dx_3}\right)\hat{\boldsymbol{\chi}}_{11}+\left(\gamma_{22,X}(\overline{\mathbf{U}})+\nu\frac{d\tilde{\mathcal{U}}}{dx_3}\right)\hat{\boldsymbol{\chi}}_{22}+\gamma_{12,X}(\overline{\mathbf{U}})\hat{\boldsymbol{\chi}}_{12},\tag{16.30}$$

where ν is the Poisson coefficient and where $\tilde{\mathcal{U}}$ is defined by

$$\tilde{\mathcal{U}}(X_1,X_2,x_3)=\mathcal{U}_3(x_3)-X_1\frac{d\mathcal{U}_1}{dx_3}(x_3)-X_2\frac{d\mathcal{U}_2}{dx_3}(x_3).\tag{16.31}$$

Remark 16.2.7. *By choosing suitable test functions and by using some very simple changes of variable like*

$$\tilde{Y}_1=Y_1,\ \tilde{Y}_2=1-Y_2,$$
$$\tilde{Y}_1=1-Y_1,\ \tilde{Y}_2=Y_2,$$

it is easy to prove that correctors $\hat{\chi}_{\alpha\beta}$ *verify*

$$\hat{\chi}_{11,1}(Y_1,Y_2)=\hat{\chi}_{11,1}(Y_1,1-Y_2)=-\hat{\chi}_{11,1}(1-Y_1,Y_2),$$
$$\hat{\chi}_{11,2}(Y_1,Y_2)=-\hat{\chi}_{11,2}(Y_1,1-Y_2)=\hat{\chi}_{11,2}(1-Y_1,Y_2),$$

$$\hat{\chi}_{22,1}(Y_1,Y_2)=\hat{\chi}_{22,1}(Y_1,1-Y_2)=-\hat{\chi}_{22,1}(1-Y_1,Y_2),$$
$$\hat{\chi}_{22,2}(Y_1,Y_2)=-\hat{\chi}_{22,2}(Y_1,1-Y_2)=\hat{\chi}_{22,2}(1-Y_1,Y_2),$$

$$\hat{\chi}_{12,1}(Y_1,Y_2)=-\hat{\chi}_{12,1}(Y_1,1-Y_2)=\hat{\chi}_{12,1}(1-Y_1,Y_2),$$
$$\hat{\chi}_{12,2}(Y_1,Y_2)=\hat{\chi}_{12,2}(Y_1,1-Y_2)=-\hat{\chi}_{12,2}(1-Y_1,Y_2).$$

Consequently,

$$\int_{\mathbf{Y}^*}\gamma_{12,Y}(\hat{\boldsymbol{\chi}}_{\alpha\alpha})dY_1dY_2=0,$$
$$\int_{\mathbf{Y}^*}\gamma_{\alpha\alpha,Y}(\hat{\boldsymbol{\chi}}_{12})dY_1dY_2=0.$$

Similarly, if we consider the change of variable $\tilde{Y}_1=Y_2$, $\tilde{Y}_2=Y_1$, *we obtain the following relations:*

$$\hat{\chi}_{22,1}(Y_1,Y_2)=\hat{\chi}_{11,2}(Y_2,Y_1),$$
$$\hat{\chi}_{22,2}(Y_1,Y_2)=\hat{\chi}_{11,1}(Y_2,Y_1),$$

and, consequently,

$$\int_{\mathbf{Y}^*}\gamma_{11,Y}(\hat{\boldsymbol{\chi}}_{11})dY_1dY_2=\int_{\mathbf{Y}^*}\gamma_{22,Y}(\hat{\boldsymbol{\chi}}_{22})dY_1dY_2,$$
$$\int_{\mathbf{Y}^*}\gamma_{11,Y}(\hat{\boldsymbol{\chi}}_{22})dY_1dY_2=\int_{\mathbf{Y}^*}\gamma_{22,Y}(\hat{\boldsymbol{\chi}}_{11})dY_1dY_2.$$

Secondly, we are going to obtain an expression for $\overline{U}_\alpha$ in terms of $\mathcal{U}_\alpha$ and $\mathcal{U}_3$. By choosing in expression (16.19)

$$\mathbf{V}(Y_1,Y_2,X_1,X_2,x_3)=\phi(x_3)\overline{V}_1(X_1,X_2)\mathbf{e}_1+\phi(x_3)\overline{V}_2(X_1,X_2)\mathbf{e}_2,$$

where $\phi\in L^2(0,L)$, $\overline{\mathbf{V}}\in H^1(\omega;\mathbb{R}^2)$, we have that

$$\int_\omega\int_{\mathbf{Y}^*}a_{ijkl}\Gamma_{ij}(\mathbf{U})\Gamma_{kl}(\mathbf{V})dY_1dY_2dX_1dX_2=\int_\omega\int_{\mathbf{Y}^*}a_{\alpha\beta\alpha'\beta'}\Gamma_{\alpha\beta}(\mathbf{U})\Gamma_{\alpha'\beta'}(\mathbf{V})dYdX=$$
$$\int_\omega\int_{\mathbf{Y}^*}\{(\lambda+2\mu)[\gamma_{11,Y}(\hat{\mathbf{u}})+\Gamma_{11}(\mathbb{U})]+\lambda[\gamma_{22,Y}(\hat{\mathbf{u}})+\Gamma_{22}(\mathbb{U})]\}\,\gamma_{11,X}(\bar{\mathbf{V}})dYdX+$$
$$\int_\omega\int_{\mathbf{Y}^*}\{(\lambda+2\mu)[\gamma_{22,Y}(\hat{\mathbf{u}})+\Gamma_{22}(\mathbb{U})]+\lambda[\gamma_{11,Y}(\hat{\mathbf{u}})+\Gamma_{11}(\mathbb{U})]\}\,\gamma_{22,X}(\bar{\mathbf{V}})dYdX+$$
$$\int_\omega\int_{\mathbf{Y}^*}4\mu[\gamma_{12,Y}(\hat{\mathbf{u}})+\Gamma_{12}(\mathbb{U})]\gamma_{12,X}(\bar{\mathbf{V}})dYdX=0,$$

where we consider the formal displacement $\overline{\mathbb{U}} = \overline{\mathbb{U}}_1\mathbf{e}_1 + \overline{\mathbb{U}}_2\mathbf{e}_2$

$$\overline{\mathbb{U}}_1(X_1, X_2, x_3) = \overline{U}_1 + \nu\left(X_1\frac{d\mathcal{U}_3}{dx_3} - \frac{X_1^2 - X_2^2}{2}\frac{d^2\mathcal{U}_1}{dx_3^2} - X_1X_2\frac{d^2\mathcal{U}_2}{dx_3^2}\right),$$
$$\overline{\mathbb{U}}_2(X_1, X_2, x_3) = \overline{U}_2 + \nu\left(X_2\frac{d\mathcal{U}_3}{dx_3} - X_1X_2\frac{d^2\mathcal{U}_1}{dx_3^2} - \frac{X_2^2 - X_1^2}{2}\frac{d^2\mathcal{U}_2}{dx_3^2}\right),$$

verifying

$$\gamma_{\alpha\alpha,X}(\overline{\mathbb{U}}) = \gamma_{\alpha\alpha,X}(\bar{\mathbf{U}}) + \nu\frac{d\tilde{\mathcal{U}}}{dx_3},\ \gamma_{12,X}(\overline{\mathbb{U}}) = \gamma_{12,X}(\bar{\mathbf{U}}).$$

Moreover, $\overline{\mathbb{U}} \in L^2(0, L; H^1(\omega; \mathbb{R}^2))$ and

$$\int_\omega \overline{\mathbf{U}}_\alpha dX = \int_\omega (X_1\overline{\mathbf{U}}_2 - X_2\overline{\mathbf{U}}_1)dX = 0,$$

since $I_1 = I_2$ and

$$\int_\omega X_1X_2dX = 0.$$

Therefore, expression (16.30) remains

$$(\hat{u}_1, \hat{u}_2) = \gamma_{11,X}(\overline{\mathbb{U}})\hat{\boldsymbol{\chi}}_{11} + \gamma_{22,X}(\overline{\mathbb{U}})\hat{\boldsymbol{\chi}}_{22} + \gamma_{12,X}(\overline{\mathbb{U}})\hat{\boldsymbol{\chi}}_{12},$$

and we have that

$$\int_\omega\int_{\mathbf{Y}^*} \left\{(\lambda+2\mu)\left[\gamma_{11,X}(\overline{\mathbb{U}})\gamma_{11,Y}(\hat{\boldsymbol{\chi}}_{11}) + \gamma_{22,X}(\overline{\mathbb{U}})\gamma_{11,Y}(\hat{\boldsymbol{\chi}}_{22}) + \gamma_{12,X}(\overline{\mathbb{U}})\gamma_{11,Y}(\hat{\boldsymbol{\chi}}_{12}) + \gamma_{11,X}(\overline{\mathbb{U}})\right] +$$
$$\lambda\left[\gamma_{11,X}(\overline{\mathbb{U}})\gamma_{22,Y}(\hat{\boldsymbol{\chi}}_{11}) + \gamma_{22,X}(\overline{\mathbb{U}})\gamma_{22,Y}(\hat{\boldsymbol{\chi}}_{22}) + \gamma_{12,X}(\overline{\mathbb{U}})\gamma_{22,Y}(\hat{\boldsymbol{\chi}}_{12}) + \gamma_{22,X}(\overline{\mathbb{U}})\right]\right\}\gamma_{11,X}(\bar{\mathbf{V}})dYdX +$$
$$\int_\omega\int_{\mathbf{Y}^*} \left\{(\lambda+2\mu)\left[\gamma_{11,X}(\overline{\mathbb{U}})\gamma_{22,Y}(\hat{\boldsymbol{\chi}}_{11}) + \gamma_{22,X}(\overline{\mathbb{U}})\gamma_{22,Y}(\hat{\boldsymbol{\chi}}_{22}) + \gamma_{12,X}(\overline{\mathbb{U}})\gamma_{22,Y}(\hat{\boldsymbol{\chi}}_{12}) + \gamma_{22,X}(\overline{\mathbb{U}})\right] +$$
$$\lambda\left[\gamma_{11,X}(\overline{\mathbb{U}})\gamma_{11,Y}(\hat{\boldsymbol{\chi}}_{11}) + \gamma_{22,X}(\overline{\mathbb{U}})\gamma_{11,Y}(\hat{\boldsymbol{\chi}}_{22}) + \gamma_{12,X}(\overline{\mathbb{U}})\gamma_{11,Y}(\hat{\boldsymbol{\chi}}_{12}) + \gamma_{11,X}(\overline{\mathbb{U}})\right]\right\}\gamma_{22,X}(\bar{\mathbf{V}})dYdX +$$
$$\int_\omega\int_{\mathbf{Y}^*} 4\mu[\gamma_{12,X}(\overline{\mathbb{U}})\gamma_{12,Y}(\hat{\boldsymbol{\chi}}_{12}) + \gamma_{12,X}(\overline{\mathbb{U}})]\gamma_{12,X}(\bar{\mathbf{V}})dYdX = 0.$$

Thanks to remark 16.2.7, the problem is written

$$\int_\omega\int_{\mathbf{Y}^*} \left\{(\lambda+2\mu)\left[\gamma_{11,X}(\overline{\mathbb{U}})\gamma_{11,Y}(\hat{\boldsymbol{\chi}}_{11}) + \gamma_{22,X}(\overline{\mathbb{U}})\gamma_{11,Y}(\hat{\boldsymbol{\chi}}_{22}) + \gamma_{11,X}(\overline{\mathbb{U}})\right] +$$
$$\lambda\left[\gamma_{11,X}(\overline{\mathbb{U}})\gamma_{22,Y}(\hat{\boldsymbol{\chi}}_{11}) + \gamma_{22,X}(\overline{\mathbb{U}})\gamma_{22,Y}(\hat{\boldsymbol{\chi}}_{22}) + \gamma_{22,X}(\overline{\mathbb{U}})\right]\right\}\gamma_{11,X}(\bar{\mathbf{V}})dYdX +$$
$$\int_\omega\int_{\mathbf{Y}^*} \left\{(\lambda+2\mu)\left[\gamma_{11,X}(\overline{\mathbb{U}})\gamma_{22,Y}(\hat{\boldsymbol{\chi}}_{11}) + \gamma_{22,X}(\overline{\mathbb{U}})\gamma_{22,Y}(\hat{\boldsymbol{\chi}}_{22}) + \gamma_{22,X}(\overline{\mathbb{U}})\right] +$$
$$\lambda\left[\gamma_{11,X}(\overline{\mathbb{U}})\gamma_{11,Y}(\hat{\boldsymbol{\chi}}_{11}) + \gamma_{22,X}(\overline{\mathbb{U}})\gamma_{11,Y}(\hat{\boldsymbol{\chi}}_{22}) + \gamma_{11,X}(\overline{\mathbb{U}})\right]\right\}\gamma_{22,X}(\bar{\mathbf{V}})dYdX +$$
$$\int_\omega\int_{\mathbf{Y}^*} 4\mu[\gamma_{12,X}(\overline{\mathbb{U}})\gamma_{12,Y}(\hat{\boldsymbol{\chi}}_{12}) + \gamma_{12,X}(\overline{\mathbb{U}})]\gamma_{12,X}(\bar{\mathbf{V}})dYdX = 0.$$

Then,

$$\int_\omega \int_{\mathbf{Y}^*} \left\{(\lambda+2\mu)\left[(1+\gamma_{11,Y}(\hat{\boldsymbol{\chi}}_{11}))\gamma_{11,X}(\overline{\mathbb{U}})+\gamma_{22,X}(\overline{\mathbb{U}})\gamma_{11,Y}(\hat{\boldsymbol{\chi}}_{22})\right]+ \right.$$
$$\left.\lambda\left[\gamma_{11,X}(\overline{\mathbb{U}})\gamma_{22,Y}(\hat{\boldsymbol{\chi}}_{11})+(1+\gamma_{22,Y}(\hat{\boldsymbol{\chi}}_{22}))\gamma_{22,X}(\overline{\mathbb{U}})\right]\right\}\gamma_{11,X}(\bar{\mathbf{V}})dYdX+$$
$$\int_\omega \int_{\mathbf{Y}^*} \left\{(\lambda+2\mu)\left[\gamma_{11,X}(\overline{\mathbb{U}})\gamma_{22,Y}(\hat{\boldsymbol{\chi}}_{11})+(1+\gamma_{22,Y}(\hat{\boldsymbol{\chi}}_{22}))\gamma_{22,X}(\overline{\mathbb{U}})\right]+ \right.$$
$$\left.\lambda\left[(1+\gamma_{11,Y}(\hat{\boldsymbol{\chi}}_{11}))\gamma_{11,X}(\overline{\mathbb{U}})+\gamma_{22,X}(\overline{\mathbb{U}})\gamma_{11,Y}(\hat{\boldsymbol{\chi}}_{22})\right]\right\}\gamma_{22,X}(\bar{\mathbf{V}})dYdX+$$
$$\int_\omega \int_{\mathbf{Y}^*} 4\mu(1+\gamma_{12,Y}(\hat{\boldsymbol{\chi}}_{12}))\gamma_{12,X}(\overline{\mathbb{U}})\gamma_{12,X}(\bar{\mathbf{V}})dYdX=0.$$

By grouping terms, we obtain that

$$\int_\omega \int_{\mathbf{Y}^*} [(\lambda+2\mu)(1+\gamma_{11,Y}(\hat{\boldsymbol{\chi}}_{11}))+\lambda\gamma_{22,Y}(\hat{\boldsymbol{\chi}}_{11})]\gamma_{11,X}(\overline{\mathbb{U}})\gamma_{11,X}(\bar{\mathbf{V}})dYdX+$$
$$\int_\omega \int_{\mathbf{Y}^*} \left[(\lambda+2\mu)\gamma_{11,Y}(\hat{\boldsymbol{\chi}}_{22})+\lambda(1+\gamma_{22,Y}(\hat{\boldsymbol{\chi}}_{22}))\right]\gamma_{22,X}(\overline{\mathbb{U}})\gamma_{11,X}(\bar{\mathbf{V}})dYdX+$$
$$\int_\omega \int_{\mathbf{Y}^*} [(\lambda+2\mu)\gamma_{22,Y}(\hat{\boldsymbol{\chi}}_{11})+\lambda(1+\gamma_{11,Y}(\hat{\boldsymbol{\chi}}_{11}))]\gamma_{11,X}(\overline{\mathbb{U}})\gamma_{22,X}(\bar{\mathbf{V}})dYdX+$$
$$\int_\omega \int_{\mathbf{Y}^*} \left[(\lambda+2\mu)(1+\gamma_{22,Y}(\hat{\boldsymbol{\chi}}_{22}))+\lambda\gamma_{11,Y}(\hat{\boldsymbol{\chi}}_{22})\right]\gamma_{22,X}(\overline{\mathbb{U}})\gamma_{22,X}(\bar{\mathbf{V}})dYdX+$$
$$\int_\omega \int_{\mathbf{Y}^*} 4\mu(1+\gamma_{12,Y}(\hat{\boldsymbol{\chi}}_{12}))\gamma_{12,X}(\overline{\mathbb{U}})\gamma_{12,X}(\bar{\mathbf{V}})dYdX=0.$$

We define the coefficients $a^*_{\alpha\beta\alpha'\beta'}$:

$$a^*_{1111}=\int_{\mathbf{Y}^*}[(\lambda+2\mu)(1+\gamma_{11,Y}(\hat{\boldsymbol{\chi}}_{11}))+\lambda\gamma_{22,Y}(\hat{\boldsymbol{\chi}}_{11})]dY, \tag{16.32}$$

$$a^*_{2211}=\int_{\mathbf{Y}^*}\left[(\lambda+2\mu)\gamma_{11,Y}(\hat{\boldsymbol{\chi}}_{22})+\lambda(1+\gamma_{22,Y}(\hat{\boldsymbol{\chi}}_{22})\right]dY, \tag{16.33}$$

$$a^*_{1122}=\int_{\mathbf{Y}^*}[(\lambda+2\mu)\gamma_{22,Y}(\hat{\boldsymbol{\chi}}_{11})+\lambda(1+\gamma_{11,Y}(\hat{\boldsymbol{\chi}}_{11}))]\,dY, \tag{16.34}$$

$$a^*_{2222}=\int_{\mathbf{Y}^*}\left[(\lambda+2\mu)(1+\gamma_{22,Y}(\hat{\boldsymbol{\chi}}_{22}))+\lambda\gamma_{11,Y}(\hat{\boldsymbol{\chi}}_{22})\right]dY, \tag{16.35}$$

$$a^*_{1212}=\int_{\mathbf{Y}^*}2\mu(1+\gamma_{12,Y}(\hat{\boldsymbol{\chi}}_{12}))dY, \tag{16.36}$$

$$a^*_{\alpha\alpha12}=0, \tag{16.37}$$

and the problem is written

$$\overline{\mathbb{U}}\in L^2(0,L;H^1(\omega;\mathbb{R}^2)),$$
$$\int_\omega a^*_{1111}\gamma_{11,X}(\overline{\mathbb{U}})\gamma_{11,X}(\bar{\mathbf{V}})dX+\int_\omega a^*_{2211}\gamma_{22,X}(\overline{\mathbb{U}})\gamma_{11,X}(\bar{\mathbf{V}})dX+$$
$$\int_\omega a^*_{1122}\gamma_{11,X}(\overline{\mathbb{U}})\gamma_{22,X}(\bar{\mathbf{V}})dX+\int_\omega\int_{\mathbf{Y}^*} a^*_{2222}\gamma_{22,X}(\overline{\mathbb{U}})\gamma_{22,X}(\bar{\mathbf{V}})dX+$$
$$\int_\omega\int_{\mathbf{Y}^*} a^*_{1212}\gamma_{12,X}(\overline{\mathbb{U}})\gamma_{12,X}(\bar{\mathbf{V}})dX=0,\ \forall\bar{\mathbf{V}}\in L^2(0,L;H^1(\omega;\mathbb{R}^2)).$$

The bilinear form given by coefficients (16.32)-(16.37) is symmetric and coercitive. In fact, the symmetry of the bilinear form is a consequence of Remark 16.2.7. Let $\Theta_{\alpha\beta}$ arbitrary, then we have that

$$a^*_{\alpha\beta\alpha'\beta'}\Theta_{\alpha\beta}\Theta_{\alpha'\beta'} = \int_{\mathbf{Y}^*} a_{\alpha\beta\alpha'\beta'}\gamma_{\alpha\beta,Y}(\hat{\mathbf{V}})\gamma_{\alpha'\beta',Y}(\hat{\mathbf{V}})dY \geq C\|\gamma_{\alpha\beta,Y}(\hat{\mathbf{V}})\|^2 \geq C|\Theta_{\alpha\beta}|^2,$$

where

$$\hat{\mathbf{V}} = \Theta_{11}\left(\hat{\chi}_{11} + Y_1\mathbf{e}_1\right) + \Theta_{22}\left(\hat{\chi}_{22} + Y_2\mathbf{e}_2\right) + \Theta_{12}\left(\hat{\chi}_{12} + Y_2\mathbf{e}_1 + Y_1\mathbf{e}_2\right)$$

due to the definitions of correctors $\hat{\boldsymbol{\chi}}_{\alpha\beta}$. For instance,

$$\begin{gathered}
\int_{\mathbf{Y}^*} a_{\alpha\beta\alpha'\beta'}\gamma_{\alpha\beta}\left(\Theta_{12}\left(\hat{\boldsymbol{\chi}}_{12} + Y_2\mathbf{e}_1 + Y_1\mathbf{e}_2\right)\right)\gamma_{\alpha'\beta'}\left(\Theta_{12}\left(\hat{\boldsymbol{\chi}}_{12} + Y_2\mathbf{e}_1 + Y_1\mathbf{e}_2\right)\right)dY = \\
\int_{\mathbf{Y}^*} 4\mu\Theta_{12}\left(\gamma_{12}(\hat{\boldsymbol{\chi}}_{12}) + 1\right)\Theta_{12}(\gamma_{12}\left(\hat{\boldsymbol{\chi}}_{12}\right) + 1)\,dY = \\
\int_{\mathbf{Y}^*} 4\mu\left[\gamma_{12}(\hat{\boldsymbol{\chi}}_{12})\gamma_{12}(\hat{\boldsymbol{\chi}}_{12}) + 2\gamma_{12}(\hat{\boldsymbol{\chi}}_{12}) + 1\right]\Theta_{12}\Theta_{12}dY = \\
\int_{\mathbf{Y}^*} 4\mu\left[-\gamma_{12}(\hat{\boldsymbol{\chi}}_{12}) + 2\gamma_{12}(\hat{\boldsymbol{\chi}}_{12}) + 1\right]\Theta_{12}\Theta_{12}dY = \\
\left(\int_{\mathbf{Y}^*} 4\mu\left[\gamma_{12}(\hat{\boldsymbol{\chi}}_{12}) + 1\right]\Theta_{12}\Theta_{12}dY\right)\Theta_{12}\Theta_{12} = a^*_{1212}\Theta_{12}\Theta_{12}.
\end{gathered}$$

So, the bilinear form associated to coefficients (16.32)-(16.37) is coercitive.

Therefore, the problem is written

$$\begin{gathered}
\overline{\mathbb{U}} \in L^2(0,L;H^1(\omega;\mathbb{R}^2)), \\
\int_\omega a^*_{\alpha\beta\alpha'\beta'}\gamma_{\alpha\beta,X}(\overline{\mathbb{U}})\gamma_{\alpha'\beta',X}(\bar{\mathbf{V}})dX = 0,\ \forall\bar{\mathbf{V}} \in L^2(0,L;H^1(\omega;\mathbb{R}^2)).
\end{gathered}$$

Since the bilinear form associated to coefficients $a^*_{\alpha\beta\alpha'\beta'}$ is coercitive, we obtain that

$$\overline{\mathbb{U}} = \mathbf{0}.$$

Therefore,

$$\overline{U}_1 = -\nu\left(X_1\frac{d\mathcal{U}_3}{dx_3} - \frac{X_1^2 - X_2^2}{2}\frac{d^2\mathcal{U}_1}{dx_3^2} - X_1X_2\frac{d^2\mathcal{U}_2}{dx_3^2}\right), \tag{16.38}$$

$$\overline{U}_2 = -\nu\left(X_2\frac{d\mathcal{U}_3}{dx_3} - X_1X_2\frac{d^2\mathcal{U}_1}{dx_3^2} - \frac{X_2^2 - X_1^2}{2}\frac{d^2\mathcal{U}_2}{dx_3^2}\right), \tag{16.39}$$

$$\hat{u}_1 = \hat{u}_2 = 0.$$

Thirdly, we are going to obtain a simpler expression for $\mathcal{U}_3$. By choosing in expression (16.19)

$$\mathbf{V}(Y_1,Y_2,X_1,X_2,x_3) = \begin{pmatrix} 0 \\ 0 \\ \mathcal{V}_3(x_3) \end{pmatrix},$$

where $\mathcal{V}_3 \in H^1(0,L)$, we have that

$$\int_0^L \int_\omega \int_{\mathbf{Y}^*} [(\lambda+2\mu)\Gamma_{33}(\mathbf{U}) + \lambda(\gamma_{11}(\mathbf{U}) + \Gamma_{22}(\mathbf{U}))] \frac{d\mathcal{V}_3}{dx_3} dY_1 dY_2 dX_1 dX_2 dx_3 = \int_0^L \int_\omega \int_{\mathbf{Y}^*} f_3 \mathcal{V}_3 dY_1 dY_2 dX_1 dX_2 dx_3,$$

that is

$$\int_0^L \int_\omega \int_{\mathbf{Y}^*} \left[(\lambda+2\mu)\frac{d\tilde{\mathcal{U}}}{dx_3} + \lambda(\gamma_{11,X}(\overline{\mathbf{U}}) + \gamma_{22,X}(\overline{\mathbf{U}}) \right] \frac{d\mathcal{V}_3}{dx_3} dY_1 dY_2 dX_1 dX_2 dx_3 = \int_0^L \int_\omega \int_{\mathbf{Y}^*} f_3 \mathcal{V}_3 dY_1 dY_2 dX_1 dX_2 dx_3,$$

where λ and μ are the Lamé coefficients.

Then, by taking into account expressions (16.38) and (16.39), we have that

$$\gamma_{11,X}(\overline{\mathbf{U}}) = \gamma_{22,X}(\overline{\mathbf{U}}) = -\nu \frac{d\tilde{\mathcal{U}}}{dx_3},$$

and consequently,

$$\int_0^L \int_\omega \int_{\mathbf{Y}^*} \left((\lambda+2\mu)\frac{d\tilde{\mathcal{U}}}{dx_3} - 2\lambda\nu \frac{d\tilde{\mathcal{U}}}{dx_3} \right) \frac{d\mathcal{V}_3}{dx_3} dY dX dx_3 = \int_0^L \int_\omega \int_{\mathbf{Y}^*} f_3 \mathcal{V}_3 dY_1 dY_2 dX_1 dX_2 dx_3,$$

that is,

$$\int_0^L \int_\omega \int_{\mathbf{Y}^*} E \frac{d\mathcal{U}_3}{dx_3} \frac{d\mathcal{V}_3}{dx_3} dY dX dx_3 = \int_0^L \int_\omega \int_{\mathbf{Y}^*} f_3 \mathcal{V}_3 dY_1 dY_2 dX_1 dX_2 dx_3.$$

Analogously, we are going to obtain a simpler expression for $\mathcal{U}_\alpha$. By choosing in expression (16.19)

$$\mathbf{V}(Y_1,Y_2,X_1,X_2,x_3) = \begin{pmatrix} \mathcal{V}_1(x_3) \\ \mathcal{V}_2(x_3) \\ -X_1 \frac{d\mathcal{V}_1}{dx_3}(x_3) - X_2 \frac{d\mathcal{V}_2}{dx_3}(x_3) \end{pmatrix},$$

where $\mathcal{V}_\alpha \in H^2(0,L)$ and by taking into account expressions (16.38) and (16.39), we have that

$$-\int_0^L \int_\omega \int_{\mathbf{Y}^*} \left((\lambda+2\mu)\frac{d\tilde{\mathcal{U}}}{dx_3} - 2\lambda\nu \frac{d\tilde{\mathcal{U}}}{dx_3} \right) \left(X_1 \frac{d^2\mathcal{V}_1}{dx_3^2} + X_2 \frac{d^2\mathcal{V}_2}{dx_3^2} \right) dY_1 dY_2 dX_1 dX_2 dx_3 = \int_0^L \int_\omega \int_{\mathbf{Y}^*} f_\alpha \mathcal{V}_\alpha dY_1 dY_2 dX_1 dX_2 dx_3.$$

Then,

$$\int_0^L \int_\omega \int_{\mathbf{Y}^*} \left\{ (\lambda + 2\mu) \left(X_1 \frac{d^2\mathcal{U}_1}{dx_3^2}(x_3) + X_2 \frac{d^2\mathcal{U}_2}{dx_3^2}(x_3) \right) - \right.$$
$$\left. - 2\lambda\nu \left(X_1 \frac{d^2\mathcal{U}_1}{dx_3^2}(x_3) + X_2 \frac{d^2\mathcal{U}_2}{dx_3^2}(x_3) \right) \right\} \left(X_1 \frac{d^2\mathcal{V}_1}{dx_3^2} + X_2 \frac{d^2\mathcal{V}_2}{dx_3^2} \right) dY_1 dY_2 dX_1 dX_2 dx_3 =$$
$$\int_0^L \int_\omega \int_{\mathbf{Y}^*} f_\alpha \mathcal{V}_\alpha dY_1 dY_2 dX_1 dX_2 dx_3.$$

By doing calculations,

$$\int_0^L \int_\omega \int_{\mathbf{Y}^*} \left(X_1^2 E \frac{d^2\mathcal{U}_1}{dx_3^2} \frac{d^2\mathcal{V}_1}{dx_3^2} + X_2^2 E \frac{d^2\mathcal{U}_2}{dx_3^2} \frac{d^2\mathcal{V}_2}{dx_3^2} \right) dY_1 dY_2 dX_1 dX_2 dx_3 =$$
$$\int_0^L \int_\omega \int_{\mathbf{Y}^*} f_\alpha \mathcal{V}_\alpha dY_1 dY_2 dX_1 dX_2 dx_3,$$

that is

$$\int_0^L EI_\alpha \frac{d^2\mathcal{U}_\alpha}{dx_3^2} \frac{d^2\mathcal{V}_\alpha}{dx_3^2} dx_3 = \int_0^L \int_\omega f_\alpha \mathcal{V}_\alpha dY_1 dY_2 dX_1 dX_2 dx_3,$$

where E is the Young's modulus.

16.2.3 Limit problems for the elementary displacement $\mathbf{U}_e$

The limit problems for the elementary displacement $\mathbf{U}_e$ are given by:

Problem $(P\mathcal{U}_3)$:

Find $\mathcal{U}_3 \in H^1(0, L)$ such that $\mathcal{U}_3(0) = 0$ and

$$\int_0^L E \frac{d\mathcal{U}_3}{dx_3} \frac{d\mathcal{V}_3}{dx_3} dx_3 = \int_0^L f_3 \mathcal{V}_3 dx_3, \quad \forall \mathcal{V}_3 \in H^1(0, L),\ \mathcal{V}_3(0) = 0. \tag{16.40}$$

Problem $(P\mathcal{U}_\alpha)$:

Find $\mathcal{U}_\alpha \in H^2(0, L)$ such that $\mathcal{U}_\alpha(0) = \frac{d\mathcal{U}_\alpha}{dx_3}(0) = 0$ and

$$\int_0^L \frac{E}{12} \frac{d^2\mathcal{U}_\alpha}{dx_3^2} \frac{d^2\mathcal{V}_\alpha}{dx_3^2} dx_3 = \int_0^L f_\alpha \mathcal{V}_\alpha dx_3, \quad \forall \mathcal{V}_\alpha \in H^2(0, L),\ \mathcal{V}_\alpha(0) = \frac{d\mathcal{V}_\alpha}{dx_3}(0) = 0. \tag{16.41}$$

Problem $(P\mathcal{R}_3)$:

Find $\mathcal{R}_3 \in H^1(0, L)$ such that $\mathcal{R}_3(0) = 0$ and

$$\int_0^L K^* \frac{d\mathcal{R}_3}{dx_3} \frac{d\mathcal{A}_3}{dx_3} dx_3 = \int_0^L \frac{1}{6} f_T \mathcal{A}_3 dx_3, \quad \forall \mathcal{A}_3 \in H^1(0, L),\ \mathcal{A}_3(0) = 0. \tag{16.42}$$

16.3 Strong convergences

Proposition 16.3.1. *The following convergences of the stress tensor hold:*

$$\mathcal{T}_\varepsilon^{\mathbf{h}}(\mathcal{T}_e^{\mathbf{e}}(\sigma_{\alpha\beta}(\mathbf{u}^{e\varepsilon}))) \to 0, \tag{16.43}$$

$$\mathcal{T}_\varepsilon^{\mathbf{h}}(\mathcal{T}_e^{\mathbf{e}}(\sigma_{33}(\mathbf{u}^{e\varepsilon}))) \to E\left(\frac{d\mathcal{U}_3}{dx_3} - X_1\frac{d^2\mathcal{U}_1}{dx_3^2} - X_2\frac{d^2\mathcal{U}_2}{dx_3^2}\right), \tag{16.44}$$

$$\mathcal{T}_\varepsilon^{\mathbf{h}}(\mathcal{T}_e^{\mathbf{e}}(\sigma_{13}(\mathbf{u}^{e\varepsilon}))) \to \mu\left(1+\frac{\partial\hat{\chi}_1}{\partial Y_1}\right)\left(-X_2+\frac{\partial\bar{\chi}}{\partial X_1}\right)\frac{d\mathcal{R}_3}{dx_3}, \tag{16.45}$$

$$\mathcal{T}_\varepsilon^{\mathbf{h}}(\mathcal{T}_e^{\mathbf{e}}(\sigma_{23}(\mathbf{u}^{e\varepsilon}))) \to \mu\left(1+\frac{\partial\hat{\chi}_2}{\partial Y_2}\right)\left(X_1+\frac{\partial\bar{\chi}}{\partial X_2}\right)\frac{d\mathcal{R}_3}{dx_3}, \tag{16.46}$$

strongly in $L^2(\mathbf{Y}^*\times\Omega)$. Moreover, convergences (15.29)-(15.32) of the strain tensor are strong in $L^2(\mathbf{Y}^*\times\Omega)$.

Proof. We choose $\mathbf{V}=\mathbf{U}$ in Problem (UP) and we obtain that

$$\int_0^L\int_\omega\int_{\mathbf{Y}^*} a_{ijkl}\Gamma_{ij}(\mathbf{U})\Gamma_{kl}(\mathbf{U})dY_1dY_2dX_1dX_2dx_3 \le$$
$$\liminf\frac{|\mathbf{Y}^*|}{e^2}\int_{\Omega_e^*} a_{ijkl}\gamma_{ij}(\mathbf{u}^{e\varepsilon})\gamma_{kl}(\mathbf{u}^{e\varepsilon})dx_1dx_2dx_3 \le$$
$$\limsup\frac{|\mathbf{Y}^*|}{e^2}\int_{\Omega_e^*} a_{ijkl}\gamma_{ij}(\mathbf{u}^{e\varepsilon})\gamma_{kl}(\mathbf{u}^{e\varepsilon})dx_1dx_2dx_3 =$$
$$\limsup\frac{|\mathbf{Y}^*|}{e^2}\int_{\Omega_e^*}\mathbf{f}^{e\varepsilon}\cdot\mathbf{u}^{e\varepsilon}dx_1dx_2dx_3 = \lim_{e,\varepsilon\to0}\frac{|\mathbf{Y}^*|}{e^2}\int_{\Omega_e^*}\mathbf{f}^{e\varepsilon}\cdot\mathbf{u}^{e\varepsilon}dx_1dx_2dx_3 \le$$
$$\int_0^L\int_\omega\int_{\mathbf{Y}^*}\{f_\alpha\mathcal{U}_\alpha + f_3\mathcal{U}_3 + (X_1^2+X_2^2)f_T\mathcal{R}_3\}dY_1dY_2dX_1dX_2dx_3 =$$
$$\int_0^L\int_\omega\int_{\mathbf{Y}^*} a_{ijkl}\Gamma_{ij}(\mathbf{U})\Gamma_{kl}(\mathbf{U})dY_1dY_2dX_1dX_2dx_3.$$

Consequently, we have that

$$\int_0^L\int_\omega\int_{\mathbf{Y}^*} a_{ijkl}\Gamma_{ij}(\mathbf{U})\Gamma_{kl}(\mathbf{U})dY_1dY_2dX_1dX_2dx_3 =$$
$$\lim_{e,\varepsilon\to0}\frac{|\mathbf{Y}^*|}{e^2}\int_{\Omega_e^*} a_{ijkl}\gamma_{ij}(\mathbf{u}^{e\varepsilon})\gamma_{kl}(\mathbf{u}^{e\varepsilon})dx_1dx_2dx_3,$$

and we obtain the strong convergences of the stress and strain tensors. □

Proposition 16.3.2. *The following convergences of the unfolded field $\mathcal{T}_e^{\mathbf{e}}(\mathbf{u}^{e\varepsilon})$ hold:*

$$e\mathcal{T}_e^{\mathbf{e}}(u_1^{e\varepsilon}) \to \mathcal{U}_1,$$
$$e\mathcal{T}_e^{\mathbf{e}}(u_2^{e\varepsilon}) \to \mathcal{U}_2,$$
$$\mathcal{T}_e^{\mathbf{e}}(u_3^{e\varepsilon}) \to \mathcal{U}_3 - X_1\frac{d\mathcal{U}_1}{dx_3} - X_2\frac{d\mathcal{U}_2}{dx_3},$$

in $H^1(\Omega)$.

Proof. It is a consequence of strong convergence (15.30) and estimates (15.6) and (15.8). □

Chapter 17

Conclusions

In Part III, we have applied the unfolding method to study the asymptotic behaviour of the catalyst support in a linear elasticity problem. These supports are strucutres made of beams, placed periodically and with inner holes.

We have obtained, after passing to the limit, three uncoupled limit problems: The first problem defines the longitudinal displacement and the second one gives the transversal bending of the structure, while the third one defines the torsion angle. Notice that the general form of longitudinal and transversal problems are the same that those obtained in the well-known Bernouilli-Navier theory of thin rods (see [80]). Nevertheless, the torsion problem does not coincide with those given in Bernouilli-Navier theory, that is, this problem takes into account, by means of torsion rigidity K^*, the periodic character and the cells geometry of the structure.

Moreover, unfolded stress tensor is similar to that obtain in classical theories, but shear components also show periodic character and cell geometry dependence by means of suitable correctors.

In a future research, we may apply the results obtained here in order to solve the fluid-structure interaction problem which occurs in an automobile's exhaust system. To do so, we will consider that the holes of the structure contain certain kind of fluid and some chemical reactions take place on the boundaries of the structure.

Acknowledgments

I would like to thank my advisors, Prof. Peregrina Quintela Estévez and Prof. Patricia Barral Rodiño for their work and support during these years. I would also like to acknowledge Prof. Francisco Guitián and Victor Valcárcel for their constant support and help in the second part of this work, and to Prof. Doina Cioranescu and Prof. Georges Griso for their huge work, help and hospitality during my three research stays in the Laboratorie Jacques-Louis Lions of the Université Pierre e Marie Curie (Paris VI), in Paris, France.

This work was partially supported by CICYT-FEDER (Spain) through projects No. DPI2004-01993 and MTM2008,05682 and by Xunta de Galicia through project No. PGIDT02PXIC20701PN. The third part of this work was partially supported by Ministerio de Ciencia y Tecnología (Spain) through project No. DPI2001-1613-C02-02 and No. DPI2004-05504- C02-02, and Xunta de Galicia projects No. PGIDIT02XI20701PN and No. PGIDIT05PXIC20701PN. Furthermore, during these years I have been funded by Ministerio de Educación y Ciencia (Spain) through grant No. AP2003-4495 of FPU program.

Resumen

Hoy en día, un conocimiento profundo de los fenómenos en mecánica de sólidos es fundamental para desarrollar nuevos métodos o técnicas que permitan ahorrar enormes cantidades de tiempo y dinero en campos como las industrias cerámicas o del aluminio. Históricamente, para simular este tipo de procesos se consideraban modelos lineales o clásicos. Sin embargo, muy a menudo los materiales reales exhiben un comportamiento no lineal y, en este momento en el que cada vez más surgen nuevos materiales, los modelos lineales están siendo llevados a su límite. Por lo tanto, el uso de modelos no lineales se hace cada vez más necesario para realizar las simulaciones numéricas de los distintos procesos en este tipo de industrias.

A lo largo de esta tesis, se pueden distinguir tres partes bien diferenciadas aunque con una temática común: el estudio matemático y la resolución numérica de problemas no lineales en mécanica de sólidos, que surgen de procesos físicos presentes en las industrias del aluminio y las cerámicas. Consideramos situaciones reales donde aparecen distintas no linealidades: leyes de comportamiento de tipo viscoplástico, condiciones de contorno tales como el contacto unilateral, etc. Así, en la primera parte de esta tesis nos centramos en el estudio matemático del proceso de colada de aluminio, e introducimos algunos algoritmos eficientes para llevar a cabo la simulación numérica del mismo. En este problema, aparecen dos no linealidades: la ley de comportamiento no lineal del aluminio y una condición de contacto con el molde que contiene el metal. A continuación, la segunda parte de la tesis está dedicada al estudio del ensayo de flexión en tres puntos y del módulo de ruptura de materiales frágiles. En este problema, aparece de nuevo una condición de contacto en su formulación. Por último, la tercera parte presenta un análisis matemático de un problema de elasticidad para soportes utilizados en catálisis.

En lo que sigue, veremos cada una de las partes de la tesis más detalladamente.

Parte 1. Procesos de colada de aluminio: Algoritmos eficientes para su simulación numérica.

El objetivo de esta primera parte de la tesis es obtener algoritmos eficientes para resolver no linealidades que provienen de leyes de comportamiento de tipo viscoplástico, o de condiciones de contorno tales como el contacto unilateral. Un situación real en la que aparecen estas dos condiciones, y que es la motivación de esta investigación, es el proceso de colada en la producción de aluminio. Durante los procesos de colada, se vierte el aluminio líquido en un molde, refrigerado por agua, llamado *falso fondo*; cuando el aluminio se empieza a solidificar, el falso fondo comienza

a descender, dejando más espacio para el nuevo metal líquido. Se puede encontrar una descripción detallada del proceso completo en [33, 41, 75].

Generalmente, el proceso de colada se divide en dos fases. Durante la fase de arranque, el campo de temperaturas, el frente de solidificación y la forma de la placa se modifican a lo largo del tiempo. Los fuertes gradientes térmicos, debidos a los chorros de agua, hacen que el la parte inferior de la placa se deforme y pierda contacto con el falso fondo. Esta deformación se conoce como *deformación del talon* y se caracteriza por un levantamiento de la base de la placa de metal. Cuando la altura de la placa es de aproximadamente 1m, el campo de temperaturas se vuelve estacionario. En esta fase estacionaria, la placa solidificada se contrae hacia dentro y la sección resultante presenta paredes laterales cóncavas.

La deformación del talon y la contracción de la placa pueden minimizarse optimizando los parámetros de colada, pero en primer lugar, es necesario ser capaz de predecir las deformaciones que sufrirá la placa para condiciones de colada fijas. Para predecir el comportamiento de la colada, las principales dificultades se deben a los efectos del acoplamiento de fenómenos, a la presencia de términos no lineales, a la existencia de fronteras libres y a que el dominio computacional varía con el tiempo (véase [6]). Concretamente, para simular la deformación del talón debemos resolver un problema de contacto unilateral sin rozamiento entre un cuerpo termo-elasto-viscoplástico de Maxwell-Norton y un sólido rígido.

El trabajo que presentamos en esta primera parte es la continuación de la investigación iniciada en [5] y [9]-[13], donde se han estudiado varios aspectos matemáticos del problema:

- La formulación como desigualdad variacional.
- La búsqueda de condiciones suficientes para la existencia de una solución.
- La implementación numérica de la presión metalostática en la interfase líquido-sólido.
- La aproximación numérica de la desigualdad variacional y la descripción de un esquema numérico para resolverla.

En la tesis doctoral [5], se obtuvo una solución aproximada de este problema usando un esquema de Euler implícito en tiempo y un método de elementos finitos en espacio. Para tratar las no linealidades, la resolución numérica se basó en el algoritmo de Bermúdez-Moreno que involucra dos multiplicadores: el multiplicador viscoplástico (que tiene en cuenta la no linealidad debida a la ley de comportamiento) y el multiplicador de contacto (que permite resolver la no linealidad debida a la condición de contacto). Estos dos multiplicadores se aproximaban usando algoritmos de punto fijo (véase [9, 10, 16]). Durante la fase estacionaria, en la que la condición de contacto no tiene una influencia significativa, este algoritmo funcionó bien; sin embargo, durante la fase de arranque, donde aparecen simultáneamente las dos no linealidades, la convergencia empeoró en gran medida, incrementando el tiempo de ejecución. Además, este algoritmo presenta una fuerte dependencia con respecto a sus parámetros, que no pueden ser determinados *a priori*. Todos estos problemas hacen muy difícil el uso masivo de este algoritmo para ayudar en los procesos de colada. El objetivo fundamental de este trabajo de investigación es desarrollar métodos numéricos eficientes que incorporen procedimientos adaptados para acelerar el tratamiento de las no linealidades y, por la tanto, ser capaces de simular numéricamente la deformación del talón en un tiempo razonable.

Para lograr este objetivo analizamos varias opciones:

- Condición de contacto. Aproximar el multiplicador de contacto utilizando métodos de Newton generalizados junto con una técnica de penalización para conservar la simetría de la matriz (véase [7, 14, 46, 54, 72]). El algoritmo resultante para resolver la condición de contacto es rápido, preciso y su convergencia es independiente de los parámetros del mismo. Sin embargo, este algoritmo necesita recalcular la matriz de rigidez en cada iteración. Por lo tanto, teniendo en cuenta que generalmente esta condición de contorno sólo involucra una pequeña parte de la frontera, proponemos usar una factorización de la matriz de rigidez adaptada a la geometría del problema.
- Ley de comportamiento viscoplástica. Se consideran dos opciones:
  - Aproximar el mutiplicador viscoplástico con técnicas de Newton estándar sin modificar la matriz de rigidez en cada iteración (véase [7, 14]).
  - Aproximar el multiplicador viscoplástico usando una generalización del algoritmo de Berúdez-Moreno con parámetros variables, que se calculan automáticamente (véase [43]).

  Cuando la no linealidad debida a la ley viscoplástica se resuelve usando técnicas de Newton, los fuertes gradientes térmicos obligan a emplear algunas técnicas numéricas para obtener una buena convergencia, como son: una adimensionalización de las tensiones, una regla de Armijo y una optimización del paso de tiempo. Para mostrar el buen comportamiento de esta metodología, presentamos ejemplos académicos diseñados para reproducir el proceso de colada. Sin embargo, al aplicarlo al proceso que se lleva a cabo en la fábrica, no siempre se alcanza la convergencia. Por ello, proponemos un segundo algoritmo que es una generalización del algoritmo de Bermúdez-Moreno con una elección automática de sus parámetros

Esta primera parte de la tesis está organizada como sigue:

Capítulo 1: Introducción. Hacemos una introducción al problema que queremos resolver y damos una descripción del problema físico asociado a los procesos de colada.

Capítulo 2: Modelo matemático. Introducimos el modelo matemático para simular la deformación del talón que se produce durante el proceso de colada, dando una descripción detallada de las condiciones de contorno, la ecuaciones de equilibrio y la ley de comportamiento no lineal asociada al aluminio. Esta última se corresponde con una ley termo-elasto-viscoplástica, donde la parte viscoplástica viene dada por una ley de Maxwell-Norton no lineal, y la parte térmica es una generalización de la ley de Arrhenius.

Capítulo 3: Estado del arte. Hacemos una revisión de los resultados más importantes del análisis matemático y de la resolución numérica de la deformación del talón. Proponemos una formulación débil para el problema en términos de espacios funcionales adecuados, siguiendo los trabajos de Geymotat y Suquet (véase [45]) y Barral y Quintela (véase [13]). Además, se presentan algunos resultados de existencia obtenidos por Barral y Quintela en [13] y por Barral *et al* en [8]. Por último, recordamos el procedimiento numérico propuesto en [5] para

aproximar la solución del problema y, de este modo, simular la deformación del talón. Este procedimiento está basado en el algoritmo de Bermúdez-Moreno.

Capítulo 4: Resolución numérica mejorada. Con el objetivo de mejorar la convergencia del algoritmo anterior para la simulación de la deformación del talón, este capítulo describe un nuevo procedimiento numérico para aproximar la solución del problema. La condición de contacto se resuelve usando el algoritmo de Bermúdez-Moreno (véase [16]), en el que el multiplicador de contacto es el punto fijo de una ecuación no lineal. Para aproximar este multiplicador proponemos un método de Newton generalizado y una técnica de penalización. Para tratar la ley de comportamiento no lineal usamos de nuevo el algoritmo de Bermúdez-Moreno y proponemos dos métodos para aproximar el correspondiente multiplicador: un algoritmo de Newton junto con algunas estrategias numéricas diseñadas para mejorar su eficiencia, y un algoritmo de Bermúdez-Moreno con parámetros variables.

Capítulo 5: Resultados numéricos. Presentamos algunos ejemplos académicos con solución analítica conocida para validar los algoritmos propuestos. Estos ejemplos se han diseñado para reproducir un comportamiento análogo al de la colada de aluminio real: fuertes gradientes térmicos con respecto al tiempo y una separación o hueco entre el dominio computacional y el sólido rígido que crece con el tiempo. Comparamos la eficiencia de las metodologías propuestas con el antiguo algoritmo de Bermúdez-Moreno introducido en [9, 10]. Por último, presentamos resultados numéricos de la simulación de la deformación del talón.

Capítulo 6: Conclusiones. Presentamos algunas de las conclusiones más importantes de esta primera parte de la tesis, remarcando que los mejores resultados numéricos se obtienen al considerar el método de Newton en contacto y el método de Bermúdez-Moreno con parámetros variables en viscoplasticidad.

Parte 2. Ensayo de flexión en tres puntos: Estudio matemático y simulación numérica.

Cada vez más surgen nuevos retos en ingeniería, ya sean nuevas aplicaciones, nuevos materiales o ambos casos simultáneamente. Habitualmente no se puede predecir correctamente el comportamiento de cierto material bajo nuevas condiciones, y es necesario realizar gran cantidad de experimentos de prueba para determinar si puede ser utilizado o no. Por lo tanto, hoy en día se está llevando a cabo un enorme esfuerzo con el objetivo de desarrollar nuevas técnicas predictivas que permitan ahorrar tiempo y dinero al testear nuevos materiales. Sin embargo, no existen demasiados estudios sobre cómo predecir el comportamiento de los materiales bajo condiciones simples. Factores como pequeñas diferencias en la composición o en la microestructura afectan en gran manera a los resultados de los experimentos más habituales, haciendo que la experiencia previa en materiales similares no haya sido de utilidad. Este hecho es particularmente crítico para los materiales cerámicos.

Generalmente, en las aplicaciones los materiales son sometidos a distintas fuerzas o cargas, con componentes más o menos complicadas de flexión, torsión, compresión y combinaciones de todas ellas. Para predecir el comportamiento de cierto material, sin llevar a cabo experimentos destructivos, es necesario entender los mecanismos que afectan a su resistencia para seleccionar

el criterio de ruptura más adecuado. Las propiedades del material se miden cuidadosamente mediante experimentos o ensayos en el laboratorio sobre una muestra del material; estos ensayos determinan las propiedades mecánicas de un material mediante la medición de la carga aplicada y el correspondiente cambio de longitud en las dimensiones de las muestras utilizadas. Hay muchos tipos de ensayos o tests para determinar las propiedades de los materiales, y se pueden clasificar en varios grupos atendiendo a la forma en que es aplicada la carga, a la condición de las muestras en el momento del ensayo o a la condición del ambiente durante el ensayo. Los más importantes son los siguientes:

- Ensayo de tensión y compresión: Se aplica una carga axial a una muestra para obtener una distribución uniforme de las tensiones sobre la sección transversal.
- Ensayo de torsión: Determina el comportamiento de las muestras sometidas a pares de cargas opuestas.
- Ensayo de flexión: Determina el comportamiento de materiales sometidos a cargas simples, por ejemplo, cargas concentradas o distribuidas uniformemente.
- Ensayo de fatiga: Utilizado para estudiar el comportamiento de materiales sometidos a cargas variables.
- Ensayo de impacto: Es un caso particular de los ensayos anteriores; la carga se aplica súbitamente.

En esta segunda parte de la tesis centraremos nuestro estudio en los ensayos de flexión. La relativa sencillez de estos ensayos ha permitido su popularización para medir las propiedades mecánicas de materiales frágiles. Uno de los ensayos más comunes es el *ensayo de flexión en tres puntos*: se coloca una muestra del material entre tres cilindros, sin sujeción adicional, dejando que el actuador o cilindro superior ejerza una carga gradualmente creciente hasta que se produzca la ruptura. La medida que generalmente se determina con este experimento es el módulo de ruptura (MOR), es decir, la máxima tensión superficial que soporta la pieza doblada antes de romper. En la literatura, el MOR viene dado por una fórmula explícita, que involucra el valor de la fuerza máxima que soporta la muestra, la distancia entre los cilindros inferiores y el segundo momento de inercia de la sección transversal de la muestra.

Sin embargo, hemos detectado que, al calcular experimentalmente distintos valores del MOR para cierto material, aparecen discrepancias importantes que dependen del tamaño de la muestra, de la relación entre el área de la sección transversal y la longitud total de la muestra o la relación entre la distancia de los cilindros inferiores y la longitud total. Es muy habitual que muestras del mismo material nos lleven a diferentes valores para el MOR, pero hasta ahora no hay estudios sobre este comportamiento.

El objetivo de la Parte II es estudiar el problema matemático asociado a los ensayos de flexión en tres puntos para mejorar el conocimiento sobre el MOR de materiales frágiles. Más específicamente, probamos la existencia de una solución única para el problema de elasticidad con contacto unilateral sin rozamiento que proviene del modelo mecánico del ensayo. Además, para justificar la fórmula clásica utilizada para calcular el MOR, nos interesa encontrar su modelo límite usando técnicas de

análisis asintótico cuando el espesor de la viga de muestra tiende a cero (véase [2, 18, 36, 80, 81]). Usando este método se han justificado teorías clásicas como la de Bernouilli-Navier, Saint Venant, Timoshenko y Vlassov (véase [18, 80]). También se ha estudiado el caso de vigas con contacto unilateral con sólido rígido (véase [82, 83]), pero únicamente en el caso de extremos anclados. A pesar de la ausencia de condiciones Dirichlet para nuestro problema mecánico tridimensional, el método asintótico nos permite obtener los problemas límites unidimensionales para la flexión y la tracción e identificar la relación entre la carga de ruptura y la correspondiente tensión normal axial. Todos los resultados teóricos han sido publicados en [70].

Además, estamos interesados en encontrar un método efectivo para calcular el MOR para materiales frágiles. Para ello, usamos todos los resultados teóricos que presentamos en esta tesis doctoral para obtener varias aproximaciones del MOR. El procedimiento es el siguiente: Una vez realizados en el laboratorio varios ensayos para vigas de cerámica, conocemos la fuerza máxima que la viga soporta antes de romper – la fuerza de ruptura. Utilizando la fórmula clásica para el MOR, obtenemos un primer valor para el mismo – el MOR teórico. En segundo lugar, realizamos simulaciones numéricas del ensayo experimental para los modelos unidimensional y tridimensional, considerando la fuerza de ruptura, de donde obtenemos dos nuevas aproximaciones del MOR – los MOR numéricos 1d y 3d. Por último, obtenemos un cuarto valor para el MOR usando una nueva fórmula obtenida del análisis asintótico de nuestro problema. Aplicamos esta metodología sobre vigas cilíndricas y rectangulares hechas de porcelana, que es un material frágil muy usado en ingeniería.

La nueva fórmula teórica que obtenemos aquí permite calcular una mejor aproximación del MOR para materiales frágiles. Esta expresión tiene en cuenta no sólo la fuerza de ruptura y la longitud total de la viga, sino también la distancia entre los cilindros inferiores, el efecto de la gravedad y la distancia entre los extremos de la viga y los cilindros inferiores (véase [51]).

Esta segunda parte de la tesis está organizada como sigue:

Capítulo 7: Introducción. Damos una descripción del problema físico asociado a los ensayos de flexión en tres puntos y presentamos la motivación del completo estudio realizado en la Parte II.

Capítulo 8: Estudio matemático del ensayo de flexión en tres puntos. Estudiamos aquí el comportamiento estático de una viga elástica tridimensional sometida al ensayo de flexión en tres puntos. Bajo condiciones de compatibilidad adecuadas sobre las fuerzas aplicadas y la geometría de la viga, probamos la existencia y unicidad de solución del problema de elasticidad con contacto asociado. Estas condiciones de compatibilidad sobre los datos son debidas a la ausencia de una condición de contorno Dirichlet sobre la frontera de la viga.

Capítulo 9: Análisis asintótico del ensayo de flexión en tres puntos. Este capítulo está dedicado a estudiar el comportamiento asintótico del problema; en particular, deducimos los modelos unidimensionales asociados al desplazamiento y damos resultados de existencia y unicidad de solución para los mismos. Además, introducimos una expresión para la tensión normal axial en la viga que está relacionada con el MOR de materiales frágiles. En la última parte del capítulo estudiamos la regularidad de solución del problema límite de flexión y damos algunas propiedades del conjunto de coincidencia.

Capítulo 10: Una fórmula mejorada para el MOR. Detallamos los experimentos reales llevados a cabo en laboratorio para vigas cilíndricas y rectangulares de porcelana y probamos que se verifican las condiciones de compatibilidad para ambos. En estos dos casos, además, presentamos soluciones analíticas para los problemas límites de flexión y tracción. Dichas soluciones se obtienen de las formulaciones diferenciales dadas por el análisis asintótico. Por último, presentamos una nueva expresión teórica para el MOR.

Capítulo 11: Calculando el MOR. En este capítulo calculamos varias aproximaciones para el MOR de la porcelana utilizando el procedimiento descrito anteriormente y hacemos una comparación de los resultados obtenidos.

Capítulo 12: Conclusiones. Como conclusión, se puede observar que las nuevas fórmulas teóricas obtenidas en esta tesis doctoral dan una mejor aproximación del MOR para materiales frágiles que las fórmulas clásicas. Además, queremos hacer notar que el MOR es una propiedad mecánica muy sensible a variaciones en las dimensiones de las muestras. Debido a esto, se pueden encontrar grandes diferencias entre los valores del MOR obtenidos aquí y el rango de valores encontrado en las bases de datos de ingeniería, en las cuales no se indican las dimensiones o geometrías de las muestras utilizadas.

Parte 3. Un problema de elasticidad para soportes de procesos de catálisis: El método de desdoblamientos.

Para reducir las emisiones de gases contaminantes a la atmósfera, desde hace poco tiempo, se incorpora al tubo de escape de los automóviles el convertidor catalítico o catalizador. En este componente se produce un proceso de catálisis heterogénea, donde un sólido que recubre los canales de un soporte de cerámica o acero inoxidable cataliza una reacción entre gases. El catalizador provee un entorno adecuado para una reacción química en la que los hidrocarburos sin quemar se oxidan completamente, de tal modo que la contaminación se reduce. Hoy en día, se está llevando a cabo un considerable esfuerzo con el objetivo de desarrollar soportes adecuados para el proceso de catálisis. En algunos casos el soporte utilizado es el factor que marca la diferencia en la viabilidad del proceso: el soporte debería permitir que el catalizador se disperse totalmente sobre su superficie, y además necesita ser estable bajo las condiciones de reacción y que los reactivos o productos no afecten a su estructura.

El objetivo de esta tercera parte de la tesis es modelar el proceso de catálisis que tiene lugar en el tubo de escape de los automóviles. Debido a la complejidad del problema, el primer paso es estudiar el comportamiento asintótico de los soportes en un problema de elasticidad lineal. Los soportes para el proceso de catálisis que consideramos aquí están formados por estructuras de múltiples celdas con forma de panal, con un espesor $e\varepsilon$ y con huecos interiores de tamaño $e\varepsilon\delta$.

Para resolver esta primera aproximación utilizamos un nuevo procedimiento, llamado método de desdoblamientos o "unfolding", desarrollado por Cioranescu, Damlamian y Griso (véase [30]). Este método es una generalización de la noción de convergencia en dos escalas introducida por G. Nguetseng [62] y desarrollada más tarde por G. Allaire [1]. El método se basa en el operador de desdoblamientos o "unfolding", $\mathcal{T}_\varepsilon^{\mathbf{h}}$, que es similar a un operador de dilatación. Si Ω es un conjunto abierto y acotado e Y es una celda de referencia en $\mathbb{R}^n$, el operador $\mathcal{T}_\varepsilon^{\mathbf{h}}$ asocia a toda función v en

$L^p(\Omega)$, una función $\mathcal{T}_\varepsilon^{\mathbf{h}}(v)$ en $L^p(\Omega \times Y)$. Una propiedad inmediata del operador "unfolding" $\mathcal{T}_\varepsilon^{\mathbf{h}}$ es que permite transformar cualquier integral en Ω en una integral en $\Omega \times Y$. Además, $\mathcal{T}_\varepsilon^{\mathbf{h}}$ permite probar que la convergencia en dos escalas en el sentido de $L^p(\Omega)$ de una sucesión de funciones v_ε es equivalente a la convergencia débil de la sucesión de funciones desdobladas $\mathcal{T}_\varepsilon^{\mathbf{h}} v_\varepsilon$ en $L^p(\Omega \times Y)$.

Uno de los resultados más importantes del método de "unfolding" es el siguiente: Para cualquier sucesión débilmente convergente w^ε en $H^1(\Omega)$, uno puede extraer una subsucesión (todavía denotada por ε) tal que

$$
\begin{aligned}
&w^\varepsilon \rightharpoonup w \text{ débilmente en } H^1(\Omega),\\
&\mathcal{T}_\varepsilon^{\mathbf{h}}(w^\varepsilon) \rightharpoonup w \text{ débilmente en } L^2(\Omega; H^1(Y)),\\
&\mathcal{T}_\varepsilon^{\mathbf{h}}(\nabla w^\varepsilon) \rightharpoonup \nabla w + \nabla_Y \hat{w} \text{ débilmente en } L^2(\Omega; H^1(Y))^n,
\end{aligned}
$$

donde $\hat{w}$ pertenece a $L^2(\Omega; H^1_{per}(\mathbf{Y}))$.

Además, mediante este método se puede obtener una nueva aproximación de los problemas de elasticidad lineal en dominios o estructuras delgadas (tales como vigas y placas). El método consiste en descomponer un desplazamiento en la combinación de un desplazamiento elemental y un alabeo asociado a la deformación de la sección transversal. Un desplazamiento elemental es un desplazamiento de la línea media de la viga junto con una pequeña rotación de la sección transversal. Esta nueva técnica ha sido introducida en [47] para estudiar vigas curvas. La misma metodología ha sido desarrollada para estudiar placas y estructuras hechas de placas (véase [48, 49]) y para estudiar problemas de uniones entre vigas y placas (véase [22, 23]).

Esta última parte de la tesis está organizada como sigue:

Capítulo 13: Introducción. Hacemos una introducción al problema que queremos resolver y damos una descripción del problema físico asociado a los procesos de catálisis.

Capítulo 14: Problema de elasticidad. Introducimos el dominio computacional y la notación que se usará en las secciones siguientes. Además, se formula el problema tridimensional de elasticidad lineal sobre las estructuras usadas como soportes en el proceso de catálisis. Estas estrucutras están formadas por una familia periódica de vigas elásticas de espesor $e\varepsilon$ y huecos interiores de tamaño $e\varepsilon\delta$.

Capítulo 15: Herramientas del método "unfolding". Presentamos algunas herramientas que se usarán al aplicar el método "unfolding". Definimos los desplazamientos elementales asociados a una viga y damos algunas estimaciones para las deformaciones correspondientes. En primer lugar, introducimos el operador "unfolding" relacionado con el parámetro de elasticidad e, junto con algunas convergencias débiles interesantes. A continuación, definimos el operador "unfolding" relacionado con el parámetro de periodicidad ε y estudiamos el límite de una sucesión acotada de desplazamientos en una estructura del tipo anterior, cuando ambos parámetros, elasticidad e y periodicidad ε, tienden a cero.

Capítulo 16: Problema de elasticidad desdoblado. Bajo hipótesis adecuadas sobre las fuerzas aplicadas, presentamos el límite del problema tridimensional de elasticidad, cuando e y ε tienden a cero, obteniendo tres nuevos problemas desacoplados: El primer problema define

los desplazamientos longitudinales y el segundo nos da la flexión tranversal de la estructura, mientras que el tercer problema define el ángulo de torsión.

Capítulo 17: Conclusiones. Presentamos algunas de las conclusiones más importantes de esta tercera parte de la tesis, remarcando que, aunque los problemas límites de flexión y tracción son los mismos que los obtenidos mediante la teoría de Bernouilli-Navier, en el caso del problema límite de torsión se tiene en cuenta, a través de la rigidez de torsión K^*, el carácter periódico de la estructura así como la geometría de las celdas.

La Parte III de esta tesis es el resultado de las estancias de investigación realizadas por la autora en el Laboratoire Jacques-Louis Lions de la Université Pierre et Mary Curie (Paris VI), en Francia, financiada por el Ministerio de Educación a través del Programa de Formación de Profesorado Universitario FPU.

Agradecimientos

Este trabajo fue financiado parcialmente por CICYT-FEDER (Spain) a través de los proyectos DPI2004-01993 y MTM2008-05682, y por la Xunta de Galicia a través de los proyectos PGIDIT02XI20701PN y PGIDIT05PXIC20701PN. Además, durante los últimos años de estudiante de doctorado recibí financiación por parte del Ministerio de Educación y Ciencia (España) a través de la beca predoctoral de Formación de Profesorado Universitario AP2003-4495.

Bibliography

[1] G. Allaire. Homogenization and two-scale convergence. *SIAM J. Math. Anal.*, 23(6):1482–1518, 1992.

[2] L. Álvarez Vázquez and J. M. Viaño. Asymptotic justification of an evolution linear thermoelastic model for rods. *Comput. Methods Appl. Mech. Engrg.*, 115(1-2):93–109, 1994.

[3] T.M. Apostol. *Mathematical analysis.* Addison-Wesley Publishing Co., Reading, Mass.-London-Don Mills, Ont., second edition, 1974.

[4] I. Arregui, J.J. Cendán, C. Parés, and C. Vázquez. Numerical solution of a 1-d elastohydrodynamic problem in magnetic storage devices. *ESAIM: Mathematical Modelling and Numerical Analysis*, 42:645–665, 2008.

[5] P. Barral. *Análisis matemático y simulación numérica del comportamiento termomecánico de una colada de aluminio.* PhD thesis, Department of Applied Mathematics, Universidade de Santiago de Compostela, 2001.

[6] P. Barral, A. Bermúdez, M.C. Muñiz, M.V. Otero, P. Quintela, and P. Salgado. Numerical simulation of some problems related to aluminium casting. *Journal of Materials Processing Tech.*, 142(2):383–399, 2003.

[7] P. Barral, C. Moreno, P. Quintela, and M. T. Sánchez. A numerical algorithm for a Signorini problem associated with Maxwell-Norton materials by using generalized Newton's methods. *Comput. Methods Appl. Mech. Engrg.*, 195(9-12):880–904, 2006.

[8] P. Barral, M. C. Naya-Riveiro, and P. Quintela. Mathematical analysis of a viscoelastic problem with temperature-dependent coefficients. I. Existence and uniqueness. *Math. Methods Appl. Sci.*, 30(13):1545–1568, 2007.

[9] P. Barral and P. Quintela. A numerical method for simulation of thermal stresses during casting of aluminium slabs. *Comput. Methods Appl. Mech. Engrg.*, 178(1-2):69–88, 1999.

[10] P. Barral and P. Quintela. A numerical algorithm for prediction of thermomechanical deformation during the casting of aluminium alloy ingots. *Finite Elem. Anal. Des.*, 34(2):125–143, 2000.

[11] P. Barral and P. Quintela. Numerical analysis of a viscoplastic problem with contact condition taking place in an aluminium casting. In *Proceedings of the 8th International Congress on*

Computational and Applied Mathematics, ICCAM-98 (Leuven), volume 115, pages 63–86, 2000.

[12] P. Barral and P. Quintela. Asymptotic analysis of a metallostatic pressure type boundary condition modelled by a fictitious domain method in an aluminium casting. *Asymptot. Anal.*, 30(2):93–116, 2002.

[13] P. Barral and P. Quintela. Existence of a solution for a Signorini contact problem for Maxwell-Norton materials. *IMA J. Appl. Math.*, 67(6):525–549, 2002.

[14] P. Barral and M.T. Sánchez. A suitable numerical algorithm for the simulation of the butt curl deformation of an aluminium slab. In *Numerical Mathematics and Advanced Applications. Proceedings of ENUMATH 2005*, pages 1108 – 1116, 2006.

[15] F.P. Beer and E.R. Johnston. *Mechanics of materials.* Mc Graw-Hill, New York, 1990.

[16] A. Bermúdez and C. Moreno. Duality methods for solving variational inequalities. *Comput. Math. Appl.*, 7(1):43–58, 1981.

[17] A. Bermúdez and M. V. Otero. Numerical solution of a three-dimensional solidification problem in aluminium casting. *Finite Elem. Anal. Des.*, 40(13-14):1885–1906, 2004.

[18] A. Bermudez and J. M. Viaño. Une justification des équations de la thermoélasticité des poutres à section variable par des méthodes asymptotiques. *RAIRO Anal. Numér.*, 18(4):347–376, 1984.

[19] A. Bermúdez de Castro. *Continuum Thermomechanics.* Birkhauser, 2005.

[20] D.P. Bertsekas. *Nonlinear Programming.* Athena Scientific, Belmont, 1995.

[21] B. Biondi and S. Caddemi. Closed form solutions of euler-bernoulli with singularities. *International Journal of Solids and Structures*, 42:3027–3044, 2005.

[22] D. Blanchard, A. Gaudiello, and G. Griso. Junction of a periodic family of elastic rods with a 3d plate. part I. *J. Math. Pures Appl. (9)*, 88(1):1–33, 2007.

[23] D. Blanchard, A. Gaudiello, and G. Griso. Junction of a periodic family of elastic rods with a thin plate. part II. *J. Math. Pures Appl. (9)*, 88(2):149–190, 2007.

[24] D. Blanchard and P. Le Tallec. Numerical analysis of the equations of small strains quasistatic elastoviscoplasticity. *Numer. Math.*, 50(2):147–169, 1986.

[25] S. F. Borg. *Matrix-tensor methods in continuum mechanics.* World Scientific Publishing Co. Inc., Teaneck, NJ, second edition, 1990.

[26] H. Brezis. *Analyse Fonctionnelle. Theorie and Applications.* Masson, Paris, 1983.

[27] M. Burguera and J.M. Viaño. Numerical solving of frictionless contact problems in perfectly plastic bodies. *Comput. Methods Appl. Mech. Engrg.*, 121(1-4):303–322, 1995.

[28] P.G. Ciarlet. *Élasticité tridimensionnelle*, volume 1 of *Recherches en Mathématiques Appliquées [Research in Applied Mathematics]*. Masson, Paris, 1986.

[29] G. Cimatti. The constrained elastic beam. *Meccanica*, 8(2):119–124, 1973.

[30] D. Cioranescu, A. Damlamian, and G. Griso. Periodic unfolding and homogenization. *C. R. Math. Acad. Sci. Paris*, 335(1):99–104, 2002.

[31] D. Cioranescu, O. A. Oleĭnik, and G. Tronel. Korn's inequalities for frame type structures and junctions with sharp estimates for the constants. *Asymptotic Anal.*, 8(1):1–14, 1994.

[32] M. Djaoua and P. Suquet. Évolution quasi-statique des milieux visco-plastiques de Maxwell-Norton. *Math. Methods Appl. Sci.*, 6(2):192–205, 1984.

[33] J.M. Drezet and M. Plata. Thermomechanical effects during direct chill and electromagnetic casting of aluminum alloys. Part I: Experimental investigation. *Light Metals*, pages 931–940, 1995.

[34] J.M. Drezet, M. Rappaz, and Y. Krahenbuhl. Thermomechanical effects during direct chill and electromagnetic casting of aluminum alloys. Part II: numerical simulation. *Light Metals*, pages 941–950, 1995.

[35] G. Duvaut. *Mécanique des milieux continus*. Masson, Paris, 1990.

[36] C. Eck, S. A. Nazarov, and W. L. Wendland. Asymptotic analysis for a mixed boundary-value contact problem. *Arch. Ration. Mech. Anal.*, 156(4):275–316, 2001.

[37] I. Ekeland and R. Temam. *Analyse convexe et problèmes variationnels*. Dunod, 1974. Collection Études Mathématiques.

[38] T.S. El-Raghy, H.A. El-Demerdash, H.A. Ahmed, and A.M. El-Sheikh. Modelling of the transient and steady state periods during aluminium dc casting. *Light Models*, pages 925–929, 1995.

[39] F. Facchinei and J.S. Pang. *Finite-dimensional variational inequalities and complementarity problems*. Springer Series in Operations Research. Springer-Verlag, New York, 2003.

[40] G. Fichera. Problemi elastostatici con vincoli unilaterali: Il problema di Signorini con ambigue condizioni al contorno. *Atti Accad. Naz. Lincei Mem. Cl. Sci. Fis. Mat. Natur. Sez. I (8)*, 7:91–140, 1963/1964.

[41] M.C. Flemings. Solidification processing. In *McGraw-Hill Series in Materials Science and Engineering*, McGraw-Hill Series in Materials Science and Engineering. McGraw-Hill, New York, 1974.

[42] A. Friaâ. Le matériau de Norton-Hoff généralisé et ses applications en analyse limite. *C. R. Acad. Sci. Paris Sér. A-B*, 286(20):A953–A956, 1978.

[43] J.M. Gallardo, C. Parés, and M. Castro. A generalized duality method for solving variational inequalities. Applications to some nonlinear Dirichlet problems. *Numer. Math.*, 100(2):259–291, 2005.

[44] J.M. Gere and S.P. Timoshenko. *Mecánica de materiales*. International Thomson Editores, Mexico, 1998.

[45] G. Geymonat and P. Suquet. Functional spaces for Norton-Hoff materials. *Math. Methods Appl. Sci.*, 8(2):206–222, 1986.

[46] R. Glowinski and P. Le Tallec. *Augmented Lagrangian and operator-splitting methods in nonlinear mechanics*, volume 9 of *SIAM Studies in Applied Mathematics*. Society for Industrial and Applied Mathematics (SIAM), Philadelphia, PA, 1989.

[47] G. Griso. Asymptotic behaviour of curved rods by the unfolding method. *Math. Methods Appl. Sci.*, 27(17):2081–2110, 2004.

[48] G. Griso. Asymptotic behavior of structures made of plates. *Anal. Appl. (Singap.)*, 3(4):325–356, 2005.

[49] G. Griso. Obtention d'équations de plaques par la méthode d'éclatement appliquée aux équations tridimensionnelles. *C. R. Math. Acad. Sci. Paris*, 343(5):361–366, 2006.

[50] G. Griso and M.T. Sánchez. Homogenization of an elasticity problem for a catalyst support by using the unfolding method. Submitted to publication.

[51] F. Guitián, P. Quintela, M.T. Sánchez, and V. Valcárcel. Three-point bending tests. Part II: An improved formula for the modulus of rupture and numerical simulations. Submitted to publication.

[52] M.E. Gurtin. *An introduction to continuum mechanics*, volume 158 of *Mathematics in Science and Engineering*. Academic Press Inc. [Harcourt Brace Jovanovich Publishers], New York, 1981.

[53] J.P. Henry and F. Parsy. *Cours d'Elasticité*. Dunod, Paris, 1982.

[54] N. Kikuchi and J. T. Oden. *Contact problems in elasticity: a study of variational inequalities and finite element methods*, volume 8 of *SIAM Studies in Applied Mathematics*. Society for Industrial and Applied Mathematics (SIAM), Philadelphia, PA, 1988.

[55] JO Kristiansson and EH Zetterlund. Thermal Stresses and Strains in the Solidifying Shell Within the Primary Cooling Zone During Continuous Casting. *Numerical Methods in Industrial Forming Processes*, pages 413–423, 1982.

[56] P. Le Tallec. *Numerical analysis of viscoelastic problems*. Recherches en Mathémathiques Appliquées. Masson, Paris, 1990.

[57] J. Lemaitre and J.L. Chaboche. *Mécanique des matériaux solides*. Dunod, Paris, 1988.

[58] J.-L. Lions and G. Stampacchia. Variational inequalities. *Comm. Pure Appl. Math.*, 20:493–519, 1967.

[59] S. Mariaux, M. Rappaz, Y. Krahenbuhl, and M. Plata. Modelling of Thermomechanical Effects During the Start-Up Phase of the Electromagnetic Casting Process. *Advances in Production and Fabrication of Light Metals and Metal Matrix Composites*, pages 175–187, 1992.

[60] R. Mifflin, L. Qi, and D. Sun. Properties of the moreau-yosida regularization of a piecewise $\mathcal{C}^2$ convex function. *Math. Program.*, 84:269–281, 1999.

[61] J. Nečas and I. Hlaváček. *Mathematical theory of elastic and elasto-plastic bodies: an introduction*, volume 3 of *Studies in Applied Mechanics*. Elsevier Scientific Publishing Co., Amsterdam, 1980.

[62] G. Nguetseng. A general convergence result for a functional related to the theory of homogenization. *SIAM J. Math. Anal.*, 20(3):608–623, 1989.

[63] V. Otero. *Estudio matemático y resolución numérica de modelos que surgen en el estudio de una colada de aluminio*. PhD thesis, Department of Applied Mathematics, Universidade de Santiago de Compostela, 2004.

[64] J.S. Pang. A B-differentiable equation-based, globally and locally quadratically convergent algorithm for nonlinear programs, complementarity and variational inequality problems. *Math. Programming*, 51(1, (Ser. A)):101–131, 1991.

[65] J.S. Pang, D. Sun, and J. Sun. Semismooth homeomorphisms and strong stability of semidefinite and Lorentz complementarity problems. *Math. Oper. Res.*, 28(1):39–63, 2003.

[66] C. Parés, M. Castro, and J. Macías. On the convergence of the Bermúdez-Moreno algorithm with constant parameters. *Numer. Math.*, 92(1):113–128, 2002.

[67] C. Parés, J. Macías, and M. Castro. Duality methods with an automatic choice of parameters. Application to shallow water equations in conservative form. *Numer. Math.*, 89(1):161–189, 2001.

[68] L. Qi. Convergence analysis of some algorithms for solving nonsmooth equations. *Math. Oper. Res.*, 18(1):227–244, 1993.

[69] L. Qi and J. Sun. A nonsmooth version of newton's method. *Math. Program.*, 58:353–367, 1993.

[70] P. Quintela and M.T. Sánchez. Three-point bending tests. Part I: Mathematical study and asymptotic analysis. Submitted to publication.

[71] M. Reed and B. Simon. *Methods of modern mathematical physics. 1. Functional analysis*. Academic Press, 1980.

[72] S.M. Robinson. Newton's method for a class of nonsmooth functions. *Set-Valued Anal.*, 2(1-2):291–305, 1994. Set convergence in nonlinear analysis and optimization.

[73] M.T. Sánchez. Simulación numérica de algunos problemas en mecánica de contacto. Master's thesis, Department of Applied Mathematics, Universidade de Santiago de Compostela, 2003.

[74] M. Schatzman. Problèmes aux limites non linéaires, non coercifs. *Ann. Scuola Norm. Sup. Pisa (3)*, 27:641–686 (1974), 1973.

[75] W. Schneider, E.K. Jensen, and B. Carrupt. Development of a new starting block shape for the dc casting of sheet ingots. Part I: Experimental results. *Light Metals*, pages 961–967, 1995.

[76] L. Schwartz. *Théorie des distributions.* Publications de l'Institut de Mathématique de l'Université de Strasbourg, No. IX-X. Hermann, Paris, 1966.

[77] J. Sengupta, S.L. Cockcroft, D.M. Maijer, and A. Larouche. Quantification of temperature, stress, and strain fields during the start-up phase of direct chill casting process by using a 3d fully coupled thermal and stress model for aa5182 ingots. *Materials Science and Engineering A*, pages 157–177, 2005.

[78] M. Sofonea. On a contact problem for elastic-viscoplastic bodies. *Nonlinear Anal.*, 29(9):1037–1050, 1997.

[79] D. Sun. A further result on an implicit function theorem for locally Lipschitz functions. *Oper. Res. Lett.*, 28(4):193–198, 2001.

[80] L. Trabucho and J. M. Viaño. Mathematical modelling of rods. In *Handbook of numerical analysis, Vol. IV*, Handb. Numer. Anal., IV, pages 487–974. North-Holland, Amsterdam, 1996.

[81] Z. Tutek and I. Aganović. A justification of the one-dimensional linear model of elastic beam. *Math. Methods Appl. Sci.*, 8(4):502–515, 1986.

[82] J.M. Viaño. Generalización y justificación de modelos unilaterales en vigas elásticas sobre fundación. In *Actas del VIII CEDYA, Santander*, pages 63–86, 1985.

[83] Juan M. Viaño. The one-dimensional obstacle problem as approximation of the three-dimensional Signorini problem. *Bull. Math. Soc. Sci. Math. Roumanie (N.S.)*, 48(96)(2):243–258, 2005.

[84] W.A. Wong and J.J. Jonas. Aluminum extrusion as a thermally activated process. *Transactions of the Metallurgical Society of AIME*, 242:2271–2280, 1968.

[85] P. Wriggers. Finite element algorithms for contact problems. *Arch. Comput. Methods Engrg.*, 2(4):1–49, 1995.

[86] E. Zeidler. *Nonlinear functional analysis and its applications.* Springer-Verlag, New York, 1990.